UNIVERSITY OF SOUTHAMPTON

The Interaction of Peptide Nucleic Acids with Free and Histone Bound DNA

by

Tracey Louise Purvis

A thesis submitted for the degree of
DOCTOR OF PHILOSOPHY

October 2003
Department of Biochemistry

UNIVERSITY OF SOUTHAMPTON

ABSTRACT

FACULTY OF SCIENCE
DIVISION OF BIOCHEMISTRY

Doctor of Philosophy

THE INTERACTION OF PEPTIDE NUCLEIC ACIDS WITH FREE AND HISTONE BOUND DNA

by Tracey Louise Purvis

Peptide Nucleic Acid (PNA) is a DNA mimic in which the phosphodiester backbone has been replaced by an uncharged peptide backbone. This can form very stable duplex and triplex complexes with DNA and, under favourable conditions, can show strand invasion of duplex DNA generating P-loop structures. This thesis studies the interaction of several polypyrimidine PNAs with both free and nucleosomal DNA under different ionic conditions. These different PNAs explore the effects of base sequence, length and polarity on the interaction. This work used variants of the *tyr*T DNA sequence, which contain PNA binding sites located at different positions with respect to the end of the fragments, thereby affecting their translational positioning when reconstituted onto histone octamers. Footprinting studies with DNaseI and S1 nuclease, together with gel retardation assays and fluorescence melting studies were used to examine the sequence specificity and binding affinity of these PNAs to free double strand DNA. At low pHs (5.0) DNaseI footprints were observed at submicromolar PNA concentrations. No binding was detected at higher pHs, consistent with the involvement of C^+•GC triplets in this interaction. Higher PNA concentrations (typically 10μM) were required to induce S1 cleavage and to produce bandshifts, suggesting strand invasion (generating 2:1 PNA:DNA complexes) is a slower and less stable process. The most stable complexes were formed when the PNA was of increased length and orientated parallel to the duplex purine strand.

Within all eukaryotic cells, DNA is associated with histone proteins in the form of chromatin. Therefore, similar studies were performed on these DNA fragments, which have been reconstituted into nucleosome core particles, thereby assessing the accessibility of each of the target sites, when located in different positions. These complexes were prepared by either challenging reconstituted nucleosomes with PNA, or by attempting to wrap pre-formed PNA-DNA complexes around the histone octamer. PNA is unable to bind to the central nucleosomal DNA core particle, though some interaction with the peripheral regions is detected. The formation of these complexes prevents DNA from wrapping around the histone octamers if the remaining regions of free DNA are insufficient in length. The N-terminal tail domains of the histone octamer interact with the DNA backbone, increasing nucleosome stability by providing additional countercharges to the polyanionic DNA backbone. Therefore, further experiments examined the interaction with nucleosomes in which the N-terminal histone tail domains had been removed. These showed improved PNA binding.

Contents

List of Figures

List of Tables

Abbreviations

2YT media	16g tryptone, 10g yeast extract, 5g NaCl per litre
Å	Ångström (10^{-10} metre)
°C	degree Celsius
A	adenine
AMPS	ammonium persulphate
AMV	Avian Myeloblastosis Virus
bis-PNA	two PNA strands covalently linking together
bp	base pair
C_{50}	concentration required to reduce bands intensity by 50%
C	cytosine
Ci	curie
CMV retinitis	cytomegalovirus retinitis
CON	control
cps	counts per second
dATP	2'-deoxy-adenosine-5'-triphosphate
dCTP	2'-deoxy-cytidine-5'-triphosphate
dGTP	2'-deoxy-guanosine-5'-triphosphate
dTTP	thymidine-5'-triphosphate
dNTP	mixture of dATP, dCTP, dGTP and dTTP
dH_2O	distilled water
DNA	deoxyribonucleic acid
DNaseI	deoxyribonuclease I
dsDNA	double stranded deoxyribonucleic acid
DTT	dithiothreitol
EDTA	ethylenediaminetetraacetic acid
G	guanine
GA	Maxam-Gilbert marker
G_o	resting phase of the cell cycle
H1	histone H1
H2A	histone H2A
H2B	histone H2B

H3	histone H3
H4	histone H4
HA	hydrogen bond acceptor
HATs	histone acetyltransferases
HD	hydrogen bond donor
HDACs	histone deacetylases
HEPES	4-(2-hydroxyethyl)-1-piperazine-ethanesulfonic acid
Hoechst 33258	2′-(4-hydroxyphenyl)-5-(4-methyl-1-piperazinyl)-2,5′-bi-benzimidazole
hrs	hours
Im	N-methyimidazole
IPTG	isopropyl β-D-thiogalactopyranoside
KDa	kilo daltons
mRNA	messenger ribonucleic acid
NTR-1	neurotensin receptor
OD	absorbance
PCR	polymerase chain reaction
pH	$-\log_{10}$ hydrogen ion concentration
PMSF	phenylmethylsulphonylfluoride
PNA	peptide nucleic acid
polyd	poly deoxy
Py	N-methylpyrrole group
R	purine
RNA	ribonucleic acid
RNaseH	reverse transcriptase heterodimer
rpm	revolutions per minute
RT	room temperature
SDS	sodium dodecyl sulphate
siRNA	short interfering ribonucleic acid
ssDNA	single stranded deoxyribonucleic acid
T	thymine
TBE	11g Tris, 5.5g boric acid and 1g EDTA per litre
TEMED	N,N,N',N'-tetramethylethylenediamine
Tris	Tris(hydroxymethyl)aminomethane

Triton X-100	polyethylene glycol mono[4-(1,1,3,3-tetramethylbutyl) phenyl]ether
T_m	thermal stability
U	units
v/v	volume per volume
w/v	weight per volume
X-gal	5-bromo-4-chloro-3-indolyl β-D-galactosidase
Y	pyrimidine

Acknowledgments

I would like to thank my supervisor Professor Keith Fox for all his help, time, patience and support throughout this research. I would like to thank the research team especially Doctor Kris Leslie for all his help and guidance and Doctor Sarah Allinson for her support. When I started my PhD I knew it would be hard work, long hours and dedication but I never thought one of my colleagues and very good friends would die at such a young age. Claire became a good friend both at work and socially and an inspiration to her friends. Her death devastated the group and we will never fully get over this loss. She was incredibly strong and determined and for our friendship and the ongoing memory I have of Claire, this work is dedicated to you. I would like to thank the Association for International Cancer Research (Cancer Research UK) for giving the grant and opportunity to undertake this research.

Throughout my academic career my parents and sister have supported, encouraged and given me the choice and opportunity to pursue my own path. I would like to thank them for everything they have done and for their continuing support. The most important person to thank is my husband Doctor Alan Purvis, who throughout this work has given me his scientific opinion, support, time, encouragement and love. Without him none of this would be worth it.

This thesis is dedicated to the memory of

Charles Douglas Gash

September 1914 to October 1987

and

Claire Fitzgerald

August 1974 to May 2002

They are both greatly missed

Chapter 1

Introduction

1.1 Introduction

The structure of deoxyribonucleic acid (DNA) was published fifty years ago on the 25th April 1953 (Watson 1953). Although largely regarded as one of the most important scientific discoveries of the twentieth century, this was only the initial stage in understanding the full extent of its molecular chemistry. DNA contains the genetic information, stored in the form of a code dictated by a sequence of organic bases, and functions by virtue of its ability to specify and control the production of a large variety of proteins. Molecules which interact with DNA may therefore be employed to target individual genes and control gene expression, and have a wide range of therapeutic and diagnostic potentials.

1.2 The structure of Deoxyribonucleic Acid

DNA is a polymer made up of a large number of deoxyribonucleotides (Bloomfield *et al* 2000). Each nucleotide consists of a common pentose sugar ring, a phosphate linkage and one of four organic nitrogenous bases (figure 1.1). The bases are categorized into two groups the purines (R) (adenine (A) and guanine (G)) and the pyrimidines (Y) (cytosine (C) and thymine (T)). Each base is attached to a sugar ring at the C1 position through a glycosidic bond with the N9 position in the purines or the N1 position in the pyrimidines. The repeating unit is formed through a phosphodiester bond between the 5′ phosphate group and 3′ hydroxyl group of the subsequent nucleotide sugar (Bloomfield *et al* 2000). This polynucleotide chain is held together to form a double helix in which there is hydrogen bonding between complementary bases, generating specific base pairs. Adenine hydrogen bonds with thymine (A:T)

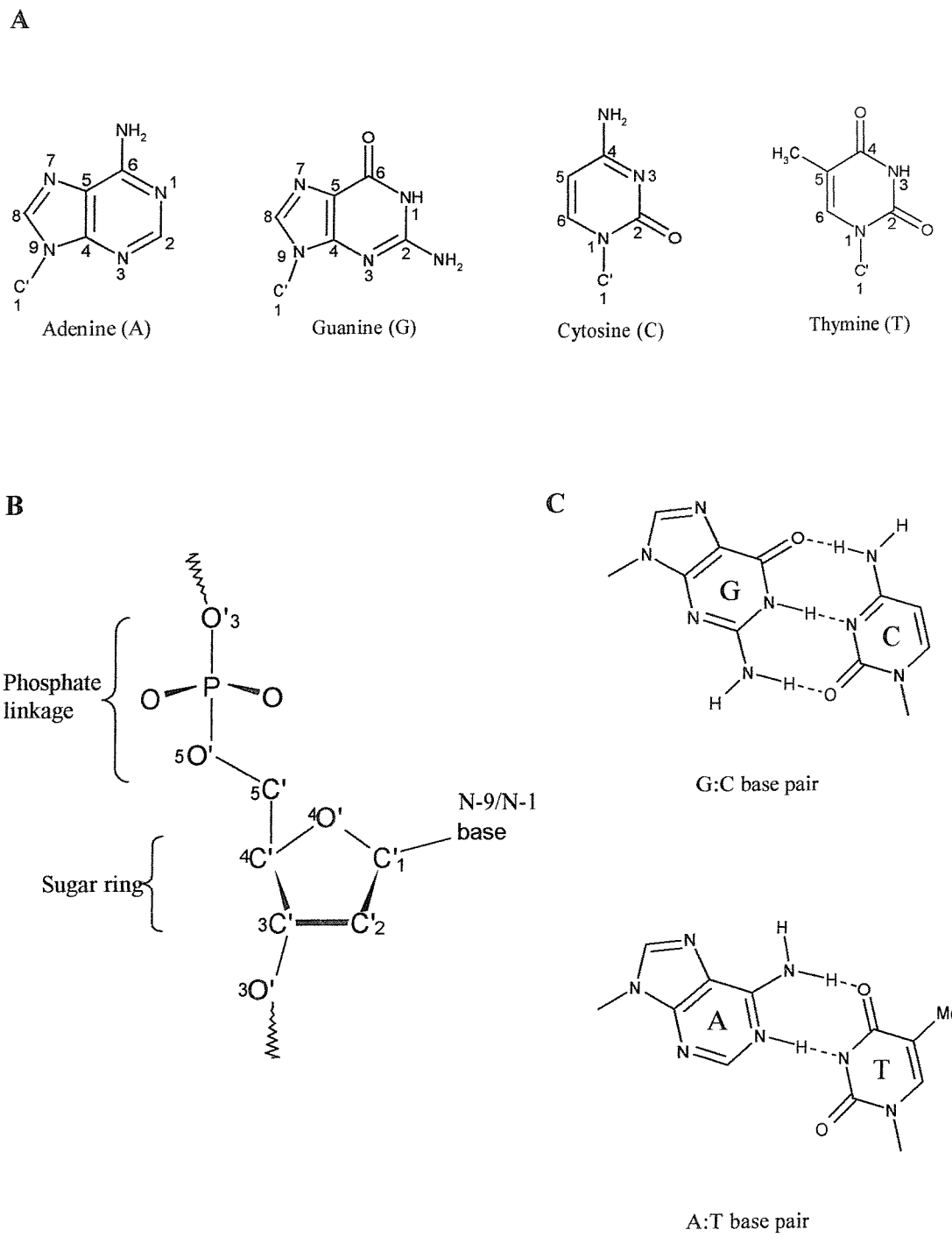

FIGURE 1.1 Basic components of DNA (A) The four different organic bases, (B) the repeating nucleotide unit, (C) A:T and G:C base pairs.

and cytosine hydrogen bonds with guanine (G:C) forming flexible base pairs (figure 1.1C). The adjacent C1′ atoms of the pentose rings are positioned 10.8Å apart for both A:T and G:C base pairs; this forms a distance constraint preventing the formation of purine-purine and pyrimidine-pyrimidine base pairing (Hunter 1993).

The base pairs are stacked perpendicular to the helical axis stabilizing the structure via Van der Waals' forces and hydrophobic interactions between adjacent base pairs. This creates a right-handed antiparallel helix with 10.4 base pairs (34Å) and on average 25 hydrogen bonds per helical turn (figure 1.2A). The helical nature of DNA arises from the non-symmetrical disposition of the glycosidic bonds across the base pairs and steric constraints imposed by the sugar phosphate backbone. This maximizes the distance between the phosphate groups thereby minimizing their electrostatic repulsion. By rotating the base pairs relative to each other the distance between the phosphates is increased thus reducing the repulsive force further. Because these glycosidic bonds are not directly opposite each other, two grooves of differing widths are created between the ribose-phosphate chains on the surface of the molecule. These are designated the major and minor grooves where the distance between the sugar-phosphate backbones is greater in the major groove than that of the minor groove. The width is usually defined by the perpendicular distance between phosphate groups on opposite strands minus their Van der Waals' diameter (5.8Å), whereas the depth is the difference in the cylindrical polar radii between phosphorus and the N2 guanine or N6 adenine atoms (Neidle 2002). Within these grooves parts of the bases are exposed to solvent, creating the potential for forming hydrogen bond contact which can be recognized by sequence specific DNA binding proteins, small molecules and triplex forming oligonucleotides.

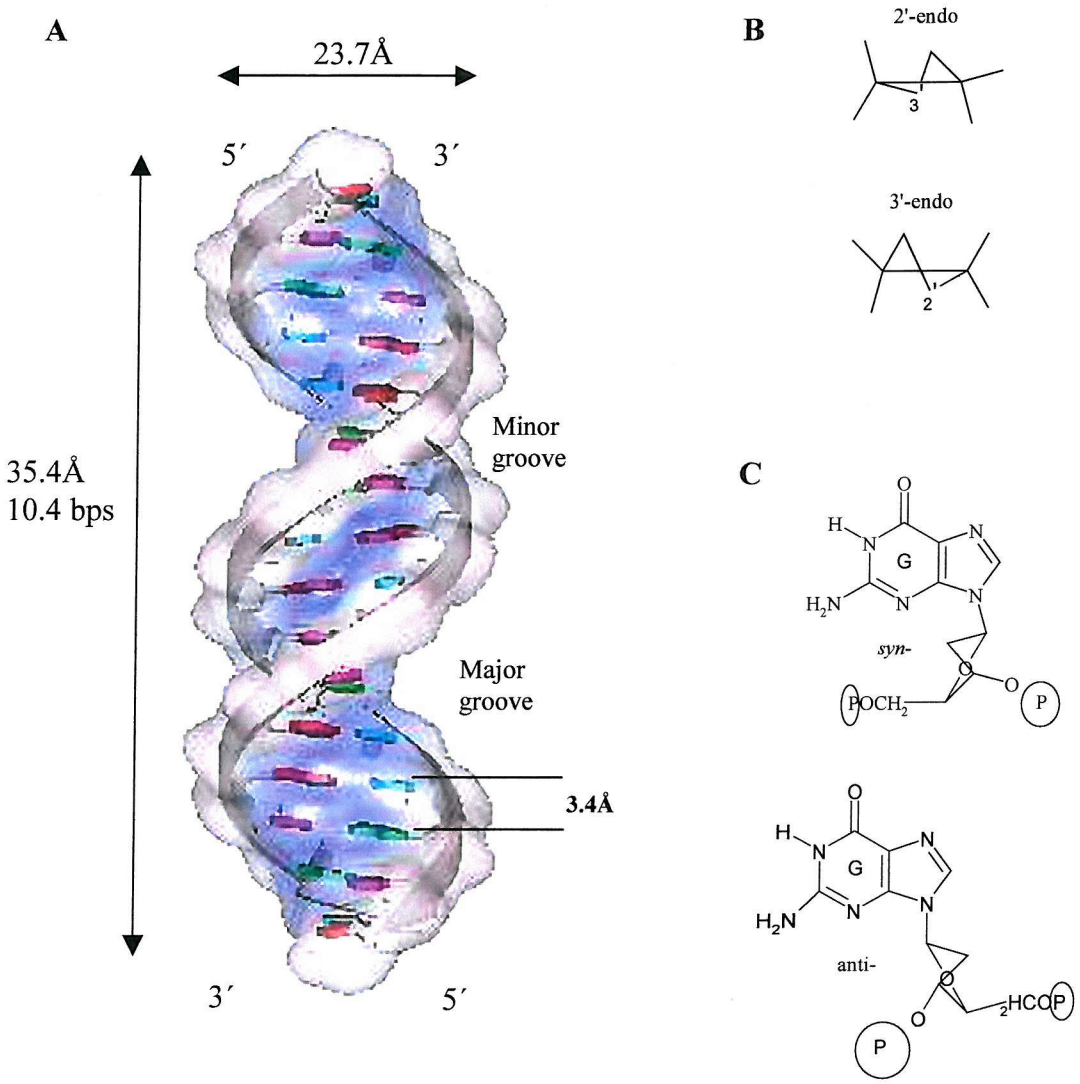

FIGURE 1.2 Structural aspects of B-DNA. (A) Graphical representation of the DNA helix (Collomb 2000) (B) C2′ *endo* and C3′ *endo* sugar pucker (C) *syn* and *anti* conformations of the base relative to the sugar.

The major and minor grooves have different hydrogen bonding potentials. This is highlighted in the T:A base pair where the major groove edge contains a methyl group (CH_3) followed by a hydrogen bond acceptor (HA), a hydrogen bond donor (HD), and a second hydrogen bond acceptor. In contrast, the minor groove edge presents only a HA, a hydrogen atom (H), and a second HA. When the T:A bases are reversed (A:T base pair) this would present a different pattern of contacts in the major groove (HA-HD-HA-CH_3) whereas the minor groove would remain the same (HA-H-HA). Similar characteristics are found in C:G and G:C base pairs in which G:C and C:G are similar in the minor groove but different in the major. Since many proteins that bind DNA recognize a specific sequences of bases, it is not surprising that most interact with the floor of the major groove, as this has greater potential for sequence specific recognition than the minor groove (Helene 1998).

DNA can adopt a variety of three-dimensional structures, exemplified by the A, B and Z forms which contain structurally distinctive major and minor grooves (Dickerson 1992; Dickerson & Ng 2001) (see table 1.1). These relate to the conformation of the sugar (C2′-*endo* or C3′-*endo*) and the orientation of the base relative to the sugar (*syn* or *anti*) (figure 1.2B & C). The B-form of DNA is the most common natural form prevalent under physiological conditions. It has a C2′ endo sugar pucker with the glycosidic bond in the *anti* configuration creating a 11.6Å wide and 8.5Å deep major groove and a 6Å wide and 8.2Å deep minor groove (figure 1.2A). The C1′-N9 (purine) and C1′-N1 (pyrimidine) glycosidic bonds are located on the minor-groove while the C6-N7 (purine) and C4 (pyrimidine) base atoms and their substituents are located in the major groove (Neidle 2002). The first observation of A-DNA was from fibre diffraction studies under conditions of low humidity. It has a much wider and shorter helix than B-DNA with the base pairs displaced from the

helical axis. Z-DNA is a left handed double helix and is formed by GC containing sequences with alternating purine and pyrimidines, under conditions of high salt or superhelical stress (Dickerson 1992). The structural features of the three different helical forms are summarized in figure 1.3 and table 1.1.

1.3 Cancer

Cancer is the second biggest killer in the Western world and over 200 genes that promote (or prevent) cancer have currently been identified in the human genome. Tumour cell growth in humans is a multi-step process caused by genetic alterations that drive the transformation of normal cells into highly malignant derivatives. Lethal effects occur when these malignant cells affect normal organ function or metastasize throughout the body. Genetic mutations occur within normal cellular genes known as proto-oncogenes producing oncogenes which leads to abnormal cell growth and division. Multiple mutations occur ranging from point mutations to chromosomal translocations. A number of theories have been proposed for the mechanism of tumour cell growth, but it is generally thought that all types of cancers usually require alterations in six steps to transform normal healthy cells into malignant growths. These mechanisms involve self-sufficiency in growth-inhibitory signals, insensitivity to growth-inhibitory signals, evasion of programmed cell death, limitless replicative potential, sustained angiogenesis and tissue invasion and metastasis (Hanahan & Weinberg 2000).

Cancer is currently treated through a combination of surgery, radiotherapy and chemotherapy. Surgery and radiotherapy are area specific whereas chemotherapy

	Helical form A	B	Z
Shape	Broad	Intermediate	Narrow
Screw sense	Right-handed	Right-handed	Left-handed
Repeating unit	1bp	1bp	2bp
Rotation/bp	33.6°	35.9°	60°/2
Tilt of base pairs relative to helix axis	19°	1°	9°
Base pairs per helical turn	11	10.4	12
Rise per base pair	2.3Å	3.4Å	3.8Å
Helix diameter	25.5Å	23.7Å	18.4Å
Pitch per helical turn	25.3Å	35.4Å	45.6Å
Glycosidic bond	*Anti*	*Anti*	*Anti* C, T *Syn* G, A
Sugar conformation	C3′ endo	C2′ endo	C3′ endo G, A C2′ endo C, T
Major groove	2.2Å wide 13.0Å deep	11.6Å wide 8.5Å deep	8.8Å wide 3.7Å deep
Minor groove	11.1Å wide 2.6Å deep	6.0Å wide 8.2Å deep	2.0Å wide 13.8Å deep

TABLE 1.1 Statistical differences between the helical forms of DNA.

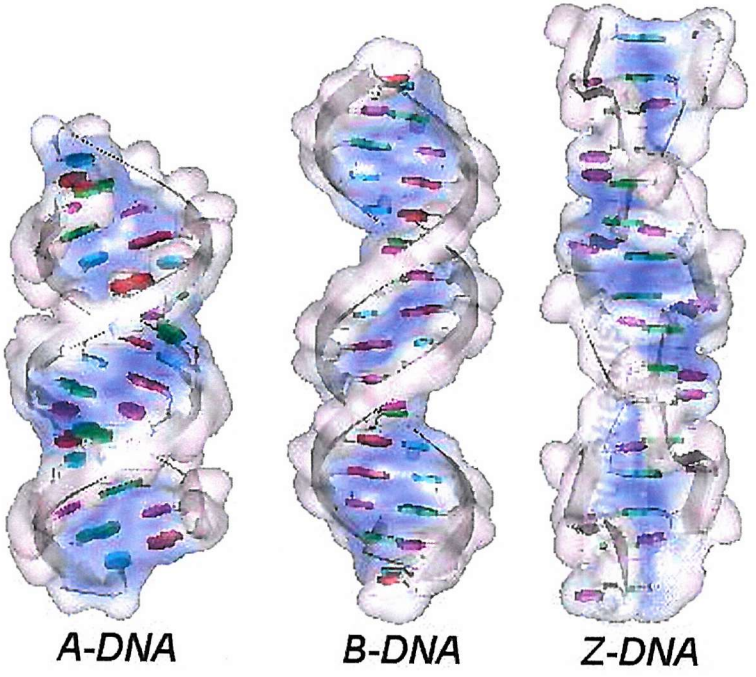

FIGURE 1.3 Structural representation of the different forms of DNA (Collomb 2000).

involves the systemic use of cytotoxic drugs. This cocktail of drugs usually contains a number of DNA binding compounds that target rapidly dividing cells in the M and S cell cycle phases but not cells in their resting phase (G_o). Chemotherapy targets all rapidly dividing cells and so is non-specific and does not distinguish between normal healthy cells and cancerous cells. These drugs therefore produce highly toxic side effects, affecting rapidly dividing cells involved in hair growth, reproduction, the immune system and bone marrow development. There is therefore an urgent need for new therapeutic approaches that target individual oncogenes or their products. One way in which this may be achieved is through antisense and antigene nucleic acid gene targeting, where the sequence specificity of these agents enables individual genes to be inhibited, avoiding the non-specific toxicity that is produced in chemotherapy.

1.4 Targeting DNA selectively

Successful targeting of DNA requires several factors to be taken into consideration. These include the sequence and structure of the particular DNA target as well as its cellular location (i.e. the nucleus) and the interaction with other proteins. Several different types of simple DNA binding ligands have been characterized; these fall into two main classes which are either intercalators or groove binders. Intercalators such as ethidium bromide, daunomycin and porphyrin insert their aromatic rings between adjacent base pairs but have very limited sequence specificity as they interact with only two base pairs. Groove binding ligands are often crescent shaped molecules which interact with the DNA minor groove. Natural ligands in this class include the agents distamycin and netropsin; these are AT selective as a result of steric clash with the two amine groups of guanine, and the narrow groove width of

these sequences. A series of synthetic minor groove binding agents (polyamides) have been developed by Dervan's group (Dervan & Edelson 2003). These compounds contain N-methylpyrrole (Py) and N-methyimidazole (Im) groups and bind within the minor groove as antiparallel dimers, which are able to distinguish between GC/CG and AT/TA sequences.

Several methods using synthetic oligonucleotides for targeting unique DNA or ribonucleic acid (RNA) sequences in the cell have been devised. Antisense oligonucleotides and ribozymes (and short interfering RNA (siRNA)) target RNA, thereby inhibiting the translation of specific genes while antigene triplex forming oligonucleotides target double stranded DNA and prevent transcription (Hanvey *et al* 1992) (see figure 1.4). Antisense oligonucleotides are derivatives of nucleic acids that hybridize to messenger ribonucleic acid (mRNA) through usual hydrogen bonding to the complementary nucleic acid bases. These prevent translation either by direct steric blockage or by activating RNaseH. Antisense therapeutic agents are currently being investigated both *in vitro* and *in vivo* for use in the treatment of human immunodeficiency virus, hepatitis virus, herpes simplex virus, papillomavirus, cancer, restenosis, rheumatoid arthritis, and allergic disorders (Kushner & Silverman 2000). Although still at the preliminary stages, some results are promising with more than ten antisense drugs currently undergoing clinical trials. For example, Vitravene is used for the treatment of cytomegalovirus retinitis (CMV retinitis) infection and is currently the only antisense drug commercially available (Crooke 1998). Ribozymes are catalytic RNAs and combine their enzymatic activity with the specificity of antisense base pairing, creating a molecule that can cleave the targeted mRNAs. Antigene agents bind to double stranded DNA (dsDNA) in the nucleus forming triple helices and blocking the production of mRNA.

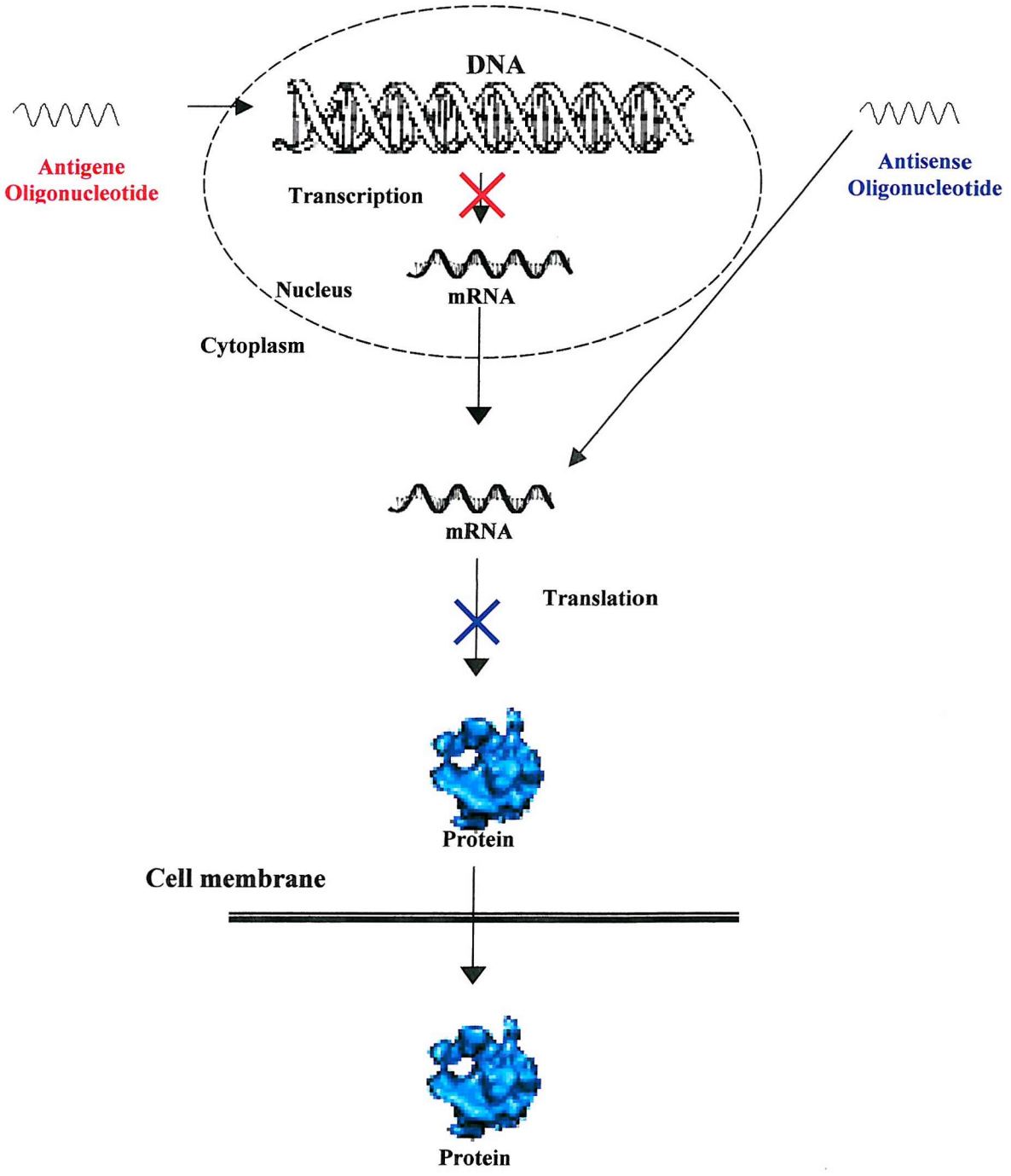

FIGURE 1.4 Illustration of the principle for antisense (blue) and antigene (red) techniques.

1.4.1 Triplex formation

The formation of a DNA triplex was first identified through the combination of polyrA/polyrU in the ratio of 1:2 in the presence of moderate concentrations of magnesium (or other cations) (Rich & Davies 1956). This forms a three stranded polynucleotide triple helix composed of U.AU triplets with a right handed screw (figure 1.5A) (Arnott *et al* 1976; Felsenfeld *et al* 1957). Since these early studies several other base triplets have been identified and these triplexes are classified into two distinct structural motifs, which differ in the orientation of the third strand. Parallel (YRY) triplexes are formed by the binding of pyrimidine containing oligonucleotides in the DNA major groove, forming C^+.GC and T.AT triplets (see figure 1.5). The third strand is oriented parallel to the duplex purine strand. Since formation of the C^+.GC triplet requires protonation of the third strand cytosine at the N3 position, the formation of these complexes requires conditions of low pH (less than 6.0). The second triplex structure is the antiparallel YRR motif in which the third strand binds antiparallel to the duplex purine strand through reverse Hoogsteen hydrogen bonding forming A.AT, G.GC and T.AT triplets. In each case the third strand oligonucleotide binds within the major groove of the DNA duplex making specific contacts with the exposed faces of the purine bases. This therefore limits triplex formation to the recognition of oligopurine tracts. Triplex stability depends on the length of the third strand and stable triplexes usually require the oligonucleotides to be at least 12-15 bases long. These complexes are very specific and are sensitive to mismatches (Chann 1997). However, the affinity of the third oligonucleotides for duplex DNA is much lower than that of double stranded DNA itself (Frank-Kamenetskii & Mirkin 1995). This is largely because of the charge repulsion between

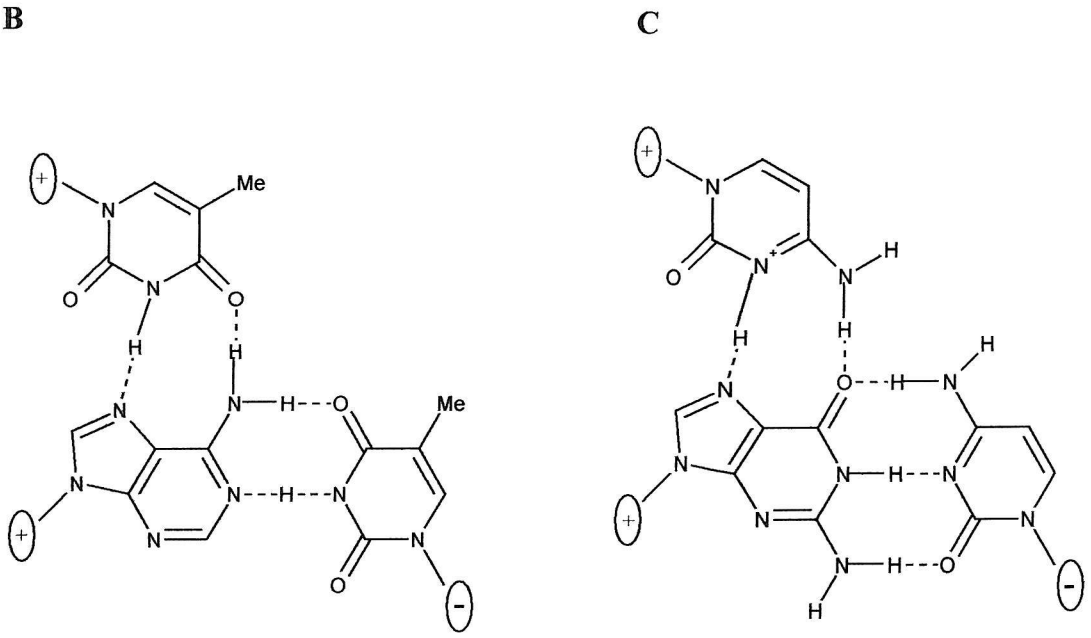

FIGURE 1.5 DNA triplex helix. (A) Cartoon representation of a triple helix, the black ribbon represents the third strand oligonucleotide (Fox 2003) (B) the T.AT and (C) C^{+}.GC triplex arrangement in a YRY triple helix.

the three polyanionic strands. It has been shown that triplex forming oligonucleotides are able to penetrate cell membranes and target dsDNA, thereby inhibiting transcription (Faria *et al* 2001). One of the main factors, which limits the use of oligonucleotides as therapeutic agents in their susceptibility to degradation by nucleases. Several modifications to the chemical structure of oligonucleotides have been devised so as to increase their stability. These include changes to the phosphodiester backbone, generating phosphorothioates, phosphoramidates and methylphosphonates, as well as modifications to the sugar such as 2′-O alky groups. The work described in this thesis concerns the DNA mimic in which the phosphodiester backbone has been replaced with a peptide backbone.

1.5 Peptide Nucleic Acids

Peptide nucleic acid (PNA) was designed by a collaboration of scientists including Peter Nielsen, Pernilla Wittung, Ole Buchardt, Michael Egholm and Rolf Berg at the University of Copenhagen in 1991 as a ligand for dsDNA recognition by triplex formation (Nielsen *et al* 1991). The concept was to mimic the function of oligonucleotides whilst maintaining binding via Hoogsteen hydrogen bonding in the major groove. The four nitrogenous bases of DNA are present in PNA enabling sequence specific targeting of duplex DNA. However, the negatively charged deoxyribose phosphate backbone of DNA is replaced with an uncharged polyamide backbone. This modification was designed with the expectation that the third strand would form a tighter triple helix with its target site, thus creating a platform for advanced recognition sequences without limiting targeting to homopurine tracts. The polyamide backbone should also increase cellular stability enabling PNA to be a more

successful antigene therapeutic agent. However, as described below, this type of simple interaction is rarely seen with most PNAs.

1.5.1 PNA chemistry

The original PNA structure was based upon an 'amino ethyl glycine' backbone and is the type used in this work. This is constructed of repeating N-(2-aminoethyl)-glycine units linked by amide bonds creating an acyclic, achiral and neutral pseudo-peptide backbone (figure 1.6A). The purine and pyrimidine bases are attached to the backbone through methylene carbonyl linkages equally aligned along the backbone. The same distance separates the bases as is found in DNA, enabling hydrogen bonding to DNA bases (figure 1.6A). PNA is chemically more related to proteins than to nucleic acids (Nielsen 1999) so consequently is characterized by a carboxylate (C) and amino (N) termini, rather than by 5′ and 3′ ends.

Several modifications have been made to the original PNA backbone to increase solubility and binding affinities. Several of these are shown in figure 1.6B. One important feature is the addition of a lysine residue at the carboxyl terminus. Lysine is doubly charged at neutral pH and thus significantly increases the solubility of the molecule (Haaima *et al* 1996).

1.5.2 PNA/DNA interactions

PNA sequence specifically targets single stranded DNA (ssDNA), dsDNA and RNA forming duplexes and triplexes. It has a remarkably strong sequence-specific binding affinity to natural nucleic acids (DNA, RNA and PNA), which is

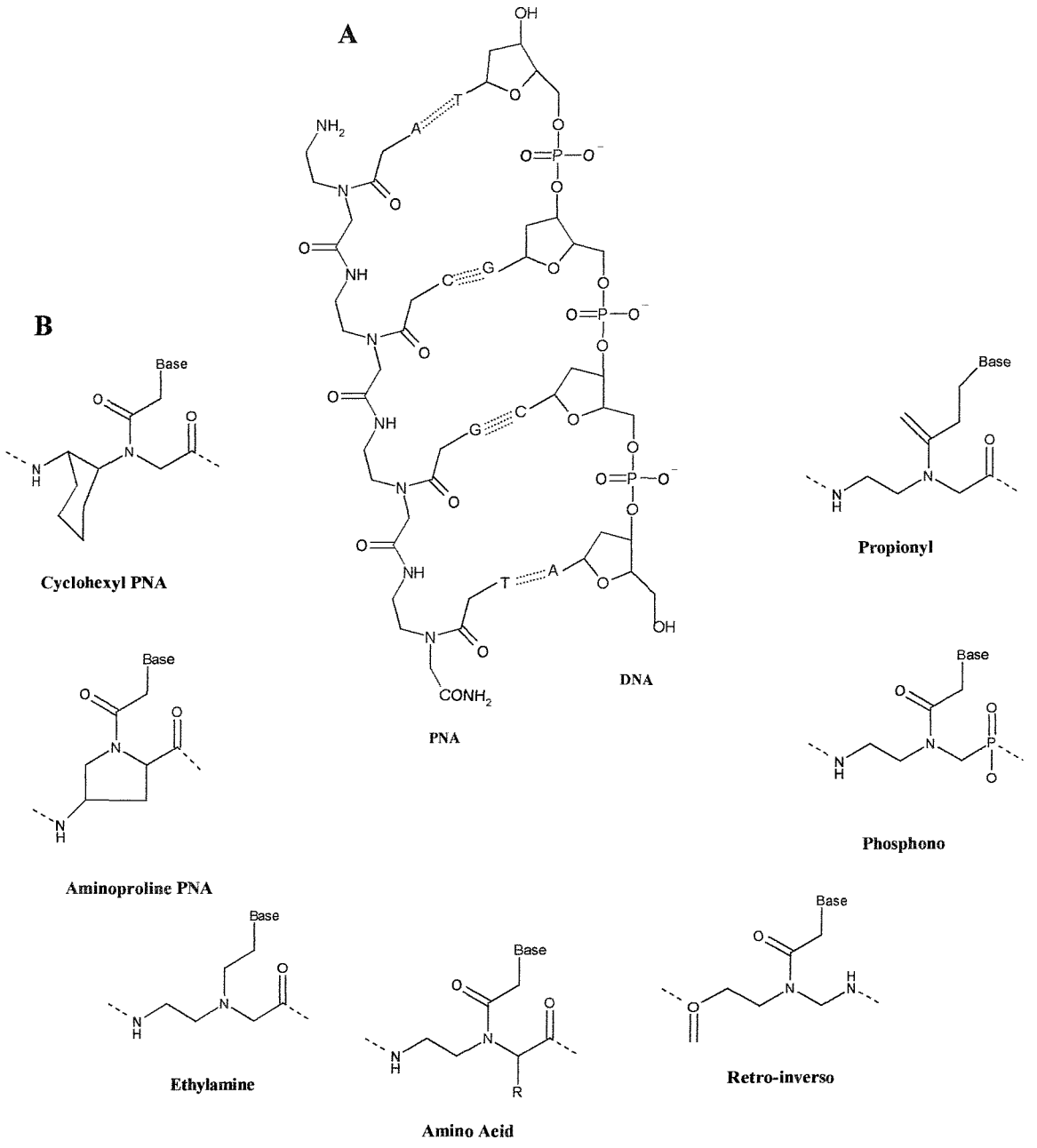

FIGURE 1.6 Chemical aspects of PNA and backbone modifications. (A) Chemical structure of DNA and PNA (B) Chemical modifications made to traditional PNA monomers including Cyclohexyl PNA (Lagriffoule *et al* 1997), Aminoproline PNA (Schwemler. *et al* 1997), Ethylamine (Hyrup & Nielsen 1996)Amino acid (Haaima *et al* 1996) and (Puschl *et al* 1998), retro-inverso (Krotz *et al* 1998), Phosphono (Efimov *et al* 1998), Propionyl (Hyrup *et al* 1994).

primarily attributed to the uncharged polyamide backbone (Schwarz *et al* 1999). When targeting ssDNA, PNA can bind in either orientation forming parallel and antiparallel PNA/DNA and PNA/RNA duplexes (figure 1.7) (Leijon *et al* 1994). This is in contrast to oligonucleotides where the polarity of binding is determined by the deoxyribose sugar. The most stable duplexes are formed with an antiparallel Watson and Crick orientation where the N-terminus of the PNA faces the 3′ end of the DNA or oligonucleotide (i.e. as if the N-terminus of PNA corresponds to the 5′ end of DNA) (Sugimoto *et al* 2001). The most stable triplexes are formed when the pyrimidine containing PNA strand binds parallel to the purine strand of the DNA duplex.

The lack of electrostatic repulsion in the PNA/DNA duplex, in comparison to the DNA/DNA duplex, gives rise to thermal stability (T_m) which is almost independent of ionic strength (figure 1.8) (Nielsen & Egholm 1999). PNA can therefore target DNA in the absence of salt, a feature which is very different to that of dsDNA, and PNA/DNA duplexes generally have higher T_m values than the corresponding DNA/DNA duplexes (Giesen *et al* 1998). At salt concentrations exceeding 500 millimolar, the T_m values are essentially the same. The T_m for PNA/DNA complexes correlates with the GC content and depends on the purine content of the PNA strand. The stability of PNA containing duplexes is length dependent with sequences less than six to eight base pairs long unable to form stable duplexes or triplexes (Doyle *et al* 2001). The introduction of mismatches also produces highly unstable complexes (Ratilainen *et al* 2000).

PNA was originally designed as a triplex forming DNA mimic and was expected to form a triple helix with dsDNA. The first studies used homo-thymine PNA sequences to target homo-adenine DNA tracts (figure 1.9). Although PNA was

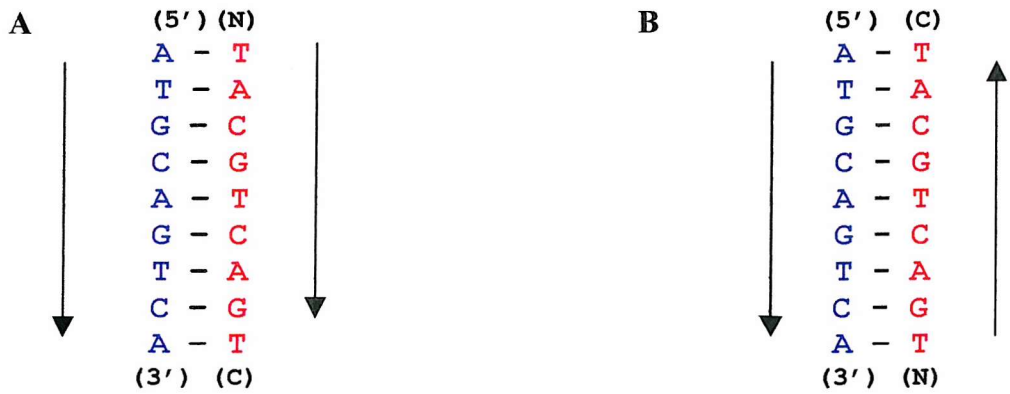

FIGURE 1.7 Orientation independent binding of PNA. (A) Parallel Watson and Crick PNA strand (B) antiparallel Watson and Crick PNA strand, both in relation to the orientation of the DNA strand. The N-C terminal region of PNA corresponds to the 5′-3′ region of DNA. The PNA strand is illustrated in red and the DNA strand is illustrated in blue.

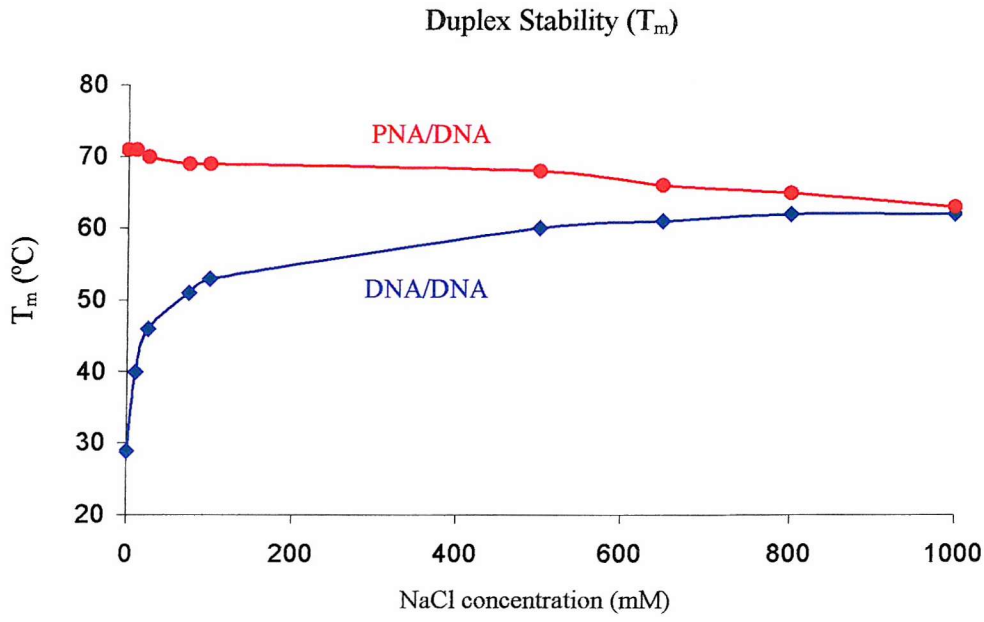

FIGURE 1.8 Thermal stability comparison for a PNA/DNA (red) and DNA/DNA (blue) duplex against salt concentration, modified from (Nielsen & Egholm 1999).

predicted to form a classic PNA/DNA_2 triplex whereas a PNA_2/DNA triplex was clearly observed. In fact the PNA had invaded the duplex, displacing the non-targeted homopyrimidine DNA strand, forming a triplex with the homo-adenine DNA strand (Wittung *et al* 1996). This was unexpected as the invading PNA had to overcome a large activation energy to displace one of the DNA strands. PNA has been shown to be able to form four different PNA/DNA complexes, which involves triplex formation and strand invasion and which are summarised in figure 1.10.

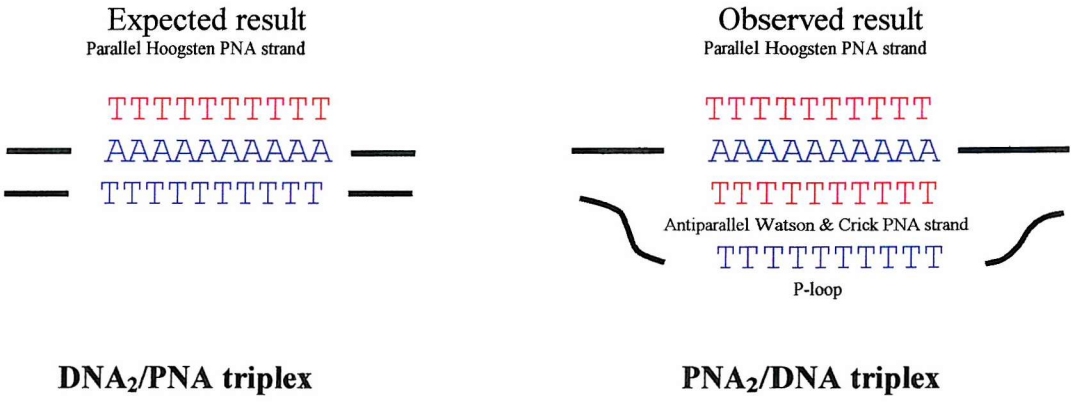

FIGURE 1.9 Early PNA experiments using polythymine PNA sequence targeted to poly A, poly T DNA targets forming a PNA_2/DNA triplex. The PNA strands are illustrated in red and the DNA strands are in blue.

The addition of PNA as a third strand to the DNA duplex can form a classic PNA/DNA_2 triplex (figure 1.10A). This is rarely observed since this complex usually progresses to a triplex via strand invasion (figure 1.10B), but is believed to be the intermediate complex. This structure is facilitated by high cytosine containing pyrimidine PNA sequences (Wittung *et al* 1997).

Triplex strand invasion (figure 1.10B) is the preferred and most kinetically stable complex formed with homopyrimidine PNA (longer than 8-10 bases). Two

PNA strands bind a single stranded polypurine tract within the DNA duplex forming a PNA_2/DNA triplex. This results in the displacement of the non-targeted single stranded pyrimidine DNA strand forming a P-loop (Wittung *et al* 1996). This complex is thermodynamically favoured but its properties are kinetically determined by its slow association rates and extremely slow dissociation rates (Demidov *et al* 1995). Purine containing and mixed sequence PNA's do not form strand invasion complexes (Nielsen & Christensen 1996).

Duplex strand invasion can occur upon PNA binding forming a PNA/DNA duplex with the single stranded polypurine tract. This displaces the non-targeted polypyrimidine strand forming a P-loop (figure 1.10C) (Wittung *et al* 1996). These structures are facilitated by purine rich PNA sequences.

Double duplex invasion (figure 1.10D) involves the interaction of a PNA molecule with both DNA strands generating two independent PNA/DNA duplexes (Lohse *et al* 1999). This complex is not possible with PNAs that contain standard bases as the two invading strands are self-complementary and form a PNA/PNA duplex in preference to targeting DNA. This is overcome by substituting the normal PNA bases with base analogues that contain bulky groups which prevent self-association (Lohse *et al* 1999).

PNA strand invasion complexes without triplex formation will be promoted under conditions where cytosine protonation is prevented thereby inhibiting binding of the Hoogsteen strand (figure 1.10 C & D). This will be achieved at low ionic strength facilitating strand invasion and high pH. Simple triplexes (figure 1.10 A) are more likely to form under conditions where cytosine protonation is promoted and strand invasion is inhibited (high ionic strength and low pH). However, triplex strand invasion complexes (figure 1.10B) require cytosine protonation for Hoogsteen

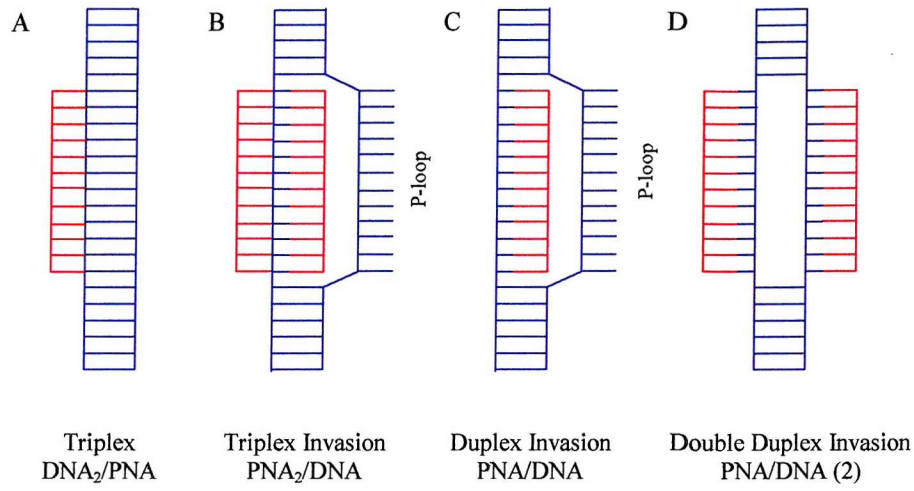

FIGURE 1.10 Binding motifs for amino ethyl PNA sequences to sequence specific complementary synthetic dsDNA sequences.

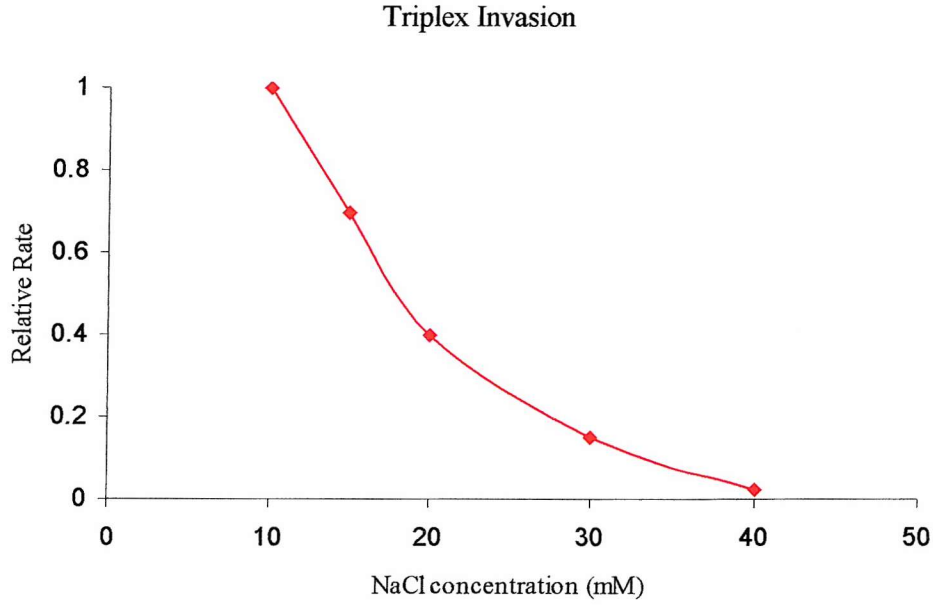

FIGURE 1.11 Ionic strength dependence of the formation of PNA triplex invasion complexes, modified from (Nielsen & Egholm 1999).

third strand binding (i.e. conditions of low pH) and low ionic strength to facilitate strand invasion. This type of complex is limited to homopurine tracts due to the involvement of third strand Hoogsten base pairing (Hyrup *et al* 1994). The rate of formation of strand invasion complexes is very slow and very sensitive to the presence of duplex stabilizing cations, such as magnesium (Mg^{2+}), spermine or spermidine and mono-cations (figure 1.11) (Hyrup & Nielsen 1996; Nielsen & Egholm 1999).

Although the mechanism of strand invasion is not clearly understood it is thought to require the opening of the helix through DNA 'breathing' (Bentin & Nielsen 1996). This would enable PNA to target the complementary sequence when the DNA is in the open state. Supercoiled and transcriptionally active DNA both have increased breathing rates, thus increasing PNA binding (Larsen & Nielsen 1996).

1.5.2.1 Bis-PNA

Triplex strand invasion complexes are very stable but their affinity specificity and stability can be improved by covalently linking the two PNA strands together in a single molecule, this is known as bis-PNA (Hansen *et al* 2001). The linkage is created via an ethylene glycol molecule from the Watson & Crick binding strand to the Hoogsteen strand. Targeting dsDNA with homopyrimidine containing bis-PNA sequences follows the same rules as triplex strand invasion, where one of the bis-PNA strands binds parallel to the purine strand of the duplex via Hoogsteen hydrogen bonding. The second strand invades the DNA duplex, binding in an antiparallel configuration forming Watson-Crick base pairs, forming a PNA_2/DNA triplex, displacing the non-targeted ssDNA forming a P-loop (figure 1.12). As well as increasing the affinity of these complexes, bis-PNA also removes any ambiguity

concerning the orientation of the PNA strands, which must now run antiparallel to each other.

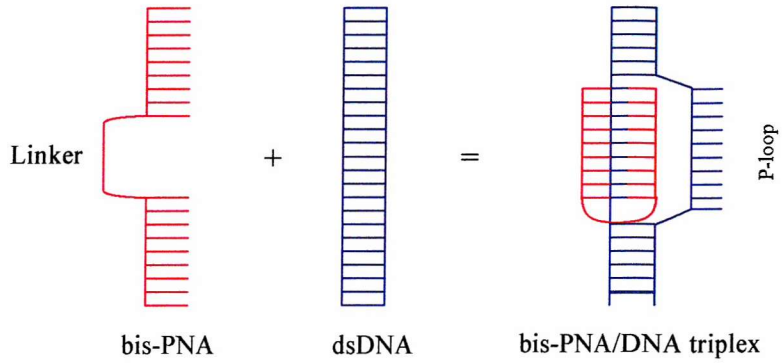

FIGURE 1.12 Binding motif for bis-PNA with sequence specific dsDNA.

1.5.3 PNA/PNA interactions

PNA has the ability to self anneal forming PNA duplexes or triplexes (Nielsen *et al* 1991). The structure of double stranded PNA has been solved by X-ray crystallography to a resolution of 1.7Å (Rasmussen *et al* 1997) while the triplex has been studied by circular dichroism using one adenine containing PNA decamer and two thymine containing decamers (Wittung *et al* 1997). Such a PNA triplex containing only T.AT triplets has been shown to form a right-handed helix. The corresponding CG.C or CG.C^+ triplets were tested, but only a duplex was formed indicating that this PNA YRY structure may not be stable.

1.5.4 Structural analysis of PNA complexes

The PNA-PNA duplex adopts a unique P-form structural configuration not seen in duplex DNA (figure 1.13 & table 1.2). The P-form helix is much wider (28Å) than the A or B-DNA or A-RNA (Rasmussen *et al* 1997) due to displacement of the Watson & Crick base pairs by 8.3Å from the helical axis. This generates a very wide central hole unique to the P-form helix. The base pairs are practically perpendicular to the helical axis, coplanar with very little tilt and prefer an A-form stacking conformation. The P-form helix has 18 base pairs per helical turn, which makes the pitch height more than double that of the B of A-form helices. A:T base pair overlaps are shown in figure 1.14, highlighting only minor variations in slide, tilt and propeller twist angles between individual base pairs and the remarkably close similarity between the P and A form helices.

Although there are important differences between PNA and DNA duplexes, when PNA targets DNA and RNA it forms different structures (figure 1.15). The pitch of a PNA/DNA duplex is 42Å (Eriksson & Nielsen 1996) which when compared to that of the PNA/PNA duplex (57.6Å) and the DNA/DNA duplex (35.4Å) it is more closely related to the B-form of DNA (Rasmussen *et al* 1997). This is due to PNA's ability to adopt the same or similar helical form as its target molecule. PNA forms an A-helix (in terms of sugar conformation) when associated in a PNA/RNA duplex (Brown *et al* 1994) (figure 1.15) and a B-helix when associated within a PNA/DNA duplex (Eriksson & Nielsen 1996) (figure 1.15). Interestingly, it can also be seen that the P-form helix is dominant in the PNA_2/DNA triplex structure (Betts *et al* 1995). Oligonucleotides lack this ability to adopt a helical conformation which is similar to its target molecule.

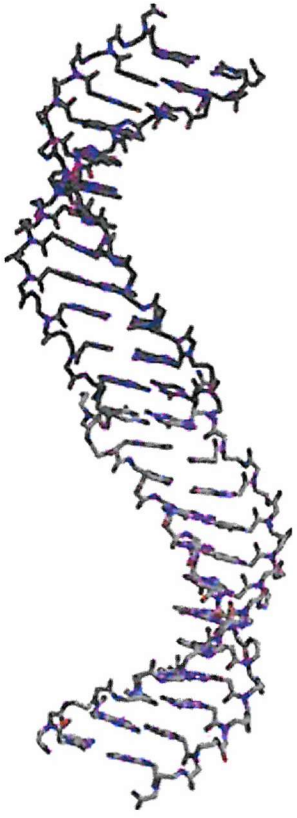

FIGURE 1.13 Graphical representation of a P-form PNA/PNA duplex (Rasmussen *et al* 1997).

	Helical forms		
	P	B	A
Helix diameter	28 Å	23.7Å	25.5 Å
Base pairs per helical turn	18	10.4	11
Rise per base pairs	3.2Å	3.4Å	2.3Å
Pitch per helical turn	57.6 Å	35.4Å	25.3 Å
Major groove	Wide and deep	11.6Å wide 8.5Å deep	2.2Å wide 13.0Å deep
Minor groove	Narrow and shallow	6.0Å wide 8.2Å deep	11.1Å wide 2.6Å deep

TABLE 1.2 Comparison of the different PNA helices

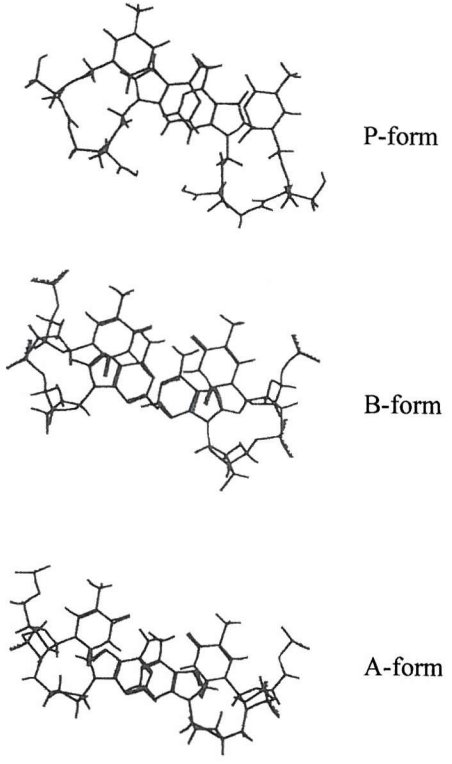

FIGURE 1.14 A:T base pair overlaps for the B, A and P-form helices (Nielsen & Haaima 1997).

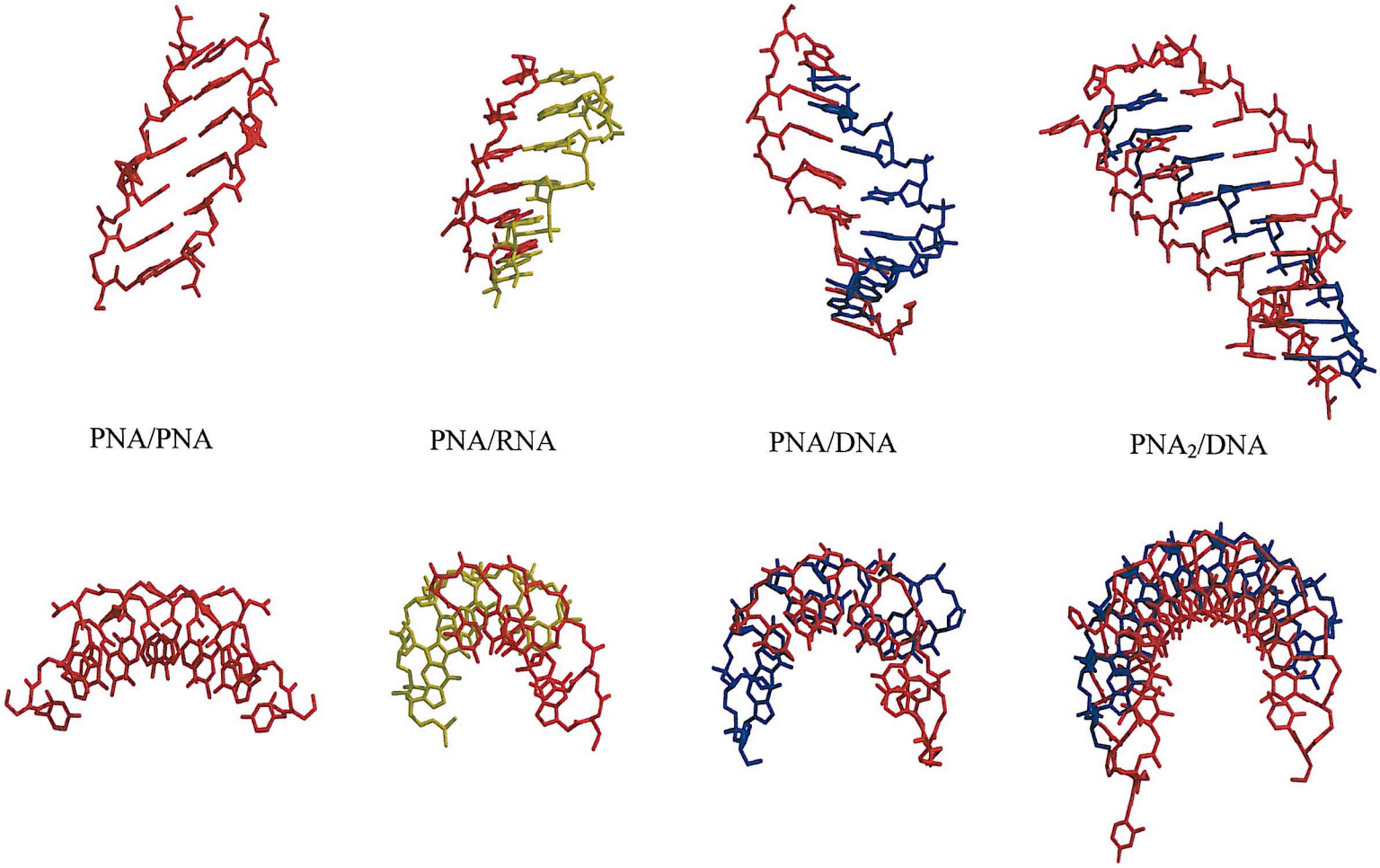

FIGURE 1.15 Molecular structure of various PNA containing duplexes and triplexes. Generated from the atomic coordinates 1pup (protein data bank (Berman *et al* 2000)) (PNA/PNA duplex), 176d (PNA/RNA duplex), 1pdt (PNA/DNA duplex) and 1pnn (PNA_2/DNA triplex). Prepared using Molscript (Kraulis 1991) and Raster3D (Merritt & Murphy 1994). PNA is shown in red, RNA is shown in yellow and DNA is shown in blue.

1.5.5 Biological applications of PNA

Genome sequencing has identified thousands of novel genes, highlighting the need for new approaches for controlling gene expression. Successful administration of potential gene controlling drugs requires good biostability, ability to cross biological membranes, sequence selectivity and solubility. The latter two have already been addressed, but what happens to PNA when it enters the cellular environment and is it able to cross the blood-brain barrier?

PNA oligomers have a high biostability in both human serum and cellular extracts (Demidov *et al* 1994) and are completely resistant to degradation by proteinase K and porcine mucosa peptidase. However, their cellular uptake through natural cellular absorption is very limited (Buchardt *et al* 1993).

Proteins, peptide and lipids have been used for the transportation of drugs into the eukaryotic cellular environment. Over the past few years a number of polycationic peptides which penetrate the cell have been identified, some of which have been shown to transport PNA oligomers into cells, in some cases crossing a number of different membranes. For example PNA-peptide conjugates have been injected into rat brains where they are transported into brain cells and affect gene expression (Aldrian-Herrada *et al* 1998). Also, the attachment of PNA to a lipid, forming a PNA-lipid complex, has been shown to successfully transport PNA across cellular membranes (Doyle *et al* 2001). PNA's specificity is length dependent but this also affects cellular uptake. Shorter PNA sequences when conjugated in a lipid complex are more readily taken up then longer sequences (Doyle *et al* 2001). Another method of cellular transportation is via the attachment to an antibody (Rusckowski *et al* 1997).

The blood-brain barrier has evolved to protect the brain against peripheral neurotransmitters, cytotoxins and microorganisms. This barrier is extremely difficult to cross in order to deliver potential drugs to the brain. Unmodified PNA sequences have been injected into rat brains where they successfully enter neuronal cells and inhibit protein synthesis in a gene specific manner (Tyler *et al* 1998). In fact, down regulation of the neurotensin receptor (NTR-1) and the mu receptor have already been observed using this technique. These results indicated that PNA could actively be taken up by neuronal cells, crossing the blood-brain barrier in a carrier free form and exerting a biological effect, a factor not previously seen with oligonucleotides.

A large variety of potential biomolecular and medical applications have been proposed for PNA, these include nucleic acid biosensors (Wang *et al* 1996), modulation of PCR analysis (Orum *et al* 1993), in situ hybridization (Lansdorp *et al* 1996), array hybridization (Weiler *et al* 1997), hybridization detection by mass spectrometry (Griffin *et al* 1997) and antisense and antigene drug technology (Hanvey *et al* 1992).

1.5.5.1 Antisense and antigene application of PNA

Within the past few years peptide nucleic acid antisense and antigene technology has entered into more detailed biological and preclinical studies. This is primarily due to the development of a number of novel methods for more efficient delivery of PNA oligomers into eukaryotic cells (Hanvey *et al* 1992). PNA is used in antisense and antigene techniques to control gene expression and cell growth (Good & Nielsen 1998). The antisense approach has shown that PNA targeted to mRNA can inhibit translation and potential cellular growth. The antigene approach has shown

that PNA targeted to dsDNA can inhibit gene transcription (Buchardt *et al* 1993). The most efficient PNA target for inhibiting specific genes, both *in vitro* and *in vivo,* is via triplex strand invasion to promoter regions of transcriptionally active genes (Nielsen *et al* 1994). The very slow annealing rate under moderate salt conditions has been overcome by placing the PNA target site and transcription binding site close together in transcriptionally active DNA (Larsen & Nielsen 1996).

Antisense PNA has also been studied as an antibacterial agent (Good & Nielsen 1998), using strains of *E.coli* cells that are permeable to PNA. One mutant showed total down regulation of β-galactosidase gene with increasing PNA concentrations when targeted to the initiator region of this gene. Further experiments examined the inhibition of bacterial growth by targeting ribosomal RNA. Bis-PNA sequences were used to target the homopurine tracts in the peptidyl transferase centre or in the α-sacrin loop (Hansen *et al* 2001). This inhibited translation at submicromolar concentrations in cell free systems and inhibited growth at micromolar concentrations. This has highlighted the potential for PNA to be developed into novel antibiotics.

Although a great deal of research has been undertaken on the strand invasion properties of PNA, less work has been carried out on the interaction with secondary structures such as quadruplexes, hairpins, cruciforms and chromatin. PNA has been targeted to quadruplex DNA, showing that a short PNA probe hybridizes to a folded DNA quadruplex (Datta & Armitage 2001). Short PNA probes have been found to disrupt folded quadruplexes forming hybrids that are stabilized by overhanging nucleotides on the DNA targeted strand.

1.6 Targeting histone bound DNA

The previous sections have shown that PNA can interact with DNA forming several types of complexes, though most of these studies have explored the interaction with free DNA. However, within the eukaryotic nucleus DNA is packaged in the form of chromatin, in which it is closely associated with a number of proteins, the first level of which involves superhelical coiling around the histone octamer. It is this environment where transcription occurs. The potential ability to target specific DNA regions with PNA whilst they are associated with histone proteins is unknown. We could imagine that association with the histone octamer could prevent binding to some target sites whilst enhancing binding to others. The work described in this thesis involves the interaction of PNA with a number of target sites on histone bound DNA, to study whether the histone octamer affects the potential PNA binding sites. However, we will first look at the properties of histone bound DNA.

1.6.1 Nucleosome core particle

The nucleosome core particle is a 205KDa protein-DNA complex, which consists of two copies of each of the core histones H2A, H2B, H3 and H4, known as the histone octamer (figure 1.16). 146 base pairs of dsDNA are wrapped around the outer region of the histone octamer forming a 1.65 left handed superhelical turn. This is the repeating unit along the chromatin fibre (figure 1.17) in which the nucleosomes are arranged as beads on a string. Located between each nucleosome core particle is a specific region of DNA known as the linker DNA, that associates with histone protein H1, promoting higher-order structures of chromatin (Harp *et al* 2000). The linker

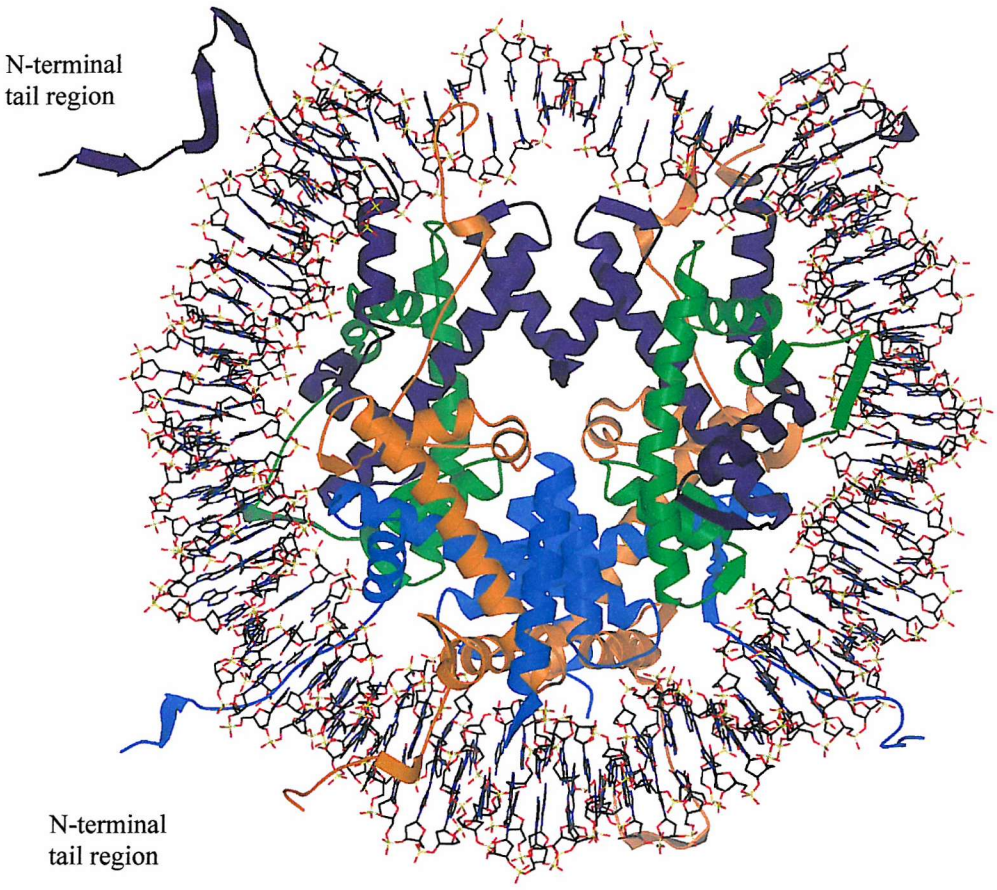

FIGURE 1.16 Three-dimensional structure of the nucleosome core particle. Generated from the atomic coordinates 1eqz (protein data bank) prepared using Molscript, GL Render (Esser 2001), and Raster3D. The histone tails can be clearly seen to protrude out the core particle. The secondary structure of the core particle is represented as arrows (β-strands), ribbons (α-helices) and cords (loops) and the DNA presented by stick models (see appendix). H2A is orange, H2B is blue, H3 is purple and H4 is green.

FIGURE 1.17 A section of the chromatin fibre. (A) A model of beads-on-a-string chromatin with a linker length of 20 nucleotide pairs (Wolffe 1995) (B) Chicken erythrocyte fibers imaged in air and low ionic strength buffer and (C) also illustrates chicken erythrocytes imaged in buffer (Leuba & Bustamante 1999).

length is variable for different species and for different cell types but generally ranges from zero to approximately 80 to 100 base pairs (Bednar *et al* 1998). Specific regions of DNA within the nucleosome core particle are protected from enzymatic attack by the histone octamer, whereas the linker regions are highly sensitive to chemical and enzymatic attack, as they are not shielded by the histone proteins.

1.6.2 Histone octamer proteins

The growth of larger crystals, availability of synchrotron radiation and computer technology has led to the successful structural determination of the nucleosome core particle and its components. The main defining X-ray structure was published in 1997 to a resolution of 2.8Å (Luger *et al* 1997). This was followed in 2000 to a resolution of 2.5Å resolution, enabling a more detailed study of the internal interactions to be examined (Harp *et al* 2000) (figure 1.16).

The five histone proteins, H1, H2A, H2B, H3 and H4, each contain two domains known as the histone fold and the N-terminal tail (figure 1.18A). The octamer proteins H2A, H2B, H3 and H4 (see appendix) are basic proteins with relatively low molecular weight and have a very high arginine and lysine content (table 1.3). The histone fold has a unique structure, which consists of three alpha helices in the shape of a shallow 'U' (figure 1.18B). The shorter helices are folded back on themselves and rotated over the longer central helix. Between each of the three helices lies a loop region, which is connected to the C-terminal and the N-terminal of the structure. Each histone protein forms this histone fold motif and it is these motifs that bind to each other to form heterodimers H2A-H2B and H3-H4 and heterotetramers $(H3\text{-}H4)_2$.

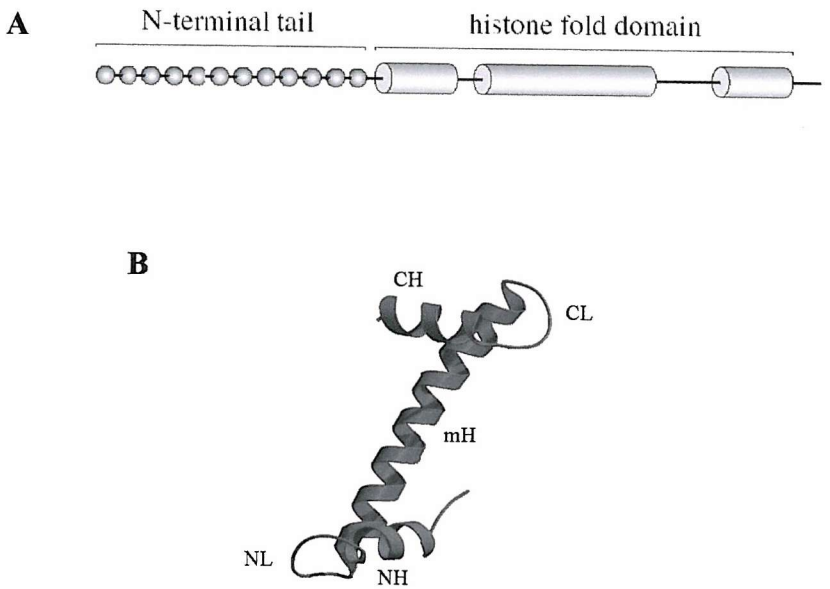

FIGURE 1.18 The structure of the histone protein motif (A) the histone fold domain formed by three α-helices (cylinders) and N-terminal tail region (beads), (B) Histone fold motif, long helix (mH), C-terminal helix (CH) and loop (CL), N-terminal helix (NH) and loop (NL). Generated from the atomic coordinated 1eqz (protein data bank) prepared using Molscript and Raster3D.

Histone protein	Molecular weight (Da)	Amino Acids	Basic amino acids proportion
H1	17,000-28,000	200-265	27% lysine, 2% arginine
H2A	13,900	129-155	11% lysine, 9% arginine
H2B	13,800	121-155	16% lysine, 6% arginine
H3	15,300	135	10% lysine, 15% arginine
H4	11,300	102	11% lysine, 4% arginine

TABLE 1.3 Statistical data for each of the five histone proteins

The N-terminal tail domain represents 30% of the overall amino acid sequence and has a poorly defined structure (Harp *et al* 2000). These are structurally important in nucleosome formation and in modulating the stability of nucleosome and the formation of the chromatin fiber. The N-terminal tail domains are highly positively charged and are the sites of posttranslational modifications such as lysine acetylation and serine phosphorylation (Hansen *et al* 1998). These modifications and removal of the tail regions reduces the positive charge and thereby 'loosens' the association between the protein and the DNA affecting the organization of chromatin (Hansen *et al* 1998).

The histone octamer consists of a tetramer of histones $(H3/H4)_2$ together with two dimers of histones H2A-H2B (Widlund *et al* 2000) (figure 1.19A). The octamer assembly is thought to be a two-step process where by the $(H3\text{-}H4)_2$ tetramer is assembled prior to the association of the H2A-H2B dimers (Worcel *et al* 1978). The two H3-H4 pairs interact through a four-helix bundle formed from the two H3 histone folds to define the H3-H4 tetramer. Each H2A-H2B pair interacts with this tetramer through a second homologous four-helix bundle between H2B and H4 histone folds. The helical motifs are associated through hydrophobic interactions between the helices and by a short β-bridge structure formed between the C-terminal loop of H2A and the N-terminal loop of H2B in the H2A-H2B heterodimers and between the C-terminal loop of H3 and N-terminal loop of H4 in the H3-H4 heterodimers. The histone octamer can be divided into two halves across the dyad axis (figure 1.19B), each half containing one copy of each histone protein. The two halves are symmetric but interact differently with one side having greater order in the histone tail regions than the other.

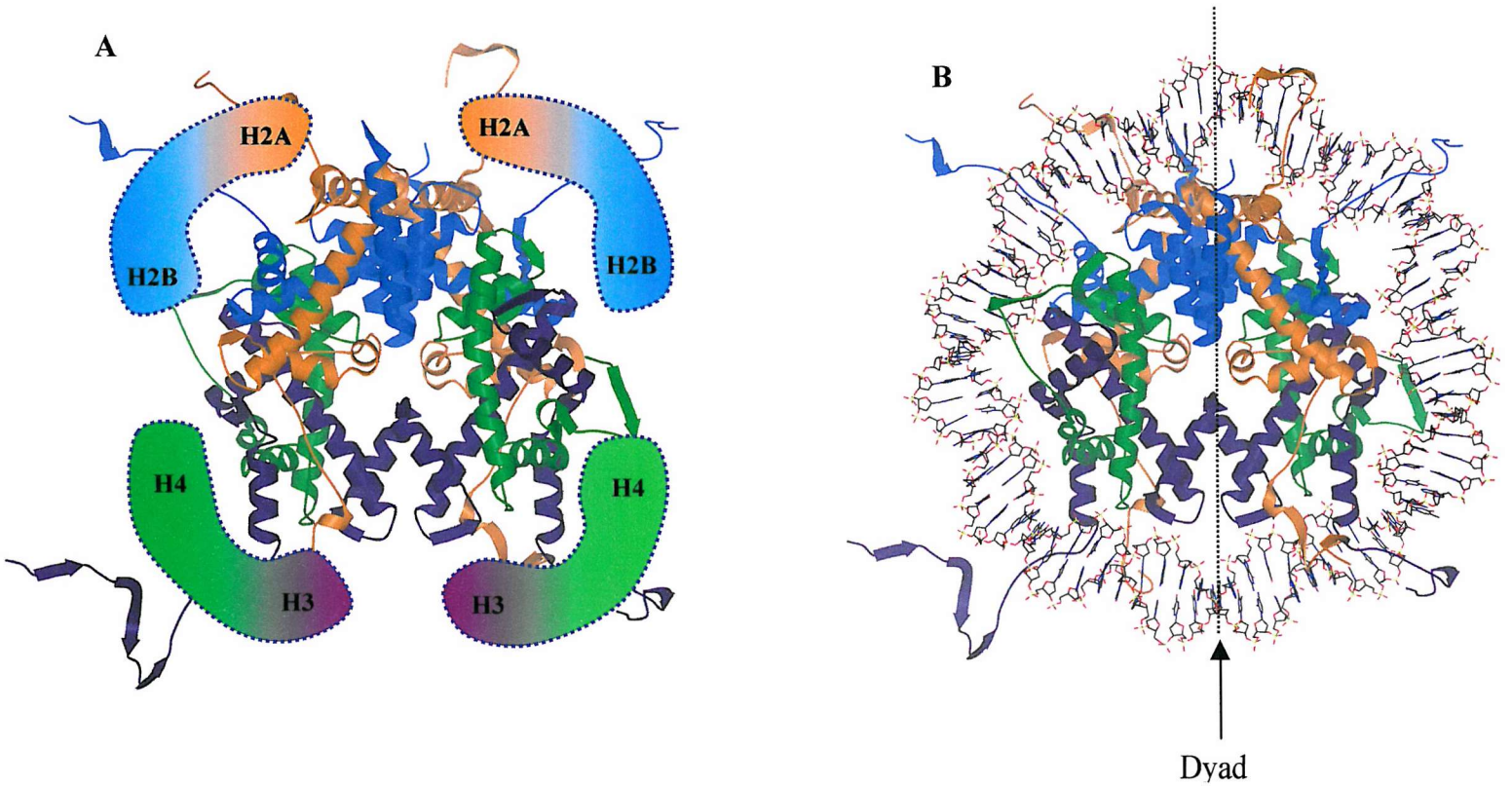

FIGURE 1.19 Three-dimensional structure of the histone octamer (A) and the nucleosome core particle illustrating the dyad axis (B). Generated from the atomic coordinates 1eqz (protein data bank) prepared using Molscript, GL Render, and Raster3D. The secondary structure of the core particle is represented as arrows (β-strands), ribbons (α-helices) and cords (loops). H2A is orange, H2B is blue, H3 is purple and H4 is green. The DNA here is represented as only a 80bp stick model.

1.7 Histone-DNA interactions

The 146 base pairs of dsDNA are wrapped around the outer surface region of the histone octamer to form a left handed 1.65 turn superhelical structure, making specific contacts with the protein surface. The structure of the nucleosome is such that the positively charged lysine and arginine residues are located adjacent to the negatively charged DNA backbone (Arents *et al* 1991). The main chain and protruding histone tails of the basic octameric histones form hydrogen bonds and ionic contacts with the negatively charged phosphodiester backbone of DNA (Luger *et al* 1997). In addition to this, 14 arginine residues are inserted into the minor grooves which face towards the protein surface (figure 1.20). When one phosphate contacts an arginine at the minor groove site, the next phosphate is one and half helical turns away and located on the other strand. This observation has led to the conclusion that as the DNA wraps around the histone octamer the minor groove is pinched and the major groove opened. Chloride ions and water molecules, including several water clusters of up to nine hydrogen-bonded groups, collect around channels to the interior of the octamer from its surface, indicating that water strengthens the cross-bridges of the helical tract (Luger *et al* 1997).

The DNA sequence associated with the histone octamer has a defined symmetry. The dyad region intersects at DNA base 73, placing 72bp of DNA on either side of the protein face (Harp *et al* 2000). The helical repeat of the bound sequence (146bp) is approximately 10.2-10.3bp, but this varies from 10.7bp in the central turns to 10bp at the flanking regions on the nucleosome core particle (Luger *et al* 1997). The helical repeat near or at the dyad axis is therefore more tightly compacted in relation to the peripheral regions.

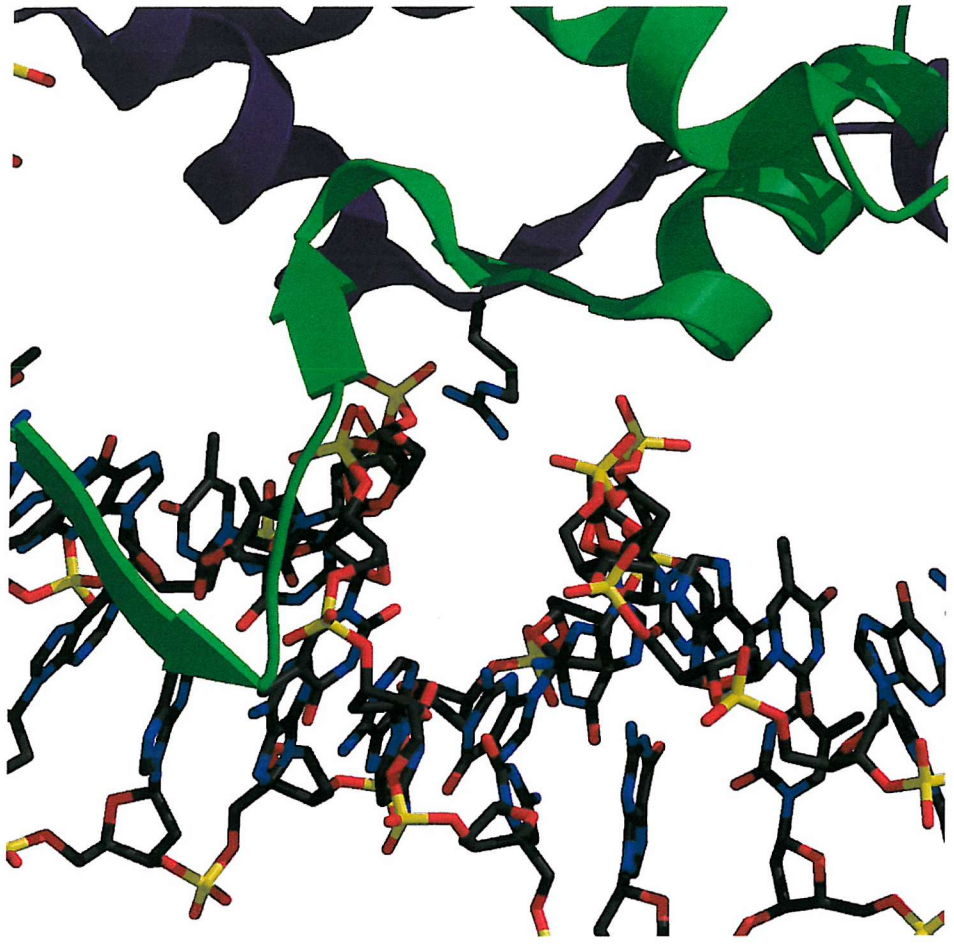

FIGURE 1.20 Three-dimensional structure of H3 (purple) and H4 (green) interaction with the DNA helix, illustrating the insertion of arginine (Arg63) from H3 into the minor groove of the DNA backbone. Generated from the atomic coordinates 1eqz (protein data bank) prepared using Molscript and Raster3D. The secondary structure and the DNA structure is represented as previously described.

The organization of DNA in relation to the protein is essential for transcription and replication and for the efficient compaction of genetic material in the eukaryotic nucleus. Although most DNA sequences must be able to wrap around the histone octamer, some sequences associate into nucleosomes more easily than others. This is a result of sequence-dependent intrinsic properties of DNA such as flexibility (Rhodes 1979) and anisotropic bendability (Drew & Travers 1985) and the interaction is not solely sequence specific. PolydAT wraps around the protein more readily than conformational rigid sequences such as polydA.polydT (Hayes *et al* 1991). Nucleosome reconstitution is more successful with DNA sequences that have a high degree of curvature (Costanzo *et al* 1990). The bending of these curved sequences requires less energy to wrap around the histone octamer and intrinsically curved DNA molecules have been shown to form more stable nucleosomes than non-curved molecules. However, once wrapped around the protein all DNA sequences are constrained to adopt a very similar conformation (Hayes *et al* 1991).

DNA sequences dictate the positioning of DNA around the nucleosome and early studies showed that on average AA/TT dinucleotides in natural DNA sequences are separated by roughly 10bp (Satchwell & Travers 1989) and are positioned so that their minor grooves face towards the protein surface. This was thought to be one of the nucleosome positioning signals and led to further studies using A/T and G/C fragments which formed very stable nucleosome DNA complexes (Shrader & Crothers 1989). Recently fragments having repeated TATAAACGCC motifs, referred to as TATA tetrads, have been shown to form the most stable nucleosome complexes (Widlund *et al* 1997). DNA sequences that have a low affinity for histone octamers are also of great significance since they form nucleosome-free regions such as the linker regions. Nucleosome-free regions are found along the

chromatin fibre, and include deoxyribonuclease I (DNaseI) hypersensitive sites that are associated with high transcriptional activity (Wolffe 1995).

1.7.1 Nucleosome positioning

The arrangement of nucleosomes along a DNA sequence will affect its accessibility and hence play a role in transcription regulation and DNA repair. Nucleosome positioning is defined in terms of rotational and translational positioning of the DNA (figure 1.21). Rotational positioning relates to the orientation of the DNA in relation to the protein surface, while the translational positioning relates to the exact position of the histone octamer along the DNA. Since nucleosomal organization requires bending of the DNA molecule, one might expect that certain sequences or sequence features will prevail in nucleosomes. PolydAT and AAT/ATT DNA sequences have been shown to affect the rotational positioning, so that the narrow minor grooves of these sequences face towards the protein surface. Sequences such as GGC/GCC and ACG/CGT face in the opposite orientation (Drew & Travers 1985).

The alignment of nucleosomes along a DNA fragment i.e. the translational position is known as nucleosome phasing. This will be determined by the way in which the DNA associates with the protein complex, and whether this occurs in a random or specific fashion. Nucleosome phasing could be determined by either the intrinsic and extrinsic properties of DNA. Intrinsic mechanisms suggest that each nucleosome recognizes a distinct segment of DNA and binds to it leading to a phasing pattern determined by the binding of each individual DNA segment (figure 1.22A). In contrast, in extrinsic mechanisms the position of one nucleosome is fixed in some way and the neighboring nucleosomes are then arranged in such a way as to maximize

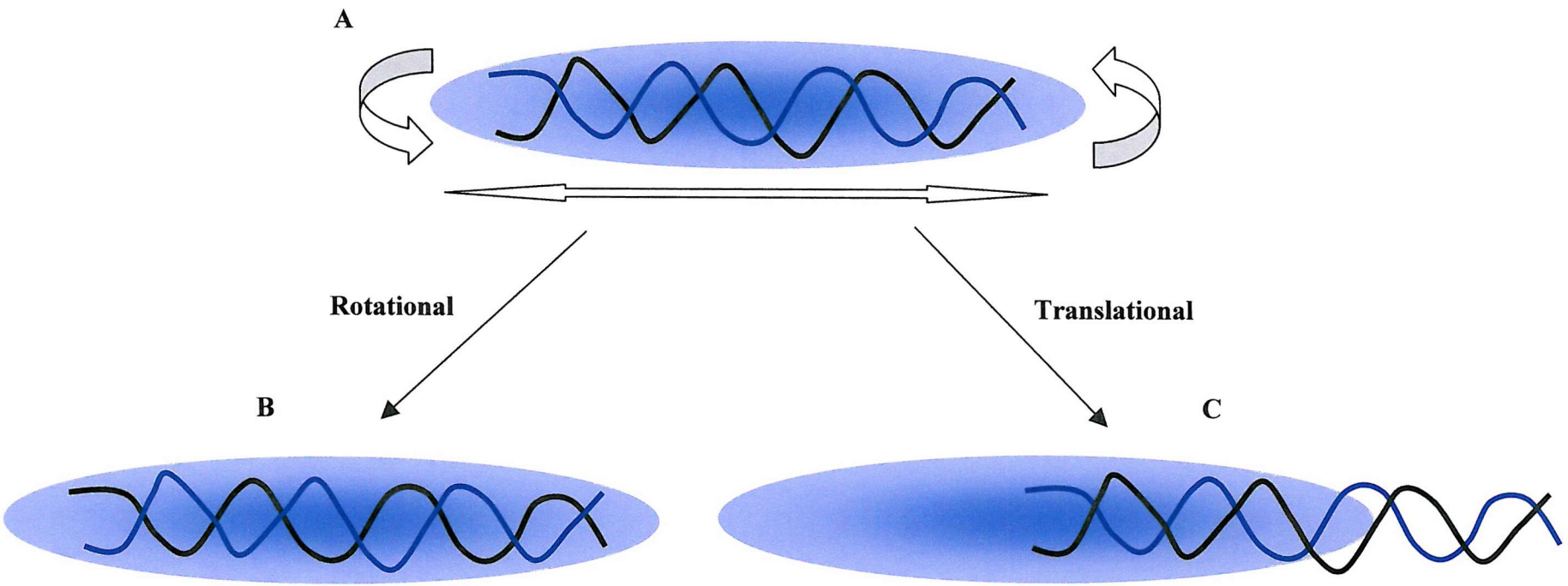

FIGURE 1.21 A graphical representation of the two mechanisms involved in nucleosome positioning. (A) Illustrating the possible mechanisms, (B) illustrating the rotational shift on the DNA helix and (C) illustrating the translational shift of the DNA in relation to the nucleosome. The light blue oval shape represents the histone octamer.

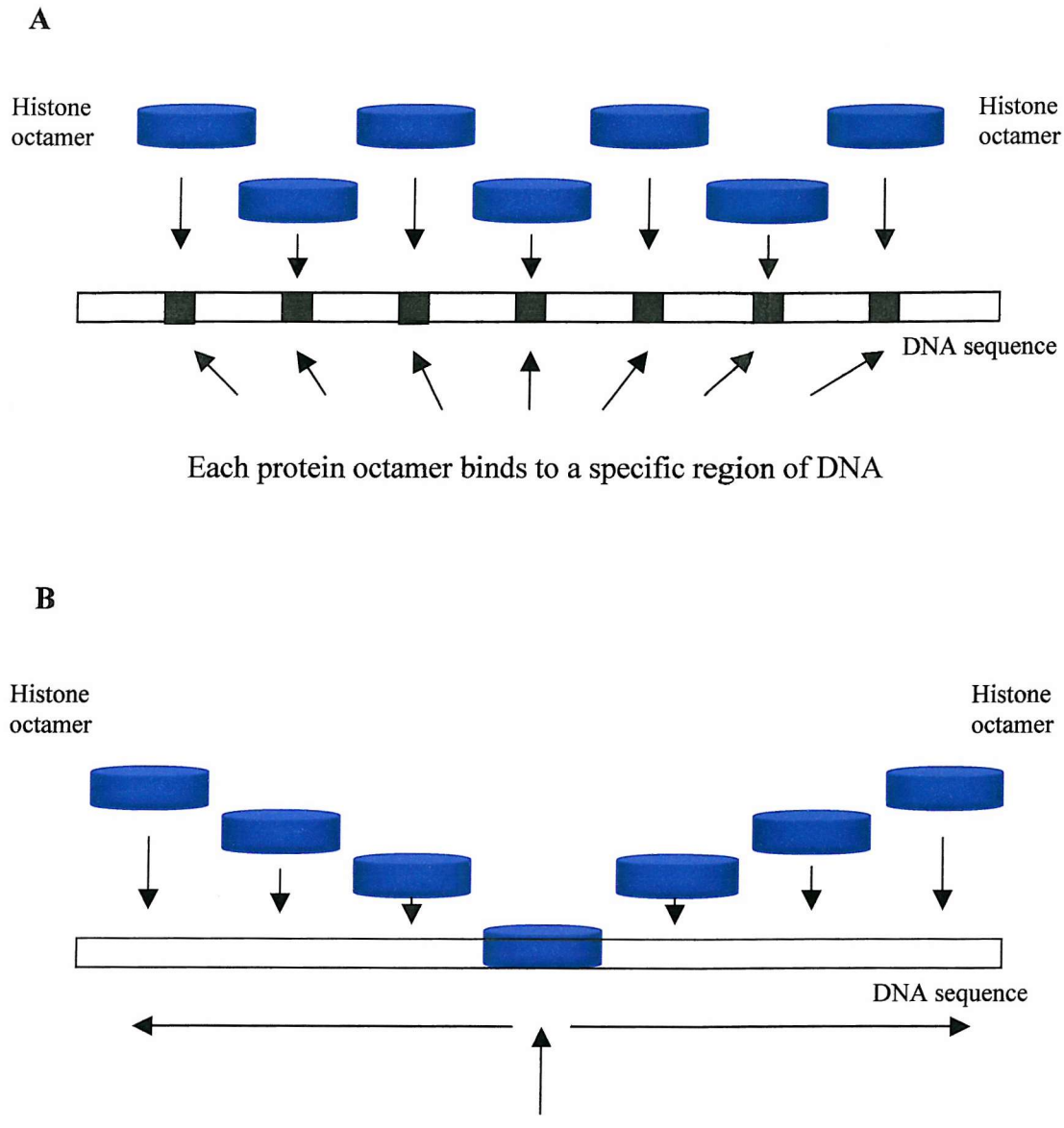

FIGURE 1.22 Illustration of nucleosome phasing. (A) Intrinsic principle for nucleosome phasing, (B) extrinsic principle for nucleosome phasing. The blue oval shape represents the histone octamer.

binding and packaging (figure 1.22B). It is thought that phasing occurs due to intrinsic rather than extrinsic mechanisms but this has not been fully proven and is very controversial in the literature (Widlund *et al* 1997). However, initiation of binding is also thought to be due to the local base composition which influences DNA structure or frequent events such as DNA replication initiation sites or transcribed genes. This could then create a cascade of protein binding downstream from the initiation site creating an equally phased chromatin fibre (Blank & Becker 1996).

1.7.2 Transcription, acetylation and chromatin remodelling

Nucleosomes must be unpackaged then repackaged during DNA replication and transcription. As the RNA polymerase advances along DNA it displaces the DNA from the nucleosome core particle forming a closed loop region. The torsion generated ahead of the RNA polymerase causes supercoiling of the DNA. This displaces the histone octamer, but keeps in contact with the DNA behind the RNA polymerase, so that each nucleosome does not totally lose contact with the DNA (Lee *et al* 1993). This can lead to the nucleosome phasing being disrupted around the genes after transcription is induced. Transcription can occur anywhere along DNA even in nucleosome bound regions. If the promoter is accessible to RNA polymerase and transcription factors, the presence of nucleosomes will not inhibit the elongation by the polymerase. It has been proposed that this packaging of DNA into chromatin may control the accessibility of genes to the binding of transcription factors.

Histone acetylation and deacetylation occurs within the chromatin fibre and is catalyzed by either histone acetyltransferases (HATs) or histone deacetylases (HDACs) respectively (Lee *et al* 1993). Acetylation of lysine residues at the N-

terminus of the histone proteins removes the positive charge, therefore reducing the affinity between the histone octamer and the DNA as shown in figure 1.23. This increases the accessibility of RNA polymerase and transcription factors to the promoter regions. Acetylation increases transcription whereas deacetylation represses transcription. A number of different histone acetyltransferases and deacetylases have been identified, one of the most proliferent one being CBP/p300, which interacts with numerous transcription regulators.

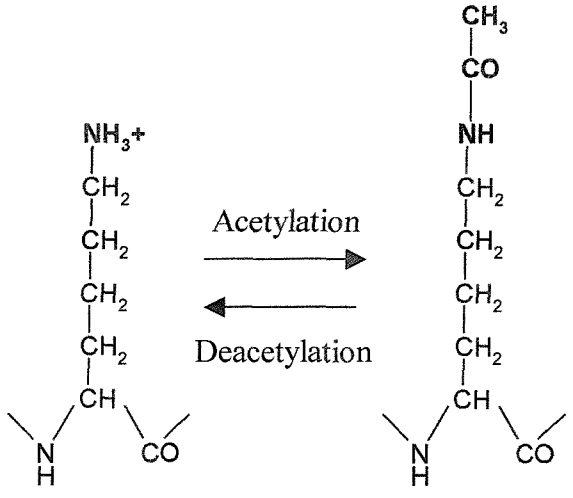

FIGURE 1.23 Acetylation and deacetylation of a lysine residue.

The organization of DNA in chromatin is not only involved with compaction but also with the regulation of gene expression (Demeret *et al* 2001). Chromatin constitutes a barrier against transcription, replication and repair, and the organization of DNA influences these genetic processes. A mechanism is therefore required that can open up the chromatin and make it more assessable. This is carried out through chromatin remodeling complexes, which are defined by their capacity to

modify the positioning of nucleosome *in vitro* and represent a major regulatory factor of gene expression (Demeret *et al* 2001). It is known that the packing of DNA into chromatin represses DNA replication so it is believed that chromatin remodeling is involved in the initiation of DNA replication (Meyer 2001). Alteration of chromatin structure has also been found to be an important factor in regulating gene expression. The initiation of DNA replication in relation to chromatin structure is poorly researched, but it is known that this results in the rearrangement of the chromatin fibre (Demeret *et al* 2001). However these chromatin remodeling complexes have only been shown to have a direct involvement in regulation processes *in vivo* in a limited number of cases.

1.8 Ligand interactions with nucleosomal DNA

The targeting of nucleosomal DNA is partially dependent upon the close association and interactions that occur between the DNA and the histone proteins. Sequence specific ligands that bind to specific DNA regions that face towards the protein surface could be sterically restricted, whereas targeting of the DNA that faces away from the protein could alter the ligand binding motif due to DNA distortion. In particular, intercalating agents such as actinomycin wedge themselves between adjacent bases along the DNA, distorting and lengthening its structure preventing polymerases and other DNA binding proteins from functioning properly. This can result in the prevention of DNA synthesis, inhibition of transcription and induction of mutations.

To date only a few studies have been carried out into the interaction of sequence specific drugs with nucleosome bound DNA. Early footprinting studies on

natural DNA restriction fragments, where the binding sites faced towards and away from the protein core, with the AT-selective minor groove binding ligands Hoechst 33258 (2′-(4-hydroxyphenyl)-5-(4-methyl-1-piperazinyl)-2,5′-bi-benzimidazole) and echinomycin indicated that at low concentrations these ligands changed the rotational positioning of the nucleosome bound DNA fragments (Low *et al* 1986; Portugal & Waring 1987). Mithramycin showed clear footprints at specific sites with nucleosomal DNA where the location of these binding sites was modified by interactions with the protein (Fox & Cons 1993). Actinomycin was only shown to bind accessible sites at low concentrations but displaced the DNA from the protein surface at higher concentrations (Portugal & Waring 1986). Synthetic DNA fragments have also been studied, one of which contains $(A/T)_4$ sites located every 10 base pairs which faced towards the protein core and showed that minor groove binding ligands also changed the rotational positioning of the DNA (Brown & Fox 1996). Studies with echinomycin and Hoechst 33258 with single and multiple binding sites show similar results (Leslie & Fox 2002). Further studies have shown that minor groove binding ligands selectively inhibit the assembly of curved DNA molecules onto the histone octamer and destabilise the nucleosome core particle (FitzGerald & Anderson 1999). More recent studies have shown that pyrrole-imidazole polyamides can bind sites facing away from the protein surface without disrupting the nucleosome core particle and have indicated that nucleosomal DNA is assessible to minor groove binding ligands (Gottesfeld *et al* 2001). Intermolecular DNA triplexes have also been formed on target sites located within the peripheral regions of the nucleosome core particle but not within 30 base pairs of the dyad axis. Increased fragment lengths have altered nucleosomal arrangements such as the translational positioning and acts as a nucleosomal barrier (Westin *et al* 1995).

1.9 DNA footprinting

One of the main techniques used in this work to study the interaction of PNA with both free and nucleosome bound DNA is 'footprinting'. Footprinting is a technique designed to study the sequence specific binding of proteins to DNA (Galas & Schmitz 1978), but was later used to detect and analyse drug DNA interactions. The basis behind this technique is the prevention of DNA cleavage by enzymes or chemical agents at the regions to which ligands are specifically bound. One strand of the DNA duplex is radioactively labelled at either the 3′ or the 5′ end. This is achieved by the incorporation of phosphorus-32 (^{32}P). Limited digestion of the DNA by an enzymatic or chemical cleavage agents results in the protection from cleavage over the binding site. The digestions conditions are such that on average each DNA molecule only cuts once i.e. single-hit kinetics. The products of digestion are then separated on the basis of size on a denaturing polyacrylamide gel. This generates a ladder of DNA bands with the protected binding site indicated by the absence of bands (figure 1.24). DNaseI footprinting can also be used to study histone bound DNA, generating a phased ladder of bands due to protection of cleavage of the DNA at regions which face towards the protein surface (figure 1.25).

Footprinting can also be used to measure ligand affinity in quantitative footprinting studies. Various concentrations of the ligand under investigation are examined, producing maximal protection at high concentrations and less protection at lower concentrations. Intermediate regions show a gradual decrease in band intensity. The concentration dependence of the cleavage pattern can be used to determine the affinity of the ligand for its target site, so long as the target DNA concentration is lower than the dissociation constant of the ligand. Analysis of the bands intensity

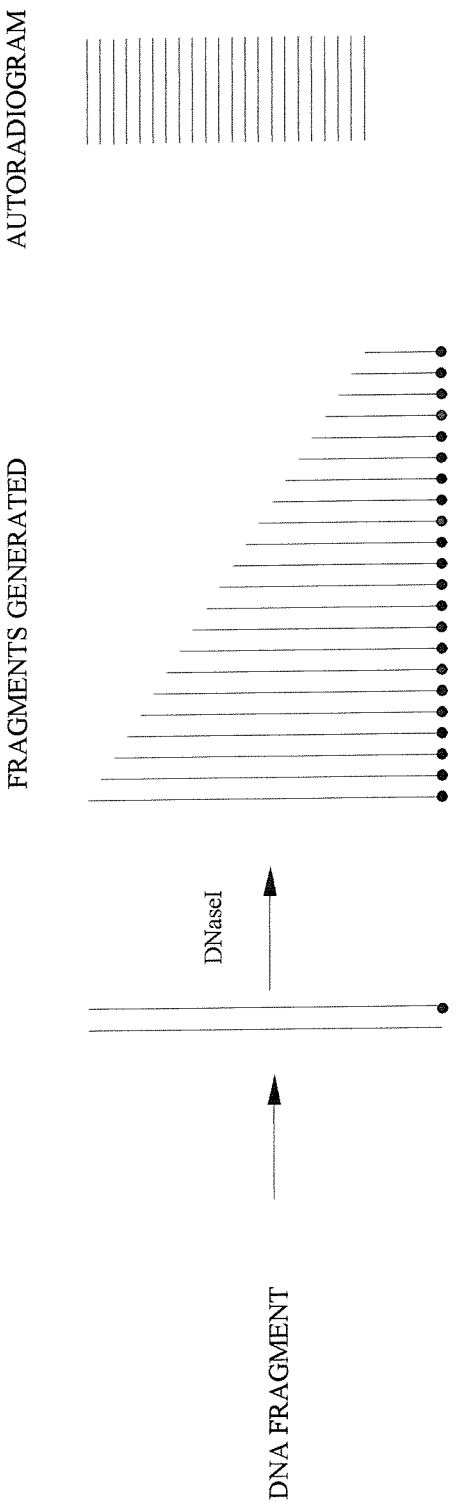

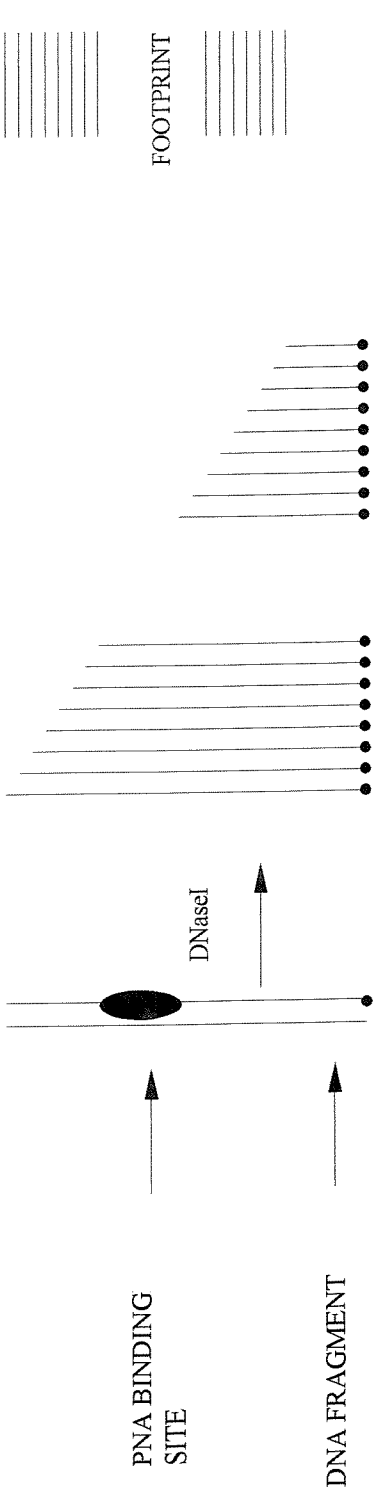

FIGURE 1.24 Illustration of DNaseI footprinting.

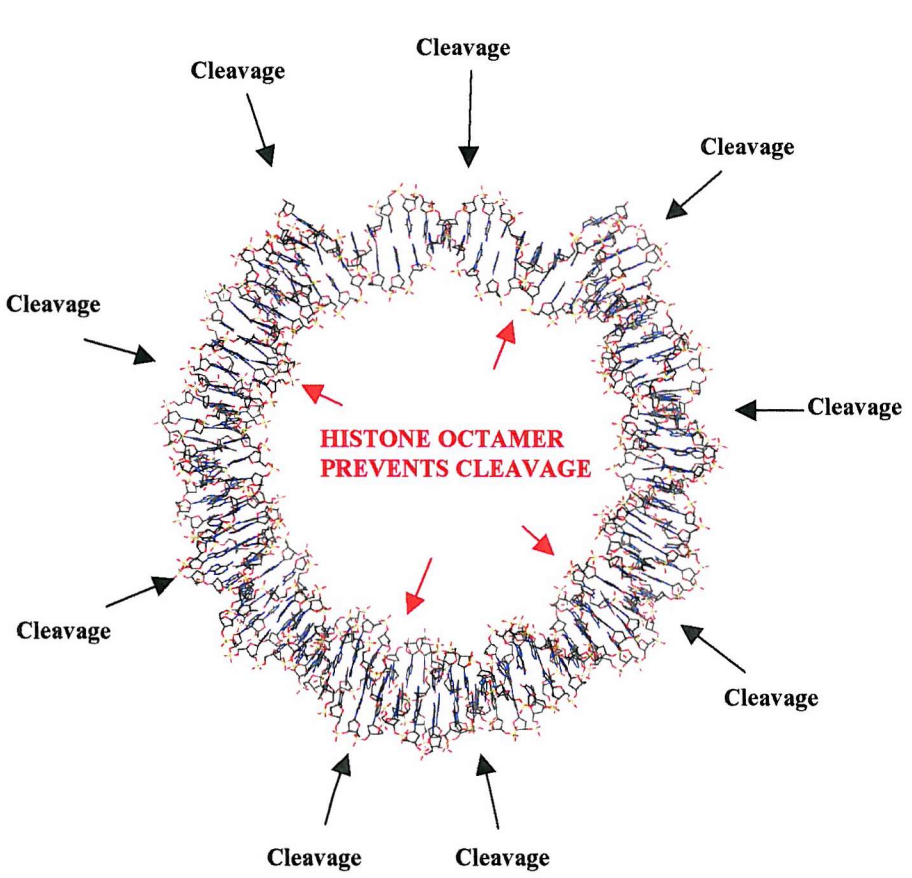

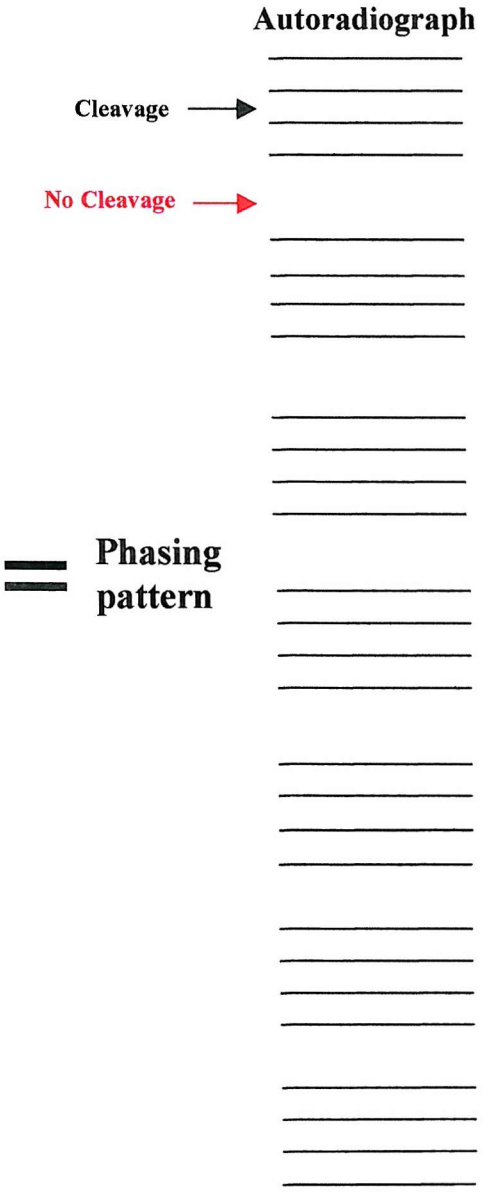

FIGURE 1.25 Illustration of the potential enzymatic and chemical cleavage mechanism when the DNA fragment is associated with the histone octamer. Highlighting the areas along the DNA fragment that can or cannot be cleaved.

allows the calculation of the ligand concentration required to achieve 50% protection of the duplex target (C_{50}).

1.9.1 DNaseI footprinting

The bovine pancreatic glycoprotein DNaseI (figure 1.26A) was used in these footprinting studies (Galas & Schmitz 1978). This enzyme requires calcium, manganese or magnesium ions for activity. DNaseI acts by inserting an exposed loop into the minor groove of DNA (Suck *et al* 1988). Acid base catalysis then occurs using amino acids E75 and H131, this results in nucleophilic attack of a water molecule causing hydrolysis of the O3′-P bond (figure 1.26B). Although DNaseI cuts most sequences it generates an uneven ladder of cleavage products (Bernardi *et al* 1973). Both AT-rich and G-rich sequences are known to be poor substrates (Drew & Travers 1985). This limitation is not directly related to the sequence composition itself but to variations in the local DNA structure. Sequences with narrow minor grooves exhibit lower cleavage by DNaseI as the enzyme cannot bind this groove (Drew & Travers 1985). The X-ray crystal structure of DNaseI bound to a short oligonucleotide revealed that the DNA was bent away from the enzyme towards the major groove (Suck *et al* 1988). It is thought that this bending may be an essential part of the cleavage mechanism and explains why less flexible sequences such as polydGC are be poorly cleaved.

DNaseI footprinting usually overestimates the size of the ligand binding site. This is due to the size of DNaseI (30.4KDa) which covers a region of 10bps and thus overestimates the footprint site by 2-3bps. DNaseI binds across the minor groove, interacting with the phosphates from the opposing strands. Since the closest

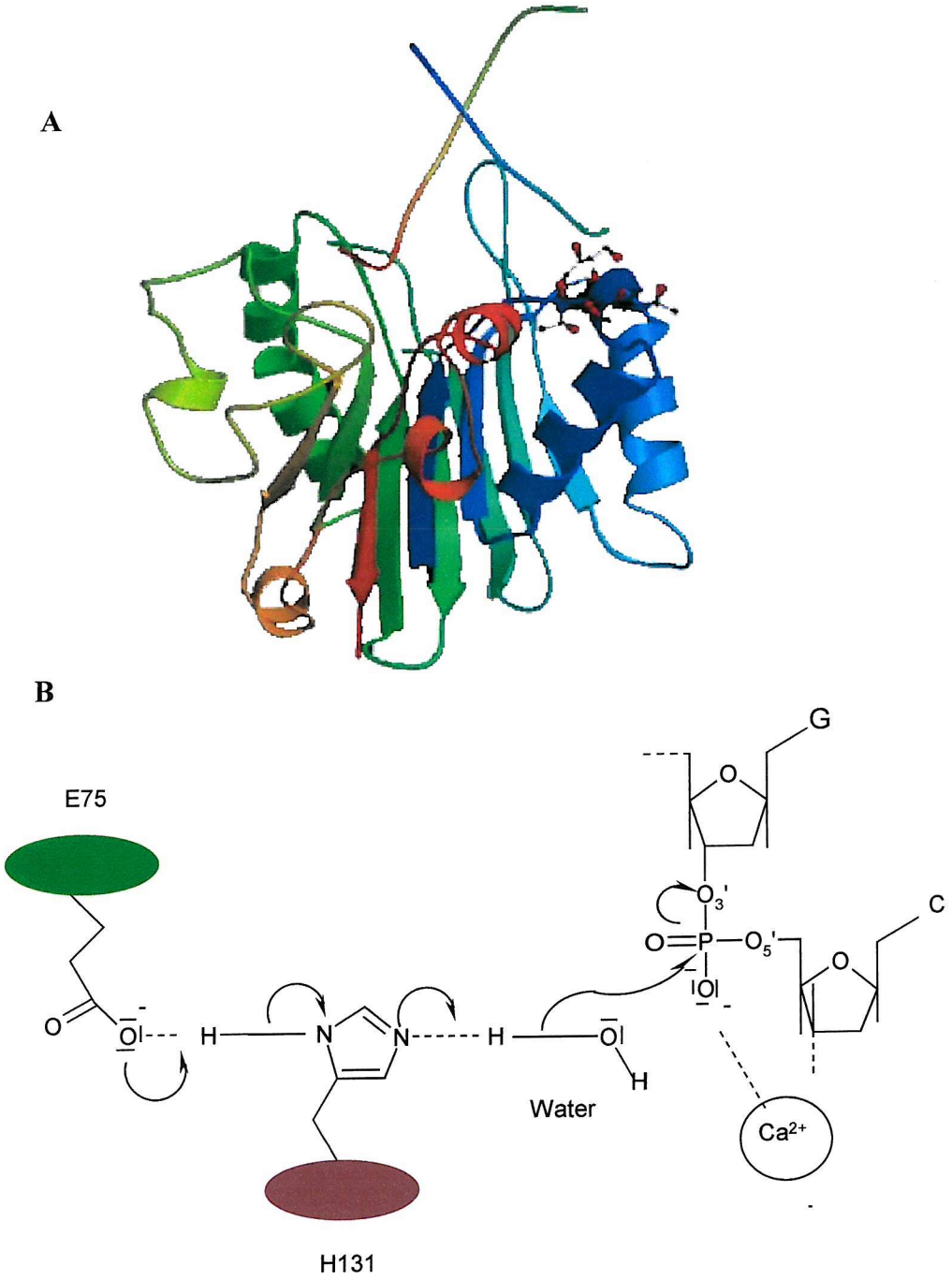

FIGURE 1.26 DNaseI structure and mechanism. (A) Crystal structure of DNaseI, (B) Proposed mechanism of action of DNaseI (E75 and H131 are sections of the protein).

phosphates across the minor groove are not attached to a base pair, but are staggered by 2-3bps, footprints are usually staggered by 2-3bps in the 3′ direction. Ligand binding in the major groove, such as in triplex formation, also produces DNaseI footprints. This must occur as a result of alterations in DNA structure and or rigidity rather than by direct steric blockage.

1.9.2 Other DNA footprinting techniques

Two additional DNA footprinting probes have been used in this work; these are micrococcal nuclease and S1 nuclease cleavage.

Micrococcal nuclease can be used as a probe for DNA-drug binding (Fox & Waring 1987). Micrococcal nuclease cuts almost exclusively at polyA/polyT bonds, cleaving the O5′-P bond. All such bonds are not equally susceptible to cleavage and alternating A-T tracts are better substrates than polydA/polydT. The crystal structure of the enzyme shows that it posses a cleft which can bind a single-stranded DNA substrate, thereby explaining the specificity for AT sequences since these are easier to denature.

S1 nuclease is a glycoprotein isolated from a crude preparation of *Aspergillus oryzae* amylase. S1 nuclease specifically hydrolyzes both terminal and internal phosphodiester bonds of single-stranded DNA and RNA. S1 nuclease can be used to remove 5′ and 3′ overhanging ssDNA and hairpin loops in DNA-RNA or DNA-DNA duplexes and in hybridization studies and genetic recombination experiments (St John *et al* 1974). In this study, S1 nuclease has been used to degrade internal single stranded loop regions.

1.10 Objectives

The work described in this thesis examines the interaction of PNA with both free and nucleosome bound DNA, using footprinting techniques. The interaction of PNA with DNA has been analyzed under conditions that promote either triplex formation or strand invasion on both free and histone bound DNA. Various target sites have been studied on different length DNA fragments. These interactions are analyzed by a number of techniques including DNaseI footprinting, gel retardation bandshift assays, micrococcal nuclease cleavage, S1 nuclease cleavage and fluorescence melting studies. The effect of the histone tail domains on PNA targeting is also examined. This study highlights the importance of the position of PNA target sites for influencing the interaction with histone bound DNA.

Chapter 2

Materials and Methods

2.1 Materials

2.1.1 General reagents

All were purchased from Sigma-Aldrich unless otherwise stated. Redivue radioactive α-[^{32}P] 2'-deoxy-adenosine-5'-triphosphate (dATP) was obtained from Amersham International, Amersham UK at a specific activity of 3,000Ci/mM and stored at 4°C.

2.1.2 DNA fragments

*Tyr*T DNA contains the *Tyr*T promoter and its flanking regions and was used as a model system in this thesis due to extensive mapping studies with histone bound DNA being well documented (Drew & Travers 1985).

The 160 base pair *tyr*T (43-59) sequence contains a 17 base pair homopurine-homopyrimidine tract between positions 43 and 59 (figure 2.1). This was obtained by mutating positions 46, 55, 56 and 58 of the original *tyr*T sequence using polymerase chain reaction (PCR) site directed mutagenesis (Brown *et al* 1998), and had been cloned between the *Sma*I and *EcoR*I sites of plasmid pUC18 (figure 2.2).

*Tyr*T (22-33) is a related DNA sequence which contains a 12 base pair homopurine-homopyrimidine tract between positions 22-33 (figure 2.1). This was obtained by mutating positions 25, 31 and 32 of the original *tyr*T sequence using PCR site directed mutagenesis (Brown *et al* 1998). Both these *tyr*T plasmids were obtained from Professor K.R. Fox.

*Tyr*T (43-59,122-133) contains the 17 base pair homopurine-homopyrimidine tract between positions 43-59 and an additional oligopurine tract,

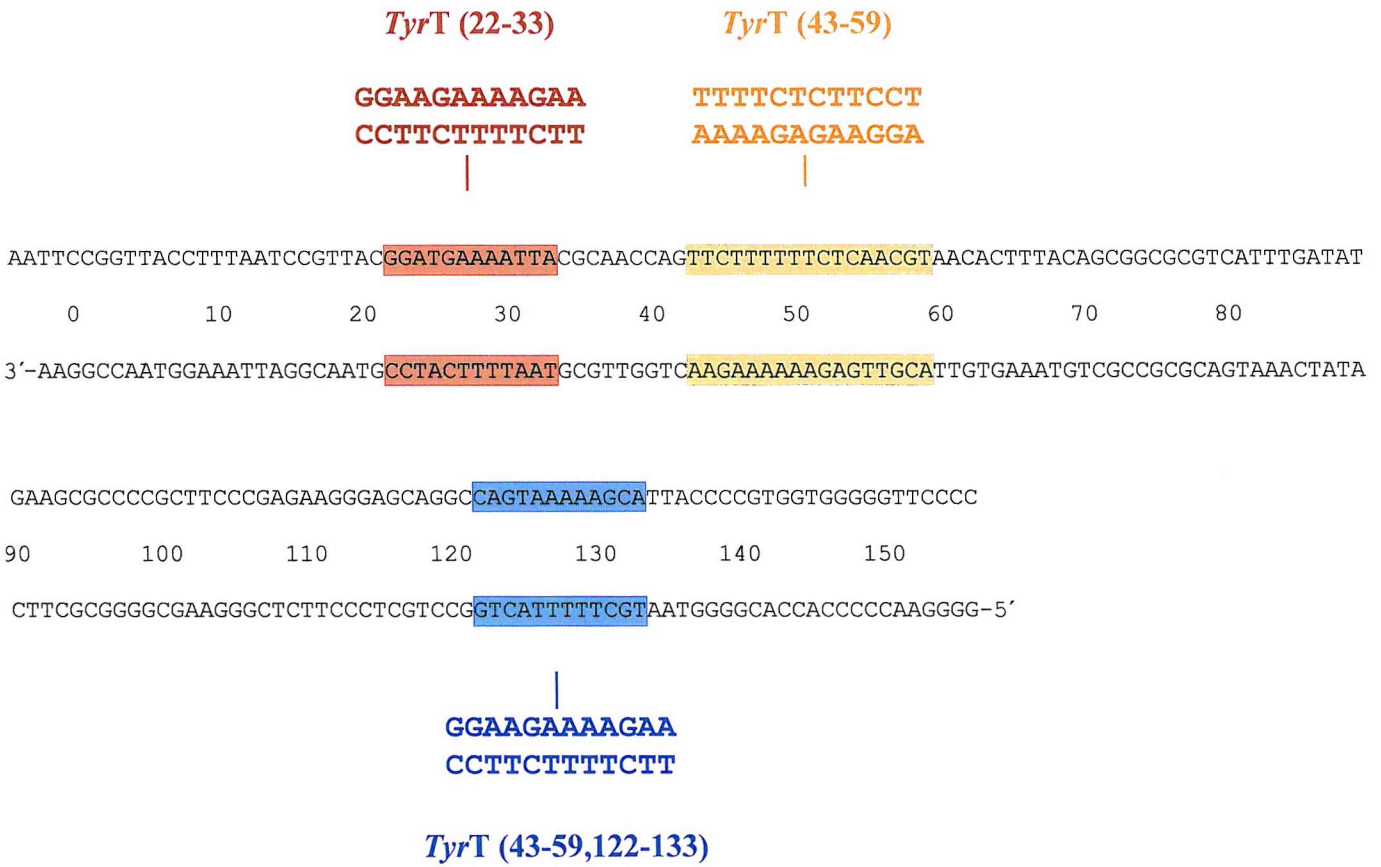

FIGURE 2.1 Base sequence of the original *tyrT* DNA sequence. The brown region is the homopurine-homopyrimidine tract of the *tyr*T (22-34) sequence that has been mutated from the original sequence and the orange region is the homopurine homopyrimidine tract of the *tyr*T (43-59) sequence that has also been mutated from the original *tyr*T sequence. These sites are targeted with PNA.

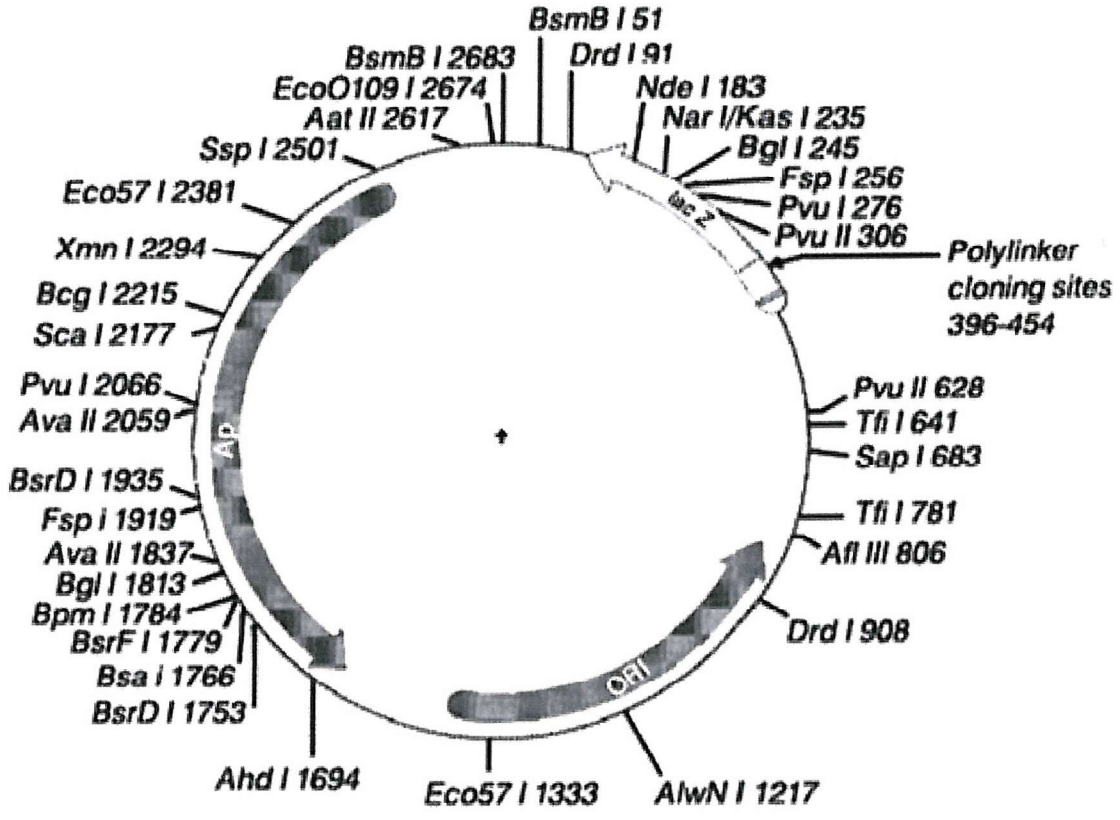

Polylinker sequence

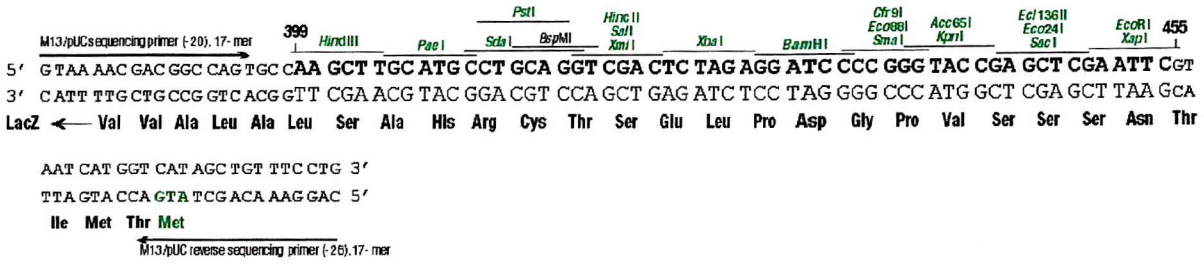

FIGURE 2.2 Illustration of plasmid pUC18 showing the sequence of the polylinker region used to clone in the relevant DNA fragments sequence. The most common restriction sites are shown around the plasmid (Yanisch-Perron *et al* 1985).

identical to that in *tyr*T (22-33), between positions 122-133. This was obtained by mutating positions 122, 123, 125, 126, 131, 132 and 133 of *tyr*T (43-59) using PCR site directed mutagenesis, as described below.

2.1.3 Enzymes

DNaseI (Type IV enzyme from bovine pancreas) was purchased from Sigma-Aldrich and stored at a concentration of 7,200U/ml and stored in a storage buffer (50mM Tris-$COOCH_3$ (pH 7.5), 10mM $CaCl_2$, 10mM $MgCl_2$ and 50% glycerol) at -20°C. Micrococcal nuclease (from *Staphylococcus aureus*) purchased from Fermentas at a concentration of 17,000U/ml and stored in a storage buffer (20mM HEPES-KOH (pH 7.6), 50mM NaCl and 50% glycerol) at -20°C. T7 Exonuclease was supplied by New England Biolabs at a concentration of 10,000U/ml and stored in a storage buffer (10mM Tris-HCl (pH 8.0), 0.1mM ethylenediaminetetraacetic acid (EDTA), 1mM dithiothreitol (DTT) and 50% glycerol) at -20°C. S1 nuclease was supplied from Fermentas at a concentration of 100U/µl and stored in a storage buffer (20mM Tris-HCl (pH 7.5), 50mM NaCl, 0.1mM $ZnCl_2$ and 50% glycerol) at 4°C. Restriction enzymes were purchased from New England Biolabs or Promega and Avian Myeloblastosis Virus (AMV) reverse transcriptase was purchased from Sigma-Aldrich.

Trypsin immobilized agarose beads were supplied by Sigma-Aldrich at a concentration of 50-100U/ml in 10mM acetic acid, pH 3.2 and stored at 4°C.

2.1.4 Oligonucleotides

All DNA oligonucleotides were purchased from Oswell DNA sequencing, Southampton, United Kingdom.

2.1.5 PNA sequences

The polypyrimidine PNA sequences were designed to target different regions of the homopurine-homopyrimidine tracts in *tyr*T (43-59), and *tyr*T (22-33) (figure 2.3 and table 2.1). Their expected binding locations and the orientation of the PNA are shown in figure 2.3. All these PNAs were supplied by Oswel DNA service (Southampton) and were stored in distilled water at concentration of 1mM at -20°C. They were diluted to working concentrations immediately before use.

2.2 Plasmid preparation

Plasmid purification was performed using Promega Wizard or Qiagen Spin Miniprep Kits for the purification of up to 20μg of high-copy plasmid DNA, generated from 5ml overnight cultures of *E.coli*. The following sections outline the experimental procedure from transformation of competent cells, through to the isolation of plasmid DNA.

2.2.1 TG2 competent cells

5 ml of 2YT media (16g tryptone, 10g yeast extract, 5g NaCl per litre) was inoculated with *E.coli* TG2 cells and grown overnight. 50ml of 2YT broth was then inoculated with 0.5ml of the overnight culture and grown at 37°C until an absorbance (OD) measured at 600nm, of between 0.3-0.5 was reached. The culture was then centrifuged at 5,000 revolutions per minute (rpm) for 5 minutes at 4°C. The supernatant was removed and the pellet was resuspended in 20ml of cold sterile

***Tyr*T (43-59)**

Site 1

```
5′  ACGCAACCAGTTCTTTTTTCTCTTCCTAACAC  3′
3′  TGCGTTGGTCAAGAAAAAAGAGAAGGATTGTG  5′
```

N-TTTTCTCTTCCT-C	PNA 20
C-TTTTCTCTTCCT-N	PNA 21
C-TTCTTTTTTCTCTTCCT-N	PNA 41
C-CTTTTTTCTCTT-N	PNA 42
N-TTCTTTTTTCTC-C	PNA 43

***Tyr*T (22-34)**

Site 2

```
5′  TTTAATCCGTTAGGAAGAAAAGAACGCAAC  3′
3′  AAATTAGGCAATCCTTCTTTTCTTGCGTTG  5′
```

N-TTCTTTTCTT-C	PNA 05
OR	OR
C-TTCTTTTCTT-N	PNA 05
N-CCTTCTTTTCTT-C	PNA 08
C-CCTTCTTTTCTT-N	PNA 09

***Tyr*T (43-59,122-133)**

Site 3

```
5′  AAGGGAGAAGGGGAAGAAAAGAATTACCCC  3′
3′  TTCCCTCTTCCCCTTCTTTTCTTAATGGGG  5′
```

N-TTCTTTTCTT-C	PNA 05
OR	OR
C-TTCTTTTCTT-N	PNA 05
N-CCTTCTTTTCTT-C	PNA 08
C-CCTTCTTTTCTT-N	PNA 09

FIGURE 2.3 PNA binding orientations in relation to the purine strand of the polypurine tract for each *tyr*T sequence.

PNA	Sequence	Sequence length	Target site	Binding orientation
005	N-TTCTTTTCTT	10 mer	2,3	Antiparallel and parallel
008	N-CCTTCTTTTCTT	12 mer	2,3	Parallel
009	N-TTCTTTTCTTCC	12 mer	2,3	Antiparallel
20	N-TTTTCTCTTCCT	12 mer	1	Antiparallel
21	N-TCCTTCTCTTTT	12 mer	1	Parallel
41	N-TCCTTCTCTTTTTTCTT	17 mer	1	Parallel
42	CTCTTTTTTC	12 mer	1	Parallel
43	N-TTCTTTTTTCTT	12 mer	1	Antiparallel

TABLE 2.1 Sequences of the PNAs used in this work together with their target sequences and the expected orientation relative to the oligopurine strand

transformation buffer (50mM $CaCl_2$, 10mM Tris-HCl, pH 7.4) and left on ice for 30 minutes. The sample was then centrifuged at 5,000 rpm at 4°C for 5 minutes. The supernatant was removed and the pellet was resuspended in 3ml of transformation buffer and stored at 4°C for a maximum of 2 weeks.

2.2.2 Transformation

1µl of plasmid stock was added to 200µl of competent cells and left on ice for 30 minutes with gentle mixing every 10 minutes. The cells were then heat shocked for 1 minute at 45°C, and cooled on ice for 2 minutes. 50µl and 100µl volumes of these transformed cells were plated on separate agar plates, containing 0.5mM isopropyl β-D-thiogalactopyranoside (IPTG), 0.5mM 5-bromo-4-chloro-3-indolyl β-D-glactosidase (X-gal) and 100µg/ml ampicillin. Plates were incubated overnight at 37°C and white colonies were used in the plasmid preparation procedure.

2.2.3 Promega Wizard Miniprep

5ml of 2YT media was inoculated with *E.coli* that contained the appropriate plasmid. Ampicillin was added to the cultures to give a final concentration of 100µg/ml and the samples were incubated at 37°C for between 8-16 hours. The 5ml cultures were divided into 3x 1.5ml Eppendorf tubes and centrifuged at 5,000 rpm for 5 minutes. The supernatant was discarded and the pellet was resuspended in 250µl of cold resuspension buffer (100µg/ml RNase, 50mM Tris-HCl pH 7.5, 10mM EDTA). The cells were then lysed with 200µl of cell lysis solution (0.2M NaOH, 1% sodium dodecyl sulphate (SDS)) and then mixed thoroughly. The

solution was then neutralized by adding 200µl of neutralization solution (2.55M KOAc, pH 4.8). These samples were centrifuged at 14,000 rpm for 10 minutes. The supernatant was removed and added to 1ml of Wizard miniprep resin (Promega) and mixed thoroughly. The solution was applied to a Wizard miniprep column supplied by Promega and drawn through the column under vacuum. The column was then washed by adding 2ml of column wash (10mM Tris, 0.1M NaCl, 2.5mM EDTA in 50% ethanol) and drawn through by vacuum. The column was dried by continuing to draw air through for 2-3 minutes, then 40µl of 65°C distilled water was added to the column, left for 1 minute then centrifuged for 1 minute at 10,000 rpm to release the plasmid from the resin.

2.2.4 Qiagen QIAprep

5 ml of 2YT media was inoculated as described in section 2.2.3. The 5ml cultures were divided equally into 3x 1.5ml Eppendorf tubes and centrifuged at 5,000 rpm for 2-3 minutes. The supernatant was removed and the pellet was resuspended in 250µl of buffer P1 (Qiagen) and then lysed with 250µl of buffer P2 (Qiagen) and thoroughly mixed. The mixture was then neutralized by adding 350µl of buffer P3 (Qiagen), gently mixed then centrifuged at 14,000 rpm for 10 minutes. The supernatant was transferred into a Qiagen spin column and was centrifuged for 1 minute at 14,000 rpm. The flow through was discarded and the plasmid was washed with 0.5ml of buffer PB (Qiagen). This was centrifuged for 1 minute at 14,000 rpm and the flow through was discarded. The plasmid was washed with 0.75ml of buffer PE (Qiagen) and centrifuged for 1 minute at 14,000 rpm and the flow through was discarded. The column was transferred into a clean Eppendorf tube and the plasmid

was eluted by incubating with 40µl of elution buffer (10mM Tris-HCl, pH 7.5), left for 1 minute and then centrifuged at 14,000 rpm for 1 minute. This plasmid stock was either stored for further transformation or was immediately used in the DNA labeling procedure.

2.3 DNA labelling

DNA fragments were labeled with α-[^{32}P] dATP by filling in the sticky ends generated by cleavage of appropriate plasmids with *Hind*III or *Eco*RI. Cleavage with a second restriction enzyme was varied so as to obtain fragments of different lengths. In each case digestion was performed by adding 10µl of 5x multi core buffer (25mM Tris-acetate, pH 7.5) 100mM potassium acetate, 10mM magnesium acetate, 1mM DTT) to 40µl of plasmid DNA that contained the sequence of interest. The different fragments obtained are shown in table 2.2. 20 units of each restriction enzyme were incubated with the plasmid for 1 hour each at 37°C (except *Sma*I, which was incubated at 25°C). The 110bp and 160bp fragments were obtained by cutting with *Eco*RI and *Sma*I or *Ava*I and were labeled at the 3′ end of the *Eco*R1 site using 10µCi (1µl) of α-[^{32}P] dATP with 0.5µl of AMV reverse transcriptase (10U/µl) at 37°C for a minimum of 30 minutes. The 190bp fragment was obtained by cutting with 10-50 units of *Eco*RI at 37°C for 1 hour, then labeled at the 3′ end of the *Eco*RI site with α-[^{32}P] dATP using 5 units of reverse transcriptase for a minimum of 30 minutes at 37°C. The mixture was then heated at 65°C for 1 minute to inactivate the reverse transcriptase enzyme, and cut with 1µl of *Hind*III at 37°C for 1 hour. The 360bp fragment was obtained by cutting the plasmid with 1µl each of *Hind*III and *Pvu*III for

Plasmid sequence	Fragment length (bps)	Restriction enzymes	Distance from labeled end Site 1	Site 2	Site 3
*Tyr*T (43-59)	110	<u>*EcoR*I</u> *Ava*I	43-59	-	-
*Tyr*T (43-59)	160	<u>*EcoR*I</u> *Sma*I	43-59	-	-
*Tyr*T (43-59)	190	<u>*EcoR*I</u> *Hind*III	43-59	-	-
*Tyr*T (43-59)	190	<u>*Hind*III</u> *EcoR*I	131-147	-	-
*Tyr*T (43-59)	360	<u>*Hind*III</u> *Pvu*II	131-147	-	-
*Tyr*T (22-33)	110	<u>*EcoR*I</u> *Ava*I	-	22-33	-
*Tyr*T (22-33)	160	<u>*EcoR*I</u> *Sma*I	-	22-33	-
*Tyr*T (22-33)	190	<u>*EcoR*I</u> *Hind*III	-	22-33	-
*Tyr*T (22-33)	190	<u>*Hind*III</u> *EcoR*I	-	157-168	-
*Tyr*T (22-33)	360	<u>*Hind*III</u> *Pvu*II	-	157-168	-
*Tyr*T (43-59,122-133)	110	<u>*EcoR*I</u> *Ava*I	43-59	-	122-133
*Tyr*T (43-59,122-133)	160	<u>*EcoR*I</u> *Sma*I	43-59	-	122-133
*Tyr*T (43-59,122-133)	190	<u>*EcoR*I</u> *Hind*III	43-59	-	122-133
*Tyr*T (43-59,122-133)	190	<u>*Hind*III</u> *EcoR*I	131-147	-	57-68
*Tyr*T (43-59,122-133)	360	<u>*Hind*III</u> *Pvu*II	131-147	-	57-68

<u>TABLE 2.2</u> DNA fragments, specific lengths and distance of the target site from the labeled end of the fragments. The underlined restriction enzyme represents the site that was radioactively labeled.

2 hours at 37°C then labeled at the 3′-end of the *Hind*III site with α-[^{32}P] dATP using AMV reverse transcriptase for a minimum of 30 minutes.

The labeled fragments were separated from the remainder of the plasmid on 8% (w/v) non-denaturing polyacrylamide gels run at 800 volts/22 Watts for 2 hours. The wet gel was exposed to X-ray film for 2 minutes followed by the excision of the relevant bands from the gel. The DNA gel slice was then suspended in 400µl of 10mM Tris-HCl pH 7.5 containing and 0.1mM EDTA and agitated at 37°C for a minimum of 16 hours. The polyacrylamide was separated from the liquid by centrifugation and the DNA was precipitated from the supernatant by adding $^1/_9$ volume of 3M NaOAc (pH 7.4) and three volumes of 100% ethanol, and put on dry ice for 10 minutes. The samples were then centrifuged for 10 minutes at 14,000 rpm at 4°C. The resulting pellet was washed with 200µl of 70% ethanol then centrifuged for 1 minute at 14,000 rpm at 4°C. The supernatant was removed and the pellet was dried under vacuum in a Speedvac concentrator. The pellet was dissolved in 10mM Tris-HCl pH 7.4 containing and 0.1mM EDTA to give an approximately 10-15 counts per second (cps) per µl, estimated using a Geiger-Muller counter.

2.4 Nucleosomes

2.4.1 Solutions for nucleosome preparation

The following solutions prepared and stored at 4°C.

Buffer A: 15mM potassium cacodylate, 60mM potassium chloride, 15mM sodium chloride, 0.5mM spermidine, 0.15mM spermine at pH 6.0. This buffer was made up as a 10x solution and diluted when required.

Solution 1: Buffer A containing 0.34M sucrose, 0.2mM phenylmethylsulphonylfluoride (PMSF), 1mM benzamidine, 15mM β-mercaptoethanol pH 6.0. Four litres of this solution was required and PMSF and β-mercaptoethanol was added directly prior to use.

Solution 2: One litre of Buffer A containing 0.34M sucrose, 0.2mM PMSF and 15mM β-mercaptoethanol (added directly prior to use) pH 6.0.

Solution 3: 500ml of 10mM Tris-HCl, pH 8.0 containing 0.2mM EDTA and 0.2mM PMSF (added directly prior to use) was prepared to lyse the cell nuclear envelope.

Solution 4: 10 litres of 20mM sodium cacodylate pH 6.0 containing 0.63M sodium chloride, 0.2M PMSF (added directly prior to use) and 1.0mM EDTA was prepared.

2.4.2 Preparation of the H1-stripped chromatin

The nucleosomes were prepared from chicken red blood cells using a method modified from Lutter (Brown *et al* 1998; Drew & Travers 1985; Lutter 1979). The following were undertaken at 4°C unless otherwise stated.

1) 50ml of freshly collected chicken blood was mixed with 1/7 volume of 84mM sodium citrate pH 7.0 to prevent coagulation and diluted to give a total volume of 500ml using solution 1.

2) The blood mixture was then centrifuged at 2,000 rpm for 8 minutes and the supernatant was discarded. The pellet was resuspended in 500ml of solution 1. This was repeated 3 times until the supernatant became clear.

3) Two litres of solution 1 was adjusted to 0.1% (w/v) nonidet P40 and the pH changed to 7.5 using Tris-base. The pellet was resuspended in 500ml of this solution,

centrifuged at 3,000 rpm for 3 minutes, and the supernatant was discarded. This was repeated three times until the pellet became clear. The pellet was then resuspended in 500ml of solution 2 and centrifuged at 3,000 rpm for 10 minutes and the supernatant was discarded. The pellet was resuspended in 100ml of solution 2 (pH adjusted to 7.4) and stored on ice.

4) The DNA concentration was determined from the absorbance at 260nm measured in 0.1M sodium hydroxide. The absorbance was adjusted to 50U/ml of nuclei (5mg/ml protein & DNA).

5) A trial Micrococcal nuclease digest was undertaken to release 70-80% of the DNA from the nuclear cell wall. One millilitre of the solution was adjusted to 1mM calcium chloride and incubated at 37°C for 3 minutes. Micrococcal nuclease was then added to the solution to give a final concentration of 40U/ml and digested for exactly 20 minutes. Adjusting to 2mM EDTA stopped the digestion. The samples were centrifuged at 5,000 rpm for 10 minutes and the pellet was resuspended in solution 3 (pH 7.5) and kept on ice for 30 minutes. After lysis for 30 minutes the samples were centrifuge at 5,000 rpm and the supernatant was measured at 260nm for the release of 70-80% of DNA. This step was then repeated for the total prep volume.

6) The total volume solution was accurately measured and placed in a flask at 4°C. 4M sodium chloride was added drop wise to give a final concentration of 0.65M.

7) The solution was then passed through a Sepharose 6B (2.5x 100cm) column, which had been equilibrated in solution 4. H1 stripped chromatin eluted after 6-8 hours.

8) The eluted samples were run on a SDS-page gel to confirm the presence of the correct histones and to show H1 had been successfully stripped from the chromatin (figure 2.4A).

SDS-page gel

10% resolving gel		**5% stacking gel**	
Acrylamide	2ml	Acrylamide	330µl
1.5M Tris pH 8.8	2.25ml	1M Tris pH 6.8	250µl
dH_2O	1.65ml	dH_2O	1.375ml
10% SDS	60µl	10%SDS	20µl
10% AMPS	60µl	10% AMPS	20µl
TEMED	5µl	TEMED	5µl

2.5 Reconstitution of nucleosomes with radiolabelled DNA fragments

Radioactively labeled DNA fragments were reconstituted onto nucleosome core particles by the salt exchange method (Drew & Travers 1985) illustrated in figure 2.4B.

1) Labeled DNA (2,000 cps) was dissolved in 12µl of 20mM Tris-HCl, pH 7.4, containing 1mM EDTA.

2) 60µl of 30mM NaOAc, pH 5.0, containing 4.5M NaCl and 1mM EDTA was mixed with 15µl of 5mM PMSF. 8µl of this was added to the dissolved labeled DNA.

3) 18µl of H1-stripped chromatin (3mg/ml) was added to the DNA solution and incubated at 37°C for 30 minutes.

4) The salt concentration was then lowered to 100mM using stepwise additions of a low salt buffer (5mM NaOAc pH 5.0, containing 1mM EDTA and 0.1% Nonidet (4 additions of 10µl then 11 additions of 20µl every 5 minutes).

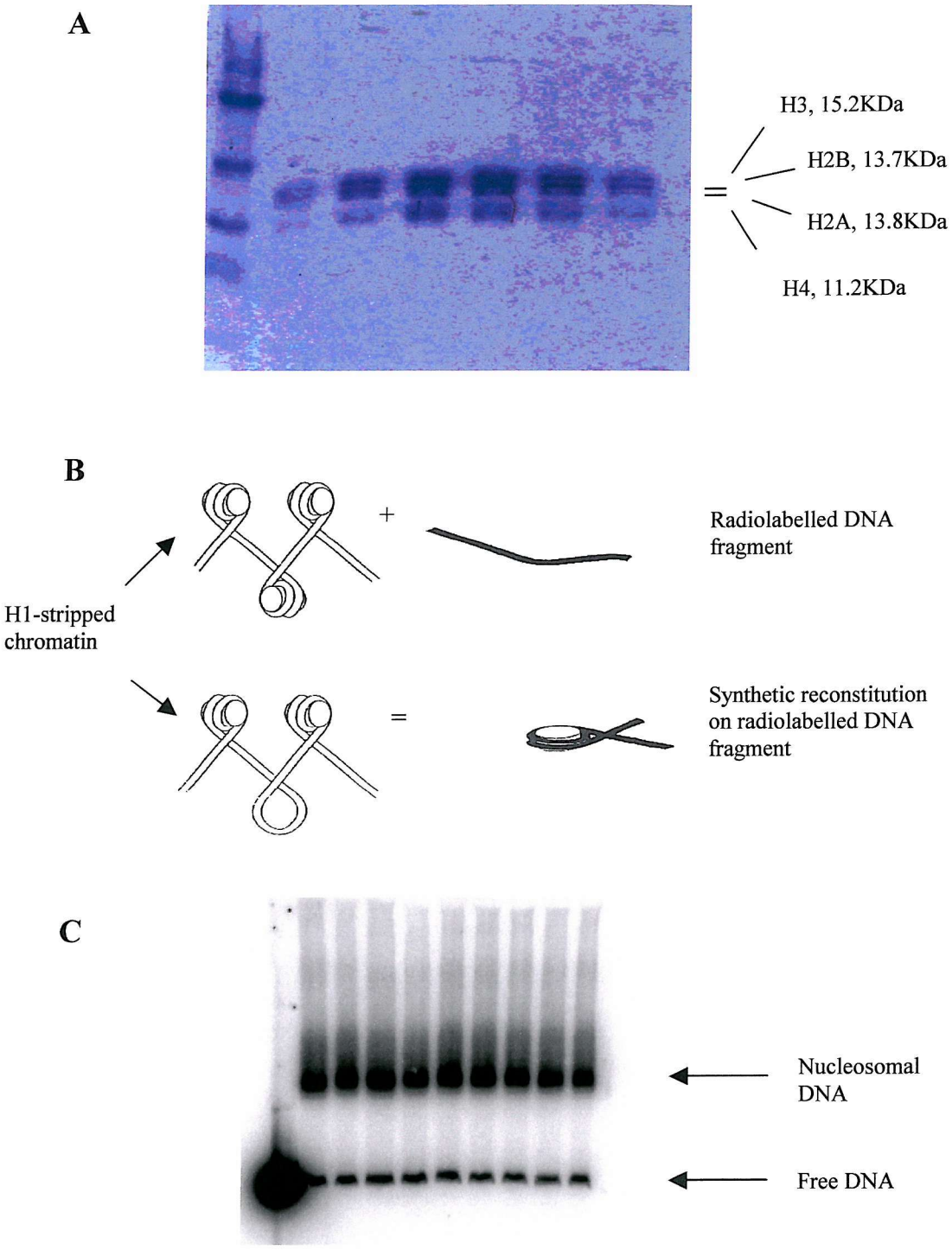

FIGURE 2.4 Summary of nucleosome reconstruction. (A) Coomassie stained protein gel showing the presence of only histones H2A, H2B, H3 and H4 in the samples eluted from the Sepharose column (B) illustration of the procedure involved in the reconstitution of radiolabelled DNA, (C) Polyacrylamide gel showing the reconstitution of the 160bp *tyr*T (43-59) sequence.

5) Successful reconstitution was confirmed by agarose gel electrophoresis to check that >95% reconstitution has been achieved (see figure 2.4C).

2.6 PNA/DNA formation

When forming a PNA/DNA complex on free DNA, 1.5µl of radiolabelled DNA was incubated with 1.5µl of PNA (diluted to appropriate concentrations in the relevant buffer) for the relevant period of time and at a range of temperatures. When targeting post nucleosome reconstitution, 10µl of preformed nucleosomes was incubated with 10µl of PNA for 24 hours at 4°C. When targeting prior to nucleosome reconstitution, 5µl of PNA was incubated with 5µl of radiolabelled DNA and incubated for the relevant time at a range of specific temperatures the reconstituted onto the histone octamer. The nucleosome samples where cleaved with their relevant cleavage enzyme and subjected to phenol extraction outlined in section 2.8. The free DNA samples were digested as outlined in section 2.7.1. All of the samples were run through gel electrophoresis (see section 2.9).

2.7 DNA cleavage reactions (Footprinting)

DNA cleavage was performed with either DNaseI, Micrococcal nuclease, S1 nuclease or T7 Exonuclease to examine the interaction of peptide nucleic acids with free and nucleosome bound DNA.

2.7.1 DNaseI cleavage

For protein free DNA, 2µl of DNaseI stock solution (7,200U/ml) was diluted in 1ml of DNaseI buffer (20mM NaCl, 2mM $MgCl_2$, 2mM $MnCl_2$). 2µl of this dilution was further diluted in 1ml DNaseI buffer to give a final working concentration. 2µl of this diluted DNaseI was added to the PNA/DNA complexes (1.5µl of radiolabelled DNA & 1.5µl of PNA). These samples were digested for 1 minute and the reaction stopped by adding 3µl of DNaseI stop solution (80% formamide, 10mM NaOH, 10mM EDTA, 0.1% (w/v) bromophenol blue). The samples were then heated at 100°C for 3 minutes and crashed cooled on ice prior to gel electrophoresis.

When cleaving the protein/DNA/PNA complex, the DNaseI concentration was increased to give a working concentration of 18 units per ml and the digest was increased to 5 minutes. Higher enzyme concentrations were required for the nucleosome work due to the presence of a large excess of unlabelled chicken DNA. For reconstituted fragments between 5-10µl of the DNaseI dilution was added to PNA/DNA complex (5µl of radiolabelled DNA & 5µl of PNA). These digested samples were phenol extracted, ether purified and ethanol precipitated as described in section 2.8 before subjecting to electrophoresis.

2.7.2 Micrococcal nuclease cleavage

For protein free DNA samples, 1µl of diluted micrococcal nuclease (1µl of the stock was diluted in 99µl of 200mM Tris-HCl (pH 8.0) 50mM NaCl and 25mM $CaCl_2$) was added to 3µl of the PNA/DNA complex (1.5µl of radiolabelled DNA &

1.5µl of PNA). After 1 minute digestion the reaction was stopped by adding 4µl of DNaseI stop solution (80% formamide containing 10mM EDTA). For the protein/DNA/PNA complexes, where the PNA/DNA complex was formed prior to reconstitution, 10µl of the diluted Micrococcal nuclease (20µl of stock in 80µl of buffer) was added to the protein/DNA/PNA complex (volume 300µl). Digestion was continued for 10 minutes and the reaction was stopped by adjusting the solution to 2mM EDTA. For the reactions in which PNA was added to reconstituted DNA, 1µl of diluted micrococcal nuclease (4µl of stock plus 90µl of buffer) was added to the 5µl samples; digestion continued for ten minutes and the reaction was stopped by adjusting the solution to 2mM EDTA. These samples were extracted with phenol, ether, and then ethanol precipitated, as described in section 2.8.

2.7.3 T7 Exonuclease cleavage

For protein free DNA, 1µl of T7 exonuclease stock (10,000U/ml) was diluted in 50µl of NE buffer and 1µl of this dilution was added to 3µl samples (1.5µl DNA & 1.5µl PNA) to give a final concentration of 66U/ml and digestion was continued for 1 minute. These reactions were stopped by adding 5µl of DNaseI stop solution.

When cleaving the protein/DNA/PNA complexes for which the PNA/DNA complex had been formed prior to reconstitution, 10µl of T7 exonuclease stock was diluted in 20µl of NE buffer and 10µl of this dilution added to each sample (volume 300µl) to give a final concentration of 166U/ml; this was digested for 10 minutes. These samples were extracted with phenol followed by ether purification then ethanol precipitated as described in section 2.8.

When cleaving the protein/DNA/PNA complexes in which the DNA had been reconstituted before adding the PNA, 1.5µl of T7 exonuclease stock was diluted in 20µl of NE buffer and 1µl of this dilution was added to each sample (volume 5µl) to give a final concentration of 150U/ml and digestion was continued for 10 minutes. These samples were extracted with phenol followed by ether and then ethanol precipitated as described in section 2.8.

2.7.4 S1 nuclease cleavage

For protein free DNA, 5µl of S1 nuclease stock (100U/µl) was added to 10µl of stock buffer (20mM Tris-HCl pH 7.5, 50mM NaCl, 0.1 mM $ZnCl_2$ and 50% glycerol) and mixed thoroughly. 1µl of this was added to the sample and digested for 3 minutes. The reaction was stopped by adding 5µl of DNaseI stop solution and boiled for 3 minutes at 100°C. The S1 nuclease dilutions where made up immediately prior to digestion.

2.8 Phenol extraction

Before phenol extraction the volume of the aqueous samples was increased to 200µl by addition of water. 200µl of phenol-chloroform (pH 8.0) was added to the samples and mixed gently, followed by centrifugation at 14,000 rpm for 1 minute. The top layer was removed and transferred into a clean 1.5ml Eppendorf tube. 200µl of ether was added (to remove residual phenol) and centrifuged at 14,000 rpm for 1 minute. The top layer was removed and discarded and the samples were placed at 37°C for 20 minutes to evaporate any excess ether. The DNA was then

precipitated by adding $^1/_9$ volume of 3M NaOAc followed by three volumes of 100% ethanol and put on dry ice for 10 minutes. These samples were then centrifuged for 10 minutes at 14,000 rpm at 4°C. The resulting pellet was washed with 200µl of 70% ethanol then centrifuged for 1 minute at 14,000 rpm at 4°C. The supernatant was removed and the pellet was dried under vacuum in a Speedvac concentrator. The pellet was then resuspended in 6µl of DNaseI stop solution. The samples were heated to 100°C for 3 minutes then cooled on ice prior to gel electrophoresis.

2.9 Gel electrophoresis

Footprinting reactions were run on 5-10% (w/v) denaturing polyacrylamide gels containing 8M (Xml Sequagel, 5ml 10x TBE-Urea (216g Tris, 110g boric acid, 18.8g EDTA, 1Kg urea in 2 litres H_2O), 28ml 50% 8M urea, 200µl 20% Ammonium Persulfate and 40µl N,N,N',N'-tetramethylethylenediamine (TEMED)), run in 10% TBE (11g Tris, 5.5g boric acid and 1g EDTA per litre) buffer. Samples were boiled for at least 3 minutes and crash-cooled on ice before loading onto the gel (400x200x0.3mm) and run at 1500V, 41W for about 2 hours. The glass plates were separated and the gel is fixed in 10% (v/v) acetic acid for 10 minutes. The gel in the transferred to Whatmann 3mm paper, dried under vacuum at 80°C for 1 hour then subjected to autoradiography at -70°C with an intensifying screen and exposed to a Kodak Phosphorimager screen. Sequencing reactions were heated at 100°C for three minutes before running on a 5% denaturing polyacrylamide gel.

For the histone bandshifts gels, 4µl of reconstituted mixture was mixed with 3µl of ficol loading buffer and run on a 5% non-denaturing polyacrylamide gel (6ml Protogel (33% solution), 5ml 5x TBE buffer, 39ml water, 200µl of 20%

ammonium persulfate (AMPS) and 40µl TEMED). The samples were loaded onto the gel (200x200x0.3mm) and run at 200V, 8W until the dye was approximately ¾ down the gel. The same procedure was undertaken for the free DNA bandshift, the only exception being 2µl of free DNA/PNA was added to 3µl of ficol. The glass plates were separated and the gel is fixed in 10% (v/v) acetic acid for 10 minutes. The gel in the transferred to Whatmann 3mm paper, dried under vacuum at 80°C for 30 minutes then subjected to autoradiography at -70°C with an intensifying screen and exposed to a Kodak Phosphorimager screen.

2.9.1 GA marker

The GA marker is used to identify the bands throughout the footprint gel. The marker highlights the purines throughout the sequence highlighting polypurine tracts. The GA marker consists of 1.5µl of labeled DNA, 5µl of DNaseI stop solution (80% formamide, 10mM NaOH, 10mM EDTA, 0.1% (w/v) bromophenol blue) and 20µl H_2O. The mixture is incubated at 100°C for 30 minutes with the cap open to allow evaporation and this consequently reduces the mixture to 5-6µl which is loaded onto the gel.

2.10 Quantitative analysis of footprinting patterns

Radioactive gels were exposed to a Kodak Phosphorimager screen for at least 12 hours. The screen was then scanned using a Molecular Dynamics Storm 860 Phosphorimager and the data analysis was undertaken using ImageQuant software. The intensity of bands over the entire footprint was calculated for each PNA

concentration and compared with that in the free DNA. The intensity of the bands was then normalized by dividing by the intensity of a clear band that was not affected by PNA added. The PNA concentration was plotted against the intensity of the bands in the footprint and C_{50} values were calculated according to the equation:

$$I/I_O = C_{50} / (L + C_{50})$$

I and I_o = Relative band intensity in the presence and absence of PNA

L = The PNA concentration

C_{50} = The PNA concentration required to reduce the intensity by 50%.

2.11 Stratagene Quikchange® Mutagenesis

The Quikchange procedure was used to undertake site directed mutagenesis on the original *tyr*T (43-59) sequence to generate a second PNA binding site at the opposite end of the nucleosome core particle. The principle of this method is explained in figure 2.5. In total seven bases were mutated, located at positions 122, 123, 125, 126, 131, 132 and 133. The first 4 bases were mutated in the first round with a second round of mutagenesis to introduce the other 3, as shown in figure 2.6. The primers started and ended with either a G or C base pair to maximize the annealing. The Quikchange reaction was set up according to Stratagene's guidelines, as shown in table 2.3. The parental DNA is dam methylated and is susceptible to the restriction enzyme *Dpn*I whereas the mutated products are not. 1µl of *Dpn*I was added to each reaction mixture and incubated at 37°C for at least 3hours. After this time, the enzyme was heated at 65°C for 15 minutes. The samples were then

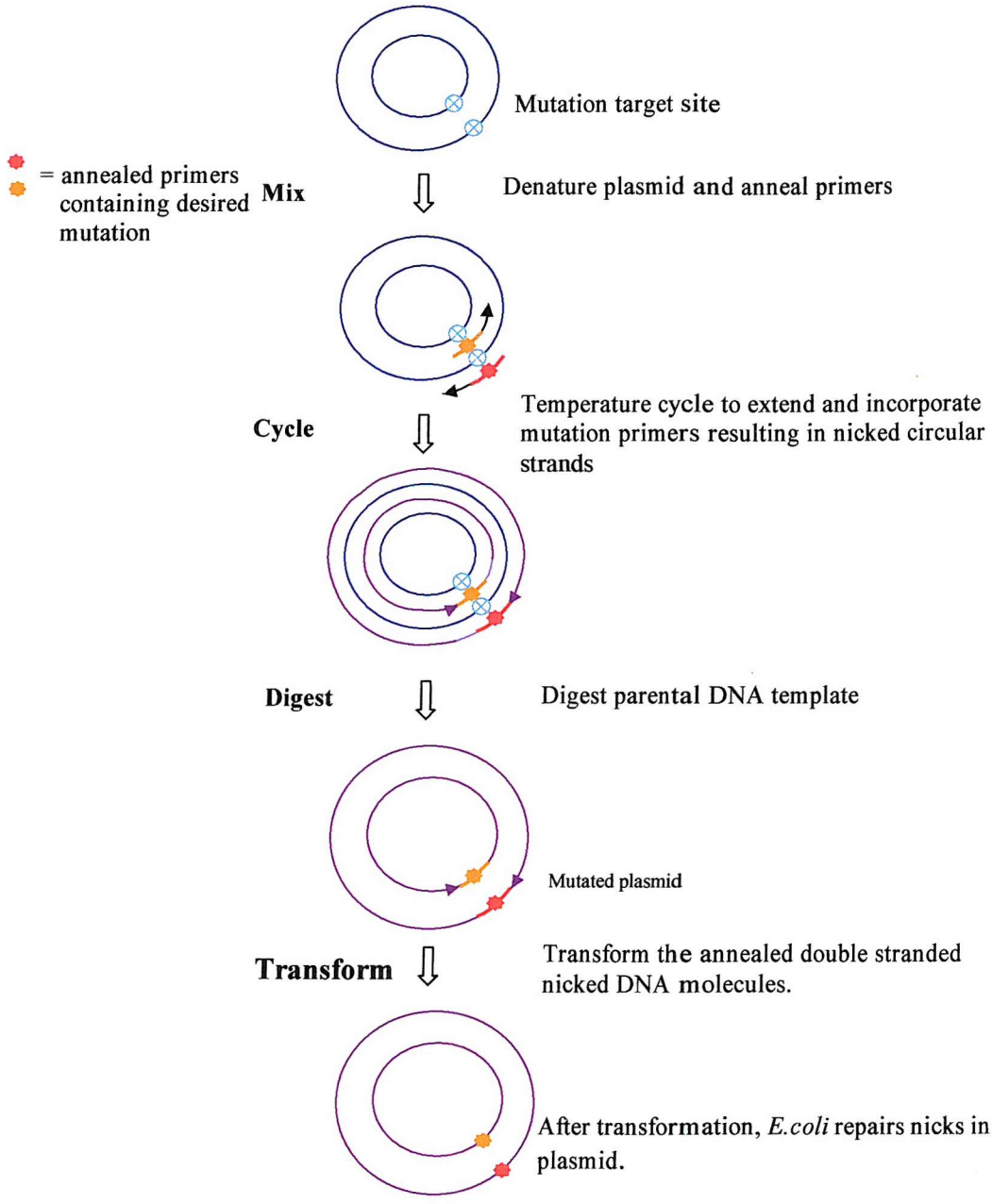

FIGURE 2.5 Diagram of Stratagene Quikchange® site-directed mutagenesis process. The mutation is inserted during the cycle step producing nicked circular strands. *Dpn*I digests the remaining parental DNA leaving the mutated DNA intact, which is transformed into *E.coli*.

1st Quickchange cycle

5′ GGCCAGTAAAAAGCATTA 3′

4 bases ↓

5′ GGGGAAGAAAAAGCATTA 3′

Primers

1 (22)
5′ GGGGTAATGCTTTTTCTTCCCCTTCTCCCTTCTCG 3′
2 (22)
5′ CGAGAAGGGAGAAGGGGAAGAAAAAGCATTACCCC 3′

2nd Quickchange round

5′ GGGGAAGAAAAAGCATTA 3′

↓ 3 bases

5′ GGGGAAGAAAAGAAATTA 3′

Primers

(2+22)
5′ GAAGGGGAAGAAAAGAAATTACCCCGTGGTGGGGG 3′
(1+22)
5′ CCCCCACCACGGGGTAATTTCTTTTCTTCCCCTTC 3′

*Tyr*T (43-59,122-133) polypurine tract between positioned 122-133bps.

5′ GG**GGAAGAAAAGAA**ATTA 3′
3′ CC**CCTTCTTTTCTTT**AAT 3′

FIGURE 2.6 Illustration of the base mutations undertaken to create site 3 in the *tyr*T (43-59, 122-133) sequence using Stratagene Quikchange® site directed mutagenesis.

Reaction conditions	Buffer
1.5µl of each primer (primers at the same concentration (125mg/ml))	100mM KCL
1µl of plasmid (pUC18 & insert)	100mM $(NH_4)_2SO_4$
1µl dNTP mix (10mM each of dATP, dTTP, dCTP and dGTP)	200mM Tris-HCl (pH 8.8)
5µl of 10x buffer	20mM $MgSO_4$
1µl of Pfu Turbo (2.5U/µl)	1% Triton X-100
> 50µl sterile water	

PCR cycles

Cycles	Temperature	Time
1	95°C	30 seconds
16	95°C	30 seconds
	55°C	1 minute
	68°C	6 minutes

TABLE 2.3 Stratagene Quikchange® site directed mutagenesis methods guideline, the top tables showing the reaction mixture and buffer used and the lower table showing the PCR cycles.

subjected to a sequencing reaction to identify the mutated sequence. The initial sequencing reaction to identify the mutated sequence. The initial sequencing gels for the first round showed that the first four bases where correctly mutated (data not shown). The second sequencing gels for the second round showed that the last three bases where also correctly mutated.

2.12 DNA Sequencing

Plasmid DNA was prepared using the Qiagen Qiaprep (see section 2.2.4). 5-10µl of each preparation was retained for further retransformation. Manual sequencing was performed using the T7 sequencing kit (Pharmacia).

Denaturing the DNA. 10µl of 2M NaOH was added to 40µl of plasmid and left at room temperature for 10 minutes. 15µl of 3M NaOAc (pH4.8), 35µl of dH_2O and 300µl of ethanol was added to the mix and placed on dry ice for 10 minutes. The sample was then centrifuged for 10 minutes at 14,000 rpm. The supernatant was removed and 100µl of 70% ethanol was added and centrifuged for 10 minutes at 14,000 rpm. The supernatant was removed and the sample was dried via the speed vac for 5 minutes until completely dry.

Annealing. The dried pellet was redissolved in 10µl dH_2O. 2µl of annealing buffer and 2µl of universal primer was added and left to anneal for 20 minutes at 37°C, then for at least 10 minutes at room temperature.

Sequencing. Four tubes where set up each containing 2.5µl of the dideoxy mixes G-short, C-short, T-short and A-short. A polymerase mix was made and was kept on ice, which consisted of 12µl label mix A, 7µl dH_2O and 1µl α-[^{32}P] dATP. An enzyme mix was made containing 6.5µl enzyme buffer and 1.5µl T7

polymerase and mixed. This enzyme mix was added to the polymerase mix and stored on ice. 6µl of this was added to the annealed DNA and left at room temperature for 5 minutes. During this time the dideoxy mixes were incubated at 37°C for 5 minutes. 4.5µl of the reaction mix was added to each dideoxy tube and left for 5 minutes. The reaction was stopped by adding 5µl stop solution stopped. The samples where then heated at 100°C for 3 minutes and transferred to ice. Half the sample was loaded onto a denaturing polyacrylamide gel in the order G, C, T, A and run for the appropriate time. The gel was then exposed onto X-ray film for 1-2 hours at -70°C to determine the sequence.

2.13 N-terminal histone tail trypsin treatment

Trypsin immobilsed agarose beads were supplied by Sigma, stored in 10mM acetic acid, pH 3.2. The required volume was filtered and washed several times by centrifugation with distilled water. After several washes the final wash was in 50mM NaOAc, pH 5.0. The agarose beads where then suspended in 100µl 50mM NaOAc, pH 5.0 (100µl=50U).

The nucleosome core particle sample was dialysed in 10mM Tris-HCl, pH 7.5, containing 25mM NaCl for 48 hours at 4°C. The protein was dialysed at a concentration of 1mg/ml. The sample was then concentrated in Saratorius tubes through centrifugation.

500µl of the nucleosome core particle (A_{260}=200) in 10mM Tris-HCl, pH 7.5 containing 25mM NaCl was digested with 28 units of immobilsed trypsin for 45 minutes. The samples where then run on an SDS-page gel and polyacrylamide gel to check the N-terminal tail regions had been removed.

2.14 Crush and Soak Method

This procedure was modified from (Sambrook *et al* 1989). The DNA band is extracted from the agarose gel and dissected into small sections and placed into a sterile Eppendorf tube (no more than 0.3g of agarose per tube). 150 to 200µl of sterile water was added along with 300 to 500µl of buffered phenol (Tris-EDTA) pH 7.5. The sample was vortexed for 1 minute and placed into liquid nitrogen for 30 seconds. The sample was then centrifuged at 14,000 rpm for 6 to 8 minutes. The vortexing, freezing and centrifuge steps were repeated several times until no agarose was visible in the lower layer. The upper aqueous layer was extracted and an equal volume of chloroform/isoamyl (24:1) was added, then mixed and centrifuged for 2 minutes. The upper layer was removed and added to this was $^{1}/_{10}$ of the total volume of sodium acetate pH 5.2 together with 3 times the total volume of ethanol. The sample was placed in dry ice for 15 to 30 minutes and then centrifuged at 14,000 rpm at 4°C. The supernatant was discarded and the pellet was washed with 70% ethanol. The pellet was dried in a speedvac and resuspended in 10µl of sterile water.

2.15 TP48 Dimer

The TP48 dimer was designed to incorporate two 160 base pair *TyrT* (43-59) fragments originally connected through a 42 base pair A_nT_n linker region to study the effect with PNA interaction on neighbouring nucleosomes. The results indicated that the DNA linker was folding back on itself and subsequent annealing procedures were unsuccessful. A modified 32 base pair A_nT_n linker region was designed as to not self anneal. The TP48 dimer was designed to bind two nucleosomes, excluding the

rigid linker region. The experimental design of this dimer is shown in figure 2.7 and the base sequence of the 352 base pair dimer is shown in figure 2.8. Site 1 located between positions 101-117bps and 235-251bps within the dimer.

The linker DNA was designed so that upon ligation, the *EcorR*1 site would be destroyed to avoid further cleavage. The 160 bp *tyr*T (43-59) fragments where originally cut with *Sma* I and blunt end ligation was performed into *Sma*1 cut pUC18 after the DNA ligation. This was unsuccessful and blunt end ligation resulted in repeated experiments where the plasmid had self-annealed. The modified design was to cut the 160 bp *tyr*T (43-59) fragments with *BamH*I instead of *Sma* I.

The following methods where used in the construction of the TP48 dimer. The DNA linker sequence was phosphorylated and allowed to anneal using the following kinase treatment.

Kinase treatment

1µl of diluted linker

2µl PNK buffer

1µl rATP

16µl dH_2O

1µl PNK

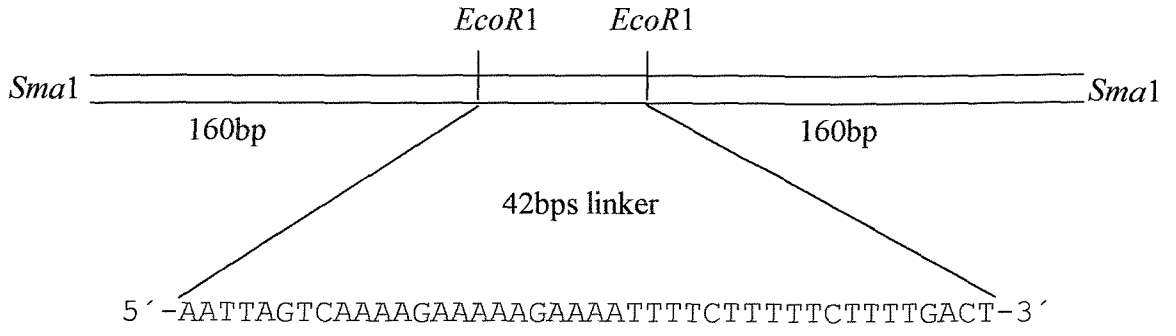

Modified design

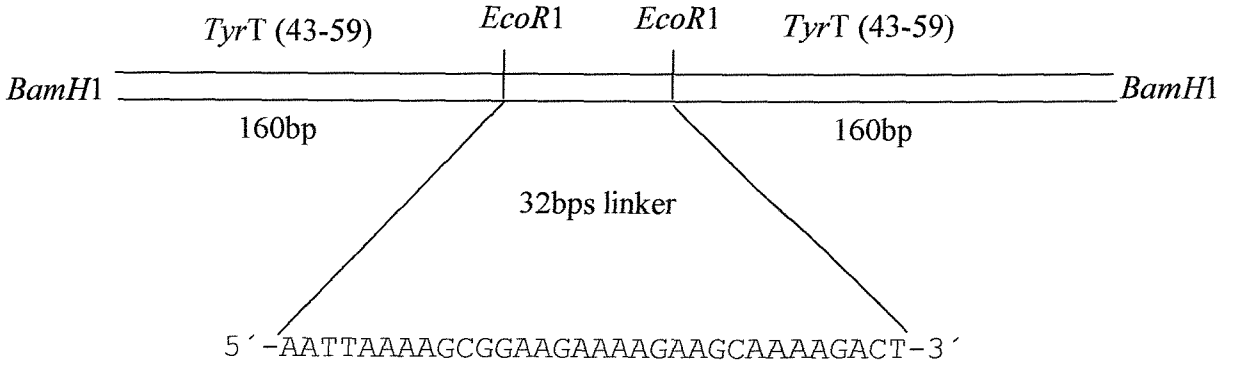

FIGURE 2.7 The original and modified design for the TP48 dimer. The double black lines represent the double helix. The restriction enzymes are labeled accordingly and the corresponding DNA linker sequence is shown.

TP48 Dimer sequence

FIGURE 2.8 TP48 base sequence. The orange region represents site 1 and their corresponding positions are labelled.

The samples were incubate at 30°C for 30 minutes, then heated to 100°C for 3 minutes and then gradually cooled to enhance annealing.

DNA ligation was preformed between the already phosphorylated and annealed DNA linker and the isolated and purified 160bp *tyr*T (43-59) fragments following the same procedure as shown in section 2.3. A variety of ligation mixtures were used however the following two methods yielding the best results. DNA ligation number 2 was the most successful procedure and it was this mixture that was used in the following procedures.

DNA Ligation 1	**DNA ligation 2**
2µl Ligase buffer	1µl Quick stick ligase
1µl T4 DNA ligase	5µl Quick stick buffer (x4)
2µl DNA (*tyr*T 43-59) 160bp	2µl DNA (*tyr*T 43-59) 160bp
1µl Linker DNA	2µl Linker DNA
14µl dH_2O	10µl dH_2O
Total Volume 20µl	Total Volume 20µl

Successful ligation was achieved when the linker DNA was at a concentration of 40pmole and the DNA fragments were at a concentration of 120pmol, a ratio of 3:1. This success was also attributed to using Quickstick ligation procedure from Bioline. The results with T4 DNA ligase were less successful. The ligation mixture was incubated through a number of ligation cycles shown in table 2.4. The most successful ligation procedure was cycle 11 and this mixture was used in the following procedures. The ligation mixture was then subjected to PCR amplification shown in table 2.5. This reaction was performed in the following mixture:

Ligation cycles

Cycle	Duration (hrs)	Temperature	Result
1	1	room temperature	-ve
2	1	15°C	-ve
3	1	37°C	-ve
4	3	room temperature	-ve
5	3	15°C	-ve
6	3	37°C	-ve
7	24	room temperature	marginal success
8	24	15°C	-ve
9	24	37°C	-ve
10	1	15°C	marginal success
	1	22°C	
	1	27°C	
	1	37°C	
11(x4)	2	15°C	+ve
	2	22°C	
	2	27°C	
	2	37°C	

TABLE 2.4 Ligation cycles for the DNA and DNA linker ligation procedure.

PCR amplification mixture

39.6µl dH_2O

5µl 10x Pfu buffer

1µl DNA dimer

2µl primer

1µl Pfu Turbo

0.4µl dNTPs

PCR amplification cycle

1	1	95°C	30 seconds
2	16	95°C	30 seconds
		55°C	1 minute
		68°C	6 minutes

TABLE 2.5 PCR cycle for the amplification of the TP48 dimer.

The resulting product was characterized through agarose gel electrophoresis, which identified the presence of the dimer (see figure 2.9). The samples were run along side a ladder and a fragment of known length to identify its presence.

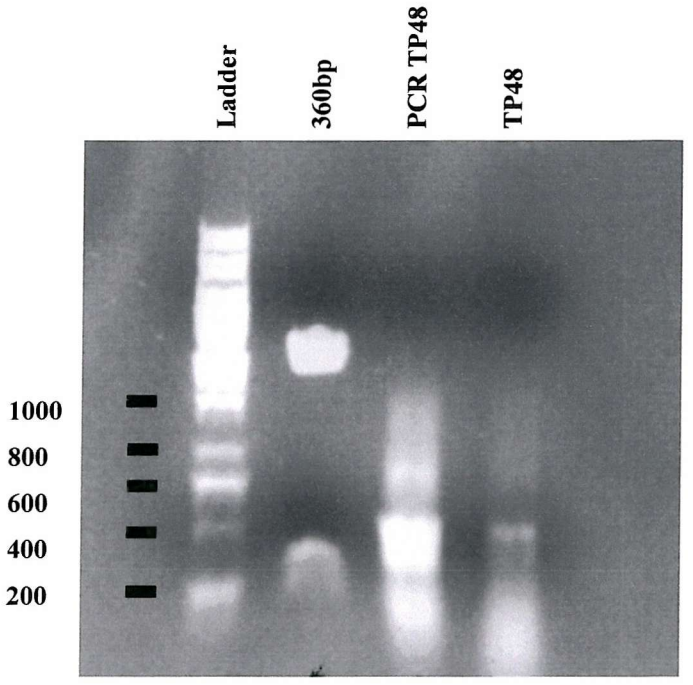

FIGURE 2.9 Agarose gel of the TP48 sequence. The lanes are labelled representing their content. The lane labelled PCR TP48 represents the TP48 sequence after PCR amplification whereas the lane labelled TP48 is prior to PCR amplification.

The next stage was to clone the dimer into the *BamH*1 cut pUC18 plasmid site. It was from this stage in the procedure that complications arose. The following reaction mixtures and various ligation methods were performed, shown below, as well as PCR amplification as shown in table 2.6.

pUC18 ligation procedure 1	**pUC18 ligation procedure 1**
1µl pUC18	1µl pUC18
1µl TP48 Dimer	1µl TP48 Dimer
1µl T4 DNA ligase	5µl T4 DNA ligase
5µl Ligase buffer	10µl Ligase buffer
>50µl distilled water	>50µl distilled water

pUC18 ligation procedure 3

1µl pUC18

1µl TP48 Dimer

1µl Quick stick ligase

5µl Quick stick buffer (x4)

>50µl distilled water

pUC18 ligation procedure 4

1µl pUC18

1µl TP48 Dimer

5µl Quick stick ligase

10µl Quick stick buffer (x4)

>50µl distilled water

pUC18 ligation cycles

Ligated at various temperatures and time spans i.e.

1. 15°C for 1 hour, 2hrs, 3hrs and 24hrs
2. 27°C for 1 hour, 2hrs, 3hrs and 24hrs
3. 37°C for 1 hour, 2hrs, 3hrs and 24hrs
4. 15°C for 1 hour, 22°C for 1 hour, 27°C for 1 hour and 37°C for 1 hour.
5. 15°C for 2 hrs, 22°C for 2 hrs, 27°C for 2 hrs and 37°C for 2 hrs

pUC18 PCR amplification

39.6µl dH_2O

5µl 10x Pfu buffer

1µl pUC18 + cloned TP48 dimer

2µl primer

1µl Pfu Turbo

0.4µl dNTPs

pUC18 ligation PCR cycle

1	1	95°C	30 seconds
2	16	95°C	30 seconds
		55°C	1 minute
		68°C	6 minutes

TABLE 2.6 pUC18 PCR cycle for the ligation of the TP48 dimer into the plasmid.

Alternative methods were used to clone the TP48 dimer into *BamHI* cut pUC18. This involved the use of a number of different DNA polymerases ie: Taq polymerase, Pfu polymerase and Pfu Turbo. The ligation was performed on both the ligated and unligated TP48 dimer. This was unsuccessful and repetitive sequencing gels showed either self-annealing of the plasmid, ligation of the DNA linker or ligation of the 160bp *Tyr*T (43-59) fragment (figure 2.10). Over a period of six months the method was modified and different ligation procedure where attempted. One method was to extract the TP48 dimer from the agarose band through the crush and soak method and ligate this sequence into the plasmid, which was unsuccessful. The ongoing issues was not the cloning into the pUC18 plasmid because different regions of the TP48 dimer were successfully cloned, however successful ligation of the TP48 dimer as one construct was not evident. One solution to this was to cut the TP48 dimer with *EcoR*1 to remove any product that had not ligated properly then clone into pUC18. This was not successful. The TP48 dimer as one construct can be successfully cloned into the pUC18 plasmid, however time restriction rather than experimental design failure was the controlling factor in the completion of this work.

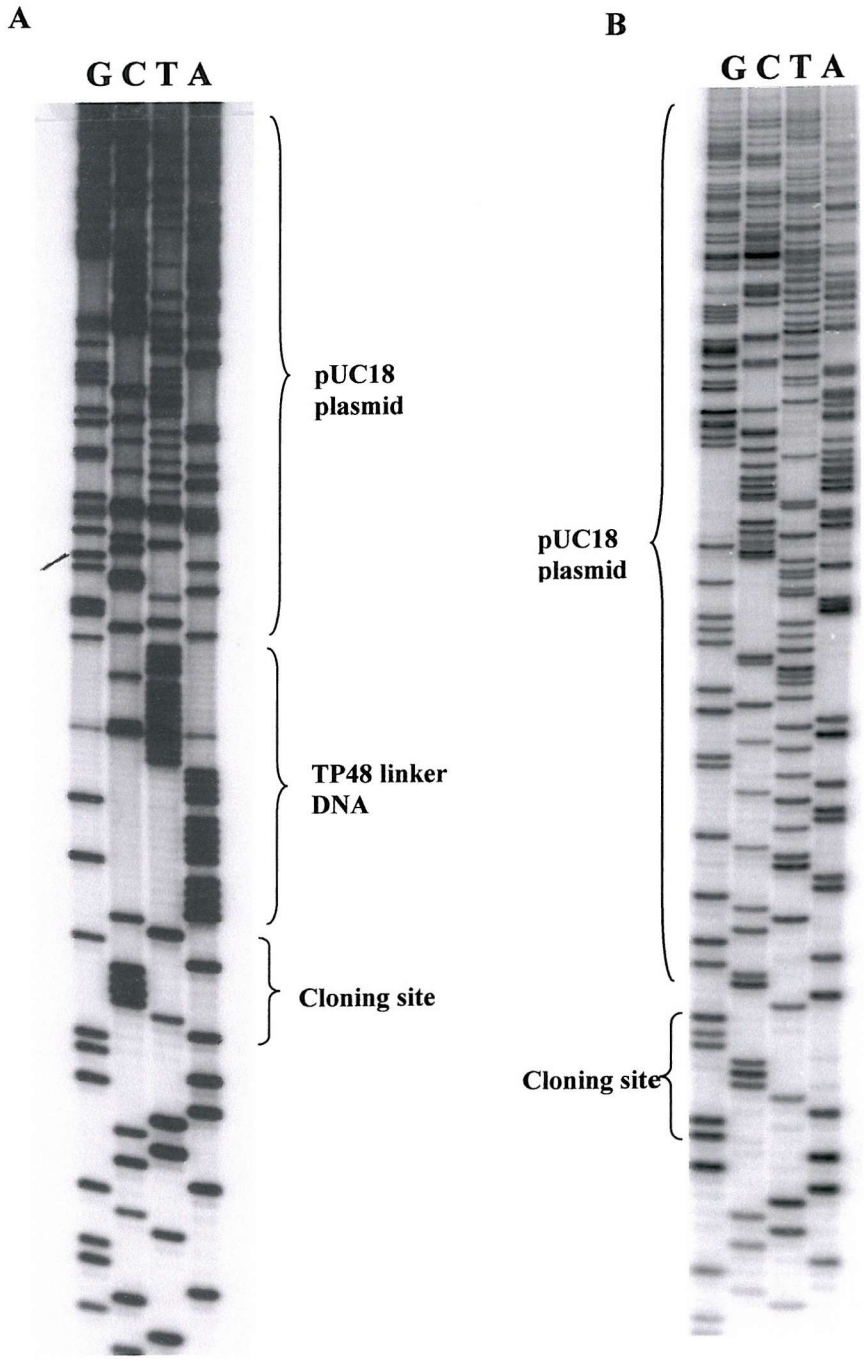

FIGURE 2.10 Polyacrylamide DNA sequencing gels of the TP48 Dimer representing (A) the ligation TP48 linker DNA and (B) self ligation of the pUC18 plasmid. The lanes are labelled according to their base content.

Chapter 3

PNA interaction with Free DNA

3.1 Introduction

The introduction to this thesis has outlined our current knowledge about the interaction of PNA with DNA. Although it is clear that these are effective sequence specific agents there are many outstanding questions regarding the interaction of individual PNAs with their targets. In particular the orientation (N→C or C→N) and mode of binding (strand invasion or triplex formation) may vary for different PNAs under different conditions. The work described in this chapter examines the interaction of several PNAs with potential targets sites on free DNA. These PNA/DNA interactions have been studied by DNaseI footprinting, gel retardation (bandshifts) and S1 nuclease cleavage. This provides the necessary background for the studies with nucleosomal DNA, which is presented later in chapter 4.

3.1.1 DNA sequences

The work described in this chapter concerns the interaction of several different PNAs with target sites, which have been prepared within DNA fragments that contain derivatives of the *tyr*T DNA sequence. Three oligopurine tracts have been examined (designated sites 1-3), which are contained within *tyr*T (43-59), *tyr*T (22-33) and *tyr*T (43-59,122-133).

*Tyr*T (43-59) contains a single 17 base oligopurine tract (5′-AGGAAGAGAAAAAAGAA) designated site 1, which is the target for PNA 20, 21, 41, 42 and 43. The length and orientation of these PNAs relative to the purine strand of site 1 are:

PNA 20	12-mer	antiparallel
PNA 21	12-mer	parallel
PNA 41	17-mer	parallel
PNA 42	12-mer	parallel
PNA 43	12-mer	antiparallel

*Tyr*T (22-33) contains a single 12 base oligopurine tract (5′-GGAAGAAAAGAA) designated site 2, which is the target for PNA 005, 008 and 009. The length and orientation of these PNAs relative to the purine strand of site 2 are:

PNA 005	10-mer	parallel or antiparallel
PNA 008	12-mer	parallel
PNA 009	12-mer	antiparallel

*Tyr*T (43-59,122-133) contains two oligopurine tracts. The first is identical to that in *tyr*T (43-59) and is located in exactly the same position. The second oligopurine target designated site 3 has the same sequence as site 2, but is located between positions 122-133.

Labelling these fragments at the 3′-end of the *EcoR*I site visualizes the purine strand of site 1, but the pyrimidine strand of sites 2 and 3. The opposite strands are seen when these fragments are labelled at the 3′-end of the *Hind*III site.

The interaction of PNA with these targets was examined using DNA fragments of different lengths (110, 160, 190 and 360 base pairs), which were prepared by digesting the parent plasmids with different combinations of restriction

enzymes. Changing the fragment length would not be expected to affect PNA binding, except that longer fragments may contain additional non-specific sites, but these fragments were prepared for studying the interaction with nucleosomal DNA (described in Chapter 4), in which longer fragments may interact with the histone proteins in several different positions.

3.2 DNaseI footprinting

The polypurine tracts in these different *tyr*T DNA fragments were targeted with their respective PNAs. These complexes were analyzed by DNaseI footprinting, to assess the specificity and strength of their interactions.

3.2.1 Site 1 on *tyr*T (43-59) targeted with PNA 20, 21, 41, 42 and 43

Figure 3.1 shows DNaseI cleavage patterns of the 110bp *tyr*T (43-59) fragment in the presence or absence of different concentrations of PNA 20 and 21. These are both 12-mer PNAs and designed to target site 1, located at the 5′- (upper) end of the 17 base oligopurine tract. PNA 20 is designed to bind antiparallel to the purine strand of the duplex, while PNA 21 is designed to bind in a parallel orientation. These experiments were performed in 50mM sodium acetate pH 5.0 in order to enable protonation of the cytosines, which is necessary for formation of the C^+·GC triplets. It can be seen that both PNA 20 and 21 produce clear footprints at the expected target site, which persist to low concentrations (about 0.5μM for PNA 20 and 21). Both footprints are located towards the 5′-end of the polypurine tract as expected. The protected region continues below the actual target site by about 3 bases, as is typically

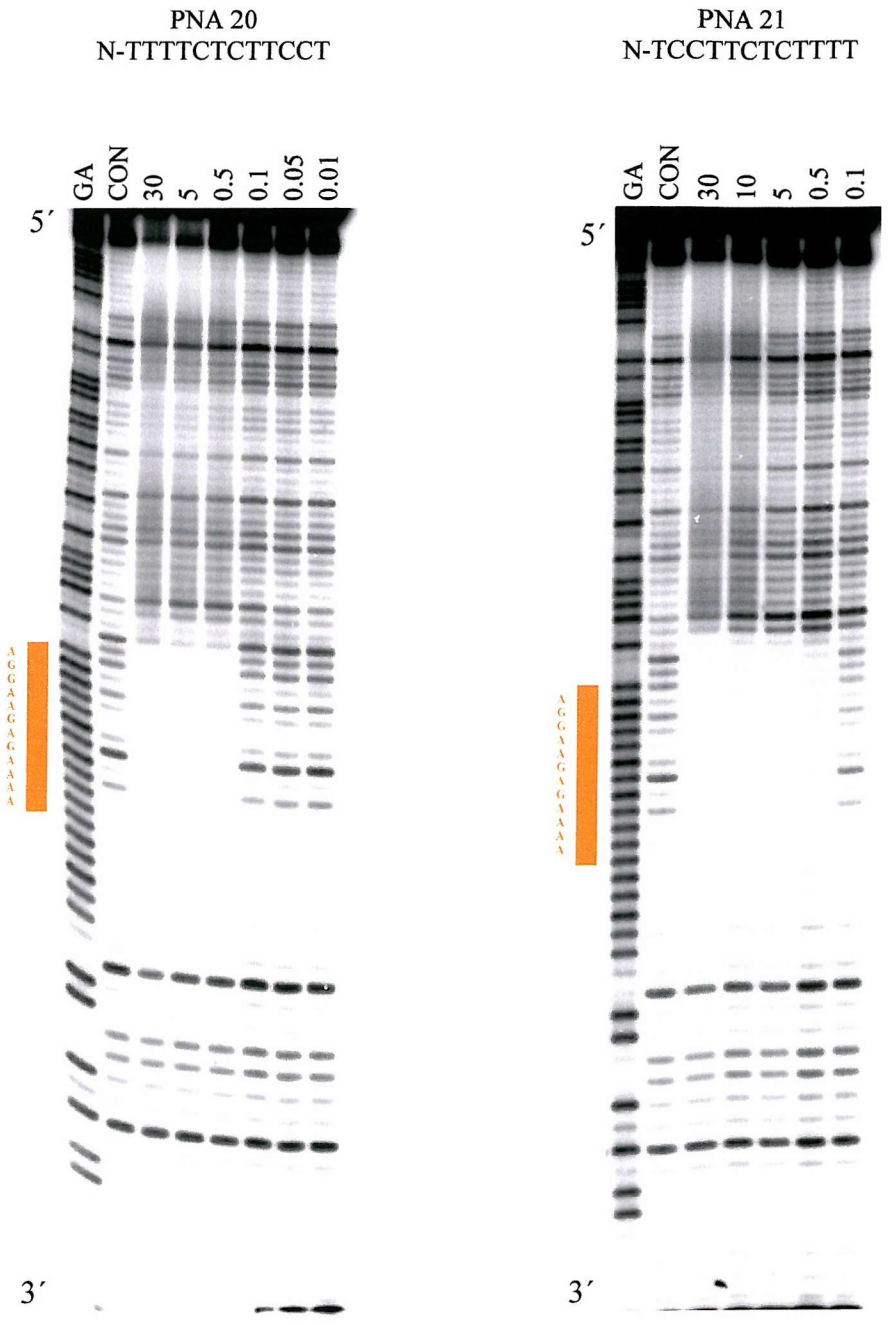

FIGURE 3.1 DNaseI cleavage of the 110bp *tyr*T (43-59) fragment in the presence or absence of PNA 20 and PNA 21. The PNA concentration (μM) is indicated at the top of each gel lane. "CON" indicates digestion of the DNA in the absence of PNA and "GA" is a Maxam-Gilbert marker specific for purines. The location of site 1 is highlighted in orange. All the complexes were incubated for 24 hours in 50mM sodium acetate pH 5.0 before digestion with DNaseI.

observed with DNaseI footprints. The footprint also extends above (5′) the target by a few bases and is similar to that seen with triplex-forming oligonucleotides (the 3′-end of the footprint is usually co-terminus with the end of the target). At high concentrations greater than 5μM there are some non-specific interactions represented as a diffuse region. Similar experiments were also performed on the 160, 190 and 360bp fragments, all of which showed similar footprinting patterns at site 1 as expected (data not shown). Close inspection of these longer fragment patterns reveals the presence of an additional, unexpected, footprint closer to the top of the gel, around position 110. This is more clearly seen with PNA 20 but is also evident with PNA 21. The identity and properties of this secondary PNA binding site are studied in greater detail below (section 3.2.2).

Figure 3.2 shows DNaseI footprints for the 110bp *tyr*T (43-59) fragment in the presence or absence of PNA 41, 42 and 43. It can be seen that, under these conditions (50mM sodium acetate, pH 5.0) all these PNAs produce clear footprints at site 1, which persist to concentrations of about 0.1-0.05μM. At high concentrations (>5μM) there is a general inhibition of cleavage throughout the entire fragment, suggesting that there is some general non-specific binding, though specific footprints are obtained at concentrations of 1μM and below. As expected the exact location and size of the footprints varies between the different PNAs. PNA 41, which was designed to bind to the entire 17-base tract, produced the largest footprint. PNA 42 and 43 bind to very similar regions, though the footprint produced by PNA 42 extends by one or two bases further up the gel (5′) than PNA 43. These footprints are lower down the gel than with PNA 20 and 21 (figure 3.1) and are consistent with their predicted binding sites. Additional experiments with the 160, 190 and 360 base pair

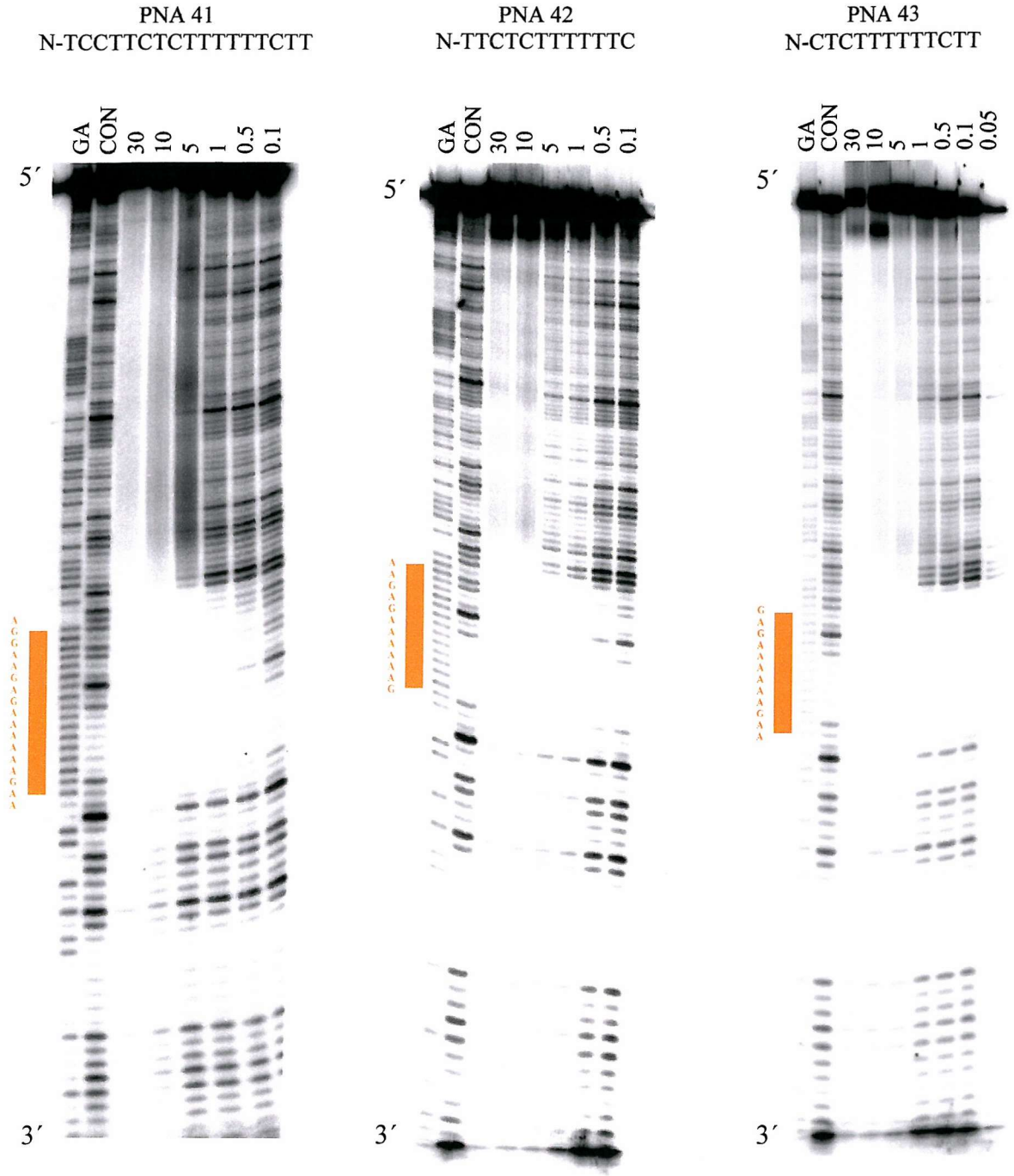

FIGURE 3.2 DNaseI cleavage of the 110bp *tyr*T (43-59) fragment in the presence or absence of PNA 41, 42 and 43. The PNA concentration (μM) is indicated at the top of each gel lane. "CON" indicates digestion of the DNA in the absence of PNA and "GA" is a Maxam-Gilbert marker specific for purines. The location of site 1 is highlighted in orange. All the complexes were incubated for 24 hours in 50mM sodium acetate pH 5.0 before digestion with DNaseI.

fragments of *tyr*T (43-59) produced very similar results and no interaction with the unexpected (secondary) binding site (data not shown).

The intensity of the bands within these footprints was determined at different PNA concentrations, and was used to produce footprinting plots, which are shown in figure 3.3. C_{50} values (the PNA concentration required to reduce the intensity of bands in the footprint by 50%) were determined by fitting simple binding curves to the data, and are presented in table 3.1. From this data is appears that the strongest binding (lower C_{50} value) is produced with PNA 41 (0.04μM ±1) for site 1. PNA 21 has a high affinity for site 1 (0.2μM ±2) whereas PNA 20 shows a weaker binding affinity (2.9μM ±4) for site 1, the difference clearly attributed to its binding polarity. PNA 42 and 43 are also both 12 bases long and differ in their cytosine content and binding locations. This is reflected in their affinities for site 1, PNA 42 having a slightly higher binding affinity (0.4μM ±6) whereas PNA 43 has a slightly low affinity (0.6μM ±2). These values are higher than PNA 21 and could be attributed to the loss of one cytosine residue, reducing the electrostatic attraction between the positively charged cytosine residue and the negative charged DNA backbone. PNA 42 and 43 have higher binding affinities than PNA 20, however the binding affinity for PNA 20 is unpredicted and lower than expected. Additional footprinting gels with PNA 20 have shown a diverse change in the C_{50} values produced. It is particularly interesting to note that the polarity of the PNA sequence only has a marginal effect upon binding, with the parallel sequences (PNA 21 and 42) having very similar C_{50} values when compared to their antiparallel counterparts (PNA 20 and 43 respectively).

These experiments were all performed by incubating the samples for 24 hours at pH 5.0, before digesting with DNaseI. On reducing the incubation period to 2 hours no footprints were observed (figure 3.4), suggesting that these complexes form

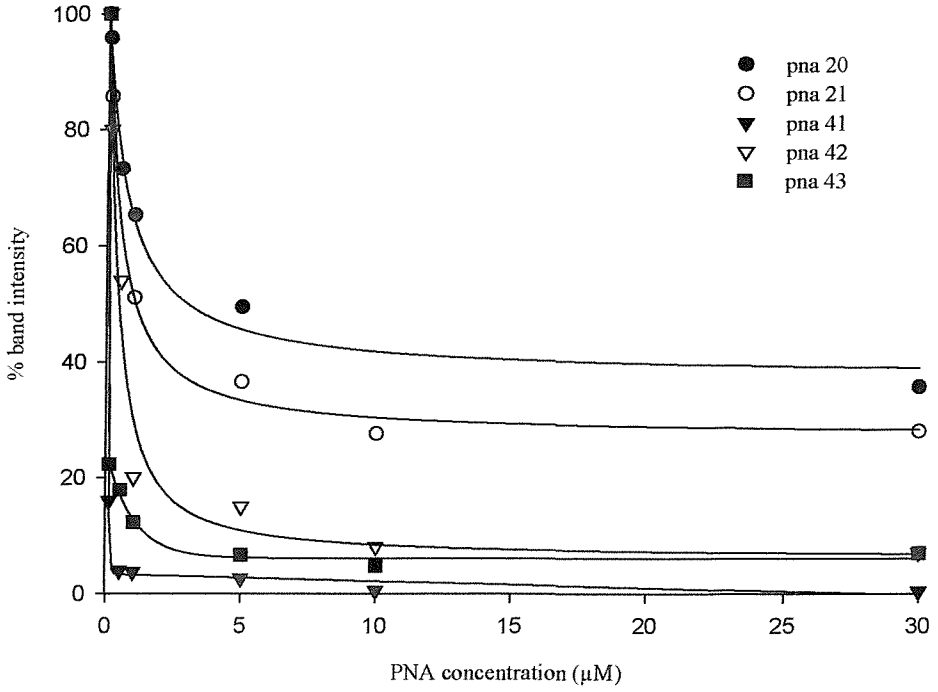

FIGURE 3.3 Footprinting plots showing the intensity of bands at site 1 on the *tyr*T (43-59) fragment as a function of the concentration of PNA 20, 21, 41, 42 and 43. The experiments were performed in 50mM sodium acetate pH 5.0. The curves shown correspond to least squares fits to a simple binding isotherm, as described in the methods section. The C_{50} values for these curves are presented in Table 3.1.

PNA sequence	C_{50} value (μM)	Standard error
20	2.9	± 4
21	0.2	± 2
41	0.04	± 1
42	0.4	± 6
43	0.6	± 2

TABLE 3.1 C_{50} values for different PNA sequences targeted to site 1 on the *tyr*T (43-59) fragment. These were calculated from the data shown in figure 3.3.

extremely slowly. This is consistent with the requirement for strand invasion, though triplexes are also known to form very slowly. Similar experiments performed at pH 7.5 also showed no footprints for any of these PNAs (figure 3.4), even after 24 hours incubation. The requirement for low pH suggests that cytosine protonation is necessary for binding, and suggest that triplex formation is involved in the binding process.

It should be noted that these simple footprinting experiments do not reveal anything about the exact mode of binding (*i.e.* strand invasion or triplex formation). However, the observation that each PNA produces a clear sequence-specific footprint, irrespective of the strand orientation, is informative. For example the sequence of PNA 20 is antiparallel to the purine strand of site 1. It should therefore be able to form an antiparallel Watson-Crick duplex with this target. Simple triplex formation should not be possible with this PNA since, according to the usual rules, the third strand should be oriented parallel to the purine strand of the duplex. However, the requirement for low pH reveals that the complex does require cytosine protonation. If this PNA binds as a third strand then the two pyrimidine strands (involved in Watson-Crick and Hoogsteen base pairing) must be oriented parallel to each other. The observed footprints suggest that PNA strand orientation is less important than with DNA oligonucleotides. Similar arguments can be made for the other PNAs.
The mode of binding of these PNAs is examined below in experiments with S1 nuclease (section 3.4) and is considered further in the Discussion. Bandshift analysis of these complexes is also described in section 3.3.

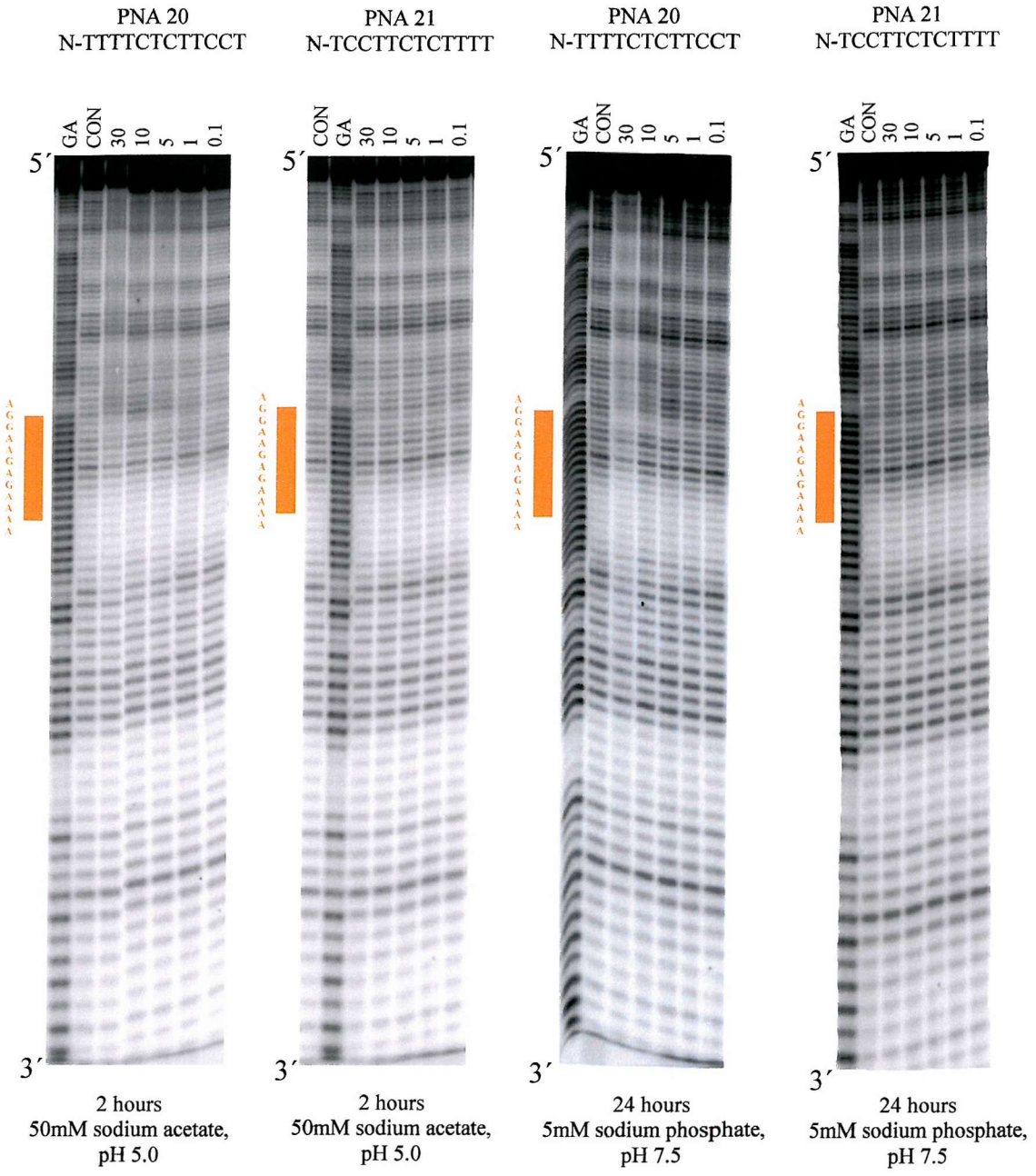

FIGURE 3.4 DNaseI cleavage of the 160bp *tyr*T (43-59) fragment in the presence or absence of PNA 20 and 21. The PNA concentration (μM) is indicated at the top of each gel lane. "CON" indicates digestion of the DNA in the absence of PNA and "GA" is a Maxam-Gilbert marker specific for purines. The location of site 1 is highlighted in orange. The complexes were incubated for 2 hours in 50mM sodium acetate pH 5.0 or for 24 hours in 5mM sodium phosphate pH 7.5 before digestion with DNaseI.

3.2.2 Secondary PNA binding site on *tyr*T (43-59)

As previously noted a second unexpected DNaseI footprint was observed with PNA 20 and 21 between positions 107-120. This region contains an imperfect oligopurine tract, which does not appear to be related to either of these PNA sequences. The properties of this site were further examined by performing DNaseI footprinting experiments with the 360 base pair fragment. This secondary site is most easily seen with this fragment since it is labelled at the *Hind*III end, bringing this site closer to the bottom of the gel. Figure 3.5 shows DNaseI footprints for the 360bp *tyr*T (43-59) fragment in the presence of absence of PNA 20 and 21. For this fragment the expected target (site 1) is labelled on the pyrimidine strand while the secondary site is labelled on the purine-rich strand. As expected both PNAs produce clear footprints at their expected target site 1, which persist to very low concentrations as seen with the 110bp *tyr*T (43-59) fragment (section 3.2.1). However, labelling on this strand reveals that the size of this footprint varies with PNA concentration, and a larger region is protected from cleavage at the higher concentrations. The reason for this is not clear, though a few explanations can be suggested. Firstly it is possible that these PNAs have secondary binding sites within the 17 base oligopurine tract, and these are only apparent at the highest concentrations. Alternatively this may reflect changes in the mode of binding of the PNA. It is possible that at low concentrations the PNA only binds as a third strand while higher concentrations may produce a strand invasion (plus triplex) complex. These possibilities will be considered further in the discussion. PNA 20 and 21 produce clear footprints at the secondary binding site, though this is much stronger for PNA 20 for which the protection persists to 0.05μM in contrast to that for PNA21, which is only evident at concentration of 30μM and

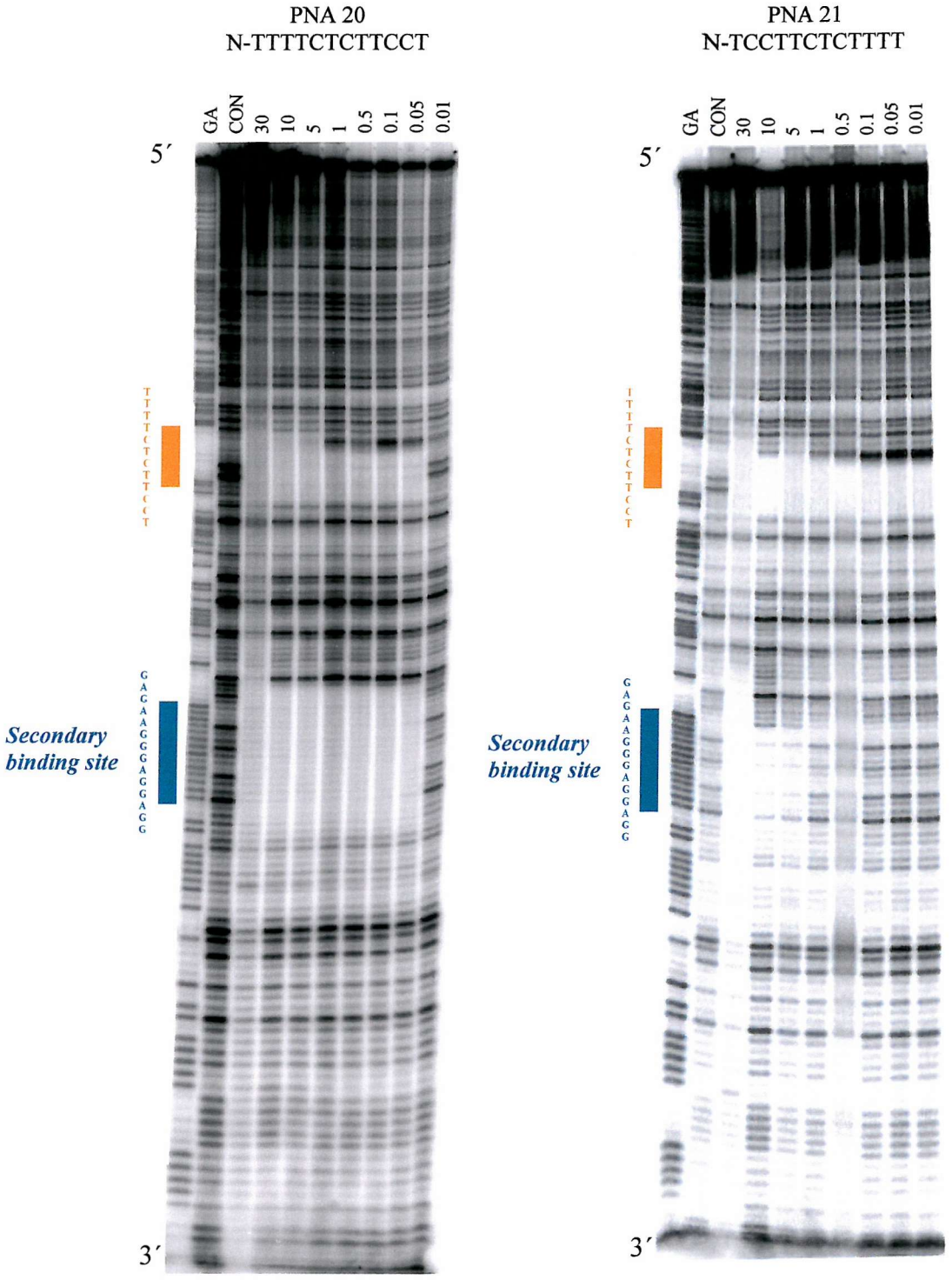

FIGURE 3.5 DNaseI cleavage of the 360bp *tyr*T (43-59) fragment in the presence or absence of PNA 20 and 21. The PNA concentration (μM) is indicated at the top of each gel lane. "CON" indicates digestion of the DNA in the absence of PNA and "GA" is a Maxam-Gilbert marker specific for purines. All the complexes were incubated for 24 hours in 50mM sodium acetate pH 5.0 before digestion with DNaseI. Site 1 is indicated in orange, while the secondary binding site is shown in green.

above. The footprints cover the entire 14 base oligopurine tract and extend by four bases towards the 5′-end and by 12 bases towards the 3′-end. The reason for this is not clear and will be considered in the discussion.

Footprinting plots for the binding of PNA 20 and 21 at this secondary site are shown in figure 3.6 from which the C_{50} values have been calculated and are shown in table 3.2. It is evident that PNA 21 binds to its intended target site much better than to this secondary site. This is reflected in its higher C_{50} values of 22.2μM ±0.9 for the secondary binding site. However, PNA 20 appears to have higher affinity for the secondary binding site in comparison to site 1 which is reflected in its C_{50} value (<0.005). The origin of this secondary binding site is not clear and will be considered further in the discussion. However, the existence of this secondary site will be important for proper interpretation of the bandshifts (section 3.3) and the interaction with nucleosomal DNA (chapter 4). Similar experiments with PNA 005, 008, 009, 41, 42 and 43 did not reveal any protection from DNaseI cleavage at this secondary binding site (data not shown).

3.2.3 Site 2 on *tyr*T (22-33) targeted with PNA 005, 008 and 009

Site 2 on *tyr*T (22-33) can be targeted with PNA 005, 008 and 009. PNA 005 is 10 bases long and since it is a palindromic sequence it can bind in either a parallel or antiparallel orientation. PNA 008 and 009 are both 12 bases long and have opposite sequences with PNA 008 parallel and PNA 009 antiparallel to the purine strand of the target.

Figure 3.7 shows DNaseI cleavage of the 110bp *tyr*T (22-33) fragment in the presence or absence of PNA 005, 008 and 009. The target is labelled on the

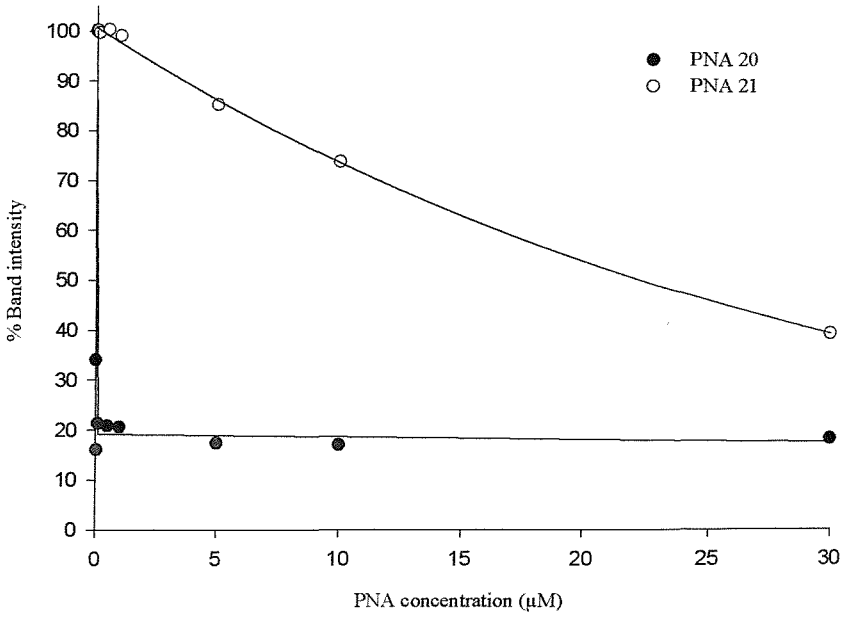

FIGURE 3.6 Footprinting plots showing the intensity of bands in secondary binding site of the *tyr*T (43-59) fragment as a function of the concentration of PNA 20 and 21. The experiments were performed in 50mM sodium acetate pH 5.0. The curves shown correspond to least squares fits to a simple binding isotherm, as described in the methods section. The C_{50} values for these curves are presented in table 3.2.

PNA sequence	C_{50} value (μM)	Standard error
20	<0.005	± 2.2
21	22.2	± 0.9
41	no footprint	-
42	no footprint	-
43	no footprint	-
005	no footprint	-
008	no footprint	-
009	no footprint	-

TABLE 3.2 C_{50} values for different PNA sequences at the secondary binding site on the 160bp *tyr*T (43-59) fragment. The C_{50} values for PNA 20 and 21 were calculated from data shown in Figure 3.6.

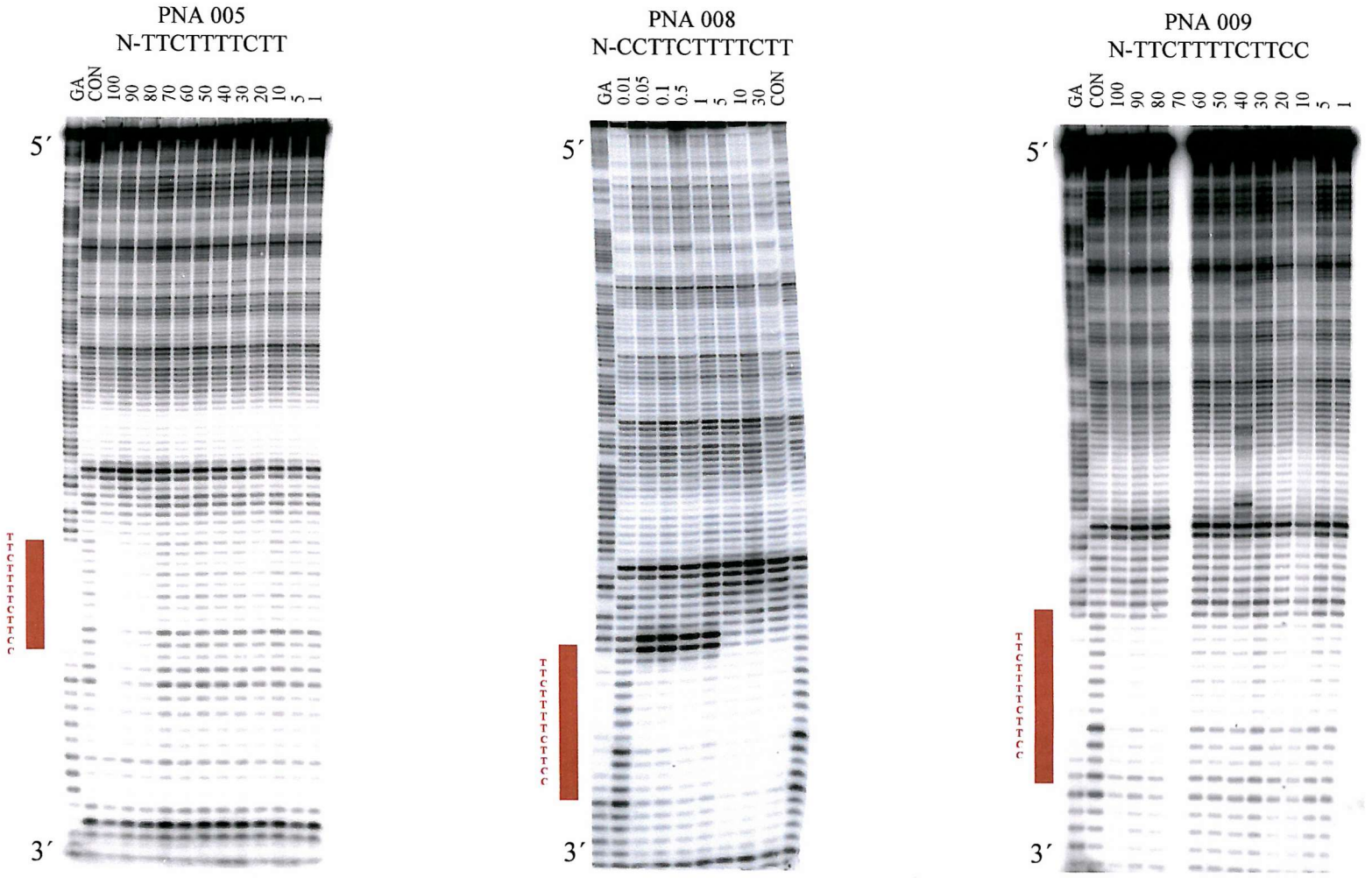

FIGURE 3.7 DNaseI cleavage of the 110bp *tyr*T (22-33) fragment in the presence or absence of PNA 005, 008 and 009. The PNA concentration (μM) is indicated at the top of each gel lane. "CON" indicates digestion of the DNA in the absence of PNA and "GA" is a Maxam-Gilbert marker specific for purines. All the complexes were incubated for 24 hours in 50mM sodium acetate pH 5.0 before digestion with DNaseI. Site 2 is indicated in brown.

pyrimidine-containing strand. It can be seen that these PNAs produce footprints at each of their targets, though at very different concentrations. PNA 005 and PNA 009 only affect DNaseI cleavage at the highest concentrations and the footprints do not persist below about 70 and 50μM respectively. In contrast PNA 008 produces a clear footprint which covers the entire oligopurine tract, and which persists to a concentration of about 0.05μM. The size of the footprint with PNA 008 varies with PNA concentration (as noted for the interaction of PNA 20 and 21 with the pyrimidine-labelled target site), and is larger at higher PNA concentrations. This may indicate a concentration-dependent change in the binding mode, which is only evident when examining the pyrimidine-labelled strand. This is not evident with PNA 005 and 009. In contrast to PNA 20 none of these PNAs show any secondary binding sites which can be clearly seen with the 360bp *tyr*T (22-33) fragment shown in figure 3.8. Additional experiments carried out on the 160 and 190 fragments derived from *tyr*T (22-33) showed similar footprints (data not shown).

These experiments were all performed by incubating the samples for 24 hours at pH 5.0, before digesting with DNaseI. On reducing the incubation period to 2 hours no footprints were observed (data not shown), suggesting that these complexes have a slow rate of complex formation. This is also consistent with the requirement for strand invasion as previously stated. Similar experiments performed at 5mM sodium phosphate pH 7.5 which also showed no footprints where present at physiological concentrations whereas at very high PNA concentrations, very weak interactions where present. The requirement for low pH suggests that cytosine protonation is necessary for binding, and suggest that triplex formation is involved in the binding process for these PNA sequences.

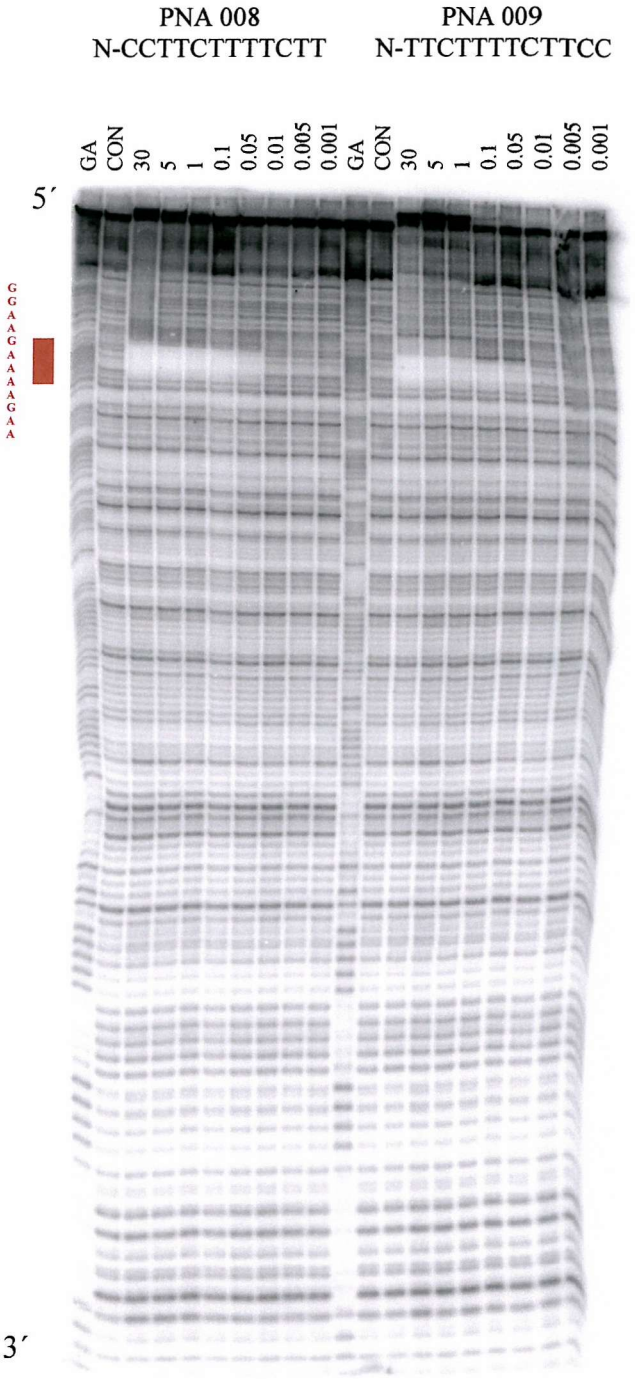

FIGURE 3.8 DNaseI cleavage of the 360bp *tyr*T (22-33) fragment in the presence or absence of PNA 008 and 009. The PNA concentration (μM) is indicated at the top of each gel lane. "CON" indicates digestion of the DNA in the absence of PNA and "GA" is a Maxam-Gilbert marker specific for purines. All the complexes were incubated for 24 hours in 50mM sodium acetate pH 5.0 before digestion with DNaseI. Site 2 is indicated in brown.

Footprinting plots derived from these data are shown in figure 3.9, and the C_{50} values for these interactions are presented in table 3.3. From this data is appears that the weakest binding (higher C_{50} value) is produced with PNA 005 (~89μM ±3), which results in very poor binding affinity for site 2. PNA 008 has a high affinity for site 2 (0.4μM ±0) whereas PNA 009 shows a weaker binding affinity (36μM ±5) for site 2, their differences attributed to binding polarity. As for PNA 005, very weak binding is present due to its 10 base pair sequence length and could also be due to a limited number of cytosine residues that has shown to be a factor that affects PNA binding affinity. The binding orientation of PNA 005 cannot be fully studied in these experiments due to low binding affinity more than likely being dependent on PNA length. The effect of cytosine content can be seen between PNA 20 and 009 where their sequence length and polarity is the same and the cytosine content is difference, PNA 21 having an additional cytosine residue, which is reflected in a lower binding affinity.

3.2.4 Sites 1 and 3 on *tyr*T (43-59, 122-133) targeted with PNA 005, 008, 009, 20 and 21

*Tyr*T (43-59,122-133) is derived from *tyr*T (43-59) and contains two oligopurine tracts. This fragment was prepared for the studies with nucleosomal DNA (described in chapter 4), so as to examine the effect of two PNAs on nucleosome structure. One of these target sites is the same as site 1 in *tyr*T (43-59), while the other has the same sequence as site 2, but is located within a different sequence context at the other end of the fragment, and is designated site 3. These two oligopurine tracts can be targeted with the same PNAs as for site 1 and 2 in *tyr*T

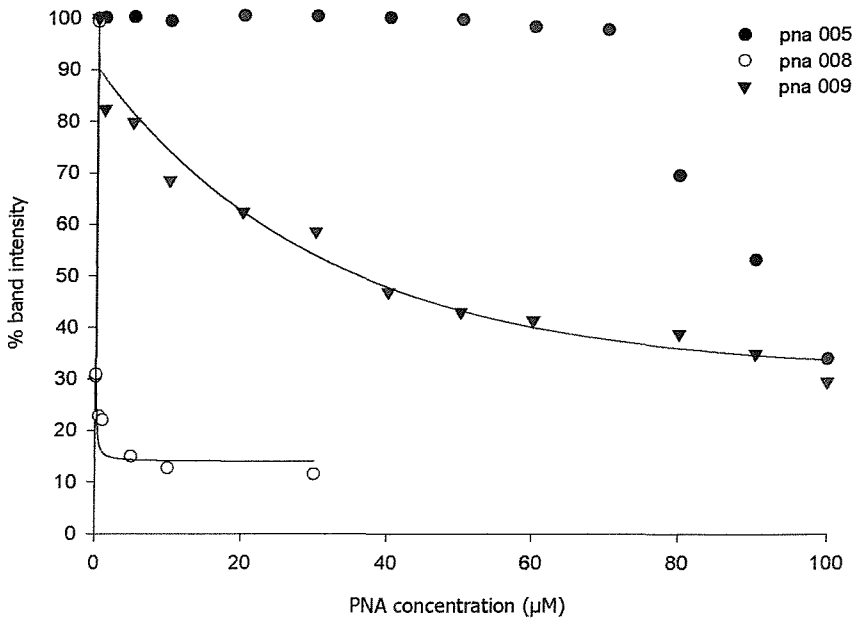

FIGURE 3.9 Footprinting plots showing the intensity of bands in site 2 on the 110bp *tyr*T (22-33) fragment as a function of the PNA concentration. The experiments were performed in 50mM sodium acetate pH 5.0. The curves shown correspond to least squares fits to a simple binding isotherm, as described in the Methods section. The C_{50} values for these curves are presented in table 3.3.

PNA sequence	C_{50} value (μM)	Standard error
005	~89	± 3
008	0.04	± 0
009	36	± 5

TABLE 3.3 C_{50} values for the interaction of different PNAs with site 2 on the 110bp *tyr*T (22-33) fragment. The C_{50} values calculated from the data shown in figure 3.9.

(43-59) and *tyr*T (22-33).

Figure 3.10 shows DNaseI cleavage patterns for the 190bp fragment, derived from *tyr*T (43-59,122-133), in the presence and absence of PNA 008, 009, 20and 21. In the left hand panel the DNA is labelled at the 3′-end of the *EcoR*I site (visualising the purine strand of site1 and the pyrimidine strand of site 3), while the right hand panel the DNA is labelled at the 3′-end of the *Hind*III site (revealing the pyrimidine strand of site 1 and the purine strand of site 3). From these patterns it can be seen that PNA 008 produces a clear footprint at site 3, which persists to low concentrations. Although this site is towards the top of the gel for the pyrimidine-labelled strand (left-hand panel) it again appears that this footprint is larger with 30μM than 10μM PNA 008. This PNA also produces a weak secondary footprint around site 1 (evident in the left hand panel) at the highest concentration. Higher concentrations of PNA 009 than 008 are required to produce a footprint at site 3 (similar to that seen with site 2 in figure 3.7) and this PNA shows no secondary binding sites. PNAs 20 and 21 show the expected footprints towards the 5′-end of site 1, which persist to low concentrations, with additional protection around the secondary binding site at positions 107-120 in the presence of PNA 20. Both sequences show no interactions at site 3. Similar experiments were performed in 50mM sodium acetate pH 5.0 with an incubation time of 2 hours and in 5mM sodium phosphate pH 7.5, all of which showed similar results as already stated (data not shown).

Footprinting plots for the interaction of PNA 005, 008 and 009 with site 3 are shown in figure 3.11 and the C_{50} values are presented in table 3.4. This data has produced C_{50} values for PNA 005, 008 and 009 (~85μM ±3, 0.06μM ±0.6, 37μM ±2 respectively) which are comparable to those obtained at site 2. Differences in binding

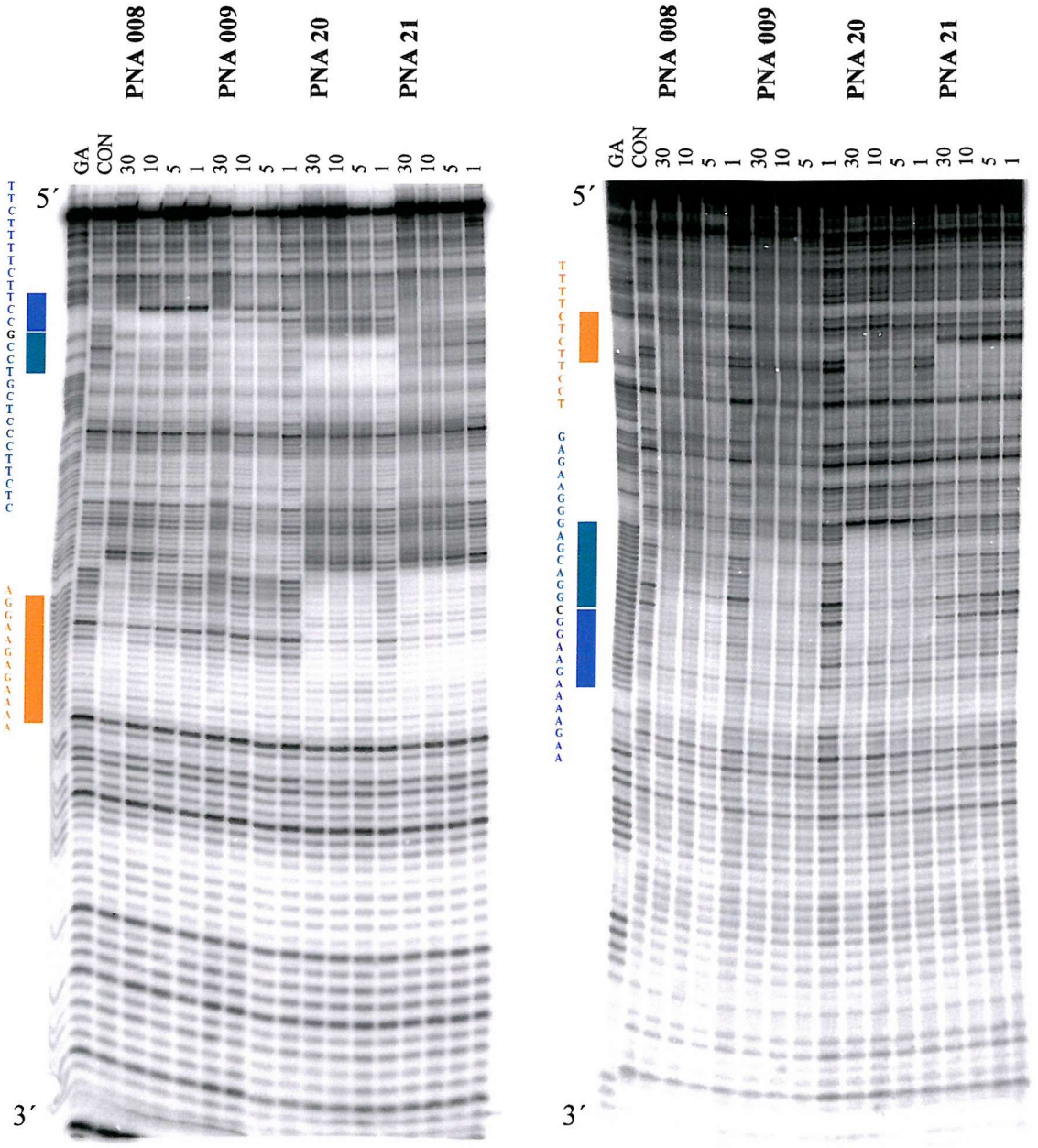

FIGURE 3.10 DNaseI cleavage patterns for the 190bp *tyr*T (43-59, 122-133) fragment in the presence or absence of PNA 008, 009, 20 and 21. The PNA concentration (μM) is indicated at the top of each gel lane. "CON" indicates digestion of the DNA in the absence of PNA and "GA" is a Maxam-Gilbert marker specific for purines. All the complexes were incubated for 24 hours in 50mM sodium acetate pH 5.0 before digestion with DNaseI. Site 1 is highlighted in orange, site 3 in blue, and the secondary binding site is shown in green.

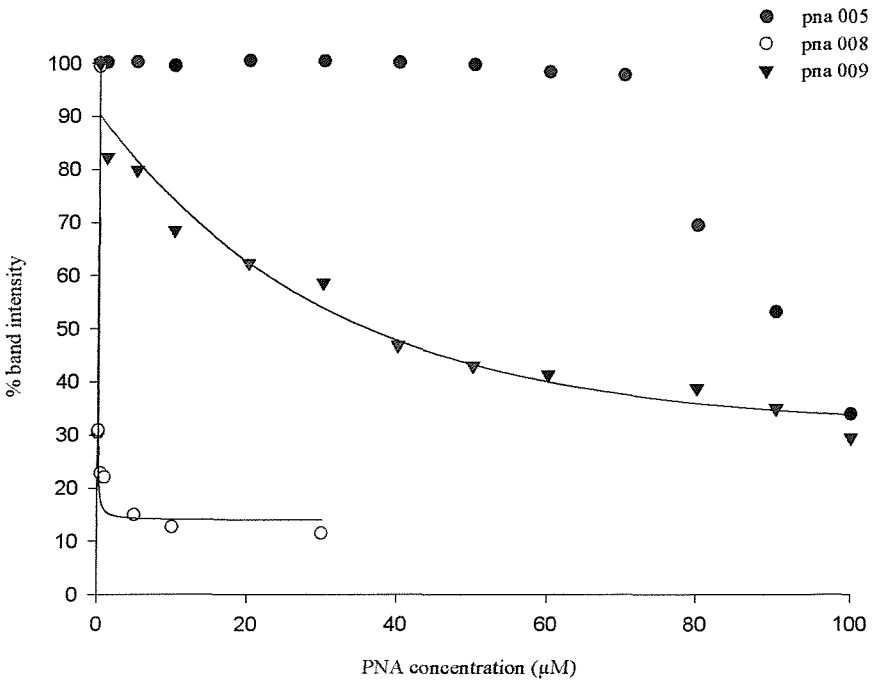

FIGURE 3.11 Footprinting plots showing the interaction of PNA 005, 008 and 009 with site 3 in the *Hind*III labelled 190bp *tyr*T (43-59,122-133) fragment. The experiments were performed in 50mM sodium acetate pH 5.0. The curves shown correspond to least squares fits to a simple binding isotherm, as described in the Methods section. The C_{50} values for these curves are presented in Table 3.4.

PNA sequence	C_{50} value (μM)	Standard error
005	~85	± 3
008	0.06	± 0.6
009	37	± 2
20	no footprint	-
21	no footprint	-

TABLE 3.4 C_{50} values for the interaction of different PNAs with site 3 on the *Hind*III labelled 190bp *tyr*T (43-59,122-133) fragment. The C_{50} values were calculated from data shown in Figure 3.11.

affinity for PNA 008 and 009 has been evident at site 3 which is also present at site 2, attributed to their binding polarity. PNA 005 has very weak binding due to sequence length and it is also partially contributed to limited cytosine residues as already discussed. These comparable affinities between site 3 and 2 show that an identical base sequence site has been mutated and targeted with their sequence specific PNAs, located in the correct position and results in no non-specific binding.

3.3 Gel retardation (bandshift) assays

The formation and stability of the PNA/DNA complexes identified by DNaseI footprinting in the previous section were also analysed using gel retardation assays (bandshift analysis) from which dissociation constants (K_d) for the interactions were calculated. This calculates the concentration required when half the active PNA sites are occupied, comparable to C_{50} values. The experiment where duplicated and run at both room temperature and 4°C, in case there was any dissociation of the complexes during running of the gel. In each case there was no significant difference between the results at these two temperatures (see figure 3.13B), and subsequent results for only the room temperature electrophoresis have been shown.

3.3.1 Site 1 on *tyr*T (43-59) targeted with PNA 20 and 21

Figure 3.12 show the effects of PNA 20 and 21 on gel mobility with the 110bp *tyr*T (43-59) fragment. Both sequences have been added individually and in combination because PNA 20 and 21 are reverse sequences, PNA 21 binding parallel

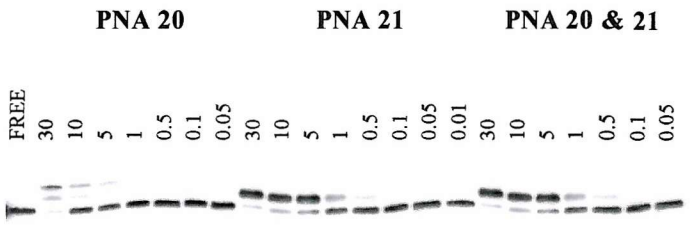

FIGURE 3.12 Bandshift assays of the 110bp fragment derived from *tyr*T (43-59) in the presence of increasing concentrations of PNA 20 and 21. The PNA concentration (μM) is shown at the top of each lane, the lane labelled "free" corresponds to DNA in the absence of added PNA. All the complexes were incubated for 24 hours in 50mM sodium acetate pH 5.0 before electrophoresis.

and PNA 20 binding antiparallel to the purine strand. This combination will promote the formation of a triple helix with strand invasion where the Hoogsteen bound third strand runs parallel to the purine strand of the Watson and Crick PNA/DNA duplex, promoting strand invasion. When added individually there is a reduction in DNA mobility in a concentration-dependent fashion, producing a single retarded species for PNA 21 and two retarded species for PNA 20. Looking first at the results for PNA 20 there is an increase in the amount of retarded DNA with increasing PNA. The higher retarded band is of greater intensity that the lower one and has a greater effect on mobility and although they have different intensities, they show similar concentration dependence. The presence of two retarded bands will be explained in more detail in section 3.5. The addition of PNA 21 produces one retarded band, which has a less significant effect on the DNA mobility in comparison to PNA 20. However, PNA 21 and PNA 20 in combination produce the same effect on mobility to PNA 21 implying that identical complexes are formed. In the presence of PNA 20 and 21 in combination, triplex strand invasion should be predominately formed which raises the

question as to whether PNA 21 is forming the same complex independent of potential polarity constraints. This will discussed further in section 3.5.

Figure 3.13 show the effects of PNA 20 on the gel mobility of the 110bp *tyr*T (43-59) fragment run at room temperature and at 4°C. This fragment contains only one oligopurine tract (site 1), and is too short to contain the secondary binding site, noted on the longer fragments, which is located beyond position 100. It can be seen that PNA 21 reduces the DNA mobility in a concentration-dependent fashion, producing a single retarded species. Looking first at the results for PNA 20 (figure 3.13A) run at room temperature there is a steady increase in the amount of retarded DNA with increasing PNA, with a concentration of around 50μM required to retard half of the DNA. Quantitative analysis of these data reveals a C_{50} value of 41μM (±8.6) at room temperature (see table 3.5 on page 155). Surprisingly this value is much higher than the C_{50} value estimated from the DNaseI footprints, suggesting that the two techniques may be measuring the formation of different types of complexes. This trend is mirrored at 4°C with a comparable C_{50} value of 42.4μM (±7.8) (figure 3.13B). This showed that there is no dissociation during gel electrophoresis at room temperature. Similar results are seen with PNA 21 at room temperature (figure 3.14), which binds more tightly than PNA 20, with a C_{50} value of 2.6μM (±6.1). This is also evident at 4°C, which has a C_{50} value of 2.7μM (±5.6) (data not shown). Again this is still much higher than estimated by DNaseI footprinting, suggesting that the binding mode detected by bandshift analysis could be measuring different complexes but does show that the parallel sequence PNA 21 binds more tightly than the antiparallel sequence PNA 20.

Bandshift analysis was performed at low salt and high pH, to promote strand invasion and confirm the DNaseI data, which identified the absence of

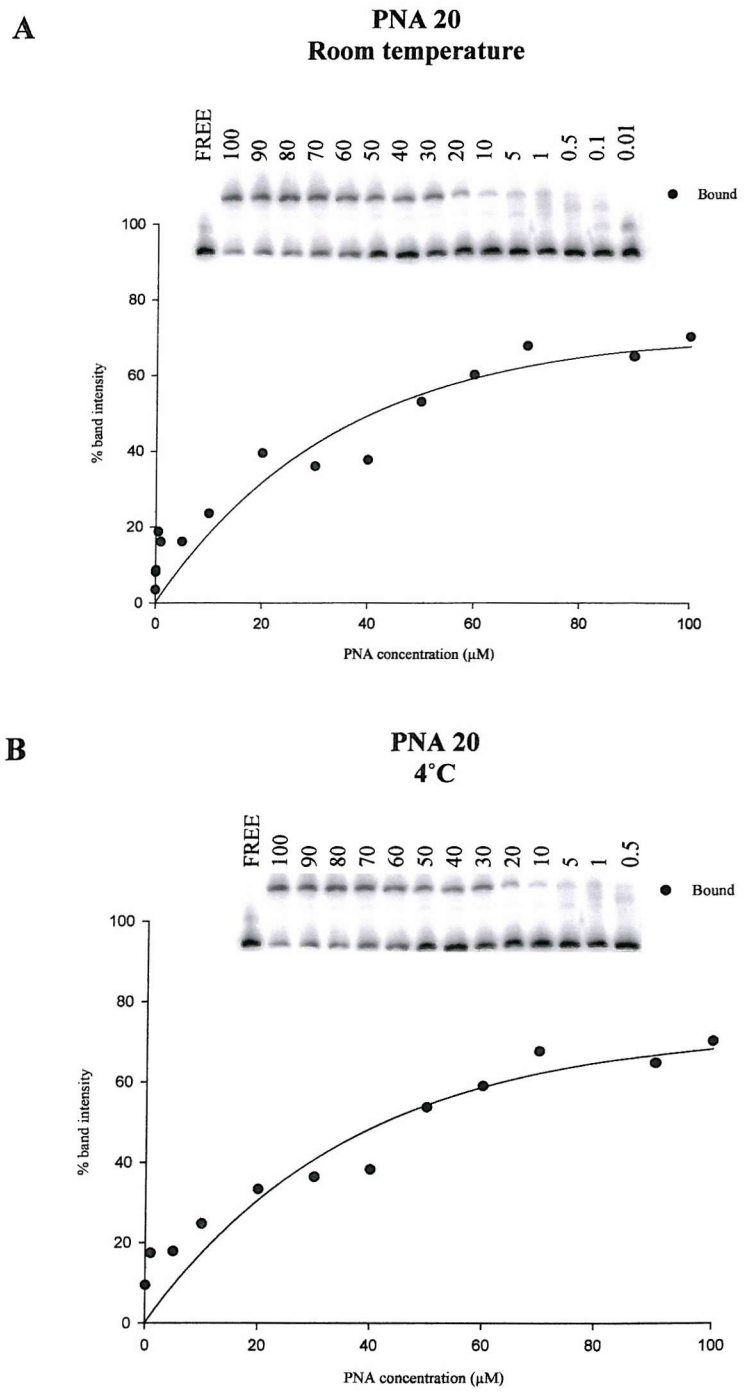

FIGURE 3.13 Bandshift assays of the 110bp fragment derived from *tyr*T (43-59) in the presence of increasing concentrations of PNA 20 run at (A) room temperature and (B) 4°C. The autoradiograph is shown along with the corresponding plot showing the percentage of DNA in the retarded band against PNA concentration. The PNA concentration (μM) is shown at the top of each lane, the lane labelled "free" corresponds to DNA in the absence of added PNA. All the complexes were incubated for 24 hours in 50mM sodium acetate pH 5.0 before electrophoresis.

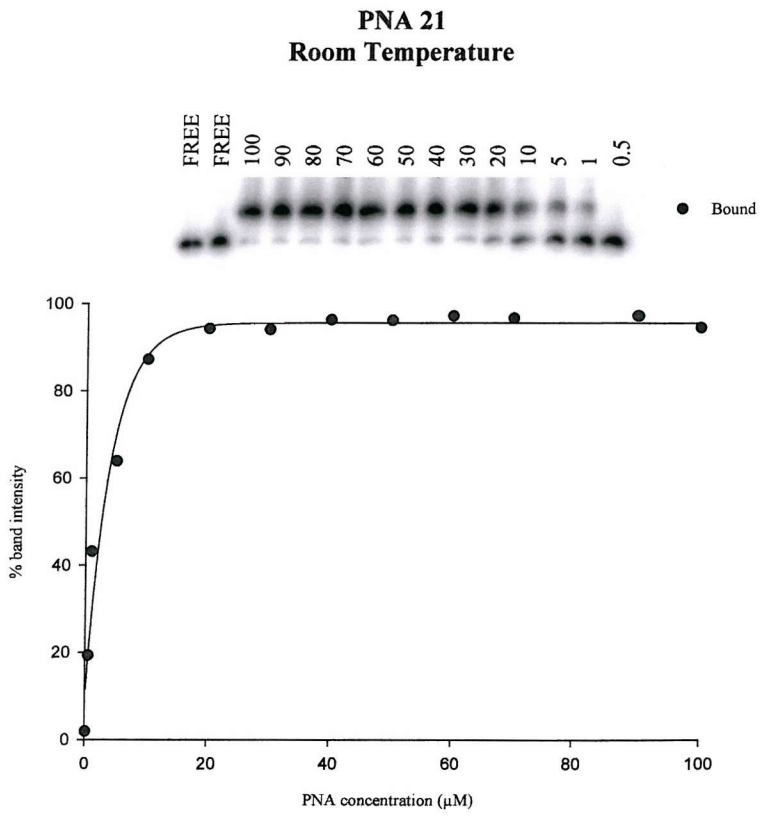

FIGURE 3.14 Bandshift assays of the 110bp fragment derived from *tyr*T (43-59) in the presence of increasing concentrations of PNA 21 run at room temperature. The autoradiograph is shown along with the corresponding plot showing the percentage of DNA in the retarded band against PNA concentration. The PNA concentration (μM) is shown at the top of each lane, the lane labelled "free" corresponds to DNA in the absence of added PNA. All the complexes were incubated for 24 hours in 50mM sodium acetate pH 5.0 before electrophoresis.

footprints at site 1 at high PNA concentrations (figure 3.4). Figure 3.15 shows the effects of PNA 20 and 21 on the gel mobility of the 110bp *tyr*T (43-59) fragment when the samples were incubated in 5mM sodium phosphate, pH 7.5 for 24 hours. For PNA 20, two very weak retarded bands are present at high PNA concentrations, the higher band having a slightly greater intensity than the lower band. Subsequent quantitative analysis shows that the higher complex, which has a greater effect on the DNA mobility, has retarded the DNA by 20% at a PNA concentration of 100μM, clarifying its weak affinity. The lower band has an even greater reduction on the retarded DNA and less of an effect on the mobility. For PNA 21 only one retarded band is present which has retarded the DNA by 45% at a PNA concentration of 100μM. The C_{50} values for both complexes cannot be resolved due to very weak binding. These results have supplemented the DNaseI results and shown that complex formation at low salt and high pH results in weak complex stability at very high PNA concentrations and reiterates the importance and requirement for triplex formation in PNA complex stability.

3.3.2 Interaction of PNA20 and 21 with longer *tyr*T (43-59) fragments

Figures 3.16 show bandshifts for the 360bp *tyr*T (43-59) fragment in the presence of PNA 20 and 21. This longer fragment contains the secondary binding site for these PNAs, noted above (section 3.2.2), as well as site 1. It can be seen that two retarded bands are produced with each of these PNAs. In each case the retarded bands appear in a concentration dependent fashion and, although they have different intensities, they show similar concentration dependence. The appearance of two retarded species is puzzling and cannot simply be explained by the presence of two

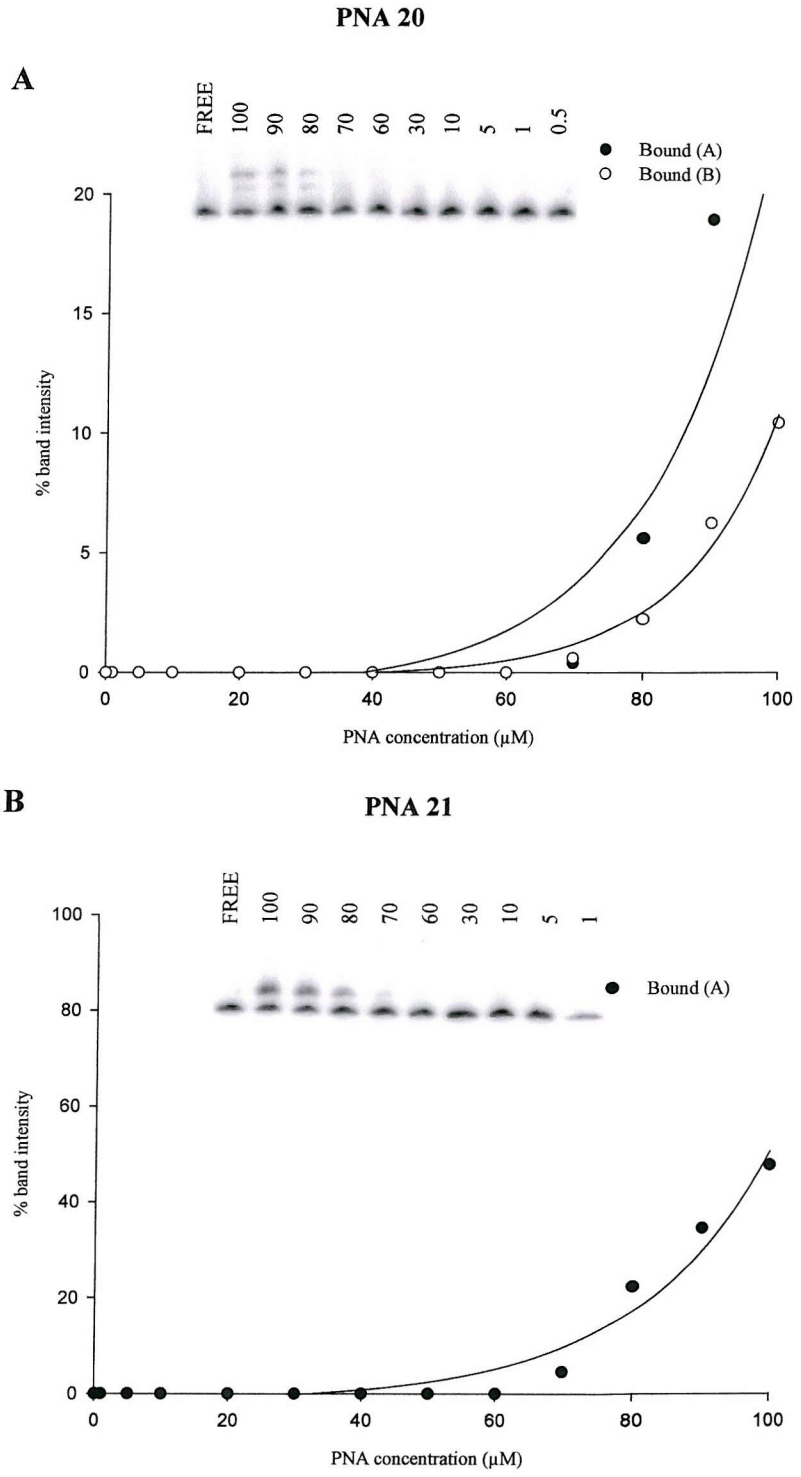

FIGURE 3.15 Bandshift assays of the 160bp fragment derived from *tyr*T (43-59) in the presence of increasing concentrations of PNA 20 (A) and 21 (B) run at room temperature. The autoradiograph is shown along with the corresponding plot showing the percentage of DNA in the retarded band against PNA concentration. The PNA concentration (μM) is shown at the top of each lane, the lane labelled "free" corresponds to DNA in the absence of added PNA. The samples were incubated in 5mM sodium phosphate pH 7.5 prior the electrophoresis.

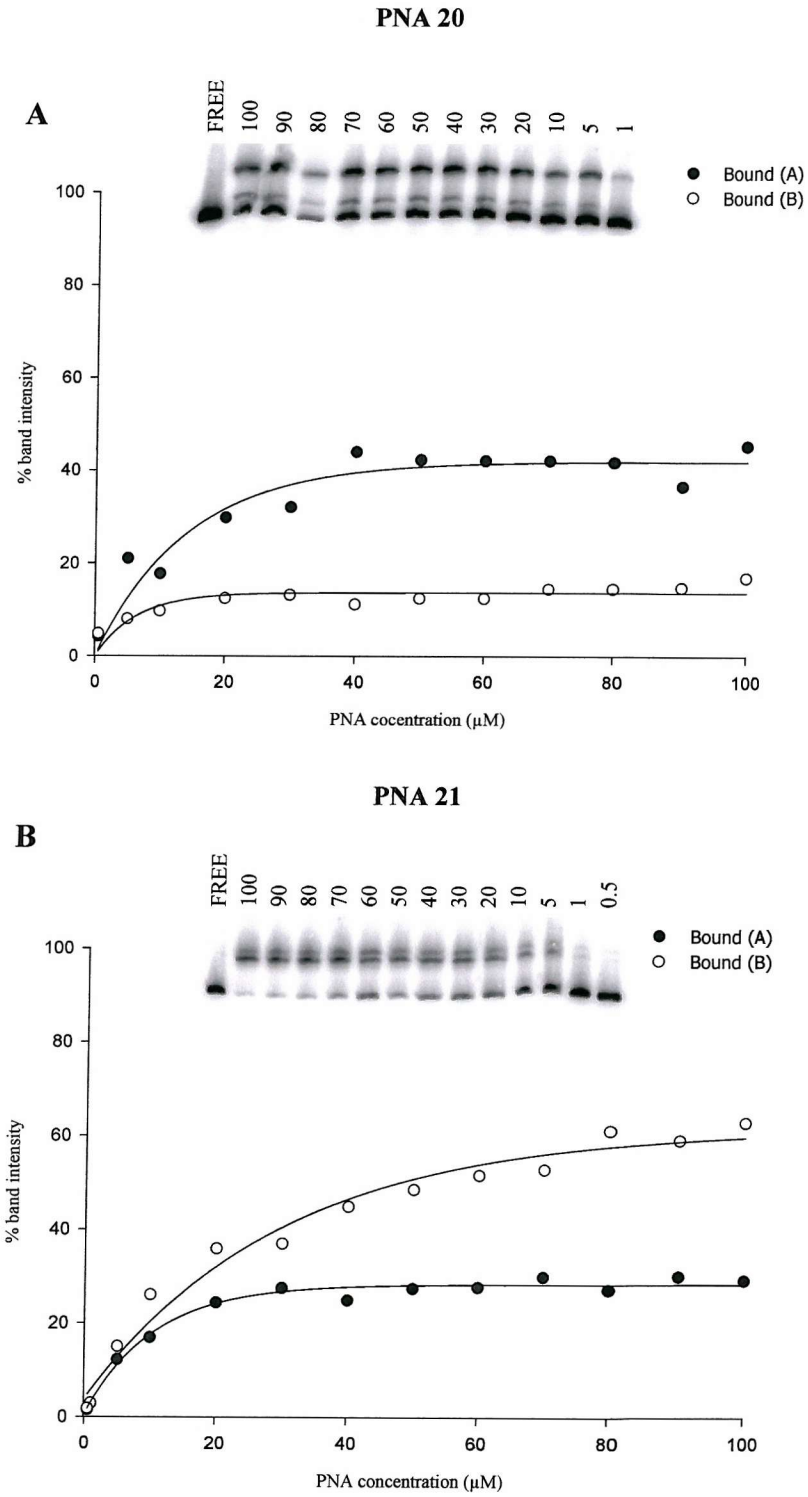

FIGURE 3.16 Bandshift assays of the 360bp *tyr*T (43-59) fragment in the presence of increasing concentrations of PNA 20 (A) and 21 (B) run at room temperature. The autoradiograph is shown along with the corresponding plot showing the percentage of DNA in the retarded bands against PNA concentration. The PNA concentration (μM) is shown at the top of each lane, the lane labelled "free" corresponds to DNA in the absence of added PNA. All the complexes were incubated for 24 hours in 50mM sodium acetate pH 5.0 before electrophoresis.

binding sites (site 1 and the secondary site). We would expect the binding of PNA to two independent sites on the fragment to produce two retarded species corresponding to DNA molecules with one or two PNA molecules bound (assuming that the two singly bound sites have similar effects on the mobility). However, at high concentrations both sites should be occupied, generating only one retarded species. Although the two retarded bands have different intensities, they are both present at all PNA concentration in approximately the same proportions. It therefore appears that these the two bands cannot correspond to the interaction of PNA with the two binding sites, though any explanation for their presence must consider why this does not occur with the shorter DNA fragment. The mobility of the two complexes are different for PNA 20 and 21. The two retarded bands A and B for PNA 20 have a different effect on the mobility, band A having a greater effect compared to band B. In comparison to PNA 21, bands A and B have a very similar mobility, band A having a slightly greater effect on mobility, which indicates that different complexes are formed which will be discussed in section 3.5. Quantitative analysis of these bandshifts are shown in figure 3.16 where the C_{50} values for the two retarded complexes can not be calculated due to the inability to retarded the DNA above 50% at the concentrations studied. This is considered further in the Discussion in the light of the DNaseI and S1 cleavage data. The concentrations required to produce these changes in mobility are again much higher than those seen with the DNaseI footprinting experiments.

3.3.3 Site 2 on *tyr*T (22-33) targeted with PNA 005, 008 and 009

Figure 3.17 show the effects of PNA 008 and 009 on gel mobility with the 110bp *tyr*T (22-33) fragment. Both sequences have been added individually, PNA

008 binding parallel and PNA 009 binding antiparallel to the purine strand. Looking first at the results for PNA 008 there is one retarded band which increases in the amount of retarded DNA with increasing PNA. The retarded band has less of an affect on mobility in comparison to the complex formed with PNA 009. For PNA 009 there is also only one retarded band present which in concentration dependent and has a greater effect on the mobility. This is comparable to PNA 20 and 21 where a greater effect on DNA mobility is present with the antiparallel sequence (PNA 20) as also seen with PNA 009 and less effect is present with the two parallel sequences PNA 008 and 20. This identifies differences in parallel and antiparallel PNA interactions on the DNA architecture and will discussed further in section 3.5.

Figure 3.18 and 3.19 shows the effects of PNA 005, 008 and 009 on the gel mobility of the 110bp fragment from *tyr*T (22-33), containing site 2. As expected these PNAs produce one retarded band, which appears in a concentration-dependent fashion. The interaction with PNA 005 is weak and the retarded band only appears at high PNA concentrations; only 40% of the DNA is retarded in the presence of 100μM PNA so a subsequent C_{50} value cannot be resolved. PNA 008 and 009 produce a retarded band at lower concentrations than PNA 005, in a similar manner to that seen with PNA 20 and 21 at site 1. PNA 008, which is parallel to the duplex purine strand, shows a lower C_{50} value of 6.1μM ±3.0 compared to PNA 009 (51.27μM ±5.2). These values are also a lot higher than the C_{50} values estimated from the DNaseI footprints, suggesting again that the two techniques may be measuring the formation of different types of complexes. This is similar to the results with PNA 20 and 21, for which the parallel sequence also showed the strongest interaction.

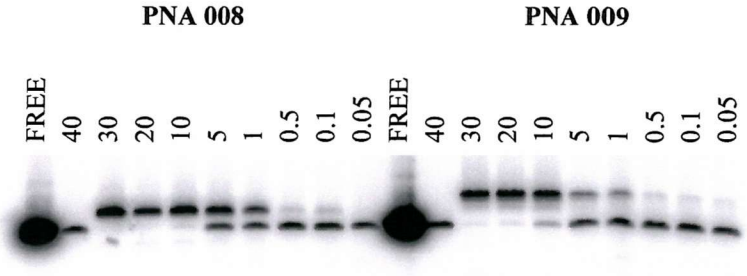

FIGURE 3.17 Bandshift assays of the 110bp *tyr*T (22-33) fragment in the presence of increasing concentrations of PNA 008 and 009. The PNA concentration (μM) is shown at the top of each lane, the lane labelled "free" corresponds to DNA in the absence of added PNA. All the complexes were incubated for 24 hours in 50mM sodium acetate pH 5.0 before electrophoresis.

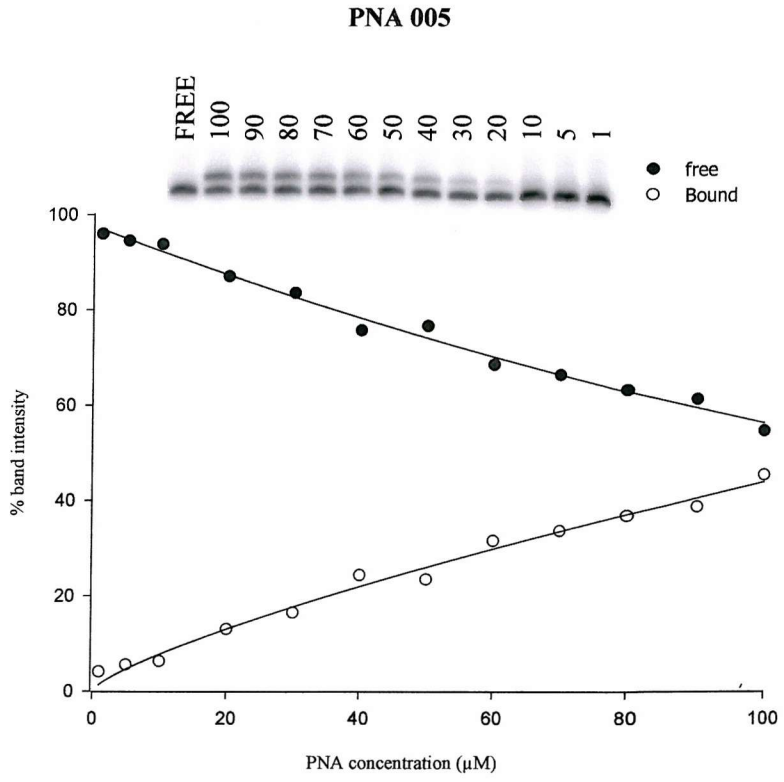

FIGURE 3.18 Bandshift assays of the 110bp *tyr*T (22-33) fragment in the presence of increasing concentrations of PNA 005 run at room temperature. The autoradiographs are shown along with the corresponding plots showing the percentage of DNA in the retarded bands against PNA concentration. The PNA concentration (μM) is shown at the top of each lane, the lane labelled "free" corresponds to DNA in the absence of added PNA. All the complexes were incubated for 24 hours in 50mM sodium acetate pH 5.0 before electrophoresis.

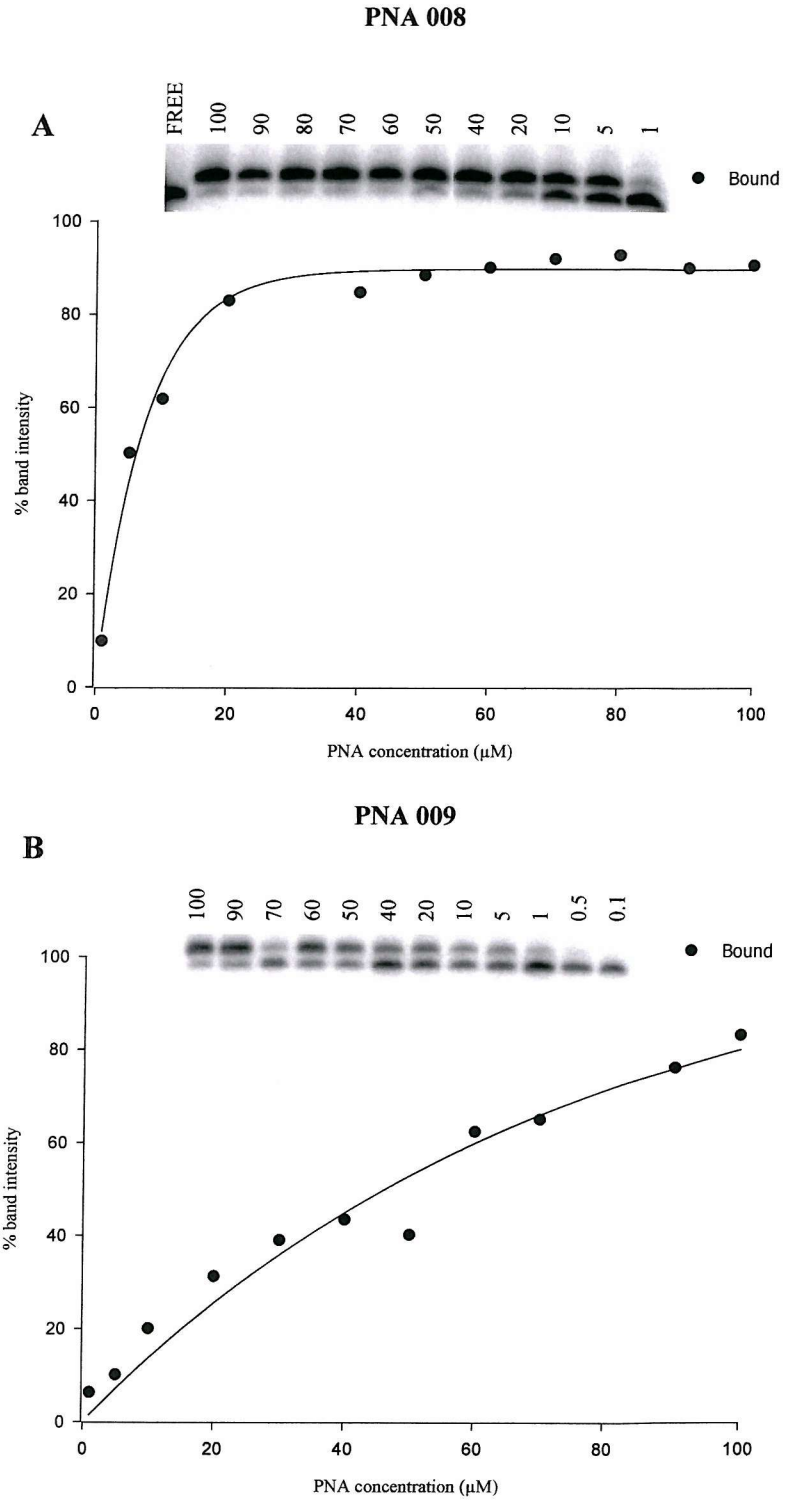

FIGURE 3.19 Bandshift assays of the 110bp *tyr*T (22-33) fragment in the presence of increasing concentrations of PNA 008 (A) and 009 (B). The autoradiographs are shown along with the corresponding plots showing the percentage of DNA in the retarded bands against PNA concentration. The PNA concentration (μM) is shown at the top of each lane, the lane labelled "free" corresponds to DNA in the absence of added PNA. All the complexes were incubated for 24 hours in 50mM sodium acetate pH 5.0 before electrophoresis.

3.3.4 Site 3 on *tyr*T (43-59,122-133) targeted with PNA 008, 009, 20 and 21

Figure 3.20 and 3.21 show bandshift assays for the interaction of PNA 008, 009, 20 and 21 with the 360bp fragment from *tyr*T (43-59,122-133), which contains targets sites 1 and 3. Since this fragment contains two independent oligopurine tracts, which bind different PNAs, we examined the effects of two PNAs targeting site 1 and 3 individually and in combination on the gel mobility. Targeting individually is shown in figure 3.20 where PNA 008 and 21 have the same effect on mobility although a diffuse higher band is present with PNA 008 and high concentrations. PNA 009 and 20 have very similar effects on DNA mobility although PNA 20 does have a greater effect. Both of these sequences have been run on lower percentage gels, which has identified two complexes as already shown with PNA 20, but a very weak band is also present with PNA 009. The mobility of the complex is identical for both sequences strongly indicating that the same complex is being formed. These results confirm that PNA 21 has a greater binding affinity than PNA20 and PNA 008 binds better than PNA 009. This will be discussed in more detail in the discussion. Figure 3.21 show bandshift assays for the interaction of PNA 008, 009, 20 and 21 in combination with the 360bp fragment from *tyr*T (43-59,122-133) fragment. It can be seen that additional bands, with lower mobility are present when either the parallel (008 and 21) or antiparallel (009 and 20) sequences are added together. It seems reasonable to suppose that the slowest band corresponds to the simultaneous binding of the two PNAs to their individual sites.

Figure 3.22 shows the effects of PNA 20 and 21 on the gel mobility of the 360bp fragment from *tyr*T (43-59, 122-133) and figure 3.23 and 3.24 shows the

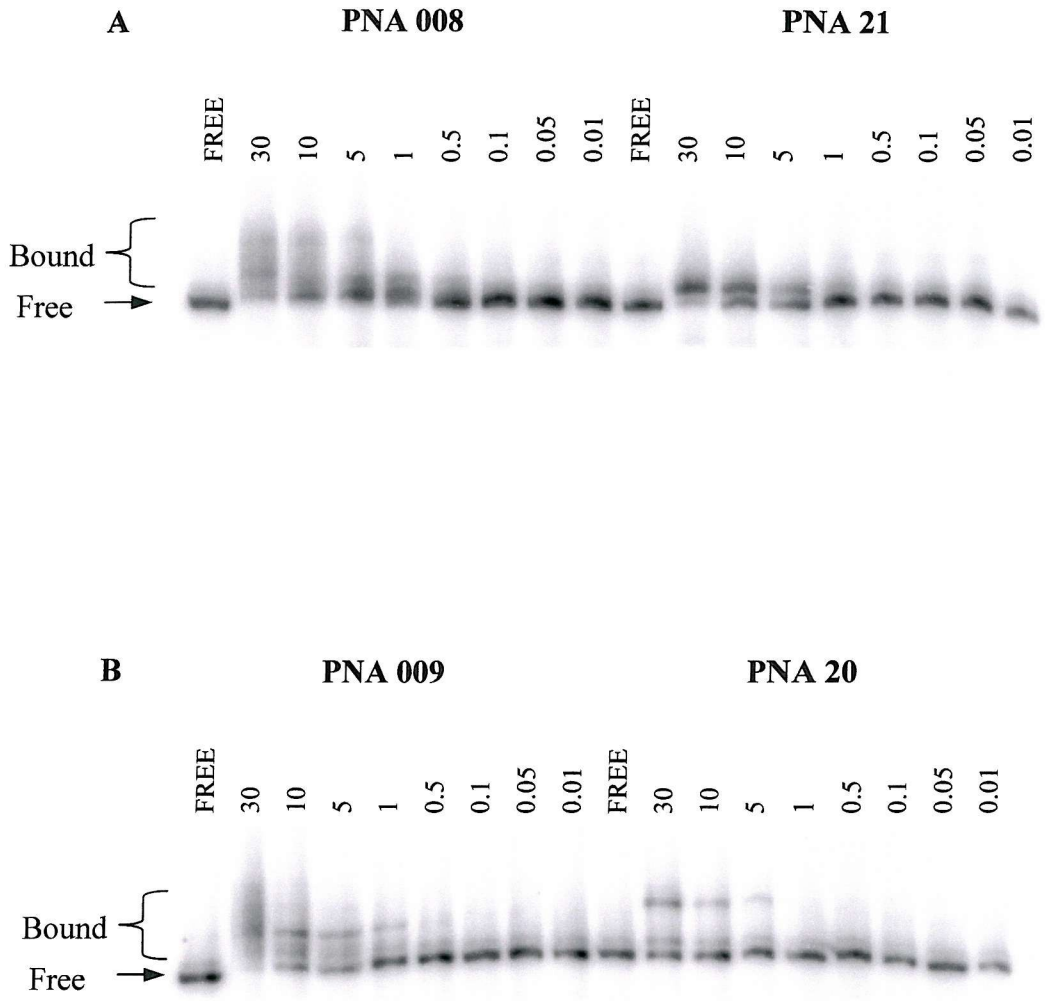

FIGURE 3.20 Bandshift assays of the 360bp *tyr*T (43-59,122-133) fragment in the presence of increasing concentrations of PNA 20, 21, 008 and 009. Panel (A) compares the effects of the parallel PNA sequence 008 and 21 and panel (B) show the effects of the antiparallel PNA sequences PNA 009 and 20. The PNA concentration (μM) is shown at the top of each lane, the lane labelled "free" corresponds to DNA in the absence of added PNA. All the complexes were incubated for 24 hours in 50mM sodium acetate pH 5.0 before electrophoresis.

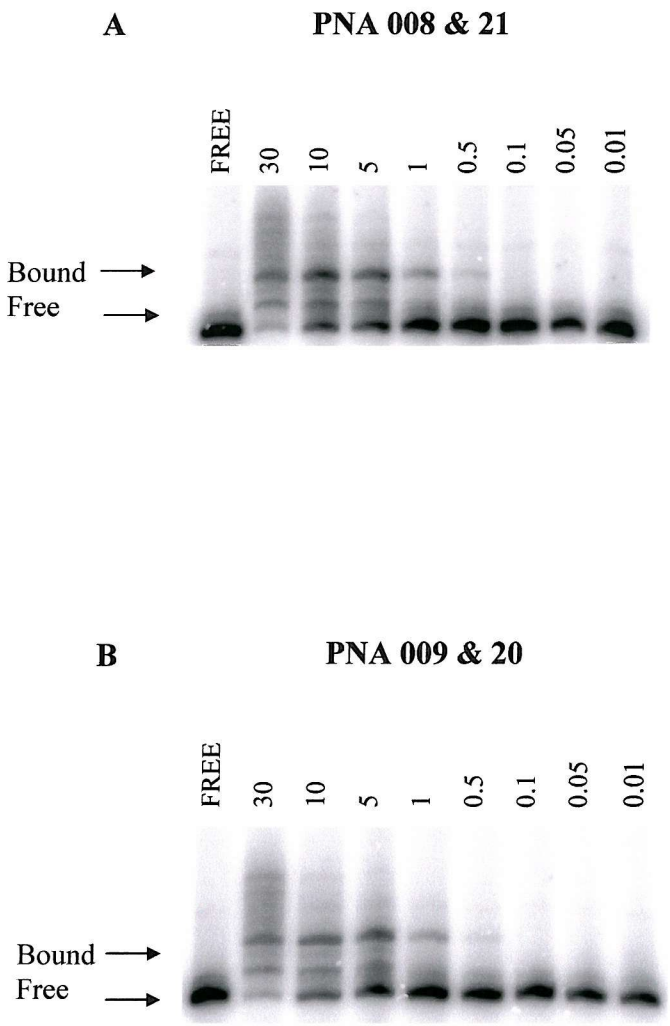

FIGURE 3.21 Bandshift assays of the 360bp *tyr*T (43-50,122-133) fragment in the presence of PNA 008 and 21, or PNA 009 and 20. Panel (A) compares the effects of the parallel PNA sequence 008 and 21 in combination and panel (B) show the effects of the antiparallel PNA sequences PNA 009 and 20 in combination. Each PNA concentration (μM) is shown at the top of each lane, the lane labelled "free" corresponds to DNA in the absence of added PNA. All the complexes were incubated for 24 hours in 50mM sodium acetate pH 5.0 before electrophoresis.

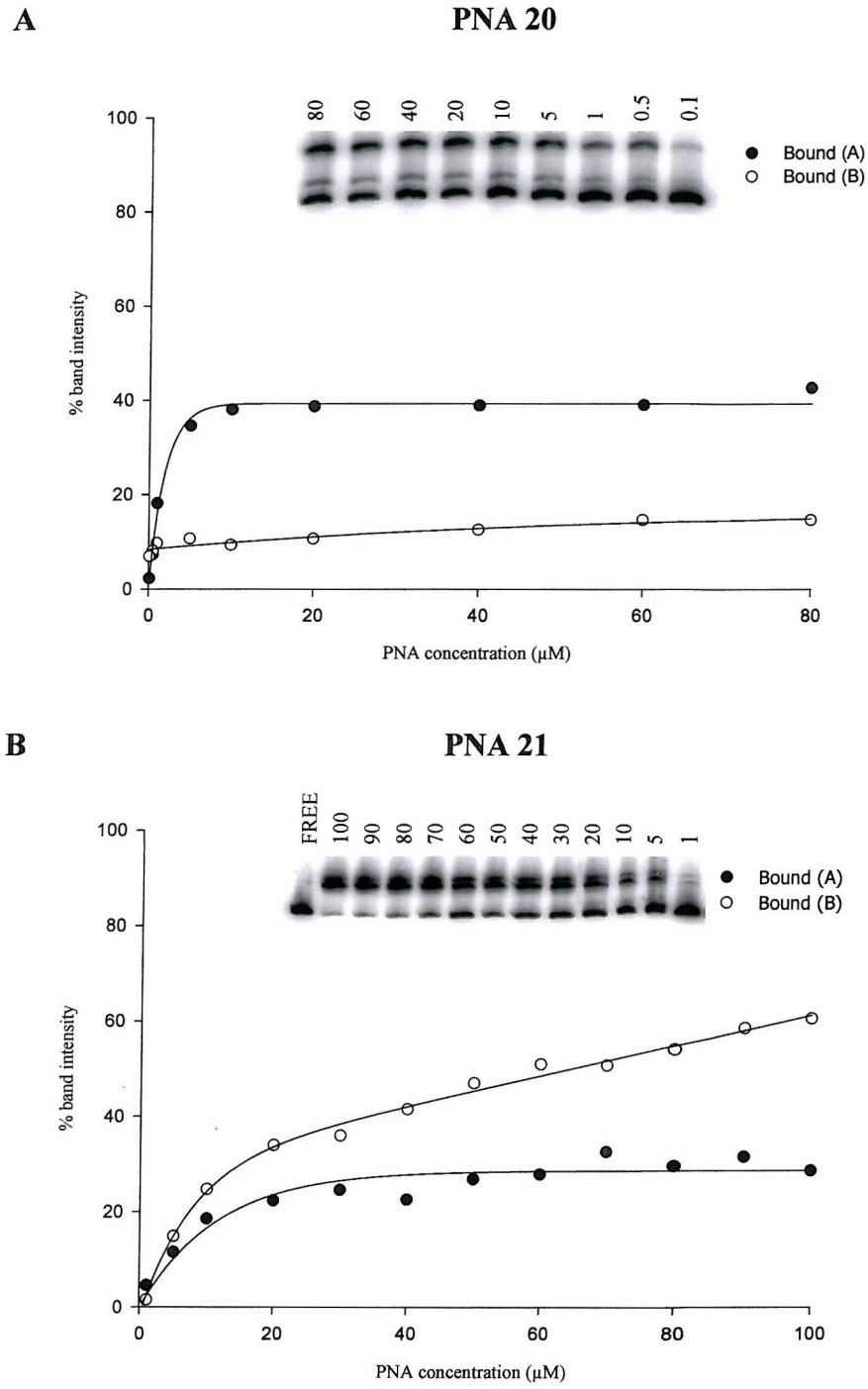

FIGURE 3.22 Bandshift assays of the 360bp *tyr*T (43-59,122-133) fragment in the presence of increasing concentrations of PNA 20 and 21. Panel (A) compares the effects of the antiparallel PNA sequence 20 and panel (B) show the effects of the parallel PNA sequence PNA 21. The autoradiographs are shown along with the corresponding plots showing the percentage of DNA in the retarded bands against PNA concentration. The PNA concentration (μM) is shown at the top of each lane, the lane labelled "free" corresponds to DNA in the absence of added PNA. All the complexes were incubated for 24 hours in 50mM sodium acetate pH 5.0 before electrophoresis.

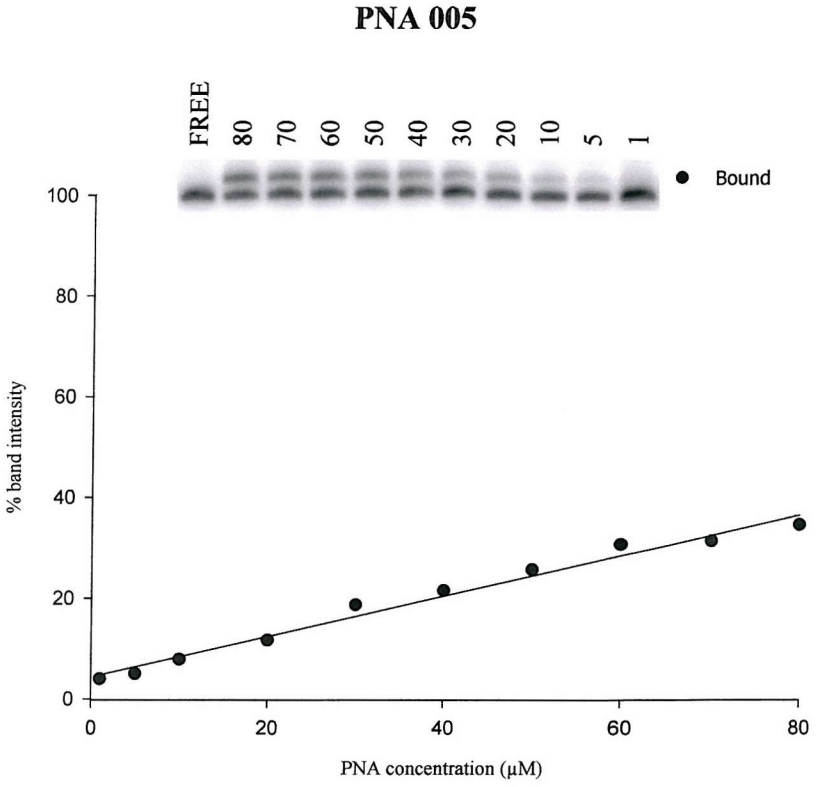

FIGURE 3.23 Bandshift assays of the 360bp *tyr*T (43-59,122-133) fragment in the presence of increasing concentrations of PNA 005. The autoradiographs are shown along with the corresponding plots showing the percentage of DNA in the retarded bands against PNA concentration. The PNA concentration (μM) is shown at the top of each lane, the lane labelled "free" corresponds to DNA in the absence of added PNA. All the complexes were incubated for 24 hours in 50mM sodium acetate pH 5.0 before electrophoresis.

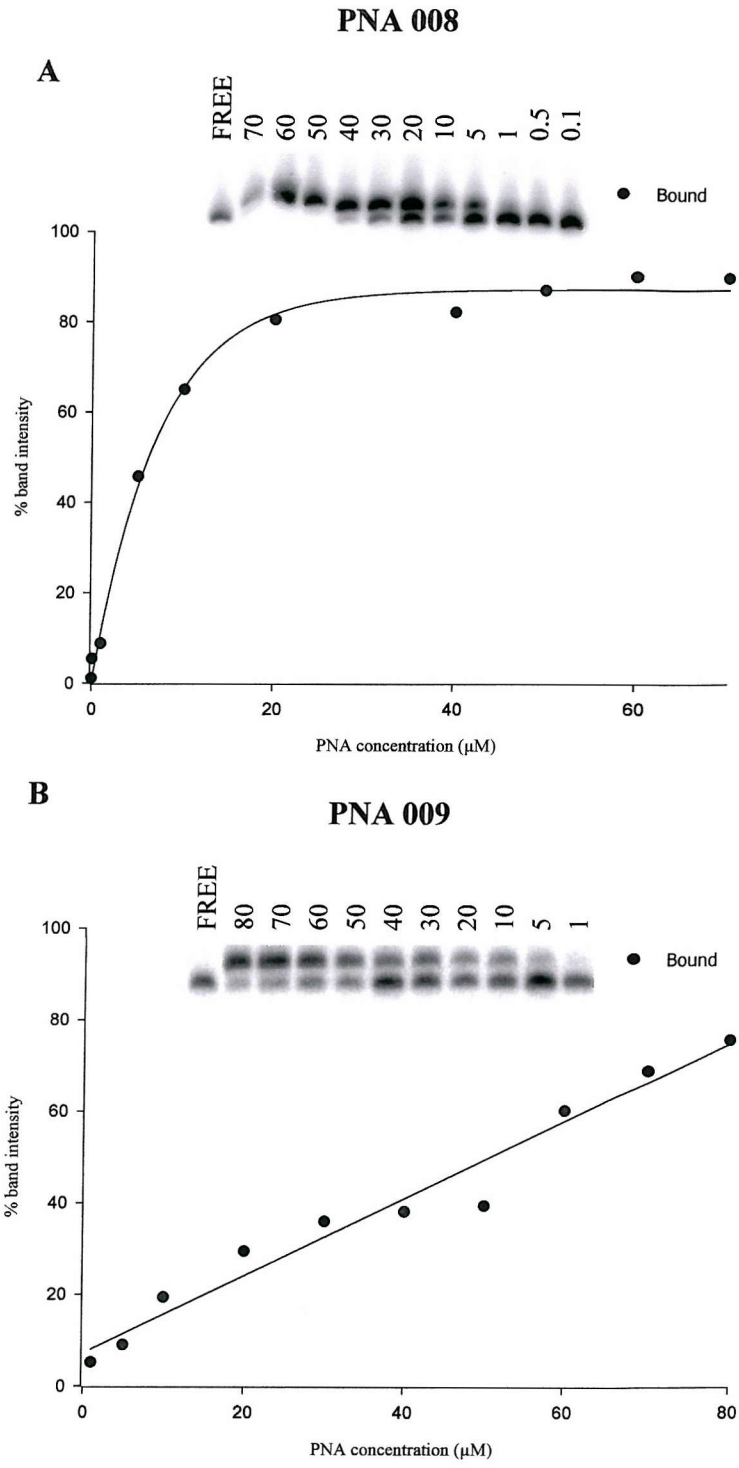

FIGURE 3.24 Bandshift assays of the 360bp *tyr*T (43-59,122-133) fragment in the presence of increasing concentrations of PNA 008 and 009. Panel (A) shows the effect of the parallel PNA sequence 008 and panel (B) show the effects of the antiparallel PNA sequence PNA 009. The autoradiographs are shown along with corresponding plots showing the percentage of DNA in the retarded bands against PNA concentration. The PNA concentration (μM) is shown at the top of each lane, the lane labelled "free" corresponds to DNA in the absence of added PNA. All the complexes were incubated for 24 hours in 50mM sodium acetate pH 5.0 before electrophoresis.

effects of PNA 005, 008 and 009 with the same fragment. As expected, PNA 20 and 21 produces two retarded bands and PNA 005, 008 and 009 produce a single retarded species, all of which are concentration dependent. The results with these fragments are similar to those with the fragments that contain sites 1 or 2 (from *tyr*T (43-59) and *tyr*T (22-33) respectively). This is reflected in their comparable C_{50} values shown in table 3.5.

The presented data in this section was obtained with samples that were incubated in 50mM sodium acetate pH 5.0 at room temperature for 24 hours. Similar bandshift experiments where performed after incubating the complexes at 37°C rather than at room temperature and incubated in 50mM sodium acetate for 2 hours. The incubation at 37°C produced similar results to those obtained at room temperature and had not altered the effect on the DNA mobility, whereas the incubation time of 2 hours resulted in no complex formation. This highlights the requirement for C^{+}·GC triplet formation and the slow complex formation with PNA complexes.

3.4 S1 nuclease footprinting

S1 nuclease digestion has been used to identify the different complexes formed with each individual PNA sequence. This nuclease (which requires low pH conditions) cleaves regions of single stranded DNA and so detects the presence of P-loop structures, which are formed as part of any strand invasion mechanism. With these pyrimidine-containing PNAs we expect the pyrimidine-containing strand of the duplex to be displaced. PNA-induced enhancements in S1 nuclease cleavage will therefore only be detected when the target site is labelled on the pyrimidine-containing strand. On the labelled purine strand the low levels of background S1 cleavage may

Polypurine tract site	Sample pH	Electrophoresis temperature	PNA sequence	Dissociation constant (μM)
1	5.0	RT	20	41.0 ±8.6
1	5.0	4°C	20	42.4 ±7.8
1	5.0	RT	21	2.6 ±6.1
1	5.0	4°C	21	2.7 ±5.6
1	7.5	RT	20	not resolved
1	7.5	RT	21	not resolved
1	5.0	RT	41	1.4 ±2.6
1	5.0	RT	42	3.7 ±1.3
1	5.0	RT	43	4.5 ±6.7
Secondary site	5.0	RT	20	not resolved
Secondary site	5.0	RT	20	not resolved
Secondary site	5.0	RT	21	not resolved
Secondary site	5.0	RT	21	not resolved
2	5.0	RT	005	not resolved
2	5.0	RT	008	6.0 ±3.3
2	5.0	RT	009	46.1 ±5.7
1+3(3)	5.0	RT	005	not resolved
1+3(3)	5.0	RT	008	6.1 ±3.0
1+3(3)	5.0	RT	009	51.27 ±5.2
1+3 (1)	5.0	RT	20	not resolved
1+3 (1)	5.0	RT	21	52.5 ±3.7
1+3(1)	5.0	RT	41	2.1 ±3.1
1+3(1)	5.0	RT	42	3.6 ±2.2
1+3(1)	5.0	RT	43	4.8 ±7.0

TABLE 3.5 Summary of the C_{50} values (μM) for the different PNAs, calculated from the bandshift analyses. Where, the abbreviation "RT" refers to room temperature.

be inhibited if addition of the PNA stabilizes the DNA duplex. These experiments were therefore performed in duplicate with the 190 base pair fragment, which can be labelled at either the *Hind*III or *Eco*RI ends.

Figure 3.25 shows the results of S1 nuclease cleavage for the 190bp *tyr*T (43-59) fragment in the presence or absence of PNA 20 and 21. On the *Eco*RI labelled fragment (first panel) site 1 is labelled on the purine strand while the secondary binding site noted above will be labelled on the pyrimidine-rich strand. Site 1 is located closer to the bottom (3′) of the gel. It can be seen that PNA 20 inhibits the low levels of S1 nuclease cleavage around site 1. In contrast there is enhanced cleavage in the vicinity of the secondary binding site, located towards the top of the gel. Both of these effects persist to PNA concentrations of about 30μM. These results confirm the stabilization of the purine strand around the intended target site1, whilst the pyrimidine strand of the secondary binding site is exposed. The second panel shows the results of PNA 20 with the *Hind*III labelled fragment, for which site 2 is located closer to the bottom of the gel. This shows intense PNA-induced cleavage around site 1, which persists to a concentration of about 5μM, indicating the presence of single-stranded DNA in this region, as expected for strand invasion, displacing the DNA pyrimidine strand. In contrast to the results with the purine strand of site 1, PNA 20 does not protect the purine-rich strand of the secondary binding site from low levels of S1nuclease cleavage.

PNA 21 produces similar effects on these two labelled 190 base pair fragments, which are shown in the third and fourth panels of figure 3.25. In the presence of PNA 21 the *Eco*RI-labelled fragment is protected from S1 cleavage around site 1, with a weak enhancement of cleavage at the secondary binding site. On the *Hind*III-labelled strand this PNA induces cleavage at site 1, indicating that PNA

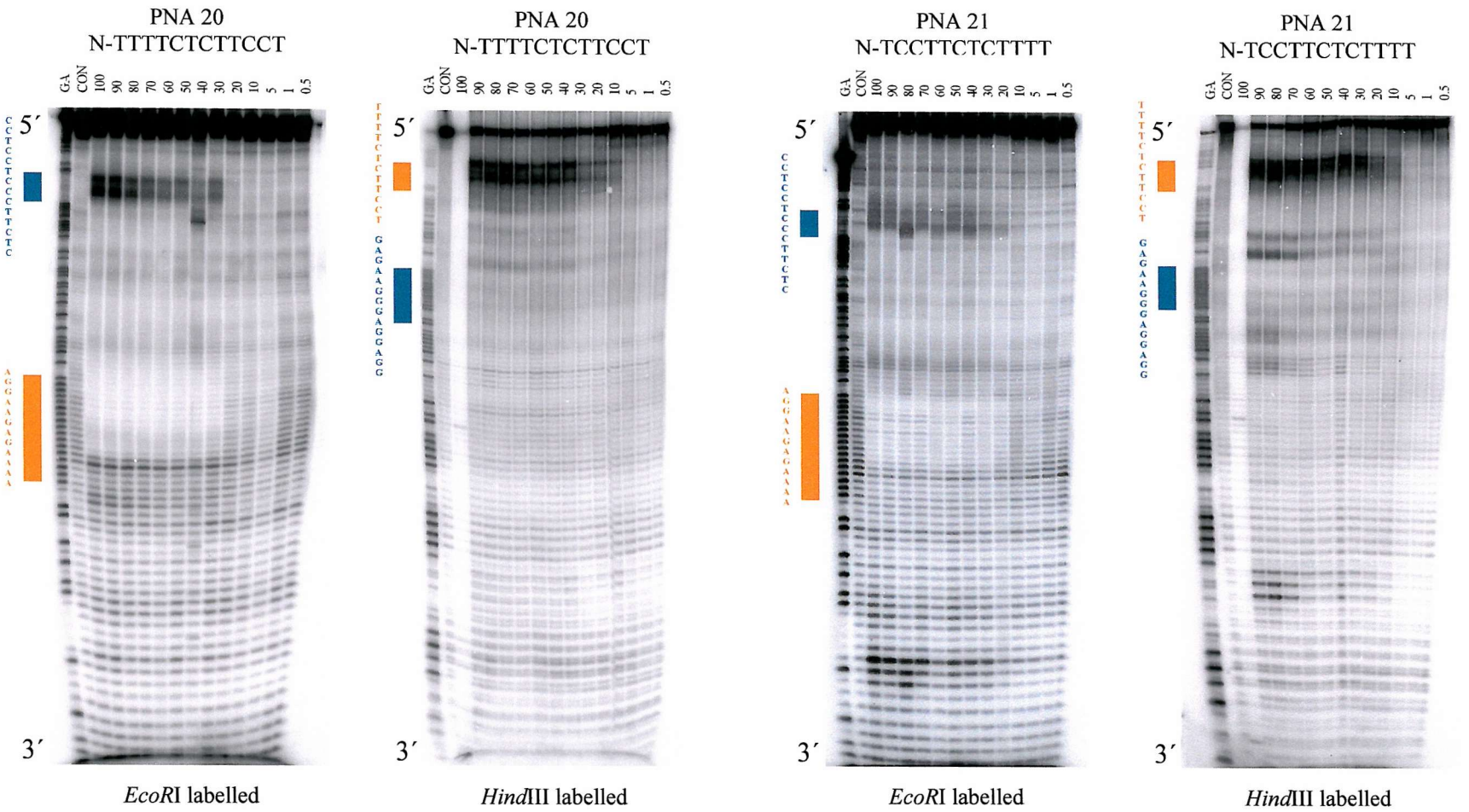

FIGURE 3.25 S1 nuclease cleavage of the 190bp *tyr*T (43-59) fragment in the presence of PNA 20 and 21. The fragments were labelled at the *Eco*R1 or *Hind*III ends as indicated. The PNA concentration (μM) is indicated at the top of each gel lane. "CON" indicates digestion of the DNA in the absence of PNA and "GA" is a Maxam-Gilbert marker specific for purines. All the complexes were incubated for 24 hours in 50mM sodium acetate pH 5.0 before digestion with S1 nuclease. The location of site 1 is highlighted in orange, while the secondary binding site is shown in green.

21 has displaced the pyrimidine DNA strand of this target site. In this case PNA 21 does not protect the purine-rich strand of the secondary binding site from S1 cleavage.

Figure 3.26 shows the results of S1 nuclease digestion of the190 base pair *tyr*T (22-33) fragment (containing site 2) in the presence and absence of PNA 008 and 009. The pyrimidine-containing strand of site 2 is visualized in the fragment labelled at the *EcoR*I end while the purine strand is seen with the *Hind*III-labelled fragment. It can be seen that PNA 008 produces enhanced cleavage of the pyrimidine strand of site 2 (left hand panel), consistent with strand displacement. However, the *Hind*III-labelled fragment (second panel) also clearly shows enhanced cleavage in the purine strand of this site. This result was not expected. PNA 009 shows similar results with enhanced S1 cleavage at site 2 for both *EcoR*I and *Hind*III-labelled fragments.

Figure 3.27 shows the results of similar experiments with the 190 base pair fragment from *tyr*T (43-59,122-133) in the presence of PNA 008 and 009. In this fragment the pyrimidine-containing strand of site 3 is visualised when it is labelled at the *EcoR*I end. Both PNA 008 and 009 produce enhanced cleavage of site 3 on the *EcoR*1-labelled fragment, and protect this site from cleavage in the *Hind*III-labelled fragment. This is the expected result for strand invasion by these PNAs at this site, and is in contrast to the unexpected results seen with at site 2 of the *Hind*III-labelled strand of *tyr*T (22-33). However, enhanced S1 cleavage is evident at the top of this fragment in a similar position to the unexpected cleavage seen at site 2 with *tyr*T (22-33). It therefore seems likely that this anomalous cleavage is an artefact. PNA 20 and 21 show similar results with *tyr*T (43-59,122-133) to those seen with *tyr*T (43-59) at sites 1 and 3.

Since the *tyr*T (43-59,122-133) fragment contains binding site 1 and 3, S1 nuclease digestion was performed in the presence of the both parallel PNAs (008 and

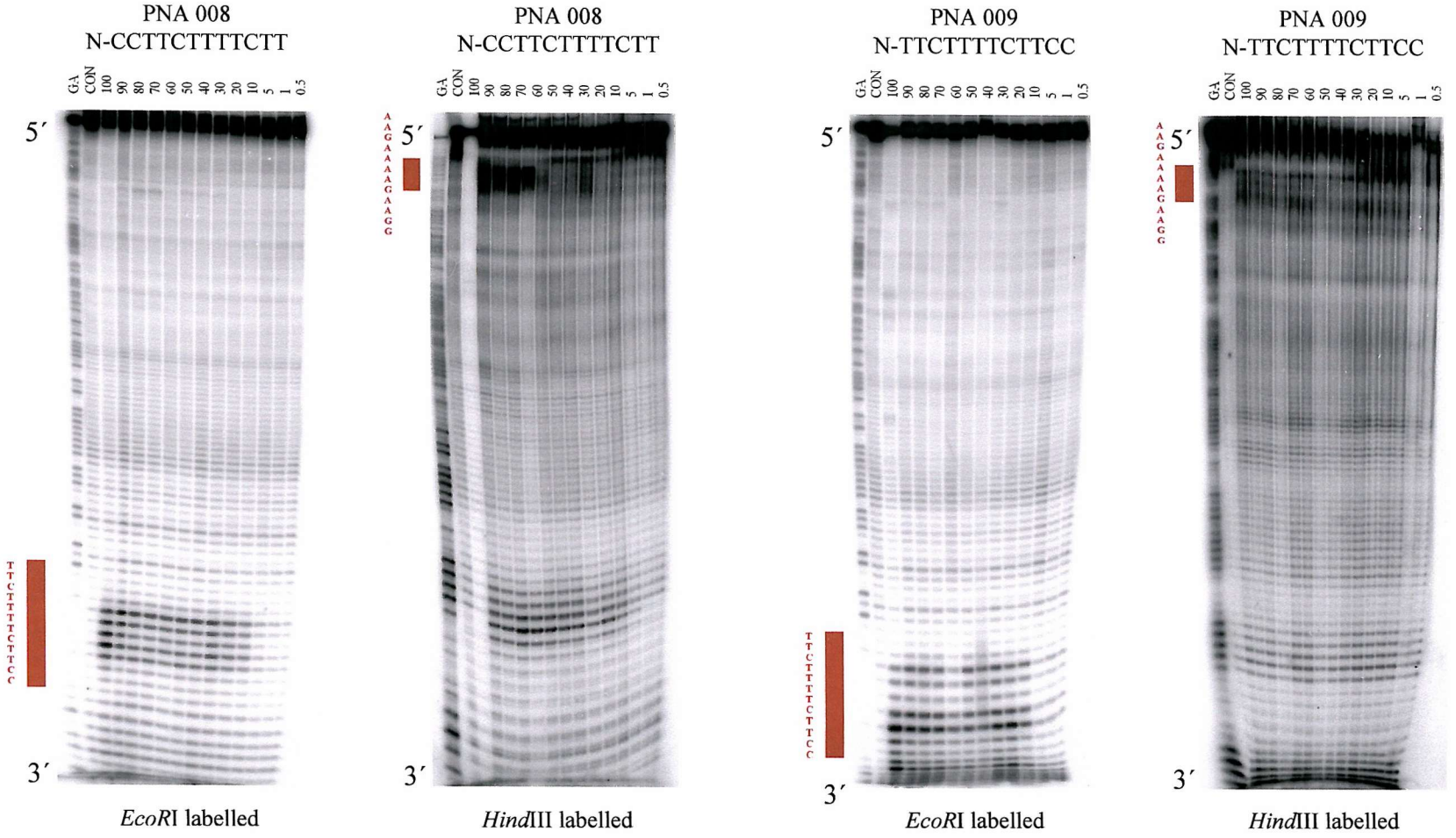

FIGURE 3.26 S1 nuclease cleavage of the 190bp *tyr*T (22-33) fragment in the presence of PNA 008 and 009. The fragments were labelled at the *EcoR*I or *Hind*III ends as indicated. The PNA concentration (μM) is indicated at the top of each gel lane. "CON" indicates digestion of the DNA in the absence of PNA and "GA" is a Maxam-Gilbert marker specific for purines. All the complexes were incubated for 24 hours in 50mM sodium acetate pH 5.0 before digestion with S1 nuclease. The location of site 2 is highlighted in brown.

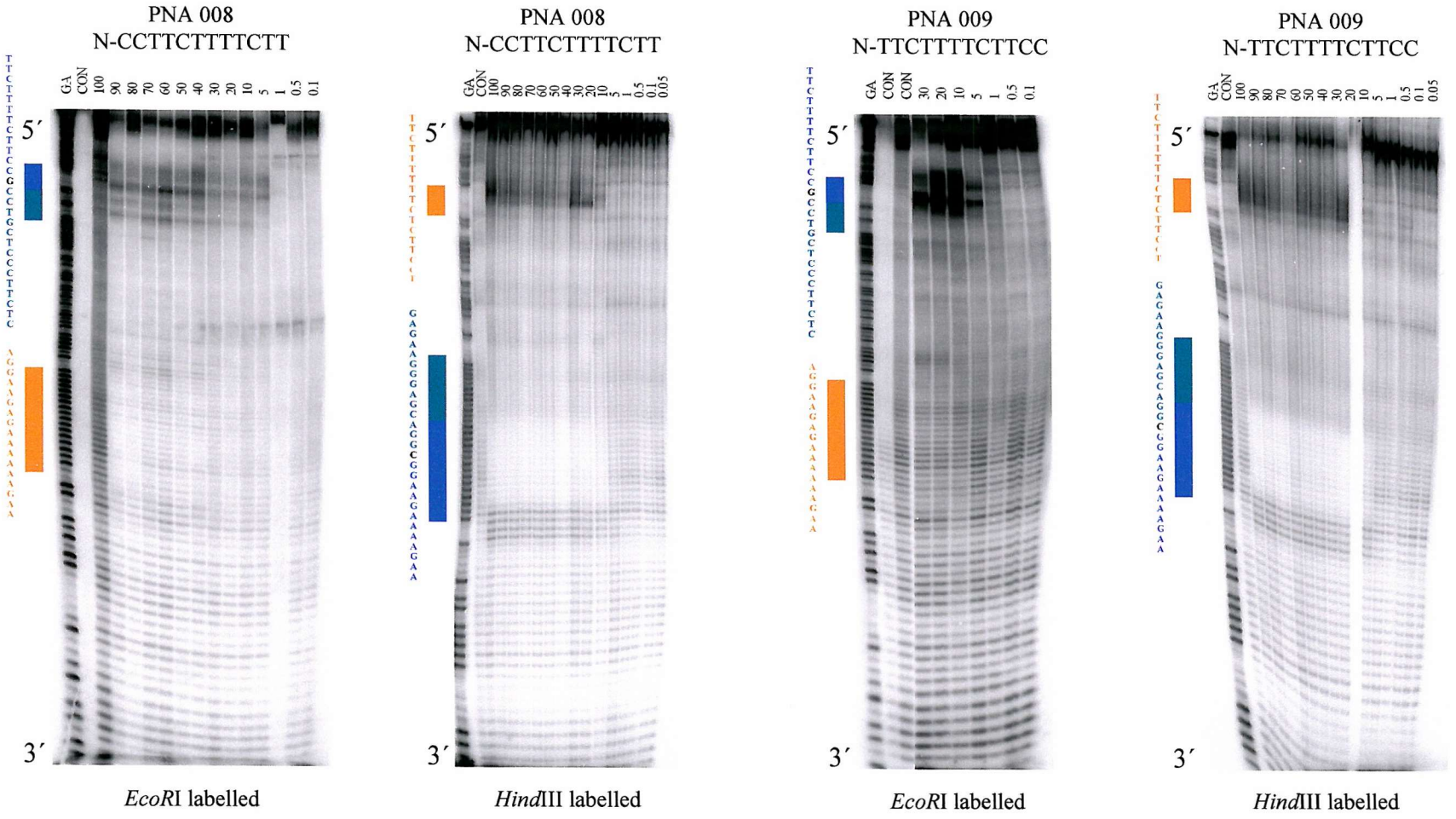

FIGURE 3.27 S1 nuclease cleavage of the 190bp *tyr*T (43-59,122-133) fragment in the presence of PNA 008 and 009. The fragments were labelled at the *EcoR*I or *Hind*III ends as indicated. The PNA concentration (μM) is indicated at the top of each gel lane. "CON" indicates digestion of the DNA in the absence of PNA and "GA" is a Maxam-Gilbert marker specific for purines. All the complexes were incubated for 24 hours in 50mM sodium acetate pH 5.0 before digestion with S1 nuclease. The location of site 1 highlighted in orange, site 3 in blue and the secondary binding site is in green.

21) or both antiparallel PNAs (009 and 20). The results of these experiments are shown in figure 3.28, for the *Hind*III-labelled strand. In the presence of either of these combinations there is enhanced cleavage at the secondary binding site for PNAs 20 and 21, along with reduced cleavage of sites 1 and 3, for which the purine-containing strands are seen.

PNA 008 and 009 or 20 and 21 in combination will promote the formation of a triple helix with strand invasion where the Hoogsteen bound third strand runs parallel to the purine strand of the antiparallel Watson and Crick PNA/DNA duplex, promoting strand invasion. These S1 nuclease cleavage gels are shown in figure 3.29. Looking first at PNA 008 and 009 interactions with site 3 on the 190bp *tyr*T (22-33) fragment, intense cleavage of the pyrimidine strand is present in the left hand panel at site 3. There is very minimal cleavage of the purine strand on the *Hind*III-labelled fragment but less intense then with targeted individually and could consequently be an artefact band. Very similar results are shown with PNA 20 and 21 interacting with site 1 on the 190bp *tyr*T (22-33) fragment. S1 nuclease cleavage protection is present on the purine strand whereas very strong cleavage is present on the pyrimidine strand at site 1. This cleavage is considerably more intense then when targeted individually indicating that in combination a triplex helix is formed promoting a P-loop structure, which has been heavily cleaved with S1 nuclease. Cleavage is only present at high concentrations above 10μM, which is not comparable to the footprinting results which footprint down to 0.05μM. This indicates that at low PNA concentrations the intermediate triplex formation could be formed and high concentrations of PNA are required to promote strand invasion complexes.

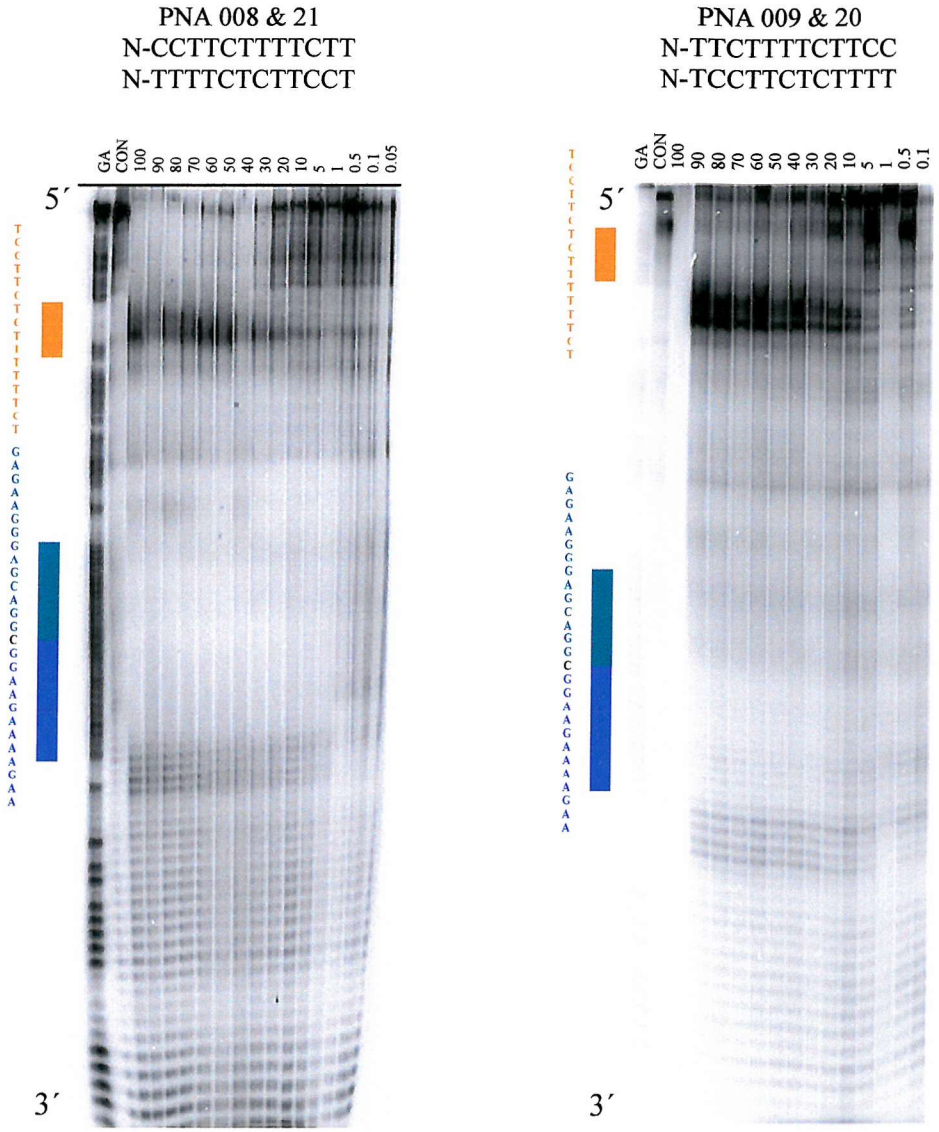

FIGURE 3.28 S1 nuclease cleavage of the 190bp *tyr*T (43-59,122-133) fragment in the presence of PNA 008 and 21 or 009 and 20. The fragments were labelled at the *Hind*III ends. The PNA concentration (μM) is indicated at the top of each gel lane. "CON" indicates digestion of the DNA in the absence of PNA and "GA" is a Maxam-Gilbert marker specific for purines. All the complexes were incubated for 24 hours in 50mM sodium acetate pH 5.0 before digestion with S1 nuclease. The location of site 1 highlighted in orange, site 2 in blue and the secondary binding site is in green.

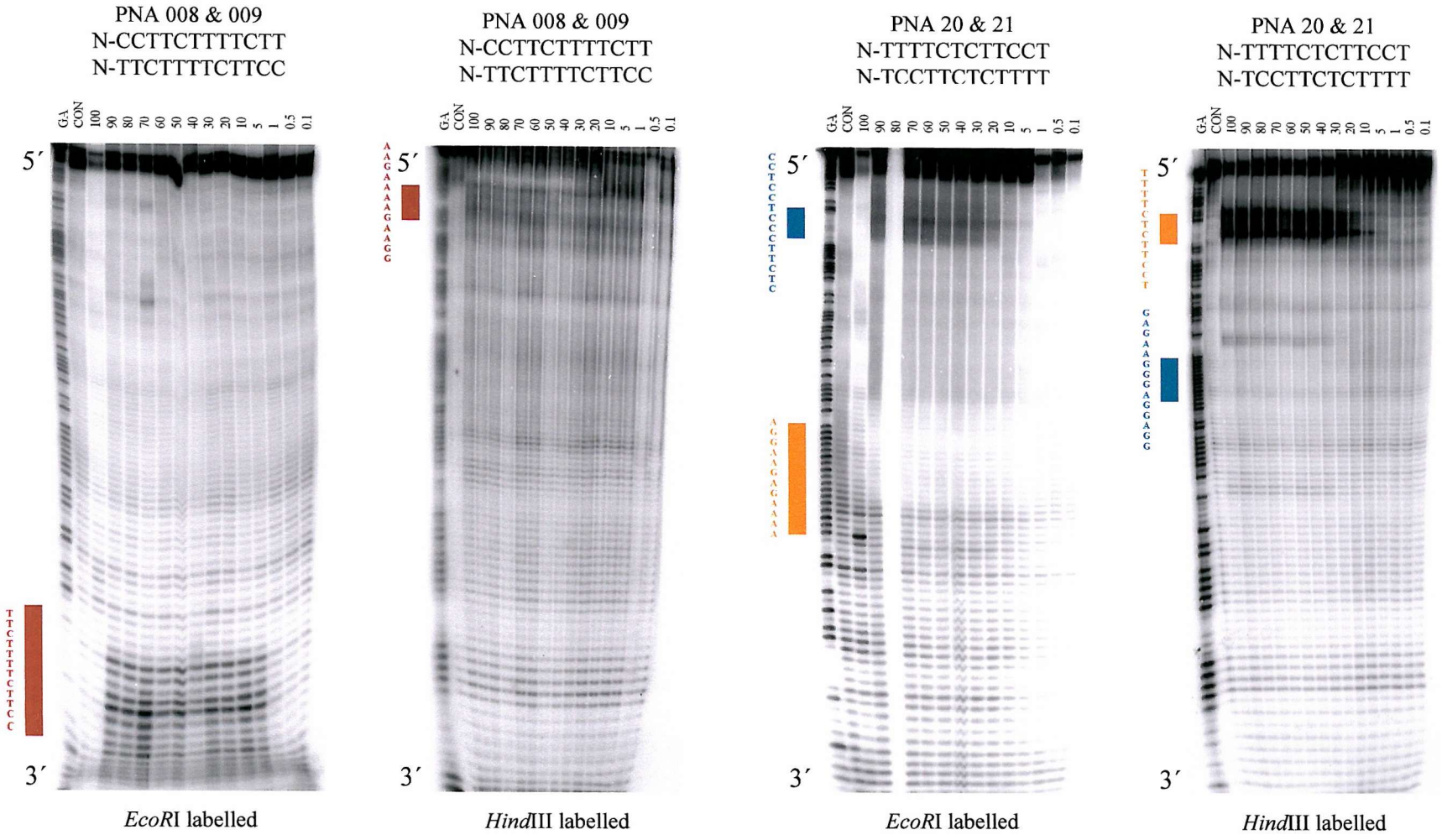

FIGURE 3.29 S1 nuclease cleavage of the 190bp *tyr*T (43-59) and (22-33) fragments in the presence of PNA 008 and 009 (left hand panels) or 20 and 21 (right hand panels). The fragments were labelled at the *EcoR*1 or *Hind*III ends as indicated. The PNA concentration (μM) is indicated at the top of each gel lane. "CON" indicates digestion of the DNA in the absence of PNA and "GA" is a Maxam-Gilbert marker specific for purines. All the complexes were incubated for 24 hours in 50mM sodium acetate pH 5.0 before digestion with S1 nuclease. The location of site 1 highlighted in orange, site 2 in brown and the secondary binding site is in green.

3.5 Discussion

This chapter had studied in depth the interaction of eight different polypyrimidine PNA sequences with various oligopurine target sites in different length double stranded DNA fragments. Each PNA sequence has shown sequence specific interactions with their intended target sites, forming complexes which involve strand invasion (as shown by the results with S1 nuclease) and triplex formation (shown by the requirement for low pH). These complexes, especially strand invasion, where also identified through micrococcal nuclease and T7 exonuclease cleavage of the P-loop (data not shown).

It has previously been reported that PNA binds (in a duplex or triplex) in the same polarity as DNA, if we consider the PNA N-terminus to be equivalent to the DNA 5′-end. However, for strand invasion triplexes at least one of the strands must be arranged in a non-canonical polarity (Wittung et al., 1996). This occurs because only one PNA sequence was used which was not symmetrical or a bis-PNA.

The DNaseI footprinting experiments confirmed that each PNA bound to its expected target site. We suggest that, under the conditions employed in these studies, PNA binds as a third strand, forming a PNA/DNA_2 triplex at low PNA concentrations. This complex was detected by DNaseI footprinting, but may not be evident in bandshift studies. However, higher PNA concentrations facilitate strand invasion, generating a PNA_2/DNA triplex. This type of complex will produce larger changes in global DNA structure, and is likely to be the one detected in the bandshift experiments. Strand invasion may also disrupt the surrounding regions of the target site extending the size of the DNaseI footprint beyond that seen with a simple triplex footprint, especially on the displaced strand. This effect is most pronounced for PNA

20, but is also evident for PNA 21, where a larger cleavage region can also be seen at site 1 at high PNA concentrations.

Each PNA sequence studied has shown to strand invade the DNA duplex producing a P-loop structure which appears to be irrespective of strand polarity. PNA 008 and 21 bind parallel whereas PNA 009 and 20 bind antiparallel. PNA 008 and 21 should bind as a third strand Hoogsteen strand whereas studies have shown that strand invasion occurs. For this to be present the PNA has to invade the duplex binding antiparallel to the purine DNA strand displacing the pyrimidine strand. This means that parallel PNA sequences appear to be able to also bind in an antiparallel orientation. This is also evident for PNA 009 and 20 however due to their antiparallel binding orientation, they could invade the DNA duplex and form a duplex invasion complex. However, if this was present then DNaseI cleavage would footprint to the same concentrations as S1 nuclease. In the absence of the invading PNA sequence only the DNA duplex would be present and DNaseI would cleave normally, this observation is not present. The dependence of PNA interactions upon polarity is contradicted in the literature and the results presented here question whether polarity determines PNA complex formation.

Cytosine content has influenced binding affinities where the increase number of cytosine residues increases their binding affinity due to the increase positive charge being attracted to the negatively charged backbone.

Bandshift analysis has identified the presence of two retarded bands for PNA 20 on the shortest fragment and two retarded bands in the presence of PNA 20 and 21 on the longer fragments as well. This cannot be attributed to the secondary binding site due to the presence of two complexes should be represented as one retarded band. However, these retarded bands are concentration dependent and could

relate to a triplex formation with and without strand invasion. Strand invasion complexes will distort the DNA architecture by potentially forming either a bend in the DNA or a bulky region, which will affect the mobility through the gel. The difference between these two retarded bands have not been experimentally proven but based in the data obtained, two different complexes appear to have been formed represented in the bandshift assays as two retarded bands. The two bands formed with PNA 20 have a different mobility whereas for PNA 21 the mobility of them are very similar. Different complexes are obviously formed but the nature of these complexes would require further investigation.

The different effects on mobility through the gel have been noted with each PNA sequence, the antiparallel sequences have a greater effect on mobility compared to the parallel PNA sequences. When PNA 20 and 21 are run in combination, there are designed to bind antiparallel and parallel to the purine strand of site 1 forming a PNA_2/DNA triplex with strand invasion. This complex is evident and also has a less of an effect on mobility and has the same effect as PNA 21 does have individually. This indicates that the complex formed with PNA 21 is potentially the same as the one formed with PNA 20 and 21 in combination concluding that PNA 21 does form the PNA_2/DNA triplex. As for PNA 20, the complex formed has changed the DNA architecture sufficiently to affect mobility. These observations are also present with PNA 008 and 009.

S1 nuclease cleavage has shown that PNA 008, 009, 20 and 21 all form P-loop structures, as evidenced by cleavage of the pyrimidine strand of their target sites. Protection of the purine strand from S1 cleavage was also observed at the specific sites, suggesting that a strong DNaseI resistant complex is formed. This protection is not evident at the secondary binding site, possibly indicating the formation of a

weaker complex. S1 cleavage is observed at higher PNA concentrations than are required to generate DNaseI footprints, consistent with the suggestion that, under these conditions triplex formation occurs at lower PNA concentrations than strand invasion.

The footprinting studies identified a secondary binding site for PNA 20 and 21 on the *tyr*T (43-59) sequence, located around position 110. PNA 20 shows a significantly higher affinity for this site than PNA 21. Although it is not clear how these PNAs bind to this sequence, antiparallel binding (PNA 20) appears to be favoured over parallel binding (PNA 21). Some possible arrangements for these PNAs at this target site are considered in figure 3.30. However, none of these is entirely convincing, as the longest contiguous stretch is only 5 base pairs long.

The results from this section have been the foundation for the interaction of PNA with histone bound DNA fragments, which will be documented, in the following chapter.

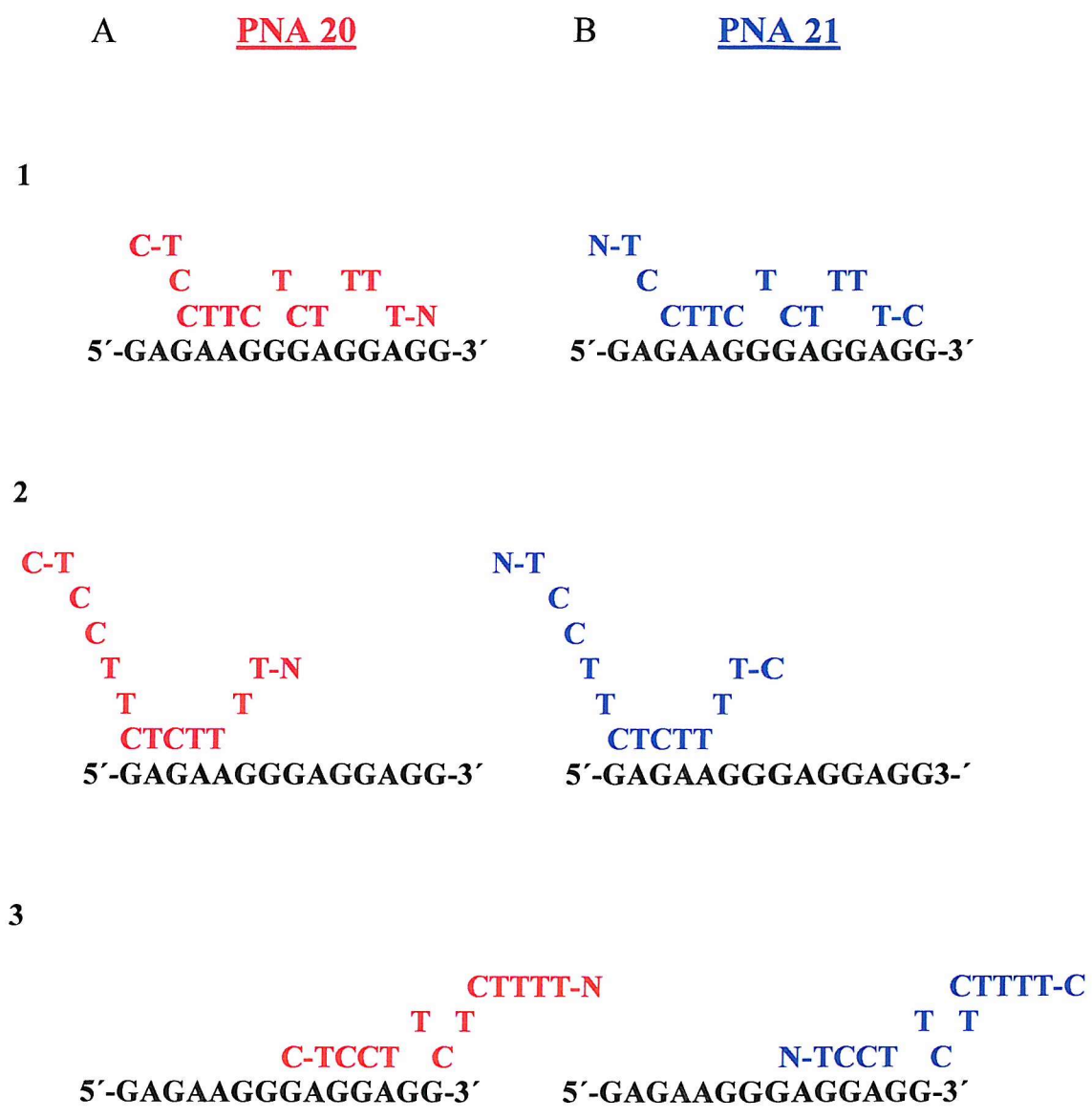

FIGURE 3.30 Proposed binding motifs for PNA 20 (A) and 21 (B) binding to the secondary binding site on the *tyr*T (43-59) sequence.

Chapter 4

PNA interaction with Histone bound DNA

4.1 Introduction

The previous chapter explored the ability of polypyrimidine PNAs to target oligopurine tracts on free DNA. These results demonstrated that stable complexes were formed, which contained P-loops and triple helices. These results are consistent with a wide range of published studies on PNA-DNA complexes. However, within all eukaryotic cells DNA is associated with proteins in the form of chromatin, which may alter its interaction with DNA. To date there have been comparatively few studies on targeting this compact protein-DNA complex with ligands. This chapter uses DNaseI and bandshift techniques to probe the interaction of the same PNAs with histone-bound DNA. In this work the PNA-DNA-protein complexes will be prepared by two different routes. In the first route the DNA is first reconstituted onto the histone proteins, and this is then targeted with PNA. This is considered to be analogous to the targeting of relatively compact chromatin. In the second route the PNA-DNA complex is formed first, and this is then reconstituted onto nucleosomal particles. This second route mimics the interaction of PNA with transcriptionally active DNA, where short DNA sequences may transiently dissociate from the protein surface, rendering them accessible for interaction with PNA. These studies used the variable length DNA fragments that were examined in the previous chapter. In this way the PNA target sites have the opportunity to relocate to other regions which are within or between the nucleosome core particles.

4.2 *Tyr*T (43-59) – site 1

4.2.1 *Tyr*T(43-59) targeted with PNA after reconstitution

Figure 4.1 shows DNaseI footprinting and bandshift gels for the interaction of PNA 20 and 21 with the histone-bound 110bp *tyr*T (43-59) fragment. It can be seen that, under these conditions, the PNAs have no effect on the DNaseI cleavage patterns, even at concentrations as high as 30μM. Examination of the DNaseI cleavage pattern of the PNA-free nucleosomal DNA reveals that interaction with the protein alters the cleavage pattern, in which regions of maximal cleavage correspond to positions where the minor groove periodically faces away from the protein core (figure 4.1A). These results are in contrast to those obtained with free DNA where visible footprints are present at site 1 at low PNA concentrations (see section 3.2.1). It therefore appears that both PNA 20 and 21 are not able to bind site 1 under these conditions, in which the target site is located approximately 10 base pairs from the dyad axis. Further experiments were performed with PNA 41, 42 and 43 all of which yielded similar results, where there was no evidence of PNA binding (data not shown). This is especially noteworthy for PNA 41, which had the highest binding affinity at site 1 of all the PNA sequences on free DNA.

These DNaseI results are substantiated by bandshift assays (figure 4.1B) which also show no disruption of the nucleosome core particle when targeted with PNA 20 or 21, even at high concentrations. Addition of PNA does not produce a visible supershift in the nucleosome-retarded bands, which might be expected if a ternary PNA-DNA-protein was formed. The presence of PNA is evident by retardation of the small amount contaminating free DNA. Additional bandshift

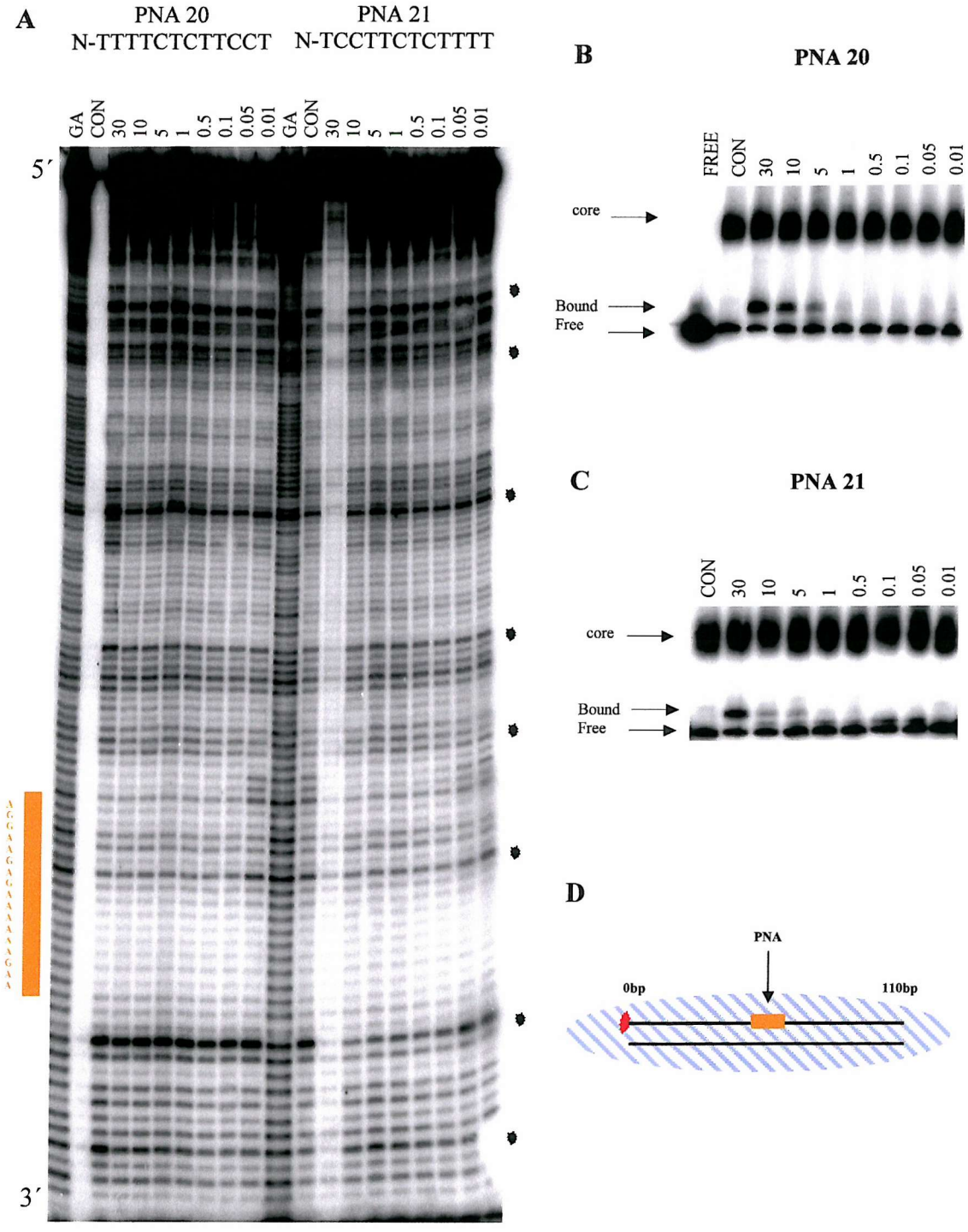

FIGURE 4.1 DNaseI cleavage (A) and bandshift assays (B,C) of the 110 base pair histone-bound *tyr*T (43-59) fragment in the presence and absence of PNA 20 and 21. The PNA concentration (μM) is indicated at the top of each gel lane. "CON" indicates digestion of the DNA in the absence of PNA and "GA" is a Maxam-Gilbert marker specific for purines. All the complexes were incubated for 24 hours in 50mM sodium acetate pH 5.0 before digestion with DNaseI. The location of site 1 is indicated in orange. The asterisks indicate the sites of maximal cleavage, where the DNA minor groove faces away from the protein core. D is a cartoon showing the likely position of the target site, relative to the histone octamer.

experiments were performed with PNA 41, 42 and 43 all of which showed no disruption to the nucleosome core particle and no supershift species (data not shown).

Figure 4.2A shows DNaseI cleavage of the longer 160 base pair *tyr*T (43-59) fragment, in the presence of PNA 20 and 21. In this instance it can be seen that both PNAs produce clear footprints at site 1, which persist to concentrations of about 10μM and 0.05μM respectively. These concentrations are considerably higher than those needed to produce footprints with free DNA, suggesting that the protein core has hindered the interaction with site 1; this effect is more pronounced with PNA 20. There is also a very weak footprint at the secondary binding at the highest concentrations (30μM) of PNA 20. Since this fragment is longer it will not necessarily sit in the same location as the 110 base pair fragment, and it is possible that the target site is located closer towards the edge of the protein. This can be justified through the ability to target this fragment. If the protein was sat in the same location as on the 110bp fragment, targeting would be prevented as previously shown in figure 4.1. However, targeting is present with the 160bp fragment so the position of the histone octamer indicates that reconstitution has occurred in a different location, further towards the 5′-end of the fragment. The phasing pattern of the 160bp fragment correlates to the cleavage pattern originally documented by Drew and Travers 1985, where the sites of maximal cleavage are shown in figure 4.2A. The purine rich region also shows limited cleavage. The DNaseI cleavage pattern of the histone bound 160bp fragment, in the absence of PNA, is not the same as the 110bp fragment and a direct comparison is shown in figure 4.3. Regions of maximal cleavage are different in intensity creating a different phasing pattern, which is not comparable to the 110bp fragment and is more pronounced towards the 5′ region of the fragment. Additional experiments were undertaken with PNA 41, 42 and 43 all of

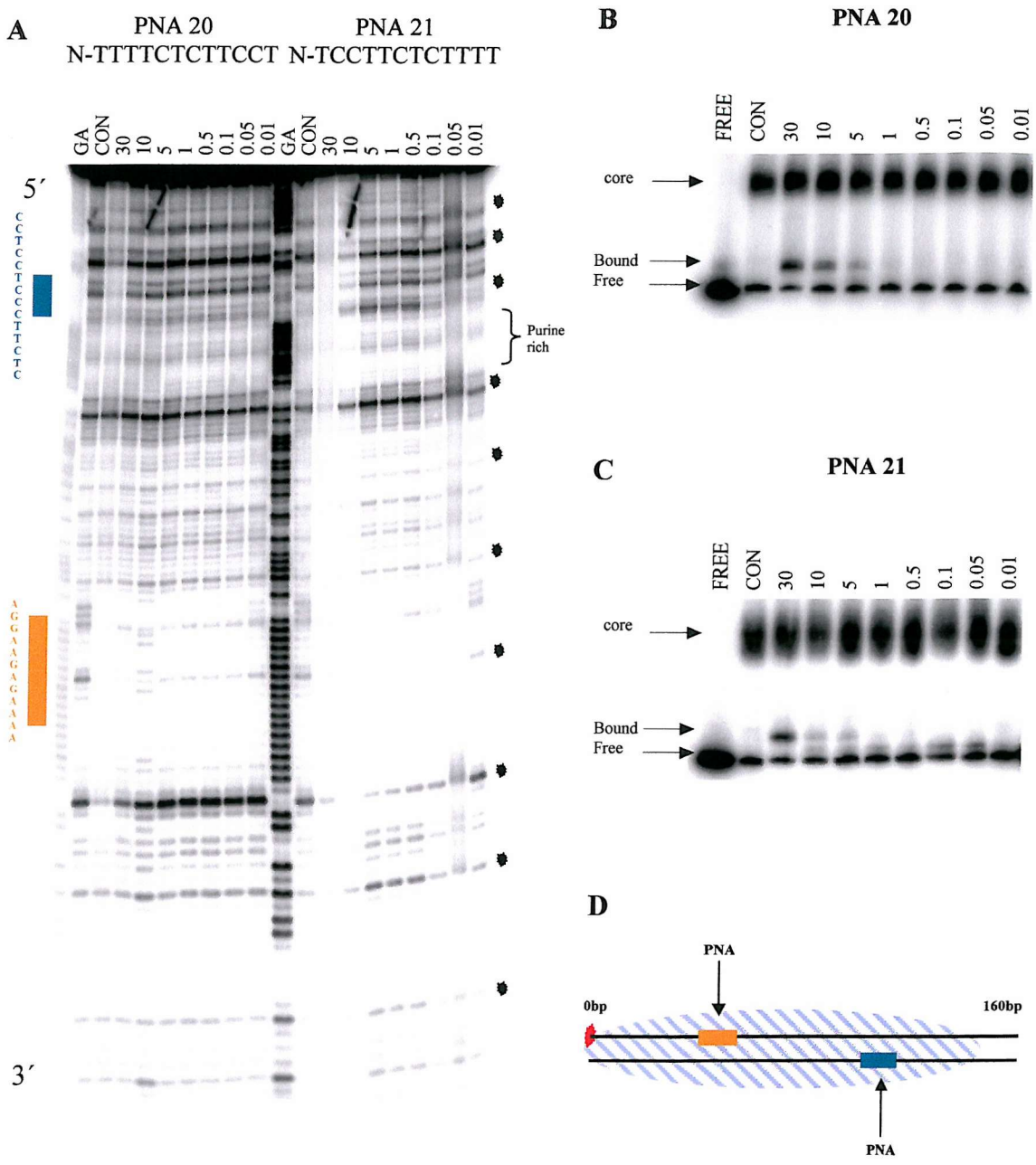

FIGURE 4.2 DNaseI cleavage (A) and bandshift assays (B,C) of the 160 base pair histone-bound *tyr*T (43-59) fragment in the presence and absence of PNA 20 and 21. The PNA concentration (μM) is indicated at the top of each gel lane. "CON" indicates digestion of the DNA in the absence of PNA and "GA" is a Maxam-Gilbert marker specific for purines. All the complexes were incubated for 24 hours in 50mM sodium acetate pH 5.0 before digestion with DNaseI. The location of site 1 is indicated in orange and the secondary binding site in green. The asterisks indicate the sites of maximal cleavage, where the DNA minor groove faces away from the protein core, corresponding to the original Drew and Travers digestion patterns (Drew & Travers 1985). D is a cartoon showing the likely position of the target site, relative to the histone octamer.

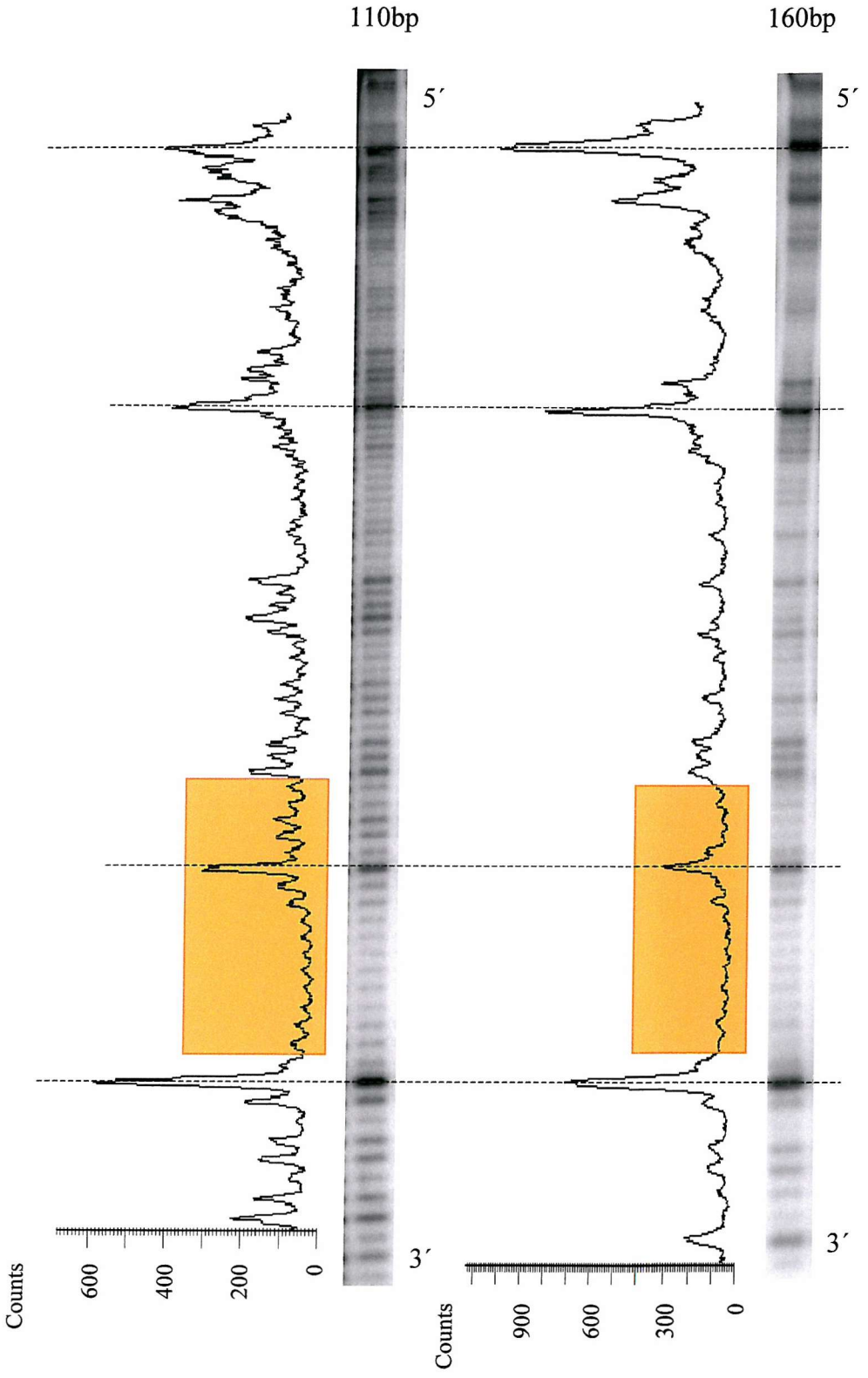

FIGURE 4.3 Differential plots of the 110 and 160bp histone bound *tyr*T (43-59) fragment in the absence of PNA. Plots are generated from imagequant analysis and the corresponding bases are identified through a dotted line. The location of site 1 is indicated in orange.

which produced footprints at site 1 at higher concentrations than with free DNA. Their C_{50} values are shown in table 4.1.

Bandshift assays of the 160bp fragment with PNA 20 and 21 are shown in figure 4.2B and C. It can be seen that addition of these PNAs does not disrupt the nucleosome core particle, even at the highest PNA concentrations, and that no supershifted species are produced. Once again retarded bands corresponding to complexes between PNA and the small amount of contaminating free DNA are evident. Additional experiments, performed with PNA 41, 42 and 43, showed no disruption to the nucleosome core particle and no supershifted species (data not shown).

The orientation of site 1 in relation to the histone octamer can be resolved through the original cleavage studies by Drew and Travers in 1985, only if you presuppose that this 160bp fragment sits in the same location and orientation as originally documented. They deduced from the electrophoretic profile shown in figure 4.4, that between positions 40-60 bases 49 and 60 are located on the inner surface of DNA whereas positions 44 and 55 are on the outer surface, facing away from the protein. The initial start position of site 1 is positioned facing away from the protein whereas the central region faces towards the surface and the end regions face away from the protein. Under this orientation, PNA is able to target but only at relatively high PNA concentrations. The orientation of this site will consequently change between different fragments.

Figure 4.5A shows DNaseI footprinting gels for the histone-bound 190 base pair *tyr*T (43-59) fragment in the presence or absence of PNA 20 and 21. In this fragment site 1 is located 43 base pairs from one end of the fragment, and 147 base pairs from the other. It is therefore possible to position the DNA so the PNA binding

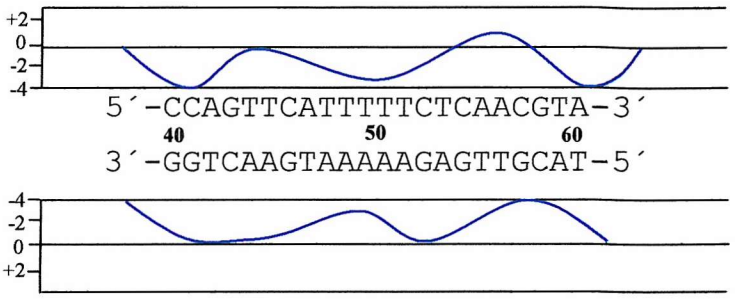

FIGURE 4.4 Digestion of a section of the *tyr*T core complex by DNaseI identifying the locations of enhanced cleavage between positions 40-60. This is taken from the original *tyr*T DNA sequence published in Drew and Travers in 1985 where they plotted the difference between two numbers, In (probability, core) –In (probability linear) plotting the difference for each bond. The vertical scales on the left are units of difference In (probability) to signify: enhanced cleavage of the core complex (+2), no difference in the cutting between core and linear (0, or reduced cleavage in the core complex compared to the linear (-2,-4) (Drew & Travers 1985).

site is not in contact with the protein, as illustrated in figure 4.5D. However, this will be more significant for the reconstitution of pre-formed PNA-DNA complexes and the translation positioning of the nucleosome core particle could be identical to the 160bp fragment. Direct comparison of the 160 and 190bp fragments is shown in figure 4.6. A similar cleavage pattern is present for both fragments indicating that the nucleosome reconstitution could be located in the same region along the fragment. However, the cleavage pattern towards the 5′ region of the gel is not visible which in turn shows that the translational positioning of the nucleosome core particle on the 190bp fragment cannot be clearly positioned through this method, but there are indications that the protein may sit in the same location. Examination of these DNaseI cleavage patterns in figure 4.5A reveal that PNA 20 produces a clear footprint at site 1, which persists to a concentration of 5μM, which is slightly lower than that required with the shorter 160 base pair fragment. PNA 21 produces similar results and a footprint is visible down to a concentration of 0.01μM. This also reiterates the observation that the protein potentially sits in the same locations as on the 160bp

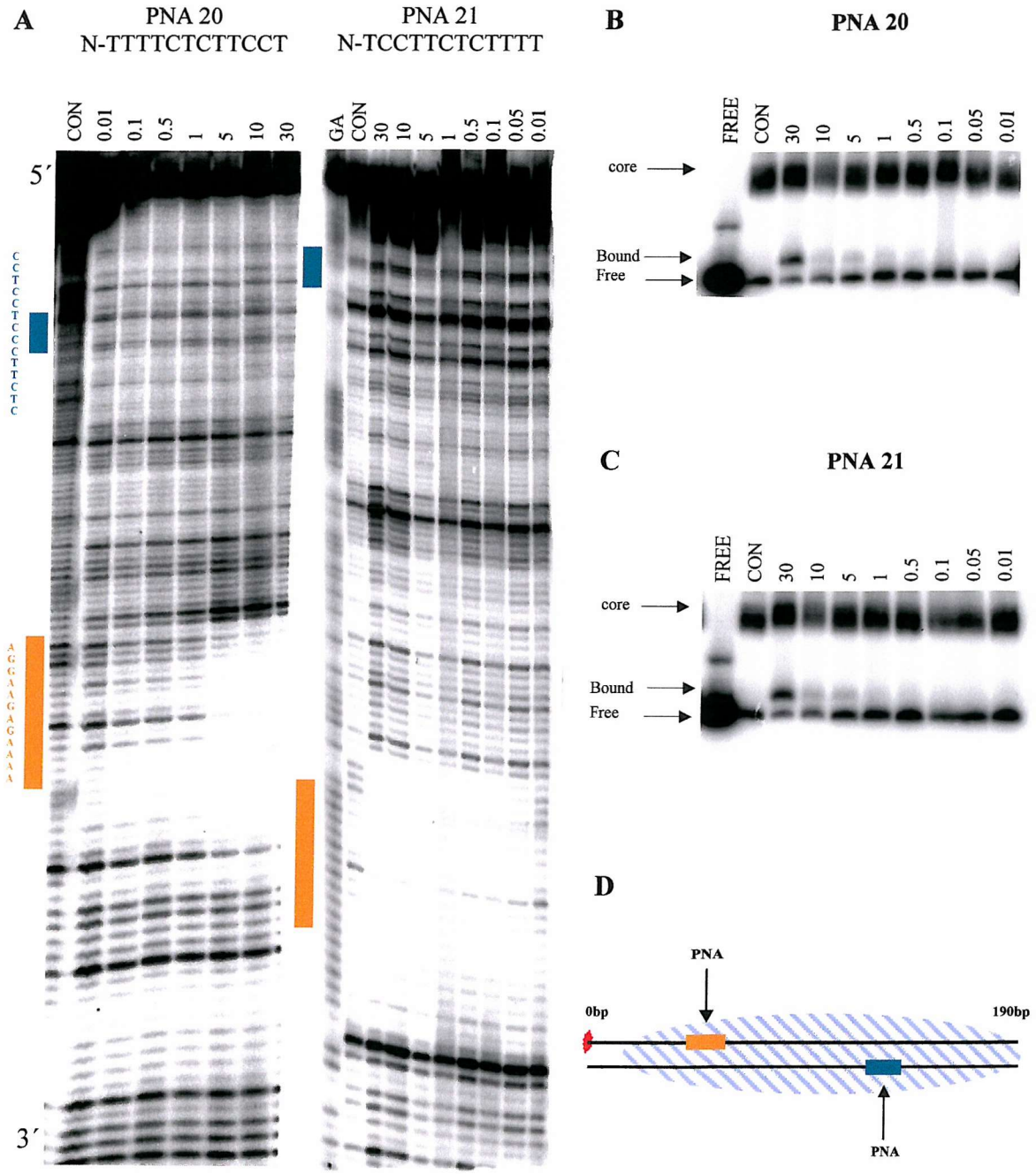

FIGURE 4.5 DNaseI cleavage (A) and bandshift assays (B,C) of the 190 base pair histone-bound *tyr*T (43-59) fragment in the presence and absence of PNA 20 and 21. The PNA concentration (μM) is indicated at the top of each gel lane. "CON" indicates digestion of the DNA in the absence of PNA and "GA" is a Maxam-Gilbert marker specific for purines. All the complexes were incubated for 24 hours in 50mM sodium acetate pH 5.0 before digestion with DNaseI. The location of site 1 is indicated in orange and the secondary binding site in green. D is a cartoon showing the likely position of the target site, relative to the histone octamer.

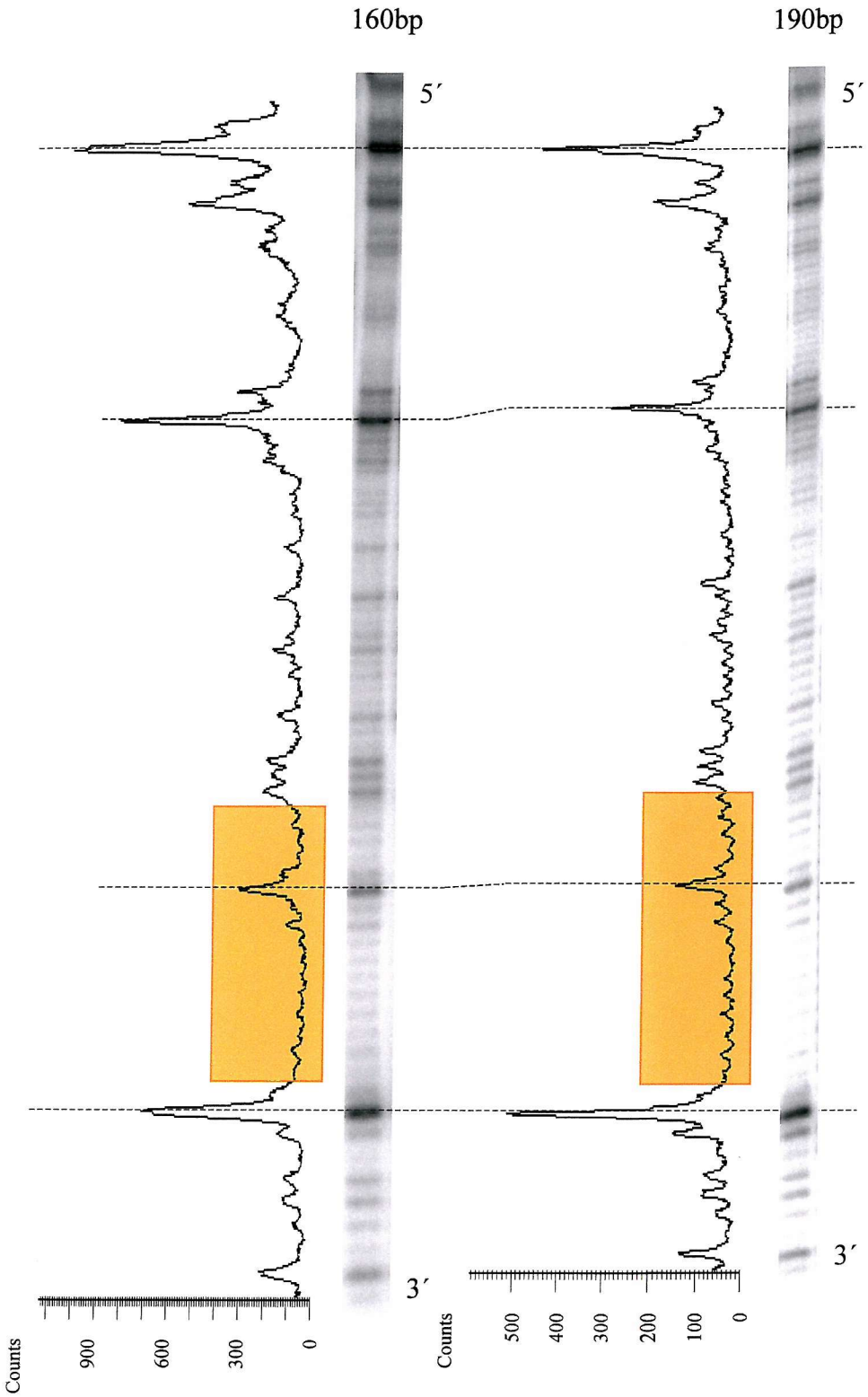

FIGURE 4.6 Differential plots of the 160 and 190bp histone bound *tyr*T (43-59) fragment in the absence of PNA. Plots are generated from imagequant analysis and the corresponding bases are identified through a dotted line. The location of site 1 is indicated in orange.

fragment. The footprint with PNA 21 produces similar PNA concentrations as those seen with free DNA however PNA 20 is still significantly higher (Section 3.2.2). In contrast no footprints are evident at the secondary binding site, even at the highest PNA concentrations, which could indicate that the protein has obstructed this site and is not located in exactly the same position as on the 160bp. The interaction of PNA 41, 42 and 43 targeting the 190bp histone bound fragment produce footprints at site 1 to a concentration of 0.1μM, 1μM and 5μM respectively which is slightly higher concentrations than those obtained with free DNA (see figure 3.2)(data not shown).

Bandshift assays with this nucleosomal 190 base pair fragment (figures 4.5Band C) show that PNAs 20 and 21 do not appear to disruption the nucleosome core particle, as the intensity of this retarded band is not altered, even at the highest concentrations. However, with PNA 21 there is a very small supershift present at PNA concentrations of 10 and 30μM. This could be attributed to a ternary PNA/DNA-protein complex, however this small increase in molecular weight potentially would not produce a visible supershift. Once again retarded bands corresponding to complexes between PNA and the small amount of contaminating free DNA are evident. Additional experiments performed with PNA 41, 42 and 43 show no disruption to the nucleosome core particle, however PNA 41 also produces a small supershift as seen with PNA 20 (data not shown).

Figure 4.7A shows DNaseI footprinting gels for the histone-bound 360 base pair *tyr*T (43-59) fragment in the presence or absence of PNA 20 and 21. The oligopurine tract site 1 is located approximately 130 base pairs from one end of the fragment and 230 base pair from the other. It is therefore possible for it to interact with two nucleosomes, with the oligopurine tract positioned close to the linker (as illustrated in figure 4.7D). It can be seen that normal cleavage over site 1 with these

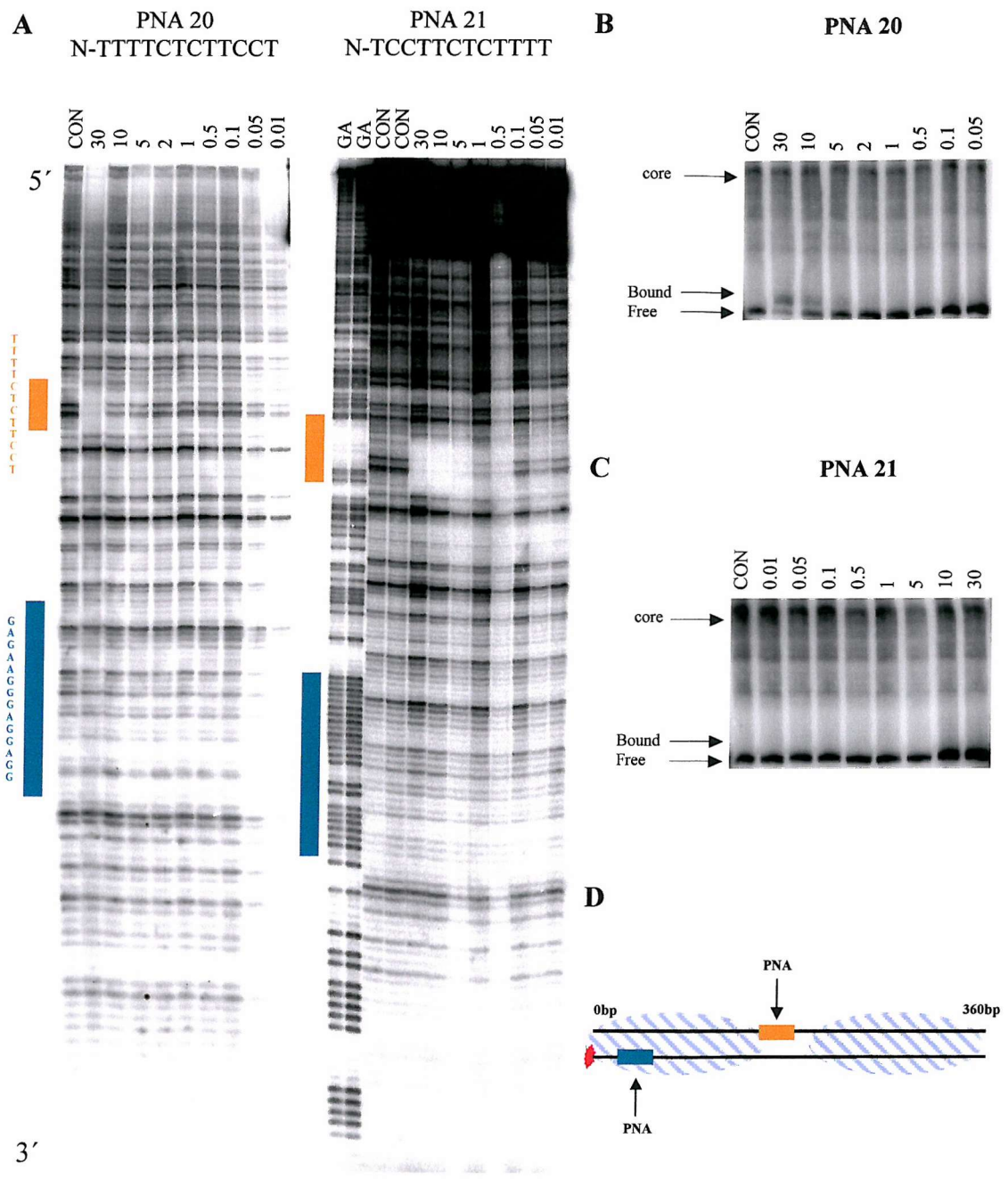

FIGURE 4.7 DNaseI cleavage (A) and bandshift assays (B,C) of the 360 base pair histone-bound *tyr*T (43-59) fragment in the presence and absence of PNA 20 and 21. The PNA concentration (μM) is indicated at the top of each gel lane. "CON" indicates digestion of the DNA in the absence of PNA and "GA" is a Maxam-Gilbert marker specific for purines. All the complexes were incubated for 24 hours in 50mM sodium acetate pH 5.0 before digestion with DNaseI. The location of site 1 is indicated in orange and the secondary binding site in green. D is a cartoon showing the likely position of the target site, relative to the histone octamer.

PNAs does only returns at concentrations below 2 and 0.1μM respectively. Interestingly, both PNAs appear to bind better to the 360bp fragment due to the nucleosome positioning in relation to site 1, this site being located towards the linker DNA region or the peripheral DNA regions of the nucleosome core particle. The phasing pattern over the secondary binding site represents nucleosomal bound DNA and this phasing continues up towards site 1. Once again there is no footprint at the secondary binding site that was noted with free DNA. Bandshift assays with this 360 base pair fragment are presented in figures 4.7B and C. These show that addition of the PNAs does not affect the amount of DNA in the retarded (nucleosomal) band. However a clear single retarded species is not present with this fragment as seen with the previous fragments indicating that potentially there are interactions with more the one histone octamer at different positions along the fragment, represented as multiple bands. We assume that the higher bands would represent potentially two proteins bound whereas the lower bands represent the presence of one nucleosome core particle. Additional experiments were performed with PNA 41, 42 and 43 all of which targeted site 1 a relatively lower concentration of 0.1 and 1μM, which is slightly higher than when targeted to free DNA. Addition of each PNA did not show any affect to the nucleosomal band as previously seen with PNA 20 and 21 (data not shown).

Footprinting plots showing the intensity of bands in these footprints as a function of PNA concentration are shown in figure 4.8 for PNA 20, 21, 41, 42 and 43, and the C_{50} values determined from these are summarised in table 4.1. None of the PNAs bind to the nucleosomal 110 base pair fragment. Some interaction with PNA is evident with the 160 base pair fragment, but the higher C_{50} values show that this is much weaker than to free DNA. PNA 41 is the least affected, which has only a 3 fold

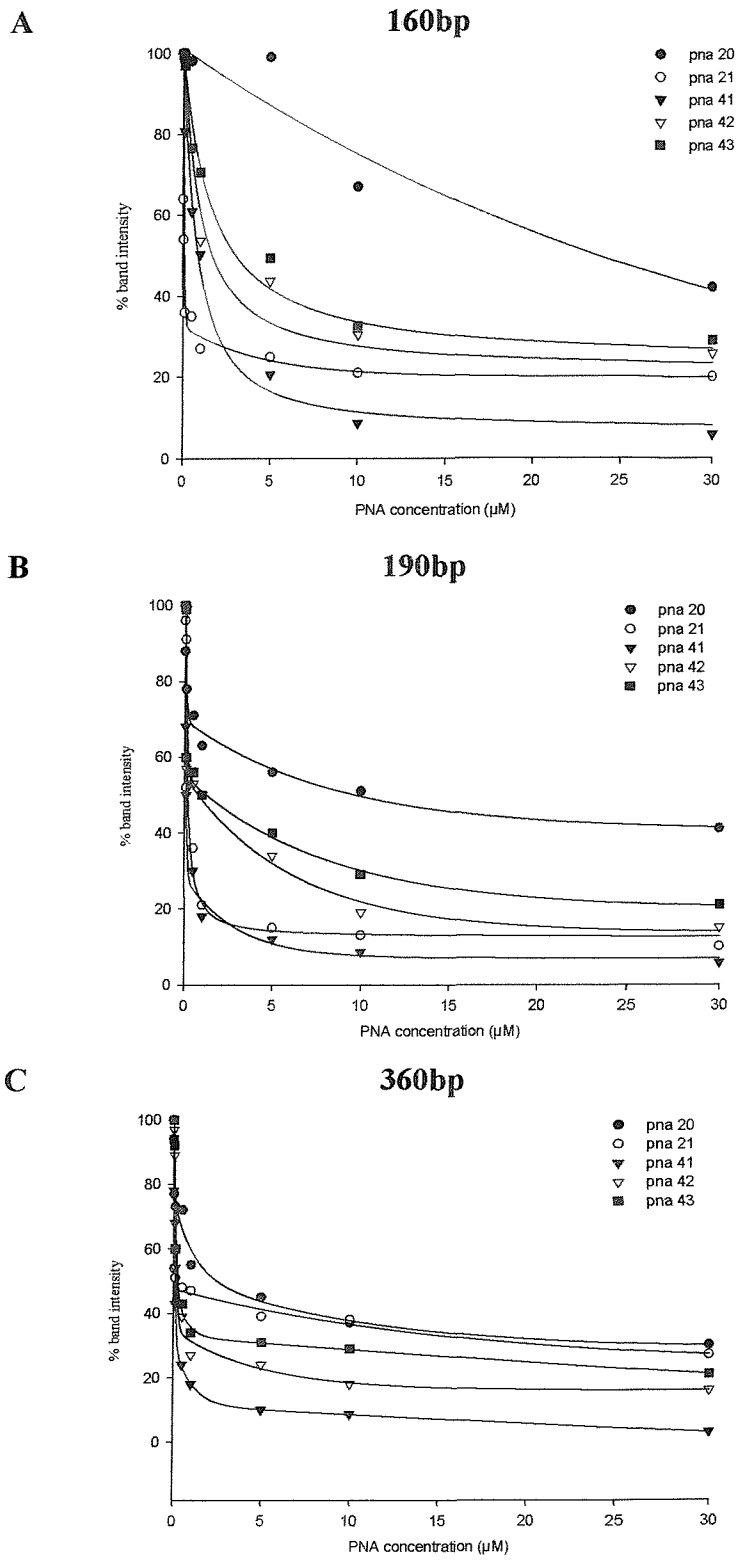

FIGURE 4.8 Footprinting plots showing the interaction of PNAs 20, 21, 41, 42 and 43 with site 1 on different length *tyr*T (43-59) fragments, when reconstituted into nucleosomal DNA. (A) 160bp, (B) 190bp and (C) 360bp fragments. The data were obtained from analysis of the footprints shown in figures 4.1-4.7.

PNA Sequence	C_{50} (μM)				
	Free DNA	Nucleosomal DNA			
		110bp	160bp	190bp	360bp
20	2.9 ±4	No footprint	23.6 ±5.52	9.6 ±4.6	0.8 ±7
21	0.2 ±2	No footprint	0.8 ±5.51	0.2 ±7.6	0.2 ±5
41	0.04 ±1	No footprint	0.9 ±4.53	0.08 ±7.2	0.08 ±8
42	0.4 ±6	No footprint	1.8 ±6.2	1.0 ±14.7	0.2 ±11
43	0.6 ±2	No footprint	3.0 ±4.4	1.9 ±13.3	0.2 ±10

TABLE 4.1 C_{50} values for different PNA sequences targeted to site 1 on the 110, 160, 190 and 360bp *tyr*T (43-59) fragments. C_{50} values were calculated from the data shown in figure 4.5.

decrease in apparent affinity to 0.12μM ±4.53, in compared to free DNA (0.04μM ±1). PNA 21 and 41 have a slightly larger change, while PNA 20, 43 are most affected. These results appear to indicate that the antiparallel sequences are more affected than the parallel ones. Increasing the sequence length to 190 base pairs further reduces the obstruction to PNA binding, decreasing the C_{50} values for all the PNAs. However, these results show that PNA is could still partly hindered from interacting with its target site, especially noticeable with PNA 20. On increasing the fragment length to 360 base pairs the histone proteins have almost no effect on PNA binding at site 1.

4.2.2 Reconstitution of *tyr*T (43-59) fragments containing pre-formed PNA-DNA complexes

The previous section examined the interaction of PNAs with DNA fragments that has already been reconstituted into nucleosome core particles. In contrast this section examines how pre-formed PNA complexes interact with histone proteins. Figure 4.9A shows the DNaseI footprinting gels for experiments in which the 110bp *tyr*T (43-59) fragment was targeted with PNA 21 and 41 prior to nucleosome reconstitution. In contrast to the results shown in figure 4.1, it can be seen that both PNA 21 and 41 produce clear footprints at site 1, which persist to concentrations of 0.5μM and 0.01μM respectively. These values are similar to those determined with free DNA. Bandshifts analysis of these complexes (figure 4.9B and C) shows a very clear reduction in the formation of nucleosome bound DNA at moderate PNA concentrations. This is accompanied by the production of large quantities of free PNA/DNA complexes. Closer inspection of the cleavage pattern in the presence of PNA in comparison to free DNA is shown in figure 4.10. The cleavage patterns for both fragments are very similar indicating that the fragment does not represent that of nucleosome bound DNA and correlates to the cleavage pattern of free DNA, which is also reiterated in the bandshift assays. Quantitative analysis of these data is shown in figure 4.11A, in which it can be seen that addition of PNA prevents reconstitution at concentrations of 1μM and above. PNA 20, 21, 42 and 43 reduce the reconstitution to about 25% of that in the absence of PNA, while PNA 41 reduced this to only 18%. These results suggest that these pre-formed PNA/DNA complexes are not able to wrap around the histone octamer. The small amount of reconstitution that is observed in each case could be due to either dissociation of some

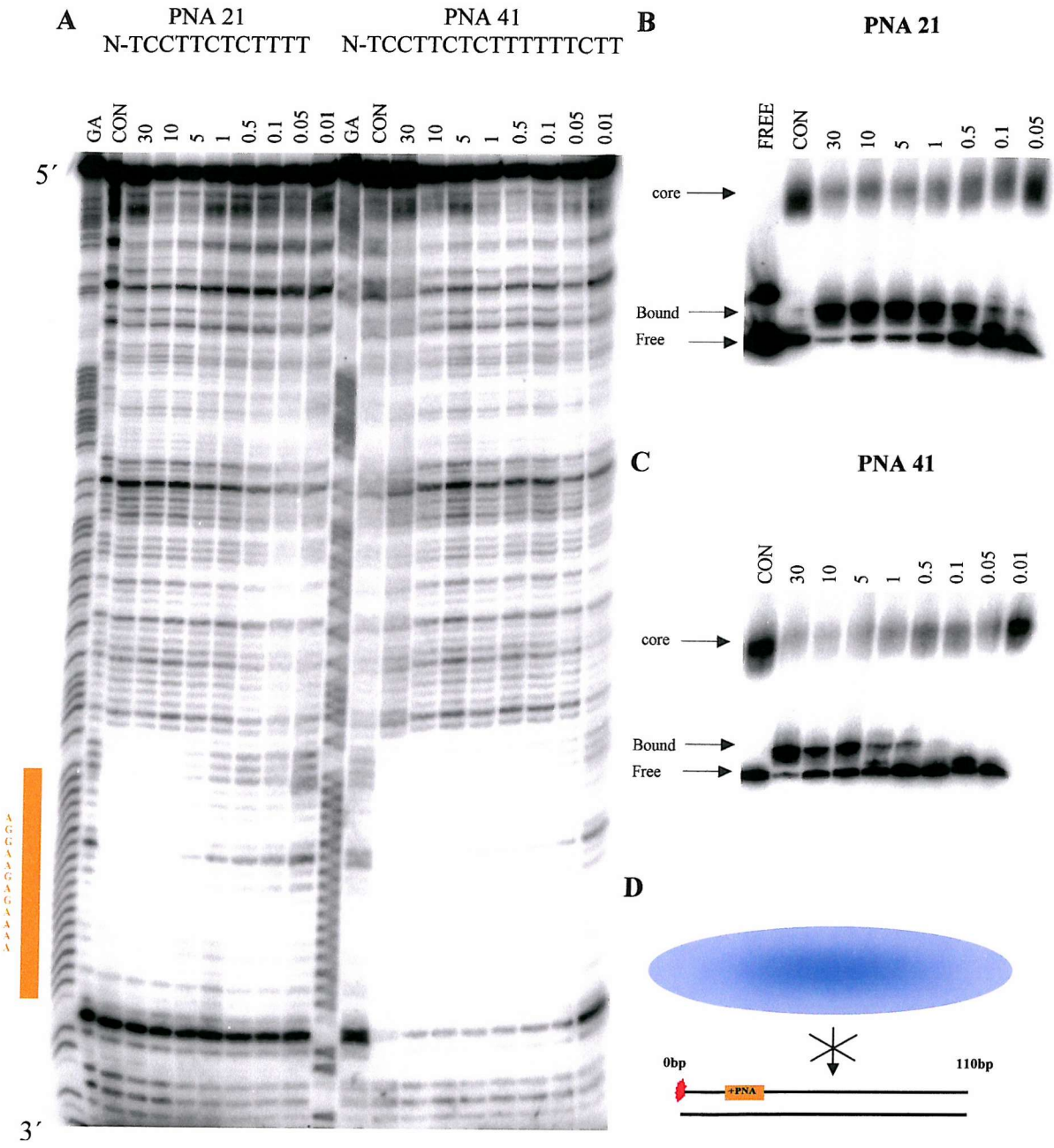

FIGURE 4.9 DNaseI cleavage (A) and bandshift assays (B and C) for the 110 base pair *tyr*T (43-59) fragment, which had been complexed with PNA 21 and 41 prior to reconstitution. The PNA concentration (μM) is indicated at the top of each gel lane. "CON" indicates digestion of the DNA in the absence of PNA and "GA" is a Maxam-Gilbert marker specific for purines. All the complexes were incubated for 24 hours in 50mM sodium acetate pH 5.0 before digestion with DNaseI. The location of site 1 is indicated in orange and the secondary binding site in green. D is a cartoon showing the likely position of the target site, relative to the histone octamer.

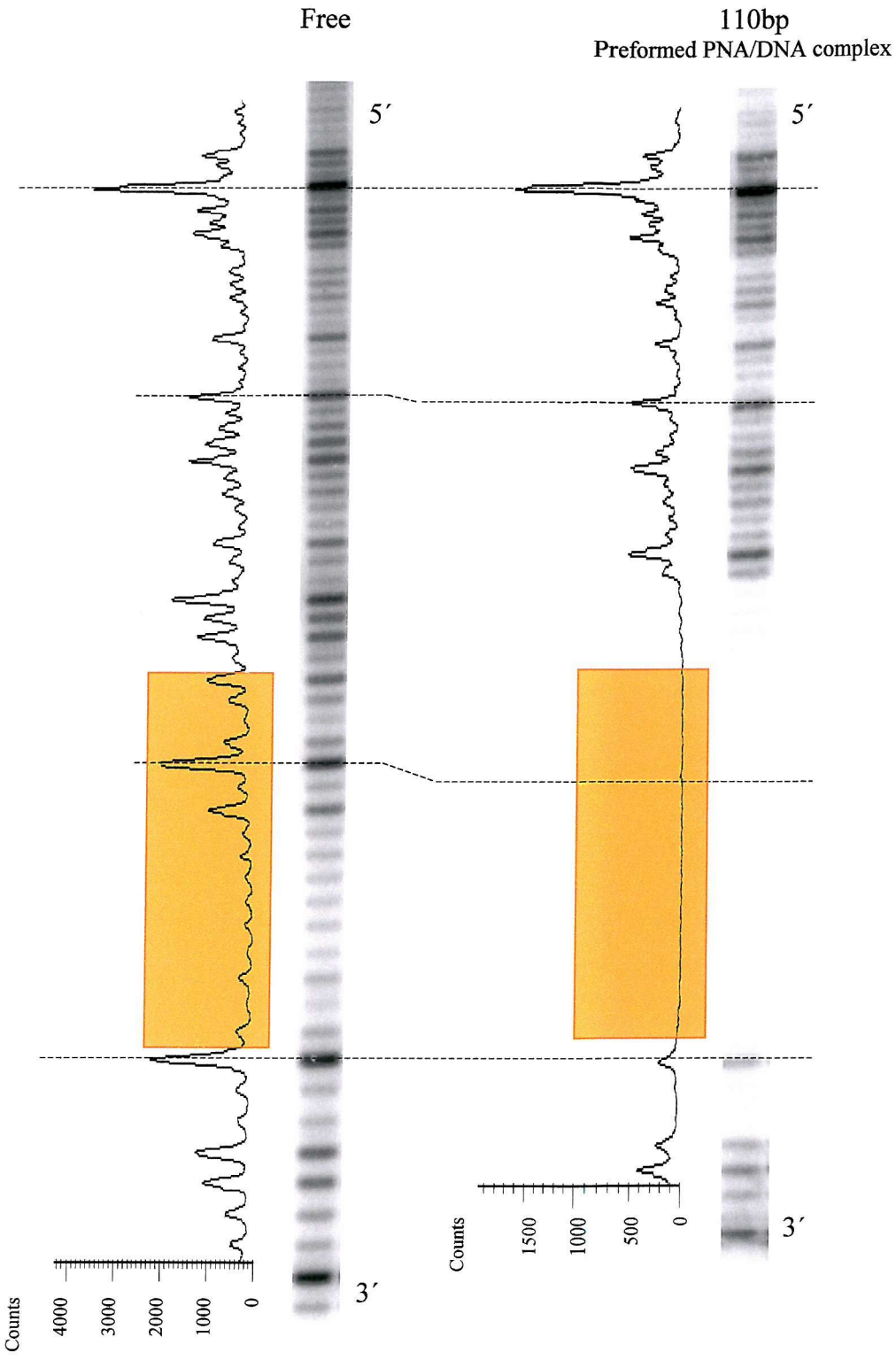

FIGURE 4.10 Differential plots of the free 110bp and the 110 base pair *tyr*T (43-59) fragment, which had been complexed with PNA prior to reconstitution. Plots are generated from imagequant analysis and the corresponding bases are identified through a dotted line. The location of site 1 is indicated in orange.

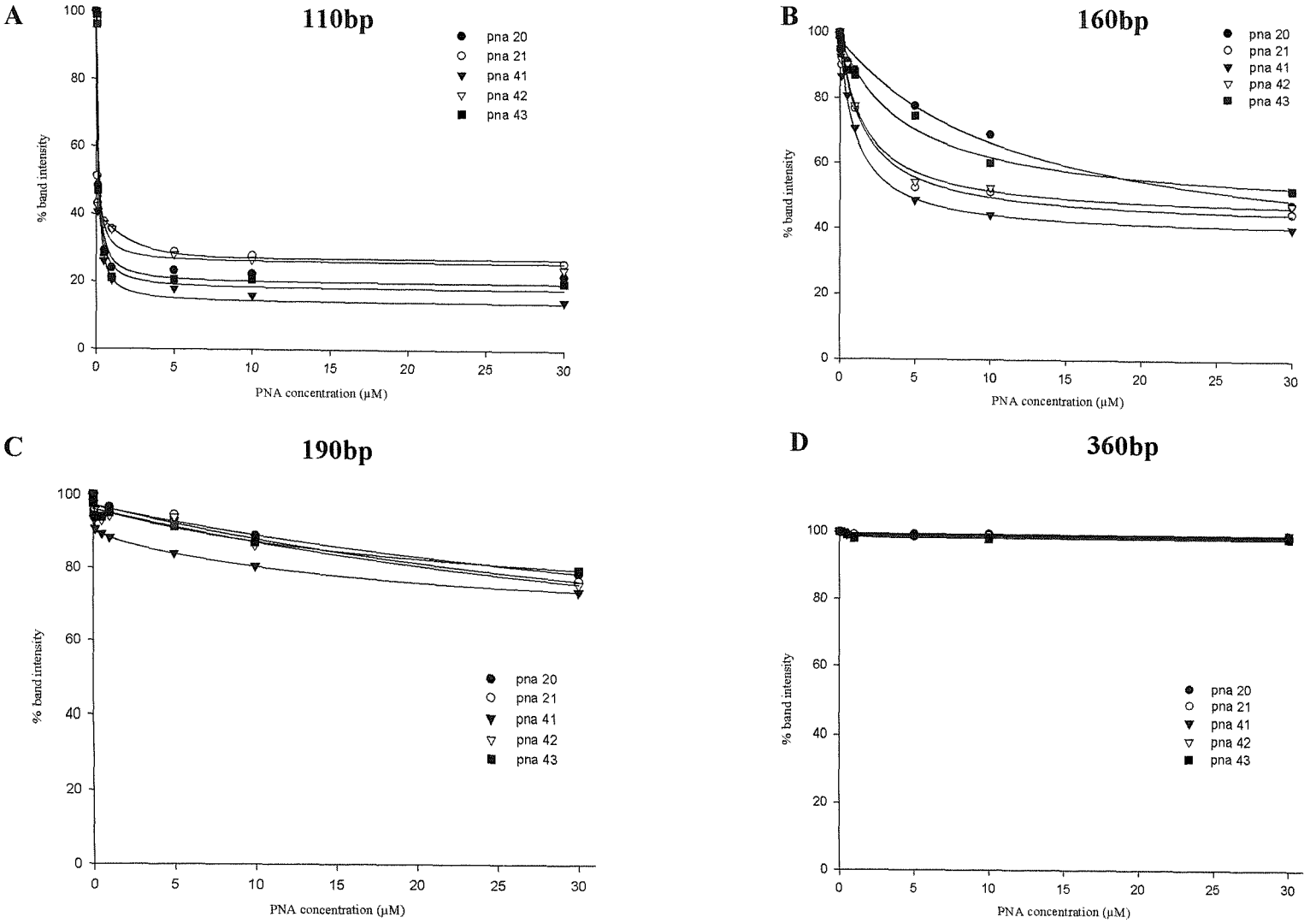

FIGURE 4.11 Effect of PNAs 20, 21, 41, 42 and 43 on the reconstitution of different length DNA containing the *tyr*T (43-59) sequence. The PNA/DNA complexes were generated before nucleosome reconstitution. A) 110, B) 160, C) 190 and D) 360 base pair fragments.

of the PNA/DNA complex during the slow process of reconstitution, or from the presence of some free DNA to which PNA is not bound. This result shows that remaining 60 base pairs of the PNA/DNA-bound fragment, beyond the PNA binding site, are not sufficient to permit nucleosome reconstitution.

Figure 4.12 shows similar DNaseI and bandshift gels in which the 160 base pair *tyr*T (43-59) fragment was targeted with PNA 20 and 21 prior to nucleosome reconstitution. Both PNA 20 and 21 produce clear footprints at site 1, which persist to concentrations of 0.01μM and 0.05μM respectively. These results are comparable to those seen with free DNA. However, it should be noticed that there is no change in the cleavage pattern around the secondary binding site indicating that the preformed complex form has been displaced. In the bandshift analysis of these samples (figures 4.12B and C) it can be seen that addition of PNA reduces the amount of DNA in the slowest moving band, which corresponds to the nucleosomal complex. In addition several retarded bands, corresponding to free PNA/DNA complexes can be seen, and are similar to those described in Chapter 3, with two retarded species for PNA 20, but one with PNA 21. A direct comparison between the histone bound 160bp fragment and the 160bp fragment that has been pre-targeted with PNA 21 (concentrations of 30μM) is shown in figure 4.13. A weaker phasing pattern is shown but this does have a similar correlation to the cleavage pattern of the histone bound fragment indicating that the protein could potentially be sat in the same location, however the translational positioning has not been fully determined. Further experiments would need to be undertaken in order to fully confirm this. Quantitative analysis of the amount of material in the nucleosomal band as a function of PNA concentration is shown in figure 4.11B. This shows a increase in the amount of histone-bound DNA, even at higher PNA concentrations. PNA 21, 41, and 42 reduce the amount of nucleosomal

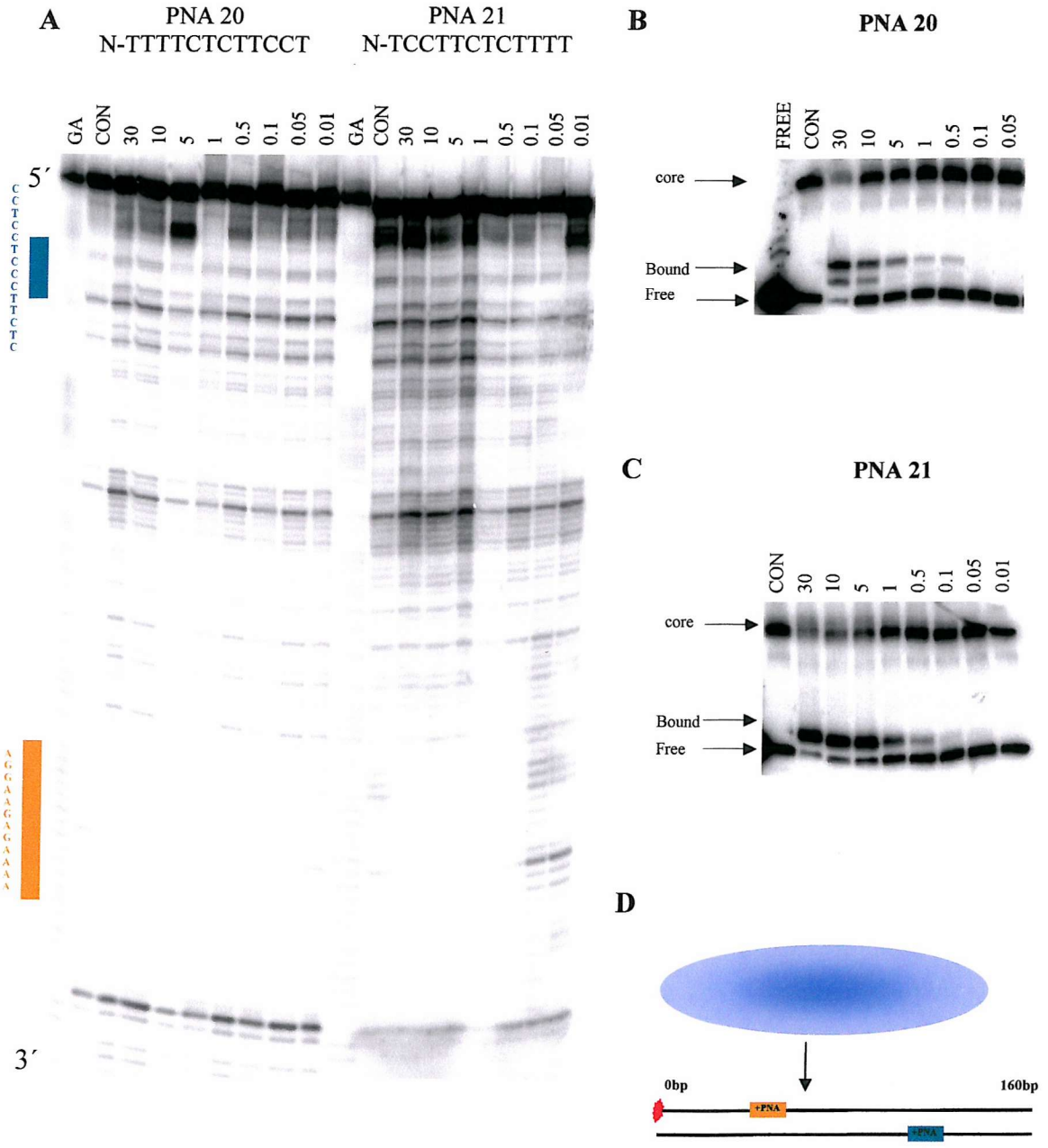

FIGURE 4.12 DNaseI cleavage (A) and bandshift assays (B and C) for the 160 base pair *tyr*T (43-59) fragment, which had been complexed with PNA 20 and 21 prior to reconstitution. The PNA concentration (μM) is indicated at the top of each gel lane. "CON" indicates digestion of the DNA in the absence of PNA and "GA" is a Maxam-Gilbert marker specific for purines. All the complexes were incubated for 24 hours in 50mM sodium acetate pH 5.0 before digestion with DNaseI. The location of site 1 is indicated in orange and the secondary binding site in green. D is a cartoon showing the likely position of the target site, relative to the histone octamer.

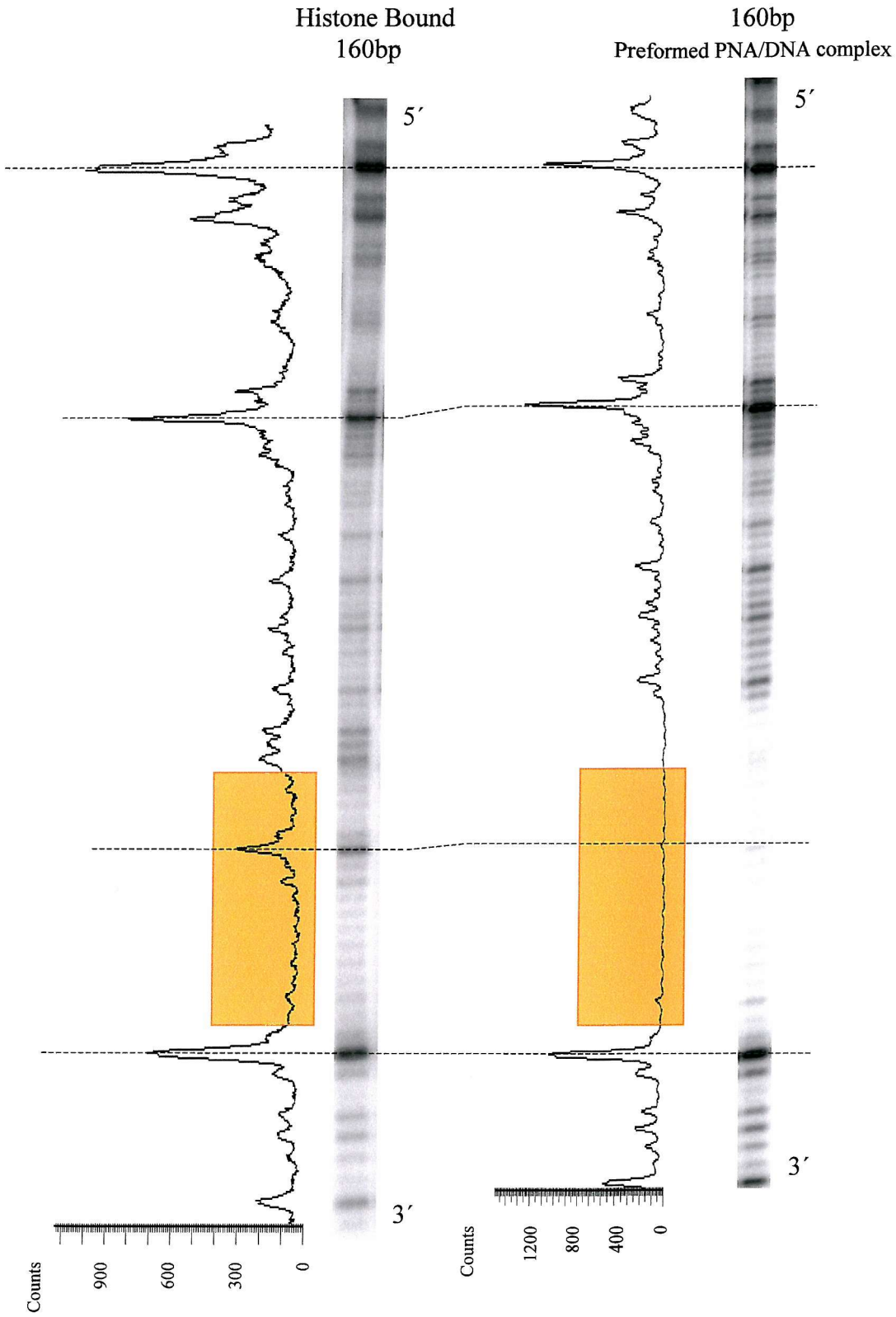

FIGURE 4.13 Differential plots of the histone bound 160bp and the 160 base pair *tyr*T (43-59) fragment, which had been complexed with PNA 21 (concentration 30μM) prior to reconstitution. Plots are generated from imagequant analysis and the corresponding bases are identified through a dotted line. The location of site 1 is indicated in orange.

DNA by 50%. PNA 20 and 43 show a more gradual decrease in reconstitution, but again reduce the amount to about 50%. Interestingly these two sequences are both antiparallel to the target site and have lower binding affinities than their corresponding parallel sequences. These results confirm that the PNA/DNA complex is not able to efficiently reconstitute onto the nucleosome core particle. However the obstruction is less than that seen with the 110bp fragment, and is presumably because the 160 base pair fragment has a longer region of PNA-free DNA, which can interact with the protein surface, however this is not confirmed. Binding to the secondary site is abolished by interaction with the protein. Interestingly, this result suggests that the 100 contiguous base pairs of PNA-free DNA on fragment could be sufficient for reconstitution onto the nucleosome core particle.

Figure 4.14 shows the DNaseI footprinting and bandshift gels from similar experiments in which the 190 base pair *tyr*T (43-59) fragment was targeted with PNA 20 and 21 prior to nucleosome reconstitution. Both PNAs show a clear footprint over the target site at concentrations greater than 10μM and 1μM respectively (figure 4.14A), which are higher than those required to produce footprints with free DNA. There is also evidence for a weak footprint at the secondary binding site with 30μM PNA 20, though PNA 21 does not affect the cleavage in this region. Bandshift analysis of these samples (figure 4.14B and C) reveals that both PNA only cause a small reduction of the amount of DNA in the retarded nucleosomal species, though the usual free PNA/DNA complexes are also evident. The reduction in the DNA-histone complex is only evident at high PNA concentrations. Direct comparison of the 190bp fragment targeted post and prior to nucleosome reconstitution in shown in figure 4.15. The cleavage patterns show very different cleavage patterns throughout the fragment. This suggests that the protein has translationally shifted along the fragment as to not

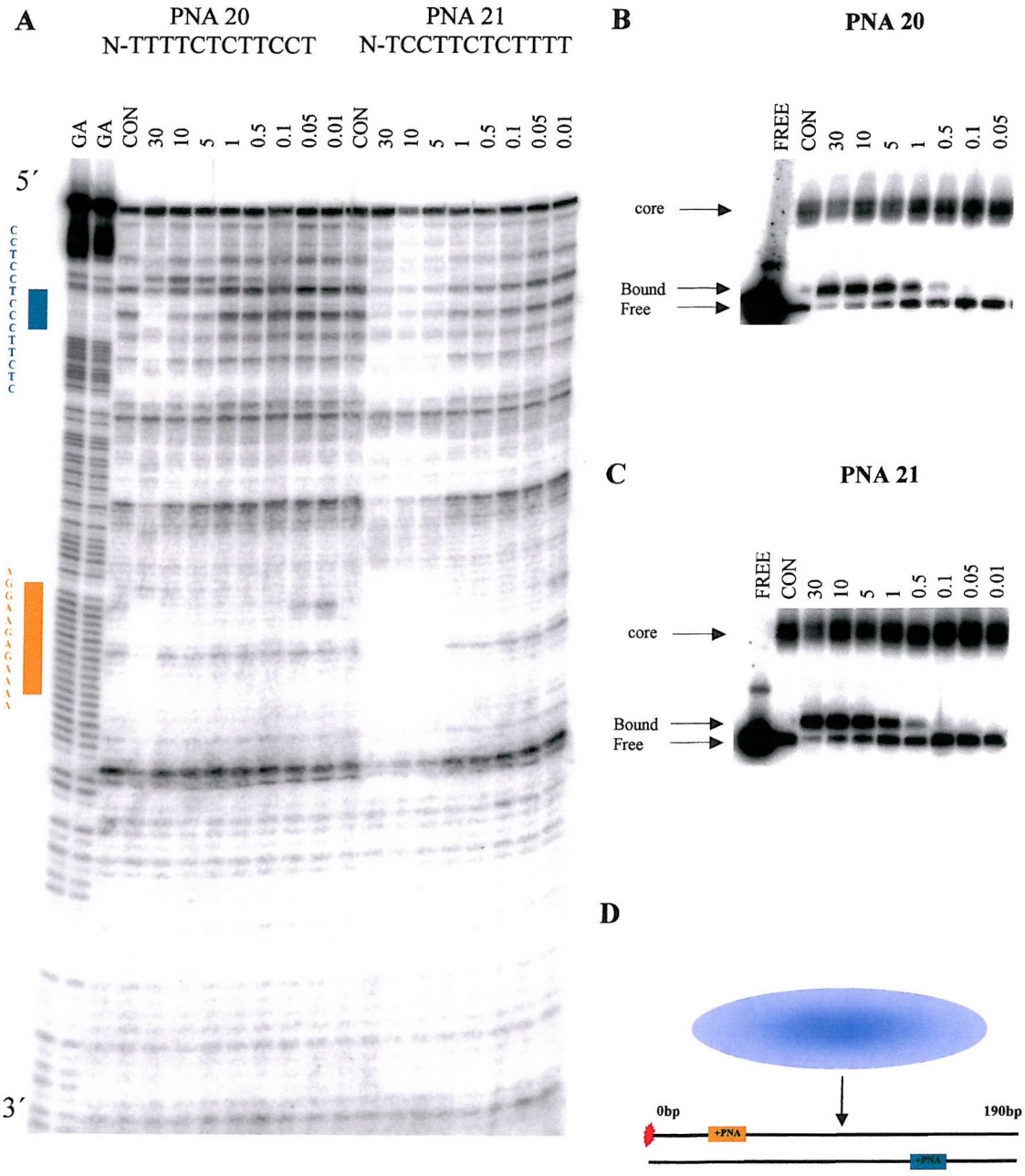

FIGURE 4.14 DNaseI cleavage (A) and bandshift assays (B and C) of the 190 base pair *tyr*T (43-59) fragment, which had been complexed with PNA 20 and 21 prior to reconstitution. The PNA concentration (μM) is indicated at the top of each gel lane. "CON" indicates digestion of the DNA in the absence of PNA and "GA" is a Maxam-Gilbert marker specific for purines. All the complexes were incubated for 24 hours in 50mM sodium acetate pH 5.0 before digestion with DNaseI. The location of site 1 is indicated in orange and the secondary binding site in green. D is a cartoon showing the likely position of the target site, relative to the histone octamer.

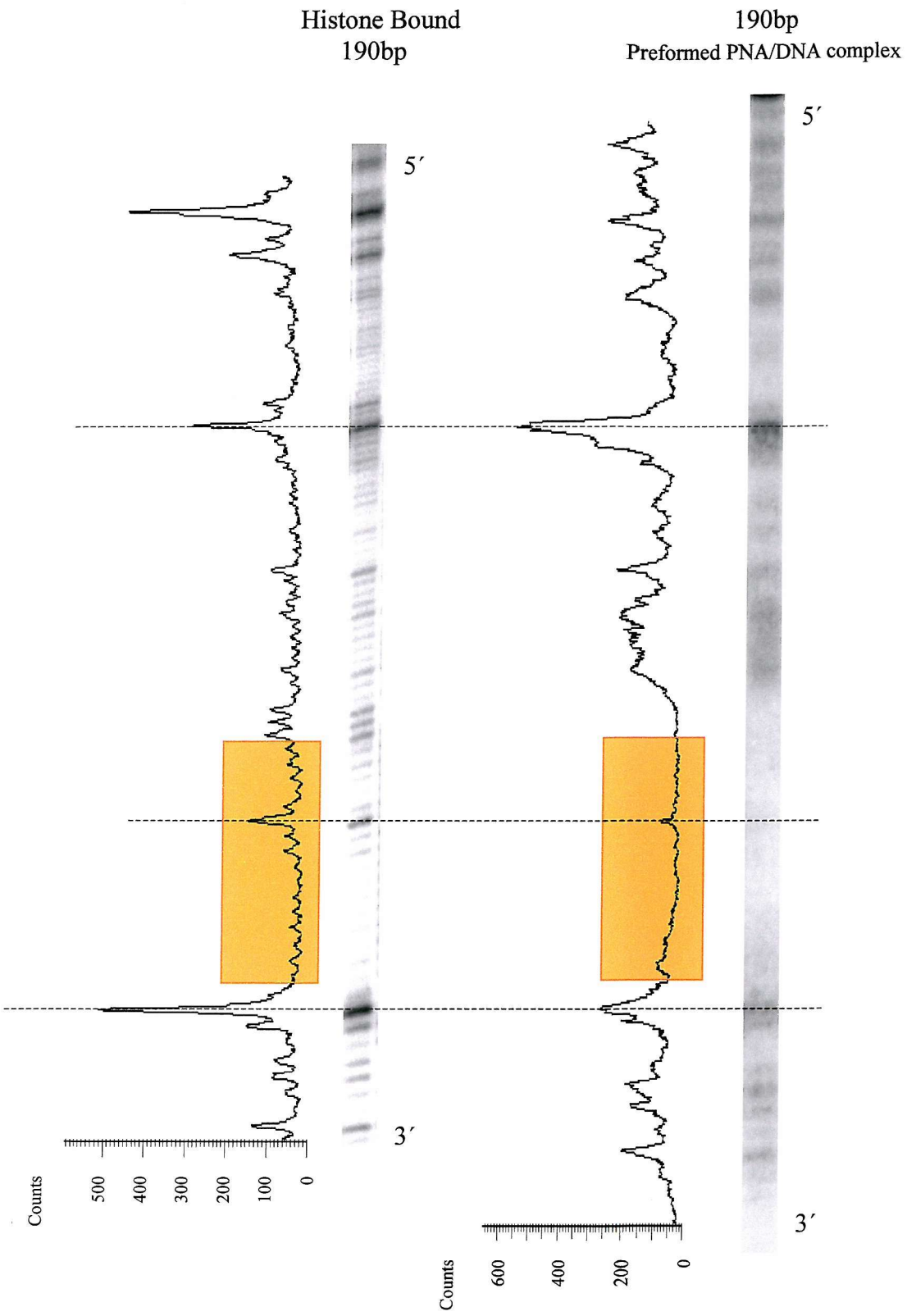

FIGURE 4.15 Differential plots of the histone bound 190bp and the 190 base pair *tyr*T (43-59) fragment, which had been complexed with PNA 21(concentration 30μM) prior to reconstitution. Plots are generated from imagequant analysis and the corresponding bases are identified through a dotted line. The location of site 1 is indicated in orange.

incorporate the PNA/DNA complex within the nucleosome core particle. Quantitative analysis of these bandshift data is shown in figure 4.11C, from which it can be seen that there is a gradual reduction in the intensity of the nucleosomal band with increasing PNA concentrations. However 80% of the nucleosomal DNA is still retained even at the highest concentrations. The reductions with this 190 base pair fragment are much less than those seen with the 160 and 110 base pair fragments. This is presumably because there is a longer contiguous region of PNA-free DNA, which can interact with the protein surface. However, it should also be noted that this abolishes the interaction with the secondary binding site as seen with free DNA.

Figure 4.16 shows DNaseI footprinting and bandshift gels from similar experiments in which the 360 base pair *tyr*T (43-59) fragment was targeted with PNA 20 and 21 prior to nucleosome reconstitution. PNA 20 and 21 both produce clear footprints over site 1 which persists to concentrations of 10μM and 1μM respectively. The concentrations are higher than those required with free DNA, but are similar to those seen with the 190 base pair fragment under similar conditions. Once again there is no interaction with the secondary binding site, even at the highest PNA concentrations. Bandshift experiments with these samples (figure 4.16B and C) show that the PNAs do not affect the nucleosome reconstitution, though the banding pattern is less clear with this longer DNA fragment. Direct comparison between the 360bp fragment targeted prior and post reconstitution has shown in figure 4.17 where the cleavage pattern is different throughout the fragment indicating that the presence of the PNA/DNA complex before nucleosome reconstitution has altered the phasing pattern which in turn shows that the protein(s) may have associated with a different region of the fragment. Quantitative analysis of these bandshifts is shown in figure 4.11D which confirms that the PNAs have little or no effect on the efficiency of

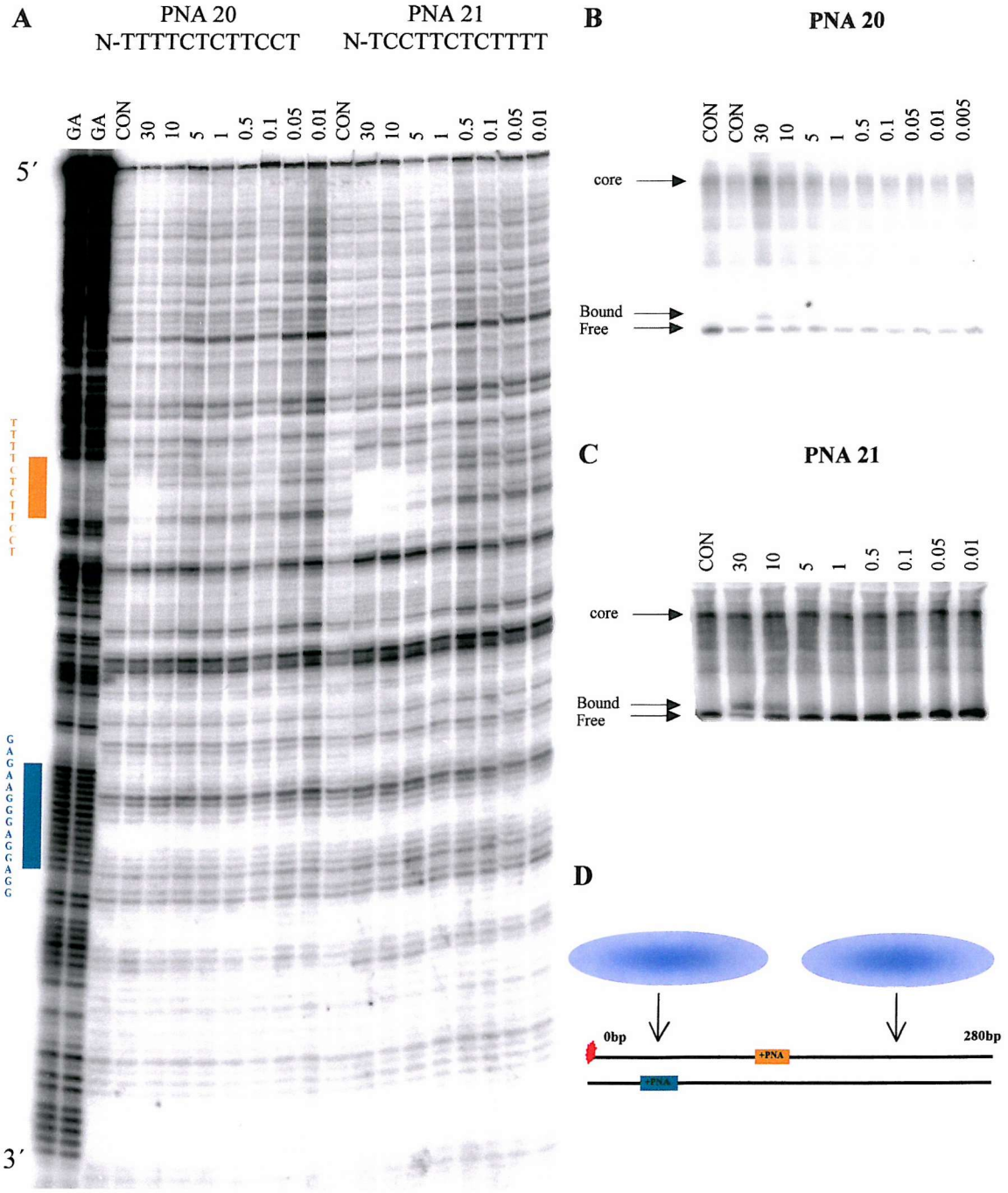

FIGURE 4.16 DNaseI cleavage (A) and bandshift assays (B and C) of the 360 base pair *tyr*T (43-59) fragment, which had been complexed with PNA 20 and 21 prior to reconstitution. The PNA concentration (μM) is indicated at the top of each gel lane. "CON" indicates digestion of the DNA in the absence of PNA and "GA" is a Maxam-Gilbert marker specific for purines. All the complexes were incubated for 24 hours in 50mM sodium acetate pH 5.0 before digestion with DNaseI. The location of site 1 is indicated in orange and the secondary binding site in green. D is a cartoon showing the likely position of the target site, relative to the histone octamer.

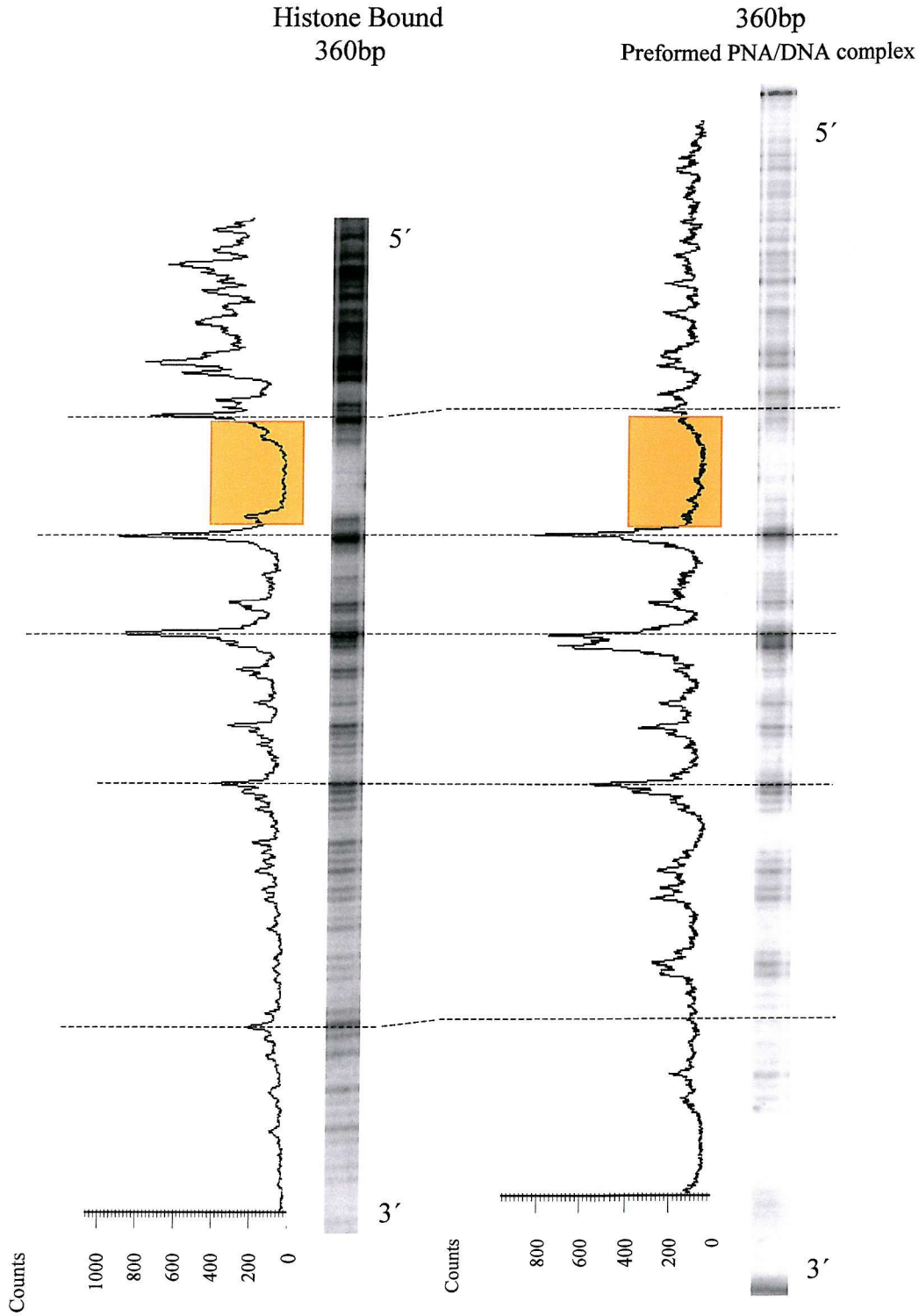

FIGURE 4.17 Differential plots of the histone bound 360bp and the 360 base pair *tyr*T (43-59) fragment, which had been complexed with PNA 21(concentration 30μM) prior to reconstitution. Plots are generated from imagequant analysis and the corresponding bases are identified through a dotted line. The location of site 1 is indicated in orange.

reconstitution. Presumably, this is again because there are long regions of contiguous PNA-free DNA, which can interact with the protein surface. In this case there are 130 and 210 base pairs either side of the target site, which may be located in the linker region between two nucleosomes and allows the proteins to sit in a variety of combinations.

4.2.3 Discussion

The results presented in this section have shown that the histone proteins can inhibit interaction of PNA with the nucleosome core particle and that these PNAs affect the reconstitution of DNA onto the nucleosome core particles. Experiments in which the DNA is first reconstituted onto the nucleosomes show that PNA does not affect nucleosome integrity. However, the PNAs are unable to bind to their targets when these closely interact with the protein surface. In contrast, when the PNA-DNA complexes are formed prior to reconstitution, the affinity for the histone octamer is severely reduced (abolished for the 110-mer) and PNA binding is attenuated. These effects are most pronounced for the shorter DNA sequences, suggesting that the location of the target site within the nucleosomal particles is an important factor. These results are most easily interpreted by suggesting the nucleosomal positioning shown in figure 4.18. The effects can be most clearly seen with the 110 base pair fragments, for which the entire sequence is covered with the histone octamer. In this instance PNAs are unable to bind to the nucleosomal DNA, even though they bind to free DNA with high affinity, and prior formation of the PNA/DNA complex completely prevents nucleosome reconstitution. On extending the DNA fragment length, PNA binding is possible if the target site is located on the periphery of the

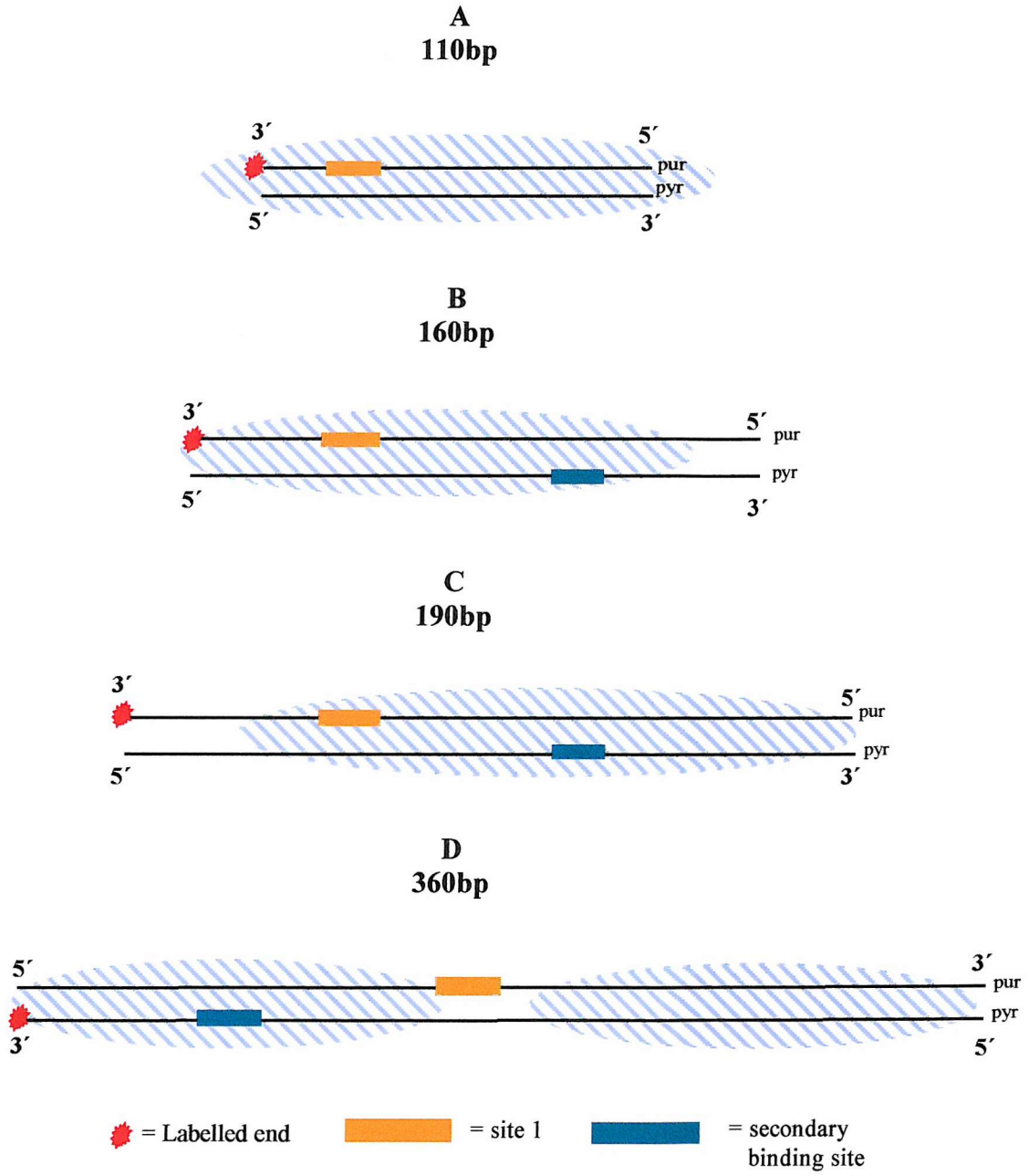

FIGURE 4.18 Cartoons showing the potential positions of the histone octamer when reconstituted with the 110 (A), 160 (B), 190 (C) and 360 base pair (D) DNA fragment containing the *tyr*T (43-59) sequence. The orange box represents site 1, while the green box represents the secondary binding site. The blue oval represents the area covered by the histone octamer. For the 360 base pair fragment the complex is shown with two octamers bound, one at each end of the fragment.

protein or within the linker region between nucleosome core particles. Multiple bands are present in the bandshift assays when the 360 base pair fragment is reconstituted onto nucleosome cores. We presume that these represent different translational positions of the nucleosome core particle or particles along the DNA fragment. In some of these configurations the PNA target site may be located in the linker regions between two nucleosomes and is available for binding.

It should also be noted that the secondary binding site has been severely affected by the protein and targeting has been prohibited. The incorporation of the complex formed at this site into the nucleosome is not evident due to reconstitution not being affected and the PNA being displaced. This highlights the important fact that only stable complexes with high binding affinities can either target the nucleosome or be incorporated within, dependent on the binding location.

4.3 *Tyr*T (22-33) – site 2

4.3.1 *Tyr*T (22-33) targeted with PNA after reconstitution

This section uses similar experiments to those described before to examine the interaction of PNA 005, 008 and 009, targeted to site 2 on the *tyr*T (22-33) sequence, with nucleosomal DNA fragments. We have assumed that the positioning of the histone octamer in relation to the DNA is the same as the *Tyr*T (43-59) sequence due to only minimal base mutations present between positions 22-33 of the original *tyr*T sequence.

Figures 4.19 and 4.20 show DNaseI footprinting and bandshift gels for the interaction of PNA 005 (figure 4.19), PNA 008 and 009 (figure 4.20) with the histone-bound 110 base pair fragment from *tyr*T (22-33). In the absence of PNA the cleavage

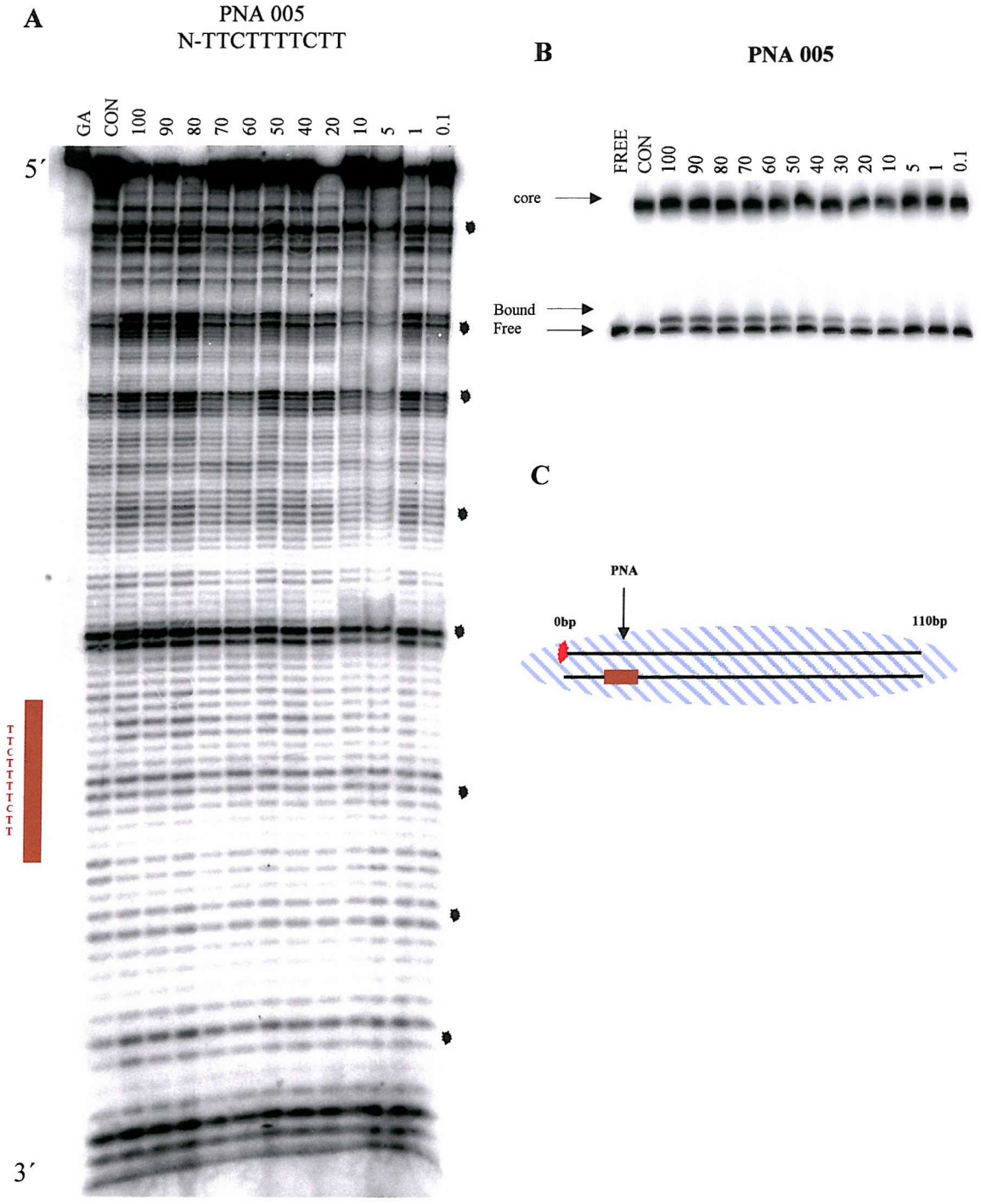

FIGURE 4.19 DNaseI cleavage (A) and bandshift assays (B) of the 110 base pair histone-bound *tyr*T (22-33) fragment in the presence and absence of PNA 005. The PNA concentration (μM) is indicated at the top of each gel lane. "CON" indicates digestion of the DNA in the absence of PNA and "GA" is a Maxam-Gilbert marker specific for purines. All the complexes were incubated for 24 hours in 50mM sodium acetate pH 5.0 before digestion with DNaseI. The location of site 2 is indicated in brown. The asterisks indicate the sites of maximal cleavage. C is a cartoon showing the likely position of the target site, relative to the histone octamer.

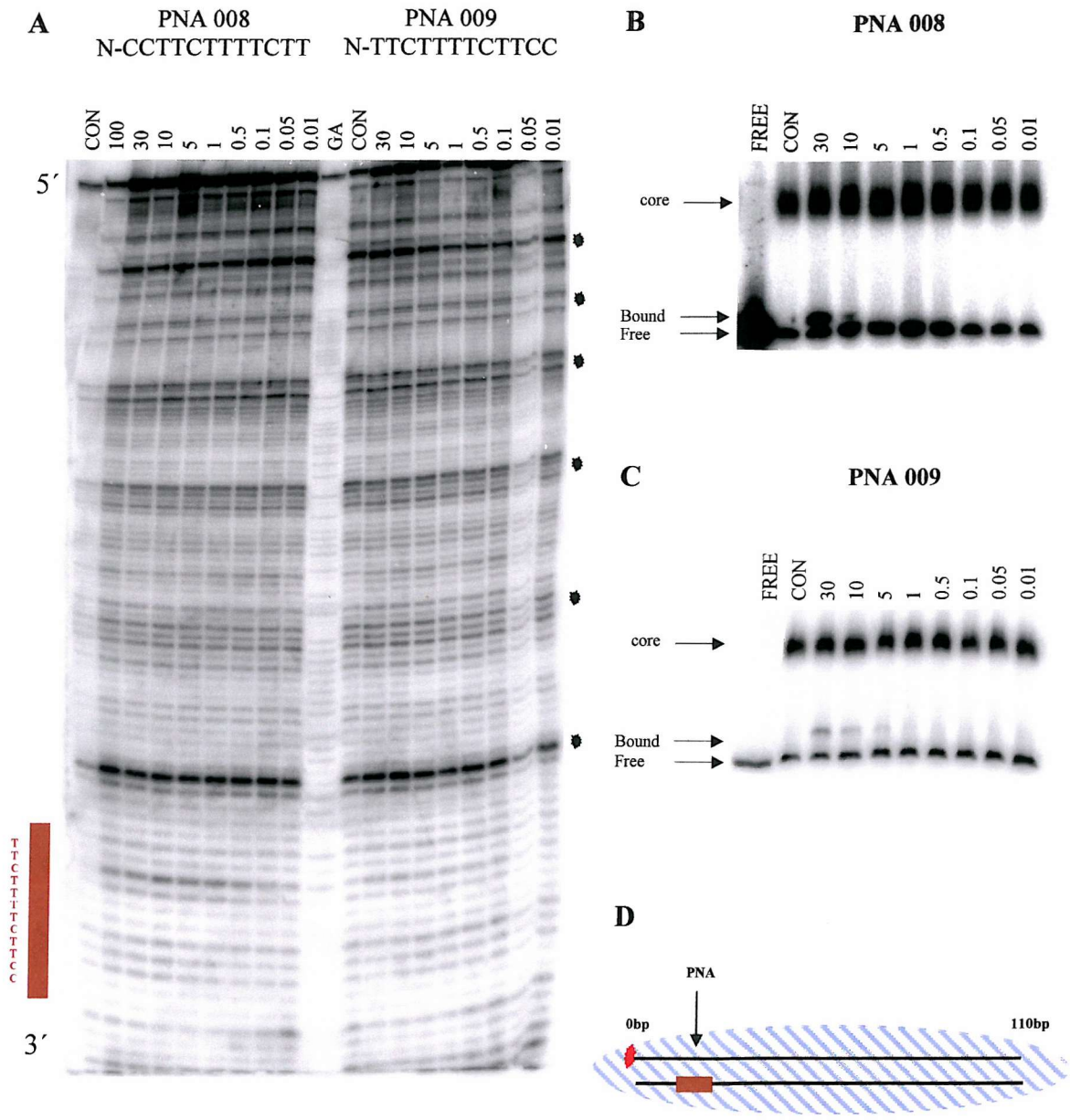

FIGURE 4.20 DNaseI cleavage (A) and bandshift assays (B,C) of the 110 base pair histone-bound *tyr*T (22-33) fragment in the presence and absence of PNA 008 and 009. The PNA concentration (μM) is indicated at the top of each gel lane. "CON" indicates digestion of the DNA in the absence of PNA and "GA" is a Maxam-Gilbert marker specific for purines. All the complexes were incubated for 24 hours in 50mM sodium acetate pH 5.0 before digestion with DNaseI. The location of site 2 is indicated in brown. D is a cartoon showing the likely position of the target site, relative to the histone octamer.

pattern is different from that of free DNA, showing good cleavage at positions where the minor groove faces away from the protein surface and which also correlates to the cleavage pattern in figure 4.1. It can be seen that these DNaseI cleavage patterns are not affected by adding the PNAs, and no footprints are evident, even at high PNA concentrations. These results are in contrast with those obtained with free DNA for which clear footprints were evident at site 2 at relatively low PNA concentrations (see section 3.3.3). The lack of interaction with this nucleosomal DNA is confirmed by bandshift assays (figures 4.19B, 4.20B and C), which show no disruption of the nucleosome core particle when targeted with PNA 005, 008 or 009, even at high concentrations. There is no visible supershift in the nucleosomal bands, though an additional band appears above the free DNA, which corresponds to the free PNA/DNA complex formed at site 2 with the small amount of contaminated free DNA.

Figure 4.21A shows DNaseI cleavage of the longer 160 base pair *tyr*T (22-33) fragment in the presence of PNA 008 and 009, which were added after nucleosome reconstitution. Although the cleavage around this target site is weak, it can be seen that PNA 008 and 009 generate footprints that persist to concentrations of 5μM and 1μM respectively. These values are considerably higher than those required with free DNA. In this fragment site 2 is located 126 base pairs from one end of the DNA and is closer towards the end of the fragment than site1 in the 160 base pair fragment from *tyr*T (43-59). These footprinting results are substantiated by bandshift assays (figure 4.21B and C), which show no disruption of the nucleosome core particle when targeted with PNA 008 or 009 even at high concentrations. Additional bands are present above the free DNA band, which correspond to PNA/DNA complexes formed with the small amount of contaminating free DNA. There is also a

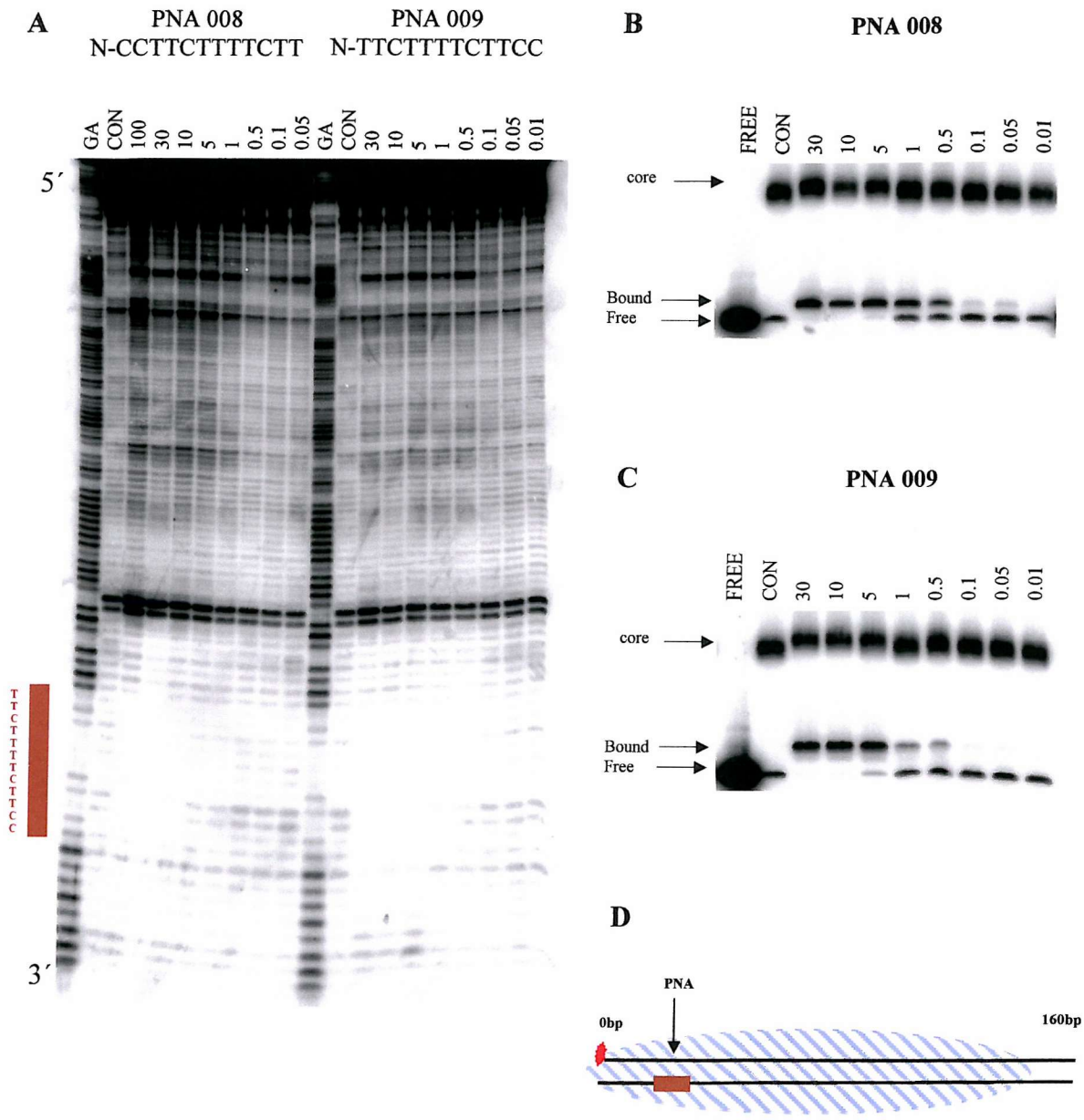

FIGURE 4.21 DNaseI cleavage (A) and bandshift assays (B,C) of the 160 base pair histone-bound *tyr*T (22-33) fragment in the presence and absence of PNA 008 and 009. The PNA concentration (μM) is indicated at the top of each gel lane. "CON" indicates digestion of the DNA in the absence of PNA and "GA" is a Maxam-Gilbert marker specific for purines. All the complexes were incubated for 24 hours in 50mM sodium acetate pH 5.0 before digestion with DNaseI. The location of site 2 is indicated in brown. D is a cartoon showing the likely position of the target site, relative to the histone octamer.

small supershift in the slowest moving band at high PNA concentrations (30, 10 and 5μM) with PNA 008 and 009. This has also been seen with PNA 21 with the *tyr*T (43-59) sequence and as stated then, this could be a ternary PNA/DNA-protein complex. Additional experiments were performed with PNA 005 however, very high PNA concentrations where required to produce very weak footprints at site 2. There was also no disruption to the nucleosome core particle even at high PNA concentrations and no visible supershift (data not shown).

The orientation of site 2 in relation to the histone octamer can also be resolved through the original cleavage studies by Drew and Travers in 1985, only if once again you presuppose that this 160bp fragment sits in the same location and orientation as originally documented. They assigned positions 28 to the inner surface of the DNA whereas positions 23 and 33 are on the outer surface, facing away from the protein. The initial start position of site 2 is positioned facing away from the protein whereas the central region faces towards the surface and the end regions face away from the protein, the same as seen with site 1. PNA is able to target but only at relatively high PNA concentrations as previous seen with the *tyr*T (43-59) sequence. The orientation of this site however will consequently change between different fragments.

Figure 4.22A shows DNaseI cleavage of the 190 base pair fragment from *tyr*T (22-33) in the presence or absence of PNA 008 and 009, added after reconstitution. Once again DNaseI cleavage is poor around site 2, but it can be seen that PNA 008 and 009 produce footprints at this site, which persist to a concentration of about 1μM. These footprints appear at similar PNA concentrations to those seen with the 160 base pair fragment and are higher than those required with free DNA. This could be due to the protein sitting in the same location as on the 160bp fragment.

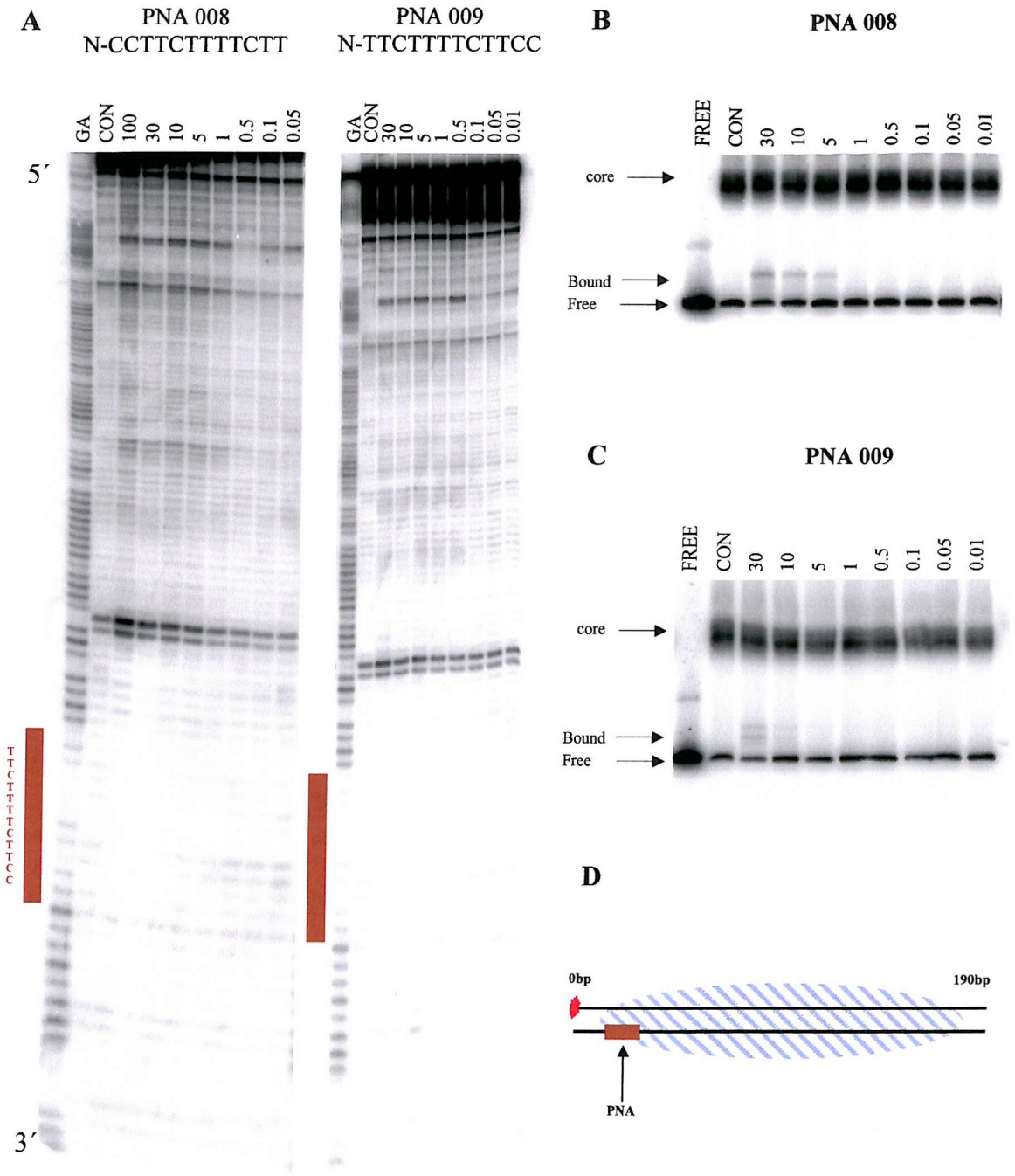

FIGURE 4.22 DNaseI cleavage (A) and bandshift assays (B,C) of the 190 base pair histone-bound *tyr*T (22-33) fragment in the presence and absence of PNA 008 and 009. The PNA concentration (μM) is indicated at the top of each gel lane. "CON" indicates digestion of the DNA in the absence of PNA and "GA" is a Maxam-Gilbert marker specific for purines. All the complexes were incubated for 24 hours in 50mM sodium acetate pH 5.0 before digestion with DNaseI. The location of site 2 is indicated in brown. D is a cartoon showing the likely position of the target site, relative to the histone octamer.

Bandshift assays (figure 4.22B and C) show that these PNAs do not disrupt the nucleosome core particle even at the highest concentration. Experiments performed with PNA 005 produced very weak footprints at high PNA concentrations and has no effect on the retarded nucleosome band (data not shown).

Figure 4.23A shows the results of DNaseI footprinting experiments with the histone bound 360 base pair *tyr*T (22-33) fragment in the presence of PNA 008 and 009. PNA 008 and 009 produce relatively weak footprints at site 2 to a concentration of approximately 1μM, which is not similar to the results with free DNA but is consistent with the lower concentrations seen with the *tyr*T (43-59) sequence (see figure 4.7). This could be due to the partial obstruction of site 2 from the protein, which was also seen with the *tyr*T (43-59) 360bp fragment. The DNaseI cleavage in the presence and absence of PNA shows the expected phased cleavage pattern. Bandshift assays (figure 4.23B and C) show that the PNAs have not disrupted the nucleosome core particle, and the intensity of this retarded band is unaltered. However, multiple bands are also present with this fragment and should correspond to the different positioning of the protein along the fragment. Additional experiments with PNA 005 produced footprints at very high concentrations and showed no disruption to the nucleosome core particle (data not shown).

Footprinting plots, derived from these DNaseI patterns with the different length fragments from *tyr*T (22-33) in the presence of PNA 005, 008 and 009 are presented in figure 4.24, and the C_{50} values derived from these are summarised in table 4.2. No footprints are produced with the 110 base pair fragment. Footprints are evident with the 160 base pair fragment, but these have much higher C_{50} values than with free DNA; this difference is greatest for PNA 009. On increasing the fragment length to 190 base pairs the C_{50} values does decrease further suggesting that there is

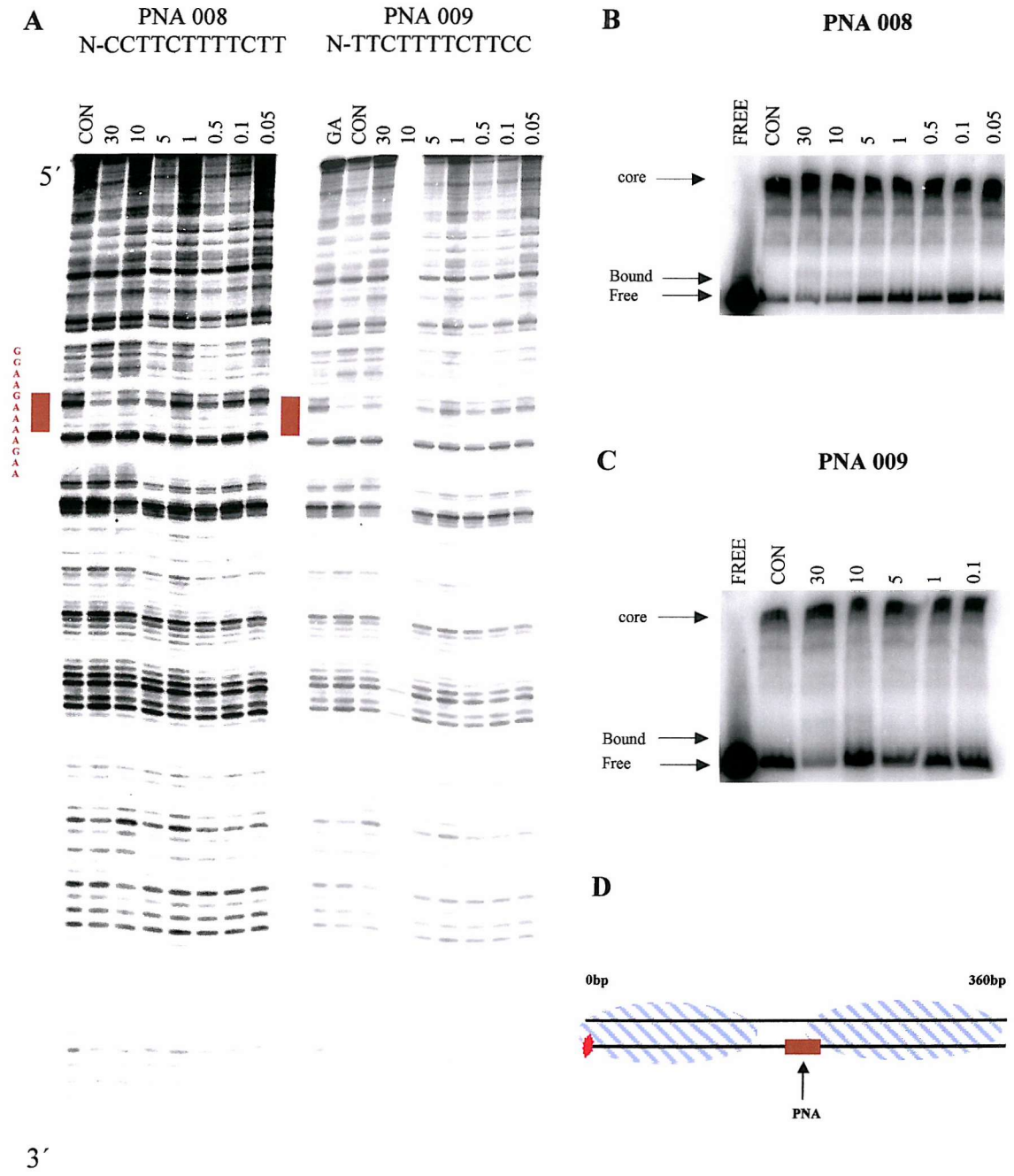

FIGURE 4.23 DNaseI cleavage (A) and bandshift assays (B,C) of the 360 base pair histone-bound *tyr*T (22-33) fragment in the presence and absence of PNA 008 and 009. The PNA concentration (μM) is indicated at the top of each gel lane. "CON" indicates digestion of the DNA in the absence of PNA and "GA" is a Maxam-Gilbert marker specific for purines. All the complexes were incubated for 24 hours in 50mM sodium acetate pH 5.0 before digestion with DNaseI. The location of site 2 is indicated in brown. D is a cartoon showing the likely position of the target site, relative to the histone octamer.

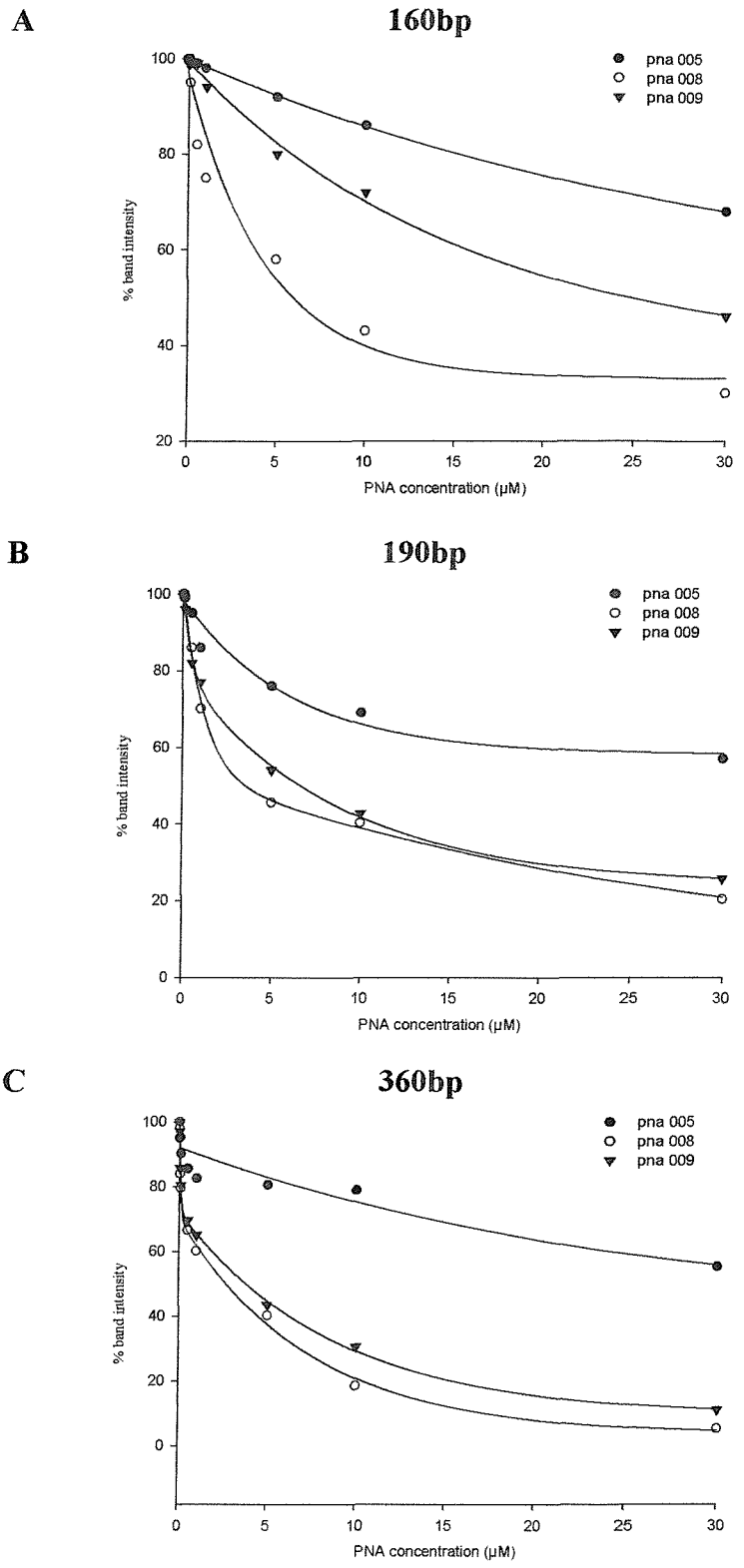

FIGURE 4.24 Footprinting plots showing the interaction of PNAs 005, 008 and 009 with site 2 on different length *tyr*T (22-33) fragments, when reconstituted into nucleosomal DNA. (A) 160bp, (B) 190bp and (C) fragments. The data were obtained from analysis of the footprints shown in figures 4.12-4.16.

PNA sequence	C_{50} (μM)				
	Free DNA	Nucleosomal DNA			
		110bp	160bp	190bp	360bp
005	~89 ±3	No footprint	not resolved	not resolved	not resolved
008	0.04 ±0	No footprint	5.9 ±5.3	3.5 ±1.6	2.7 ±1.9
009	36 ±5	No footprint	24.7 ±1.4	6.2 ±1.1	3.8 ±0.9

TABLE 4.2 C_{50} values for different PNA sequences targeted to site 2 on the 110, 160, 190 and 360 base pair *tyr*T (22-33) fragments. These values were determined from the footprinting plots shown in figure 4.17.

less obstruction from the protein core over site 2. This data does indicates that the protein could sit further away from site 2 compared to the 160bp fragment. When the fragment length is further increased to 360 base pairs, the PNA binds with higher affinity but not the same C_{50} as to free DNA, indicating that the protein does not fully obstruct this site.

4.3.2 Reconstitution of *tyr*T (22-33) fragments containing pre-formed PNA-DNA complexes

The previous section examined the interaction of PNAs with different length *tyr*T (22-33) fragments that has already been reconstituted into nucleosome core particles. In contrast this section examines how pre-formed PNA complexes interact with histone proteins, using similar experiments to those described with *tyr*T (43-59) in section 4.2.2.

Figure 4.25A shows the DNaseI footprinting gels for experiments in which the 110bp *tyr*T (22-33) fragment was targeted with PNA 005 prior to nucleosome reconstitution. In contrast to the results with histone bound DNA shown in figure 4.19, a footprint is evident at site 2 at the highest PNA concentration. Although this is higher than that require with free DNA, this may be attributed to the weak binding of this PNA resulting in some being displaced during the reconstitution process. The results of bandshift experiments with these samples are shown in figure 4.25B. It can be seen that PNA 005 only has a small effect on the efficiency of nucleosome reconstitution (the presence of PNA can be seen from its effect on the small amount of contaminating free DNA). This suggests that there is a greater length of PNA-free DNA region to reconstitute. Nearly 80 base pairs of free DNA is present which when reconstituted only has a marginal effect on the reconstitution. Quantitative analysis of the amount of radiolabelled DNA in the retarded species is shown in figure 4.26A and shows a small decrease in the intensity of the nucleosomal DNA band, with 75% of the complex remaining at PNA concentrations above 10μM.

Figure 4.27 shows the results of similar experiments in which the 110 base pair fragment has been targeted with PNA 008 and 009 before reconstitution. These PNAs produce DNaseI footprints (figure 4.27A), which persist to concentrations of about 0.1μM, which is only slightly higher than seen with free DNA. The bandshifts also show a small reduction in the formation of nucleosomal DNA at high PNA concentrations, and a quantitative analysis of these data is shown in figure 4.26A revealing a gradual decrease in the intensity of the nucleosomal band to about 60% for PNA 008 and 63% for PNA 009 of that in the uncomplexed DNA at a concentration of 30μM. This is greater than the effect of PNA 005, presumable because of their greater binding affinity.

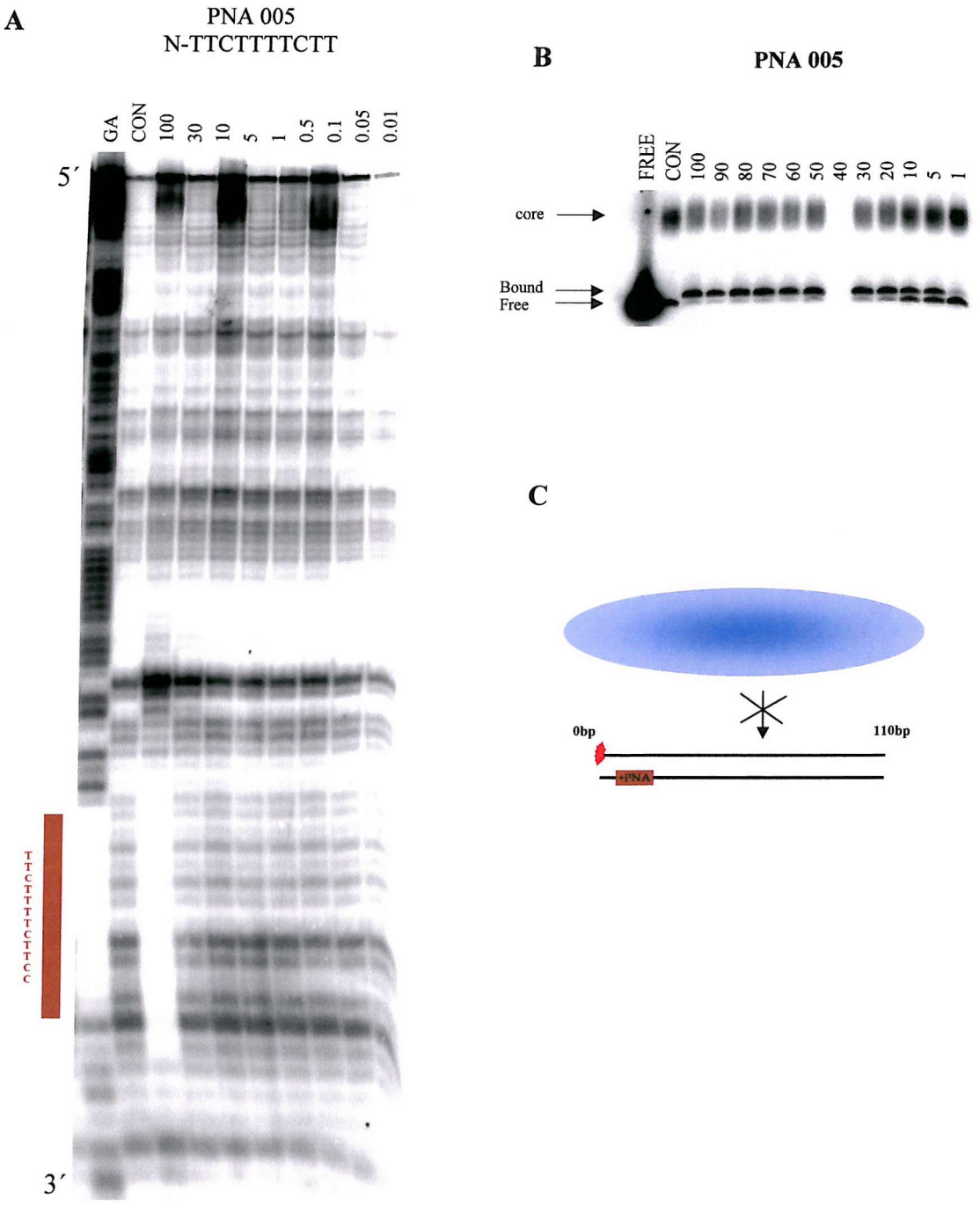

FIGURE 4.25 DNaseI cleavage (A) and bandshift assays (B) for the 110 base pair *tyr*T (22-33) fragment, which had been complexed with PNA 005 prior to reconstitution. The PNA concentration (μM) is indicated at the top of each gel lane. "CON" indicates digestion of the DNA in the absence of PNA and "GA" is a Maxam-Gilbert marker specific for purines. All the complexes were incubated for 24 hours in 50mM sodium acetate pH 5.0 before digestion with DNaseI. The location of site 2 is indicated in brown. C is a cartoon showing the likely position of the target site, relative to the histone octamer.

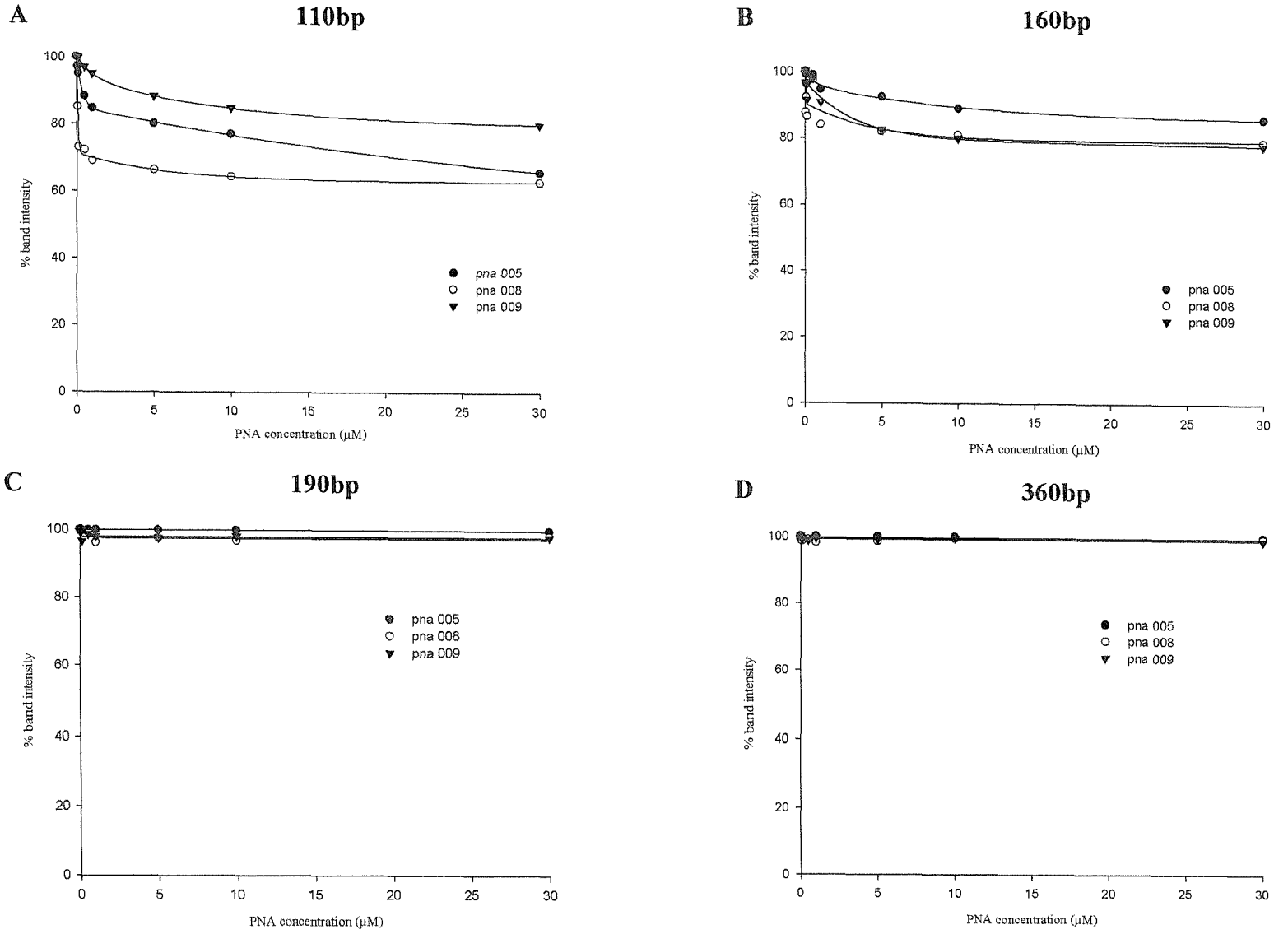

FIGURE 4.26 Effect of PNAs 005, 008 and 009 on the reconstitution of different length PNA containing the *tyr*T (22-33) sequence. The PNA/DNA complexes were generated before nucleosome reconstitution. A) 110, B) 160, C) 190 and D) 360 base pair fragments.

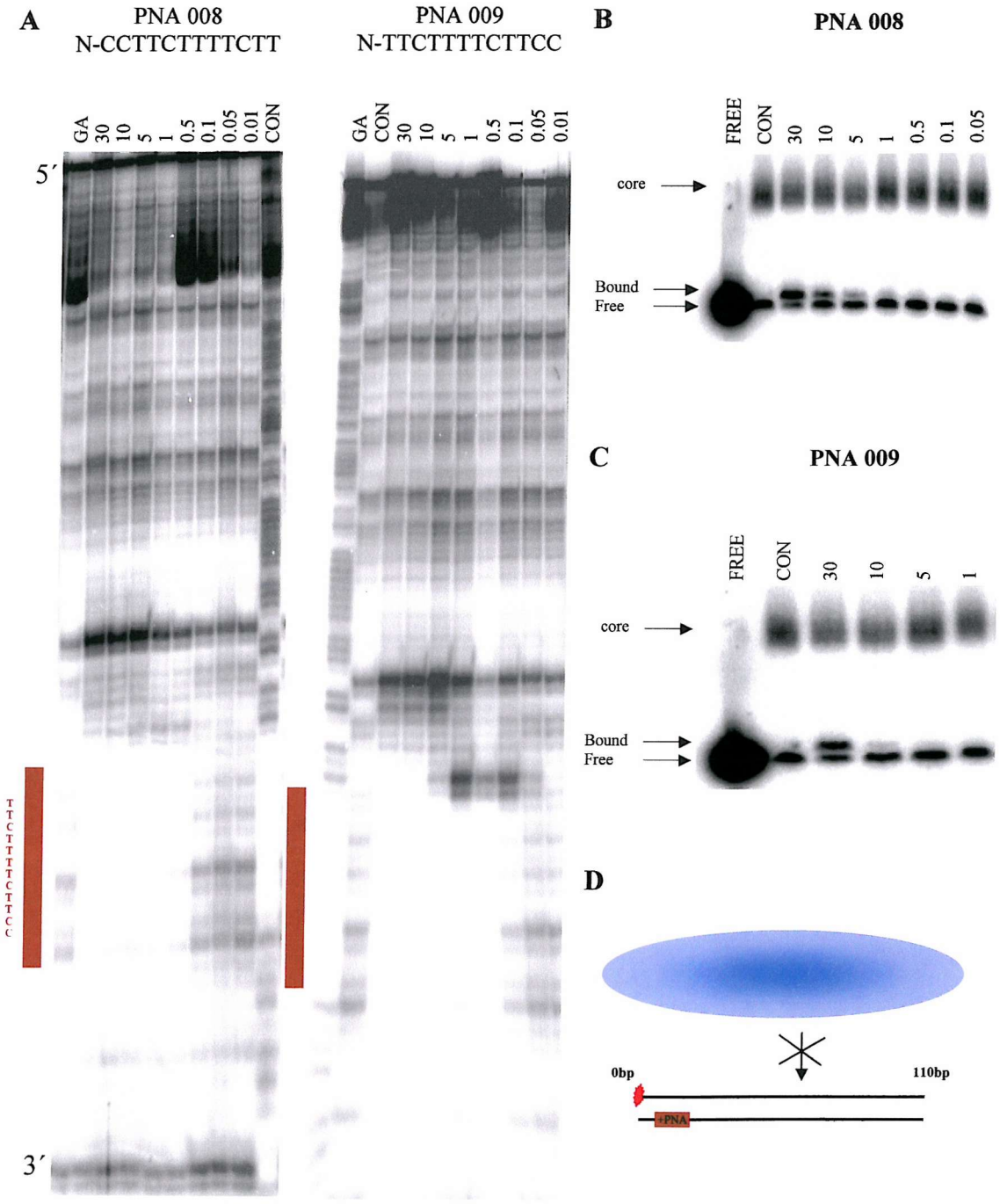

FIGURE 4.27 DNaseI cleavage (A) and bandshift assays (B and C) for the 110 base pair *tyr*T (22-33) fragment, which had been complexed with PNA 008 and 009 prior to reconstitution. The PNA concentration (μM) is indicated at the top of each gel lane. "CON" indicates digestion of the DNA in the absence of PNA and "GA" is a Maxam-Gilbert marker specific for purines. All the complexes were incubated for 24 hours in 50mM sodium acetate pH 5.0 before digestion with DNaseI. The location of site 2 is indicated in brown. D is a cartoon showing the likely position of the target site, relative to the histone octamer.

Figure 4.28 shows DNaseI footprinting and bandshift gels for the 160 base pair *tyr*T (22-33) fragment, targeted with PNA 008 and 009 prior to nucleosome reconstitution. These produce footprints at site 2 which persist to concentrations of about 1μM for PNA 008 and 10μM for PNA 009 which is higher than that with free DNA, probably due to displacement of weaker complexes during reconstitution. The bandshift experiments with these samples (figure 4.28B and C) show that this PNA has little effect on nucleosome reconstitution. However, there appears to be a small supershift in the retarded band, evident at the highest concentrations of PNA 008 and 009. This has to due to the presence of high PNA concentrations but this does not seem reasonable to attribute this shift the addition of PNA due to only a small increase in molecular weight. This shift is not present with PNA 005. Quantitative analysis of these data (figure 4.26B) shows only a small reduction in the amount of nucleosomal DNA at the highest PNA concentrations (10% reduction for PNA 005 and 20% reduction for PNA 008 and 009).

Figure 4.29 shows DNaseI footprinting and bandshift gels for the 190 base pair *tyr*T (22-33) fragment, targeted with PNA 008 and 009 prior to nucleosome reconstitution. It can be seen that these PNAs produce DNaseI footprints at PNA concentrations of about 1μM for PNA 008 and 10μM for PNA 009. These concentrations are not comparable to those obtained with free DNA however they are consistent with the footprinting concentrations shown in figure 4.28, highlighting the possibility that these weaker complexes are displaced through the reconstitution process. Bandshift assays with these samples (figure 4.29B and C) show that the PNAs have no effect on the efficiency of reconstitution, which is confirmed by the quantitative analysis shown in figure 4.26C. This indicates that the protein has potentially shifted to the PNA free region. Additional experiments were performed

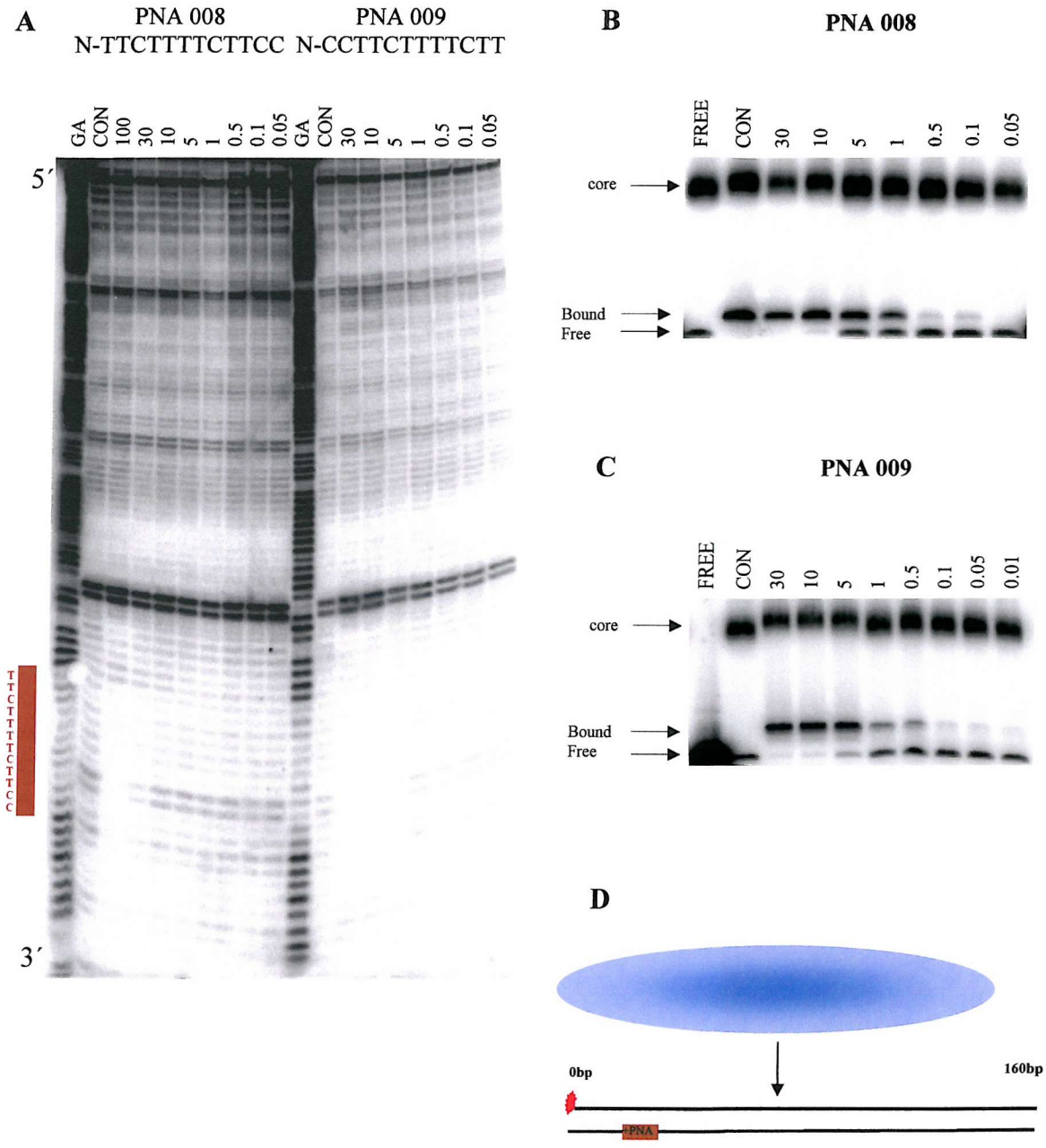

FIGURE 4.28 DNaseI cleavage (A) and bandshift assays (B and C) for the 160 base pair *tyr*T (22-33) fragment, which had been complexed with PNA 008 and 009 prior to reconstitution. The PNA concentration (μM) is indicated at the top of each gel lane. "CON" indicates digestion of the DNA in the absence of PNA and "GA" is a Maxam-Gilbert marker specific for purines. All the complexes were incubated for 24 hours in 50mM sodium acetate pH 5.0 before digestion with DNaseI. The location of site 2 is indicated in brown. D is a cartoon showing the likely position of the target site, relative to the histone octamer.

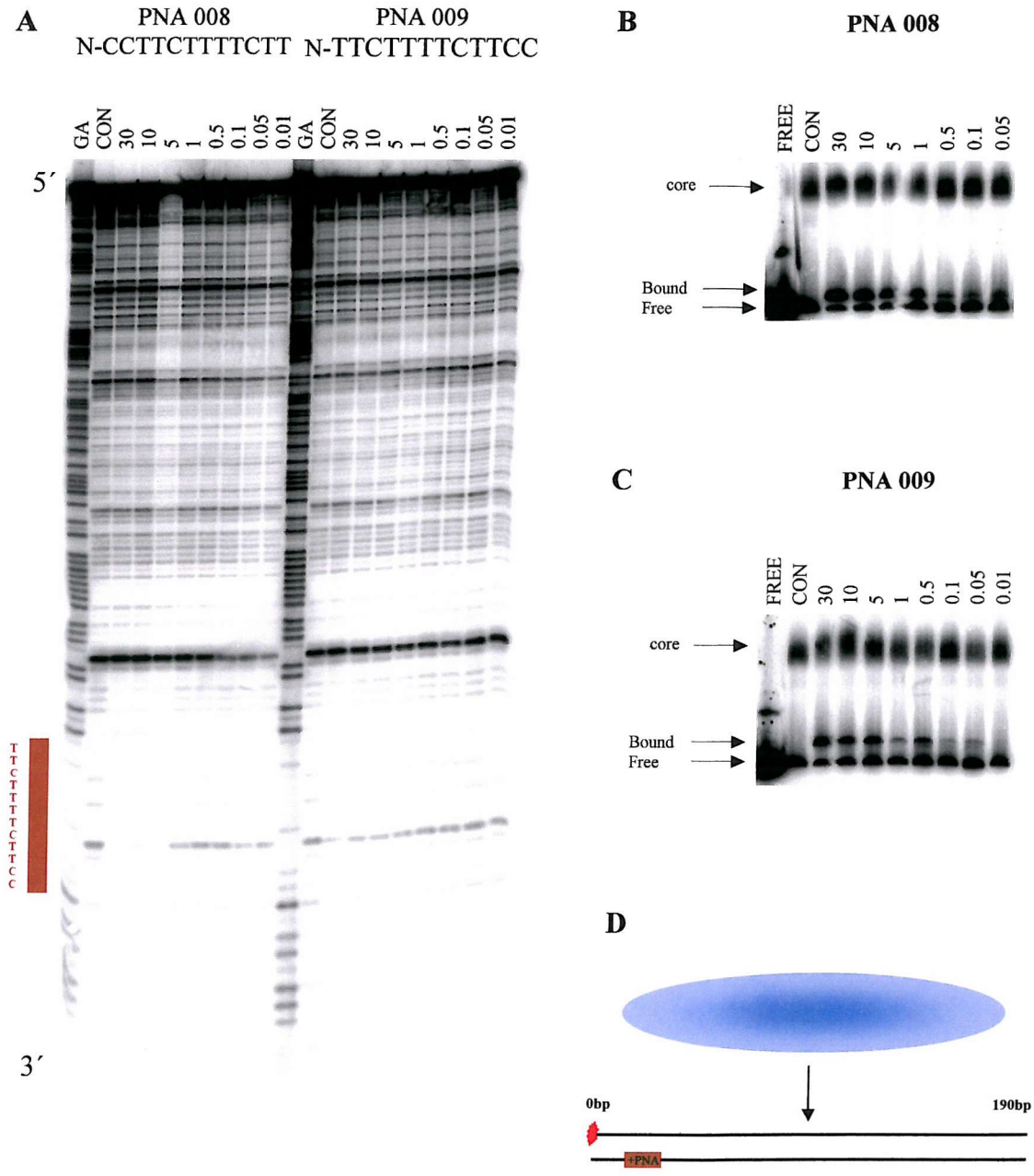

FIGURE 4.29 DNaseI cleavage (A) and bandshift assays (B and C) for the 190 base pair *tyr*T (22-33) fragment, which had been complexed with PNA 008 and 009 prior to reconstitution. The PNA concentration (μM) is indicated at the top of each gel lane. "CON" indicates digestion of the DNA in the absence of PNA and "GA" is a Maxam-Gilbert marker specific for purines. All the complexes were incubated for 24 hours in 50mM sodium acetate pH 5.0 before digestion with DNaseI. The location of site 2 is indicated in brown. D is a cartoon showing the likely position of the target site, relative to the histone octamer.

with PNA 005, which produced footprints at very high PNA concentrations and had not effect on the nucleosome reconstitution (data not shown).

Figure 4.30 shows DNaseI footprinting and bandshift gels for the 360 base pair *tyr*T (22-33) fragment, targeted with PNA 008 and 009 prior to reconstitution. These PNA produce very weak footprints to a concentration of 0.1μM with PNA 008 and 10μM with PNA 009. The bandshifts show that these PNAs have not affected the reconstitution efficiency; this is confirmed by the quantitative analysis shown in figure 4.26D. As noted with *tyr*T (43-59) sequence these bandshifts with this fragment reveal multiple retarded bands, which presumably correspond to different translational positions of the DNA within the nucleosome particles. There also appears to be a small supershift in the lowest band with high concentrations of PNA 008 and 009. This band should represent only one nucleosome core particle and this evident supershift, which was also seen with other fragments, could verify this theory. Additional experiments were performed with PNA 005, which produced footprints at very high PNA concentrations and had no effect on the nucleosome reconstitution and no supershift was present (data not shown).

4.3.3 Discussion

The DNaseI footprinting and bandshift results presented in this section confirm that PNA can affect the efficiency of nucleosome reconstitution and wrapping the DNA around the protein core affects the accessibility of PNA binding sites. The location of the PNA target site within the nucleosome core particle is an influencing factor and by moving the target site further away from the protein, interactions and reconstitution is increased. The accessibility of each target site is affected by the

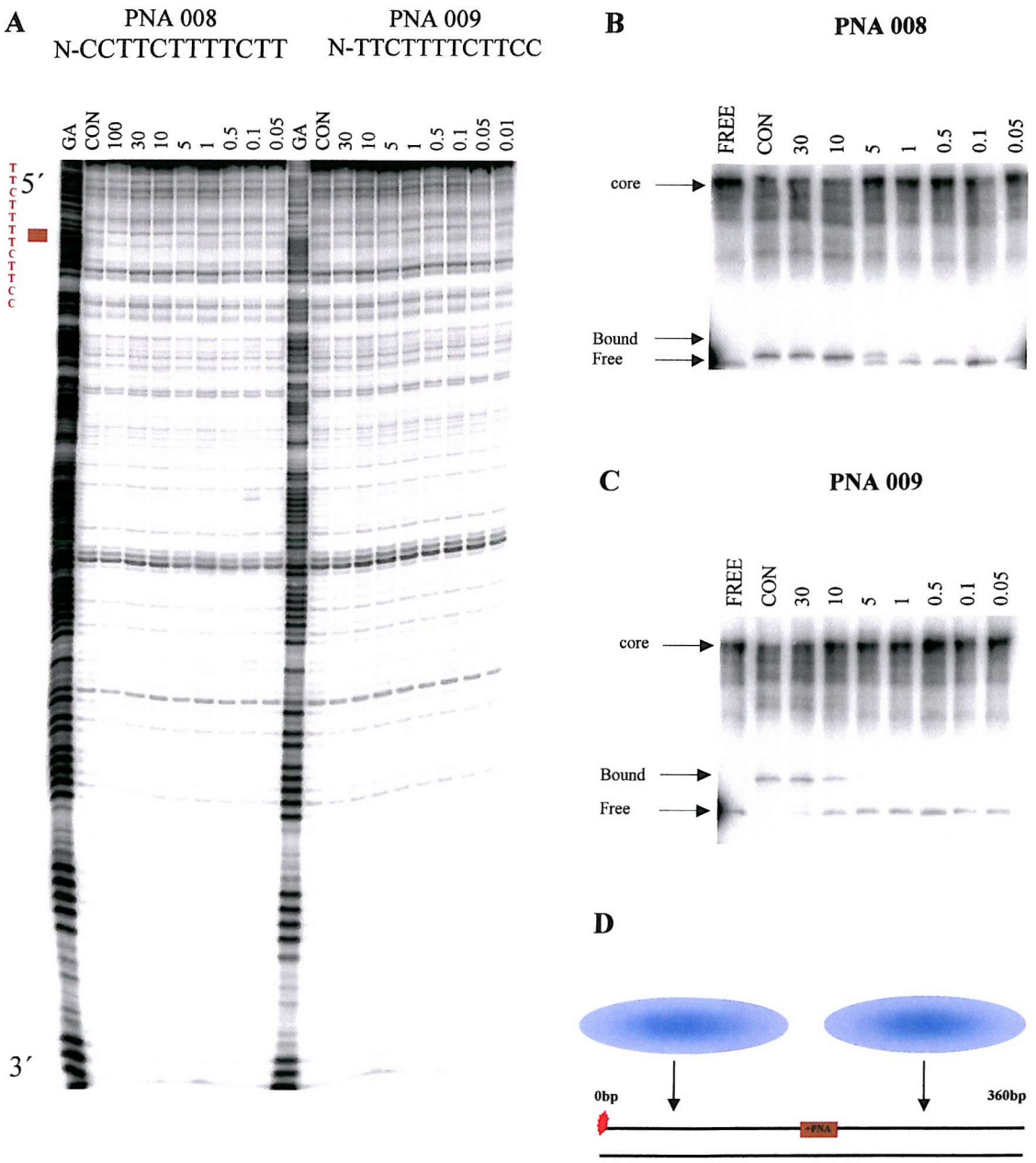

FIGURE 4.30 DNaseI cleavage (A) and bandshift assays (B and C) for the 360 base pair *tyr*T (22-33) fragment, which had been complexed with PNA 008 and 009 prior to reconstitution. The PNA concentration (μM) is indicated at the top of each gel lane. "CON" indicates digestion of the DNA in the absence of PNA and "GA" is a Maxam-Gilbert marker specific for purines. All the complexes were incubated for 24 hours in 50mM sodium acetate pH 5.0 before digestion with DNaseI. The location of site 2 is indicated in brown. D is a cartoon showing the likely position of the target site, relative to the histone octamer.

length of the DNA fragment, which alters the amount of contiguous PNA-free DNA that is available for reconstitution. Also once DNA is wrapped around the protein it is generally less accessible for PNA binding. For short DNA fragments prior binding of PNA can prevent nucleosome assembly but has less of an effect with the PNA target site is further away from the protein as seen with the 110 base pair fragment. These results are similar to those seen with *tyr*T (43-59) and are most easily interpreted by suggesting the nucleosomal positioning shown in figure 4.31. One observation that was not frequently observed with the *tyr*T (43-59) sequence was a supershift in the nucleosome core particle band at high concentrations of PNA 008 and 009. There is not clear explanation for this but the high concentrations will effect the molecular weight marginally but a different complex could be formed which in turn would affect its mobility. These results will be considered further in the discussion at the end of this chapter.

4.4 *Tyr*T (43-59,122-133) – sites 1 and 3

The location of the PNA target sites within each DNA fragment appears to be one of the important factors, which influence the accessibility of the site for binding, and affect the efficiency of reconstitution. The previous sections examined the binding of PNAs to oligopurine tracts, which were located towards one end of each DNA fragment. In several of these instances there was still sufficient PNA-free DNA beyond the target site to allow nucleosome assembly, even though this may have been forced into a different location. The PNA/DNA complex would then be positioned toward the edge end of the protein, or dangling at the end of the nucleosome. We were therefore interested to examine the interaction of PNA with a

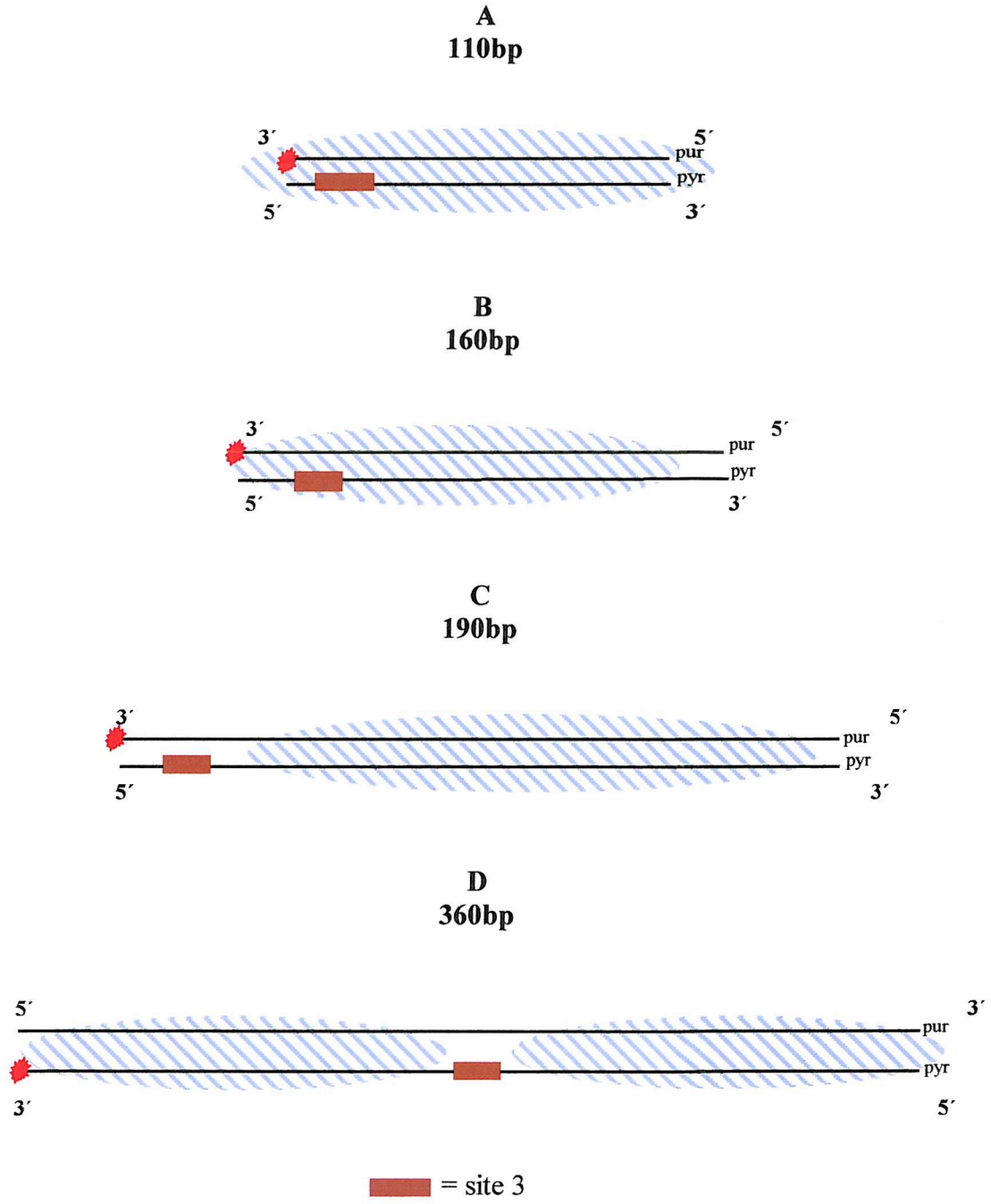

FIGURE 4.31 Cartoons showing the potential positions of the histone octamer when reconstituted with the 110 (A), 160 (B), 190 (C) and 360 base pair (D) DNA fragment containing the *tyr*T (22-33) sequence. The yellow box represents site 1, while the green box represents the secondary binding site. The blue oval represents the area covered by the histone octamer. For the 360 base pair fragment the complex is shown with two octamers bound, one at each end of the fragment.

fragment that contains target sites at both ends. We therefore modified the *tyr*T (43-59) sequence, and introduced a second oligopurine tract between positions 122-133. This second site (site 3) was designed so as to have the same sequence as site 2 in *tyr*T (22-33) and so can be targeted with PNA 008 and 009. The section examines the effects of PNA 008, 009, 20 and 21 at these two target sites on this fragment *tyr*T (43-59,122-133). These two sites are less than 70 base pairs apart, and it is therefore unlikely that the nucleosome formation could occur between them. We therefore expected so see large effects with the 190 base pair fragment, the 160bp fragment was not studied due to the same distance between sites 1 and 3. In contrast the 360 base pair fragment containing these two sites may still have sufficient free DNA to be able to bind both PNAs as well as one histone octamer. This is illustrated in figure 4.32. Site 3 was created by site directed mutagenesis of seven bases between positions 122-133 base pairs as described in Chapter 2. These base changes are shown in figure 4.33.

4.4.1 *Tyr*T (43-59,122-133) targeted with PNA after reconstitution

This section examines the interaction of PNA 008, 009, 20 and 21 with sites 1 and 3 in *tyr*T (43-59,122-133) when this sequence has been reconstituted into nucleosomes. The results with free DNA were presented in sections 3.2.1 and 3.2.3. The most interesting aspect of these studies in when the two PNA sites are targeted in combination but targeting individually has also been studied. Figure 4.34 shows the DNaseI and bandshift gels for the interaction of PNA 008, 009, 20 and 21 with the histone-bound 190 base pair fragment from *tyr*T (43-59,122-133). PNA 20 and 21 produce footprints at site 1 at concentrations above 1μM are no footprints are present

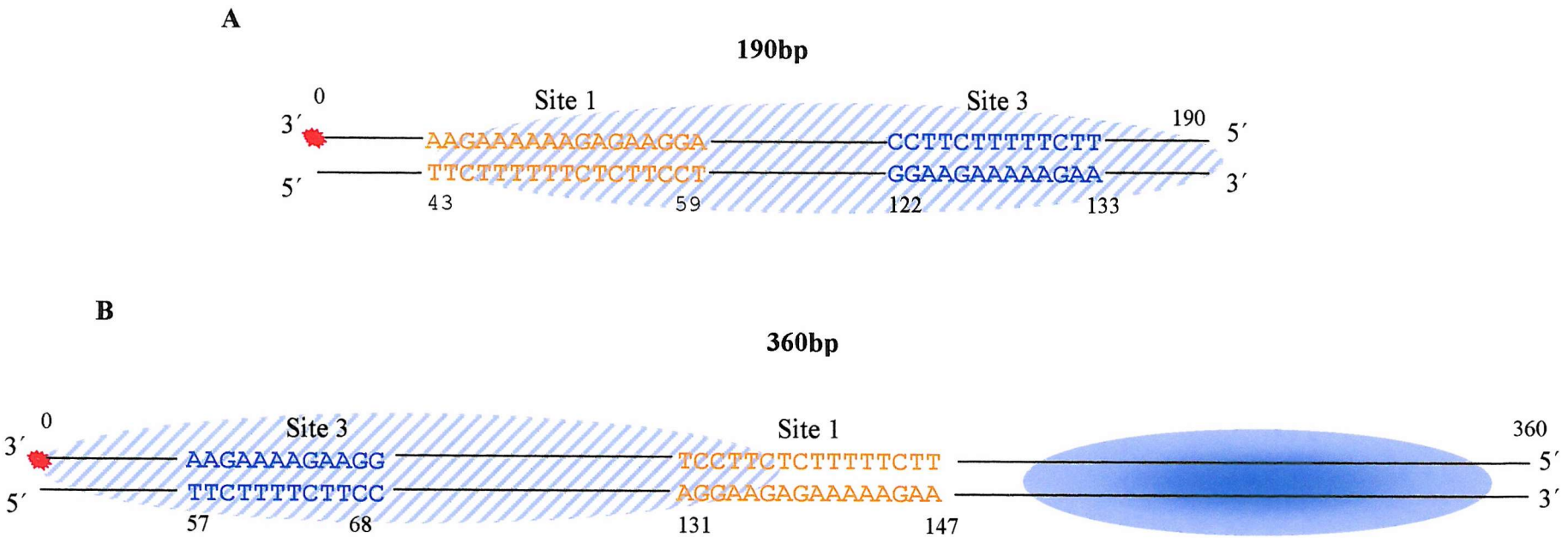

FIGURE 4.32 The location of sites 1 and 3 on the 190 (A) and 360 (B) base pair *tyr*T (43-59,122-133) fragments and their potential for interaction with the histone octamer. The ovals represent the histone octamers, while the sequences of the two oligopurine sites are as indicated.

*Tyr*T (43-59,122-133)

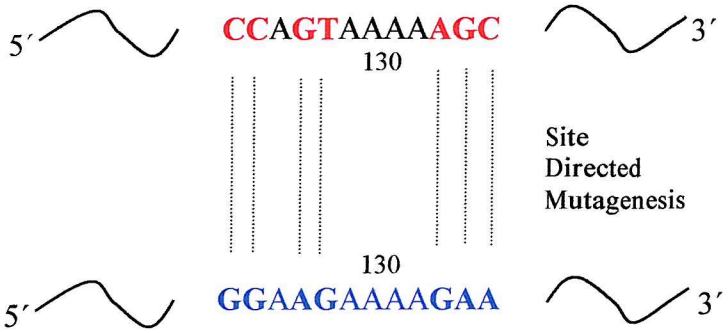

Site 3 located between position 122-133 on the *Tyr*T (43-59,122-133)

```
5′  AAGGGAGAAGGGGAAGAAAAGAATTACCCC  3′
3′  TTCCCTCTTCCCCTTCTTTTCTTAATGGGG  5′
```

FIGURE 4.33 Illustration of the seven base pairs changed between positions 122-133, generating site 3 on *tyr*T (43-59, 122-133).

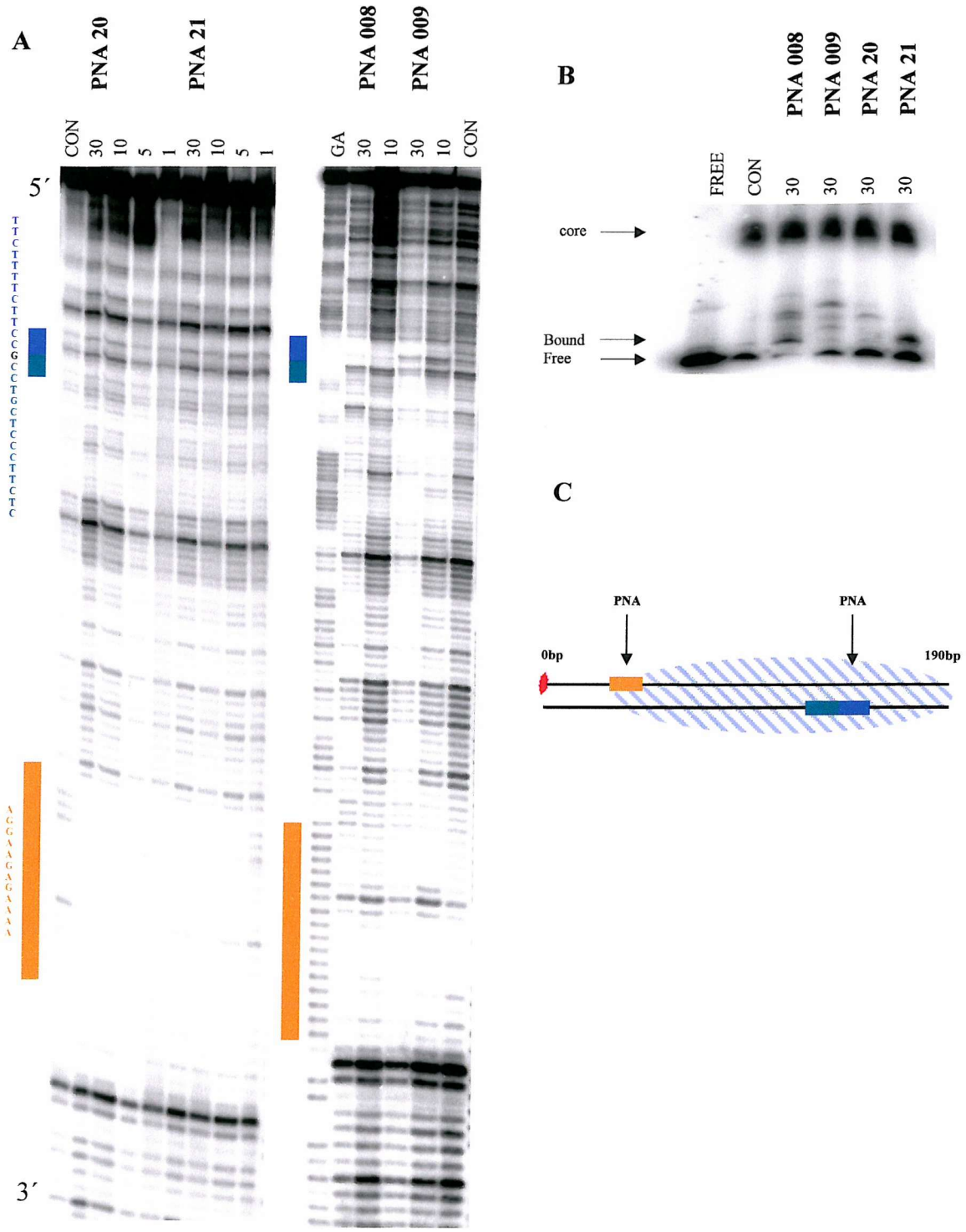

FIGURE 4.34 DNaseI cleavage (A) and bandshift assays (B) of the 190 base pair histone-bound *tyr*T (43-59,122-133) fragment in the presence and absence of PNA 008, 009, 20 and 21. The PNA concentration (μM) is indicated at the top of each gel lane. "CON" indicates digestion of the DNA in the absence of PNA and "GA" is a Maxam-Gilbert marker specific for purines. All the complexes were incubated for 24 hours in 50mM sodium acetate pH 5.0 before digestion with DNaseI. The location of site 1 is indicated in orange, while site 3 is shown in blue. C is a cartoon showing the likely position of the target site, relative to the histone octamer.

at site 3 or the secondary binding site, whereas PNA 008 and 009 show no targeting of site 3. The nucleosome reconstitution onto the 190bp *tyr*T (43-59,122-133) fragment should be the same as when reconstituted onto the 190bp *tyr*T (43-59) fragment. A direct comparison of the two is shown in figure 4.35 where very similar cleavage patterns are present indicating that the protein sits in the same location and seems more evident that the histone octamer sits further towards site 3. The bandshift assays show no disruption to the nucleosome core particle with each PNA sequence, though some bands corresponding to the interaction of these PNAs with free DNA are evident. Quantitative analysis of this data in shown in figure 4.38 and will be discussed at the end of this section.

Figure 4.36A shows the DNaseI and bandshift gels for the interaction of both PNA 009 and 20 or PNA 008 and 21 in combination with the histone-bound 190bp *tyr*T (43-59,122-133) fragment. PNA 20 and 21 produce footprints at site 1 whereas there is no interaction at site 3 with PNA 008 or 009. Lack of interaction has to be due to obstruction from the protein over site 3. There is also no evidence for any interaction at the secondary binding site with PNA 20 or 21. The corresponding bandshifts (figure 4.36B) show no disruption to the nucleosome core particle at high concentrations of PNA 008, 009, 20 or 21 targets both sites 1 and 3. However, when the PNA sequences are in combination there in an increase number of lower retarded bands, which correspond to the different PNA/DNA complexes formed. There is also a small supershift in the nucleosomal band with the parallel PNA sequences 008 and 21. This will be discussed further in section 4.4.3.

Figure 4.37 shows the DNaseI and bandshift gels for the interaction of PNA 008, 009, 20 and 21 with the histone-bound 360 base pair fragment from *tyr*T (43-59,122-133). PNA 20 and 21 produce footprints at site 1 at the highest

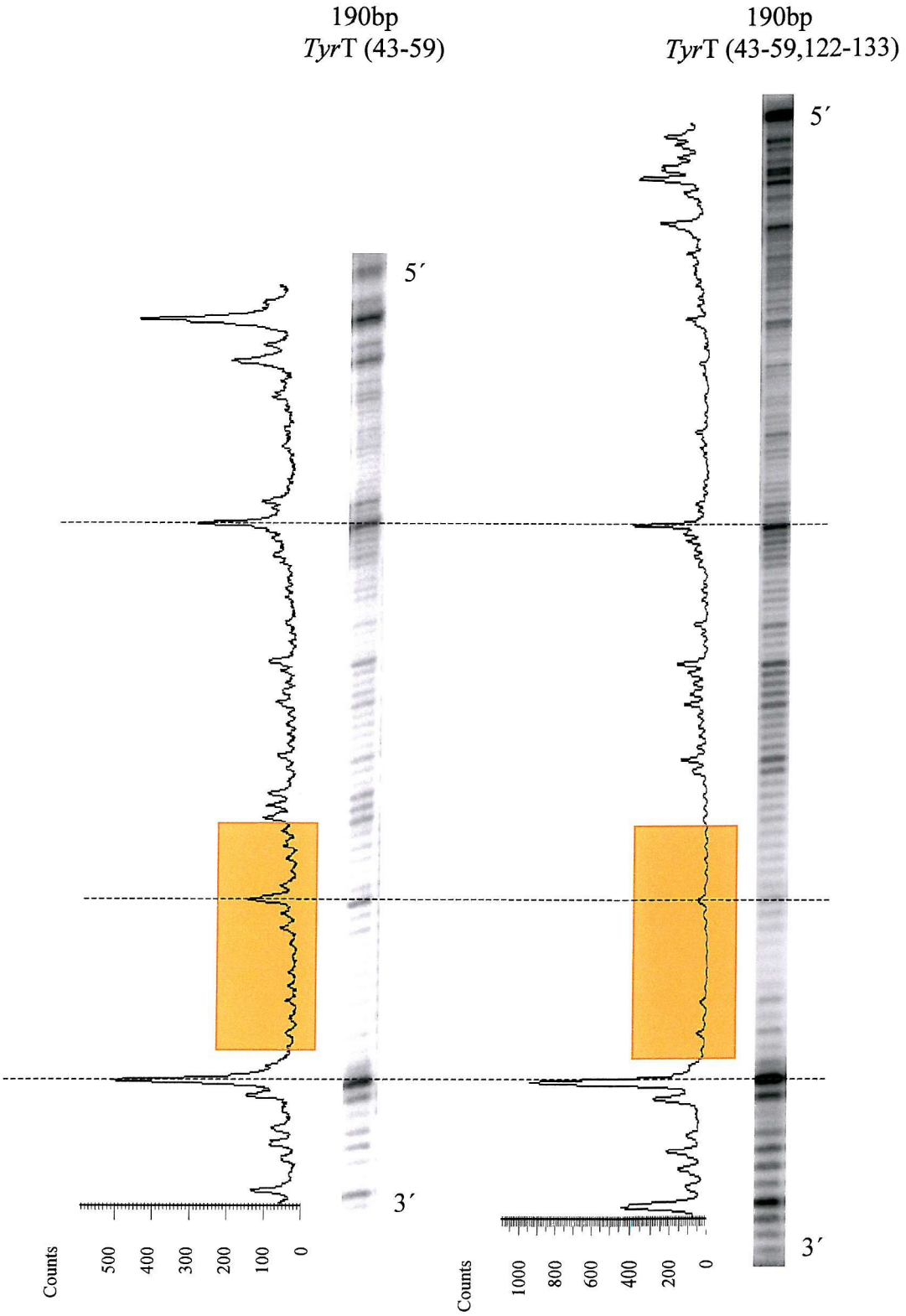

FIGURE 4.35 Differential plots of the histone bound 190bp *tyr*T (43-59) fragment and *tyr*T (43-59,122-133) fragment. Plots are generated from imagequant analysis and the corresponding bases are identified through a dotted line. The location of site 1 is indicated in orange.

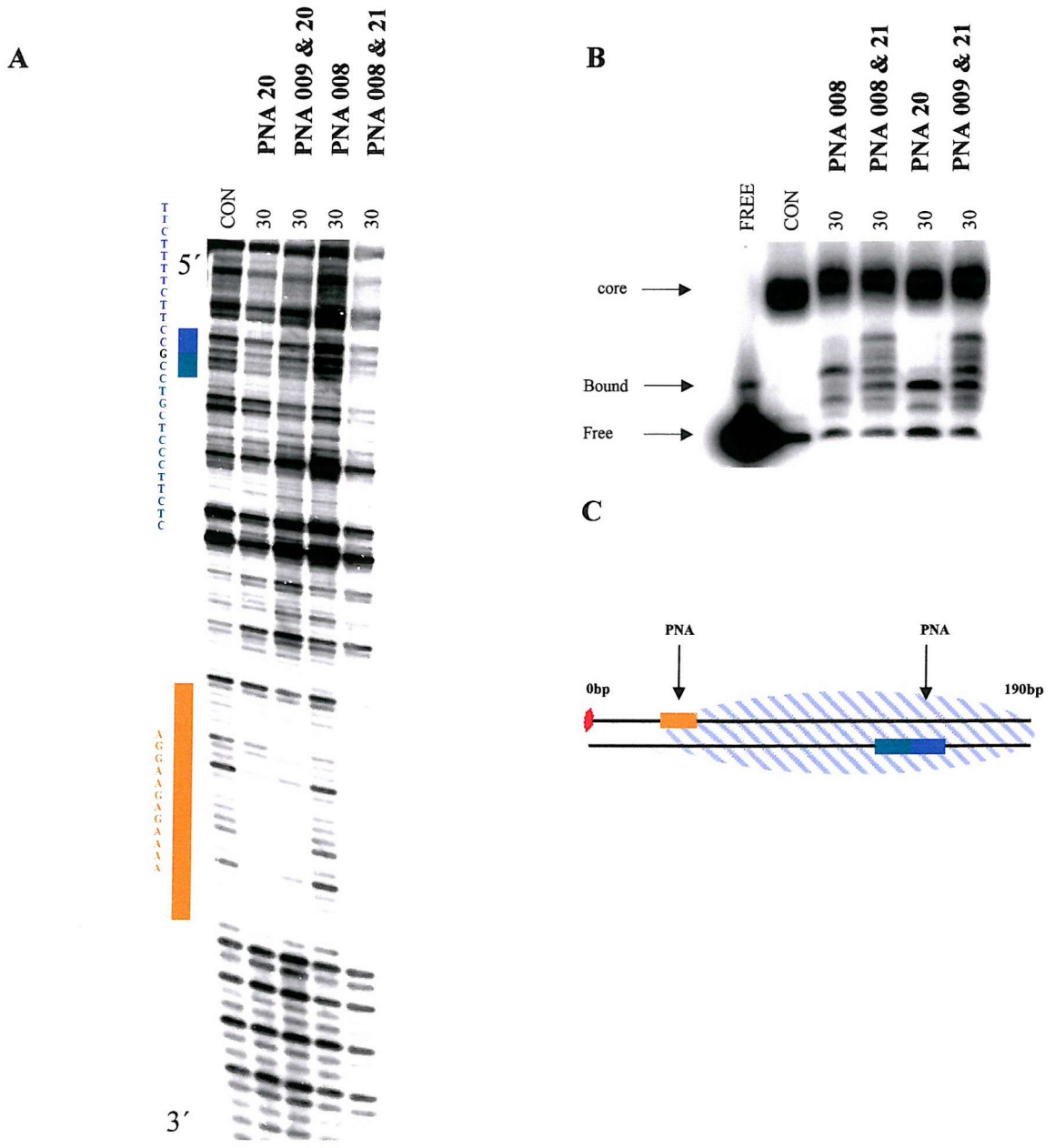

FIGURE 4.36 DNaseI cleavage (A) and bandshift assays (B) of the 190 base pair histone-bound *tyr*T (43-59,122-133) fragment in the presence and absence of PNA 008, 009, 20 and 21 in combination. The PNA concentration (μM) is indicated at the top of each gel lane. "CON" indicates digestion of the DNA in the absence of PNA and "GA" is a Maxam-Gilbert marker specific for purines. All the complexes were incubated for 24 hours in 50mM sodium acetate pH 5.0 before digestion with DNaseI. The location of site 1 is indicated in orange, while site 3 is shown in blue. C is a cartoon showing the likely position of the target site, relative to the histone octamer.

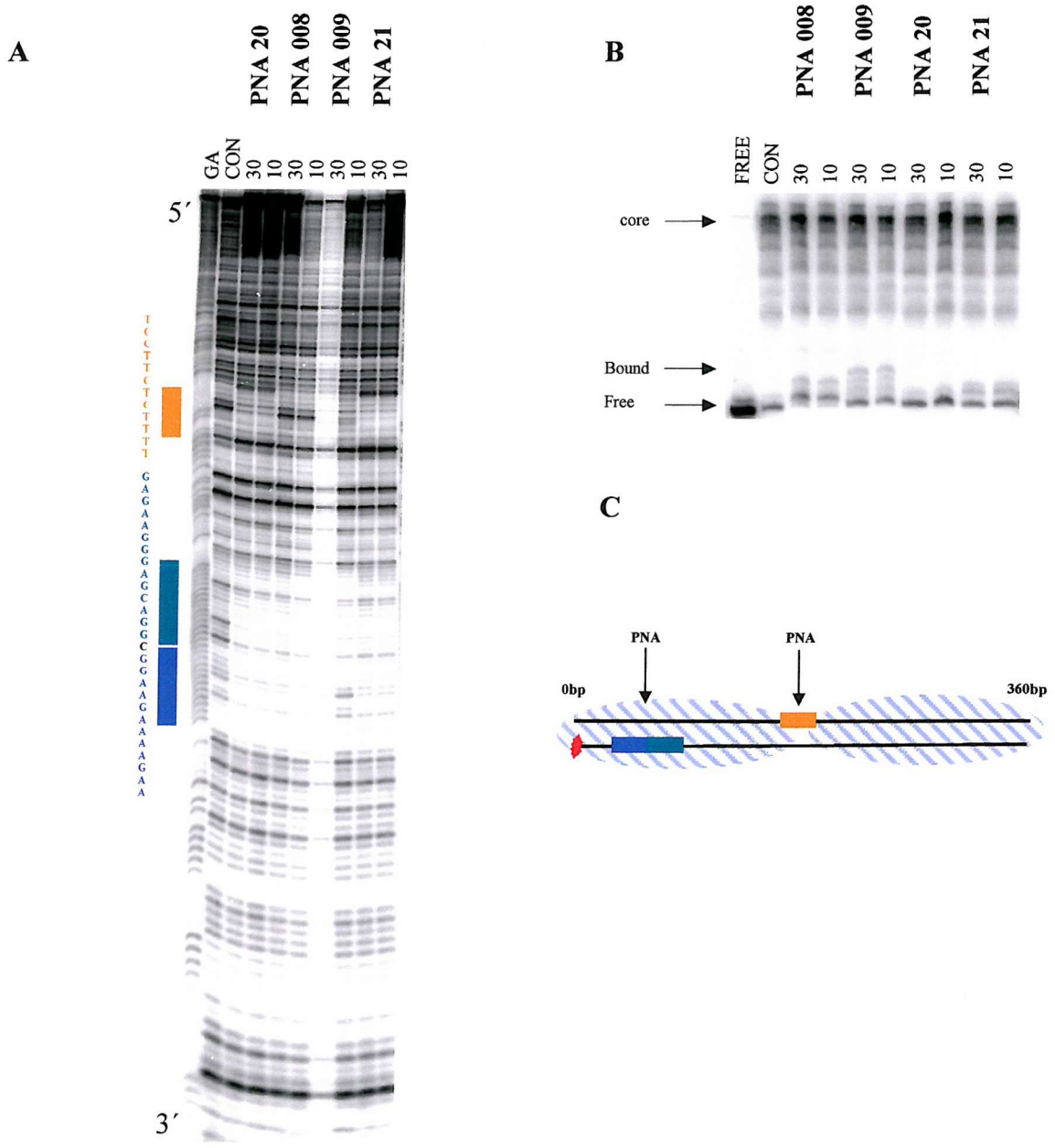

FIGURE 4.37 DNaseI cleavage (A) and bandshift assays (B,C) of the 360 base pair histone-bound *tyr*T (43-59,122-133) fragment in the presence and absence of PNA 008, 009, 20 and 21. The PNA concentration (μM) is indicated at the top of each gel lane. "CON" indicates digestion of the DNA in the absence of PNA and "GA" is a Maxam-Gilbert marker specific for purines. All the complexes were incubated for 24 hours in 50mM sodium acetate pH 5.0 before digestion with DNaseI. The location of site 1 is indicated in orange, while site 3 is shown in blue. D is a cartoon showing the likely position of the target site, relative to the histone octamer.

concentrations (30 and 10μM). PNA 008 and 009 do not produce footprints at site 3and no interactions are visible at site 1 or the secondary binding site. The bandshift assays also show that these PNAs do not disrupt the pre-formed nucleosome core particles.

Footprinting plots showing the intensity of bands in these footprints as a function of PNA concentration are shown in figure 4.38 and the C_{50} values determined from these are summarised in table 4.3. Only site 1 interactions have been graphically presented due to no interactions present at site 3 with either PNA sequences. The C_{50} values with PNA 20 and 21 are higher for the 190bp fragment than the 360bp fragment indicating that site 1 on the 190bp fragment in less assessable that on the longer fragment. The values for the 190bp fragment are 4.7μM ±1.2 for PNA 20 and 5.7μM ±0.8 for PNA 21. These are 1.6 fold and 28.5 fold higher than with free DNA showing that there has to be protein obstruction. Due to the increased concentrations required to target site 1 this indicates that the site is still located within the peripheral regions of the nucleosome core particle when compared to the same site on the histone bound 190bp *tyr*T (43-59) fragment. For the 360bp fragment, the values are more comparable to the 190bp fragment indicating that there is potentially little obstruction from the protein and that site 1 in more than likely positioned in the linker DNA region but also could be dangling off the end of the nucleosome core particle. These results also indicate that the parallel binding sequences are more effective than the antiparallel ones when targeting histone bound DNA.

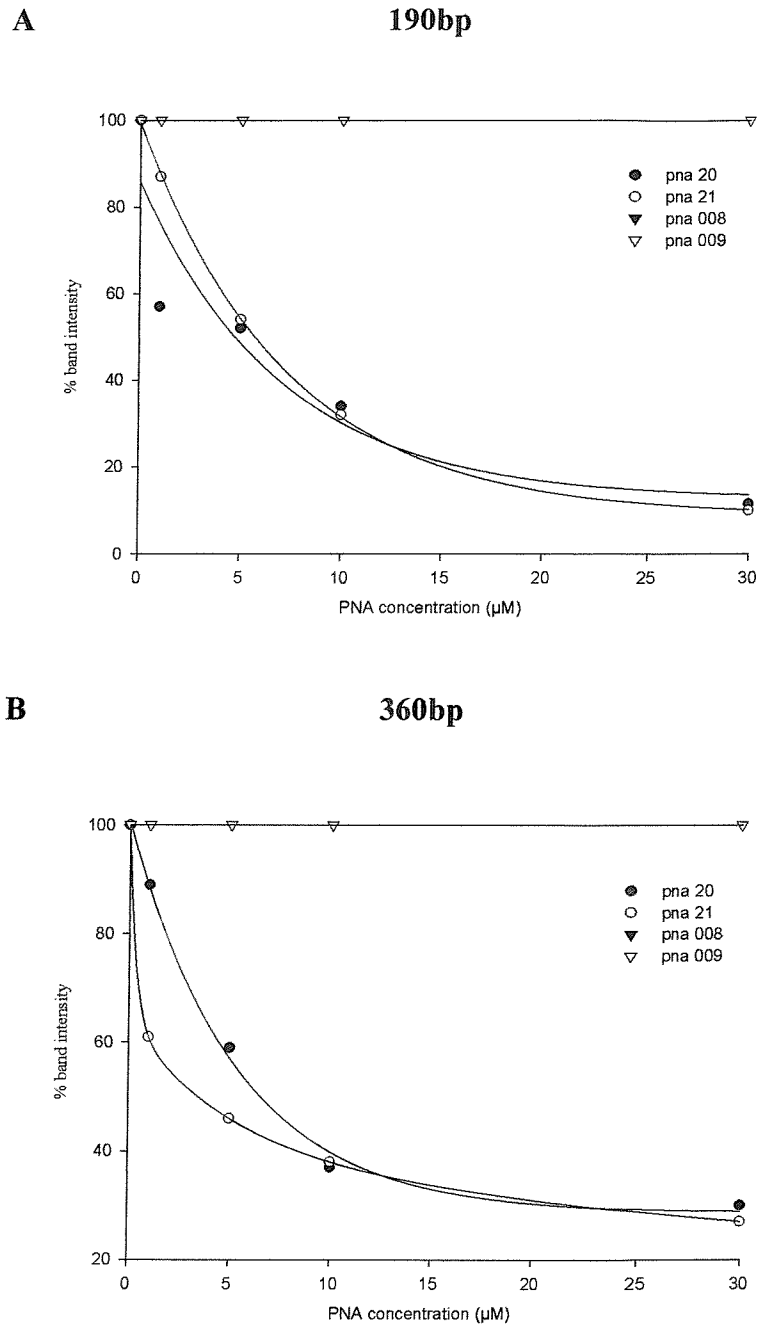

FIGURE 4.38 Footprinting plots showing the interaction of PNAs 008, 009, 20 and 21 with site 1 on the 190 and 360 base pair fragment containing the *tyr*T (43-59,122-133) sequence, when reconstituted into nucleosomal DNA. (A) 190, (B) 360 base pair fragments. The data were obtained from analysis of the footprints shown in figures 4.34 and 4.37.

PNA sequence	C_{50} (μM)				
	free DNA	190bp Site 1	190bp Site 3	360bp Site 1	360bp Site 3
008	0.04 ±0	No footprint	No footprint	No footprint	No footprint
009	36 ±5	No footprint	No footprint	No footprint	No footprint
20	2.9 ±4	4.7 ±1.2	No footprint	4.1 ±2.8	No footprint
21	0.2 ±2	5.7 ±0.8	No footprint	6.9 ±2.5	No footprint

TABLE 4.3 C_{50} values for different PNA sequences targeted to site1 and 3 on the 190 and 360 base pair *tyr*T (43-59,122-133) fragments. These values were determined from the footprinting plots shown in figure 4.29.

4.4.2 Reconstitution of *tyr*T (43-59,122-133) fragments containing pre-formed PNA-DNA complexes

This section examines the interaction of pre-formed PNA-DNA complexes with *tyr*T (43-59,122-133) interact with histone proteins, using similar experiments to those described with *tyr*T (43-59) and *tyr*T (22-33) in sections 4.2.2 and 4.3.2.

Figure 4.39A shows the results of DNaseI footprinting experiments with the 190 base pair *tyr*T (43-59,122-133) fragment, which had been targeted with PNA 008, 009, 20 and 21 prior to reconstitution. Footprints can be seen at site 1 for PNA 20 and 21 with no interactions at site 3 or the secondary binding site. PNA 008 and 009 produce footprints at site 3 with no interactions at the secondary binding site or at

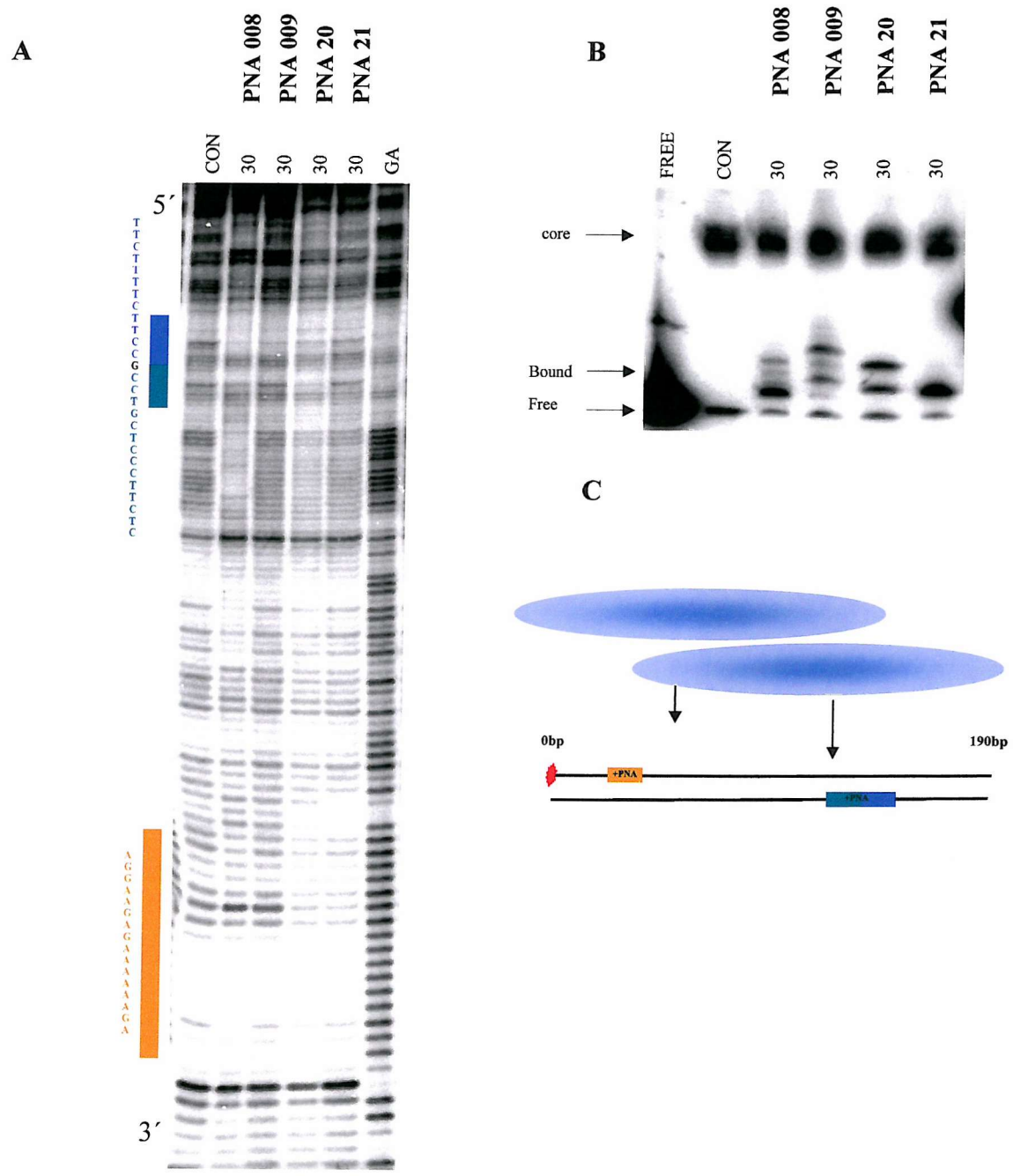

FIGURE 4.39 DNaseI cleavage (A) and bandshift assays (B) of the 190 base pair histone-bound *tyr*T (43-59,122-133) fragment in the presence and absence of PNA 008, 009, 20 and 21. The PNA/DNA complexes were prepared before nucleosome reconstitution. The PNA concentration (μM) is indicated at the top of each gel lane. "CON" indicates digestion of the DNA in the absence of PNA and "GA" is a Maxam-Gilbert marker specific for purines. All the complexes were incubated for 24 hours in 50mM sodium acetate pH 5.0 before digestion with DNaseI. The location of site 1 is indicated in orange, while site 3 is shown in blue. C is a cartoon showing the likely position of the target site, relative to the histone octamer.

site 1. Examination of the bandshift experiments (figure 4.39B) shows that the prior addition of PNA has not reduced the amount of DNA in the nucleosomal band, indicating that targeting these individual sites has not affected the efficiency reconstitution. However, there appears to be a difference in the cleavage pattern when targeting site 1 or site 3. This is especially noticeable with PNA 008 along the region of DNA beyond site 1 in comparison to the cleavage pattern with PNA 20 and 21. This could indicate a shift in the nucleosome positioning however further investigation would be required to clarify this. Quantitative analysis of the bandshift data is shown in Figure 4.40A in which it can be seen that each PNA causes only a small decrease in the amount of histone-bound DNA, and that reconstitution is maintained at a level above 95%.

Figure 4.41 shows the results of DNaseI footprinting experiments in which the 190 base pair *tyr*T (43-59,122-133) fragment has been targeted with PNA008 and 21 or PNA 009 and 20 in combination. The experiment shows the presence of footprints at both sites 1 and 3, though those at site 3 are much clearer. The footprints confirm that the PNA is still bound to the DNA fragments, but do not give direct information on the nucleosome reconstitution. However the bandshift assays with these samples show that when either the parallel (008 and 21) or antiparallel (009 and 20) PNA sequences are added together there is a greater reduction in the efficiency of reconstitution. This shows that targeting both ends of the fragment potentially could prevent of reduce the nucleosome reconstitution due to only 70 bases being present between the two sites, which appears to be an insufficient length for nucleosome reconstitution. There are also an increased number of free PNA-DNA bands, which must correspond to multiple types of complexes when the PNAs are added in combination. Quantitative analysis of these data is shown in figure 4.40B revealing

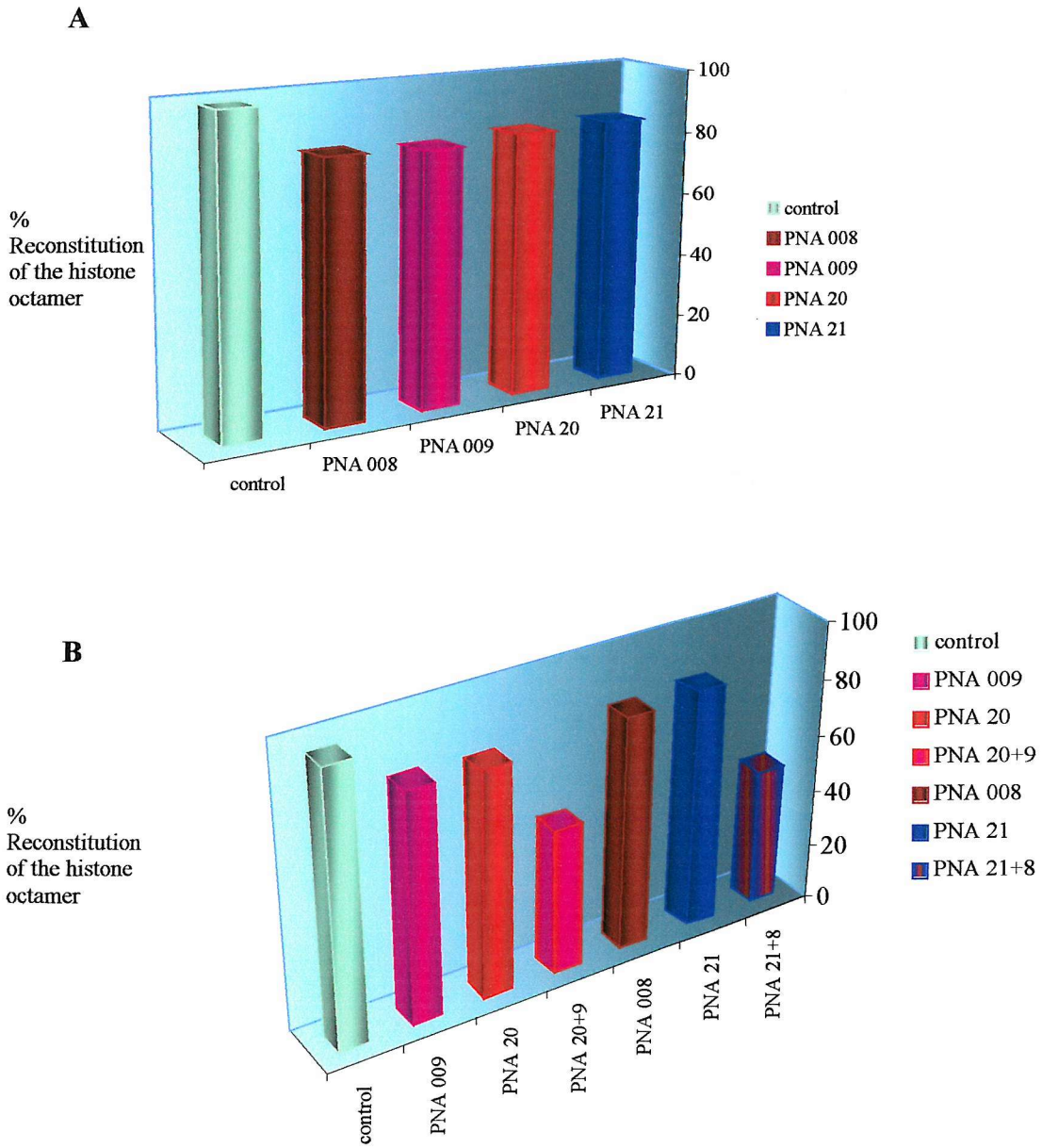

FIGURE 4.40. Graphical representation of the percentage reconstitution of the 190 base pair *tyr*T (43-59,122-133) into nucleosomes, in the presence of (A) 30μM PNA 008, 009, 20 and 21 individually and (B) 30μM of PNA 21 and 008 or 20 and 009 in combination. The PNA/DNA complexes were generated before nucleosome reconstitution.

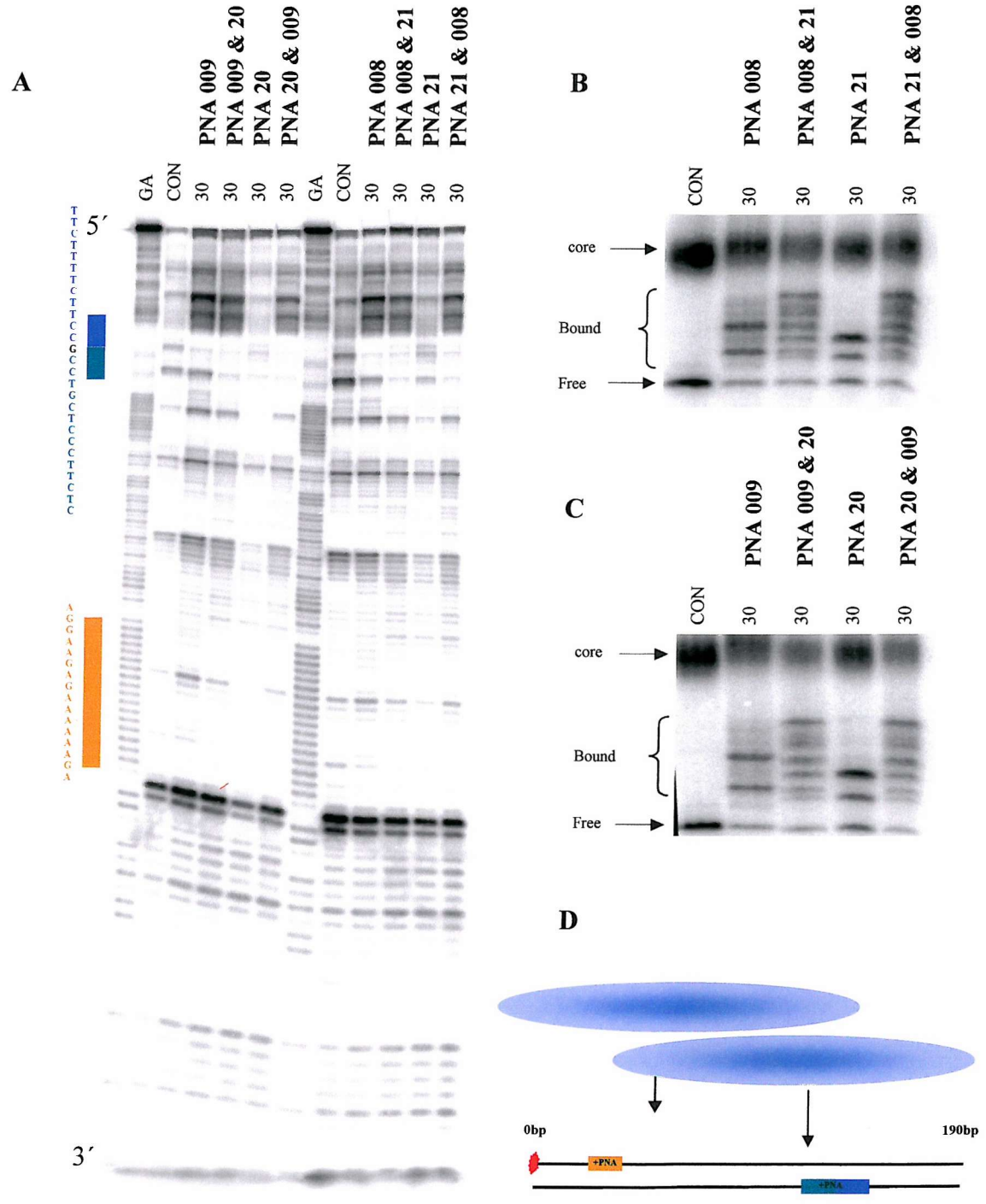

FIGURE 4.41 DNaseI cleavage (A) and bandshift assays (B,C) of the 190 base pair histone-bound *tyr*T(43-59,122-133) fragment in the presence and absence of combinations of PNA 008 and 21 or 009 and 20. The PNA/DNA complexes were prepared before nucleosome reconstitution. The PNA concentration (μM) is indicated at the top of each gel lane. "CON" indicates digestion of the DNA in the absence of PNA and "GA" is a Maxam-Gilbert marker specific for purines. All the complexes were incubated for 24 hours in 50mM sodium acetate pH 5.0 before digestion with DNaseI. The location of site 1 is indicated in orange, while site 3 is shown in blue. D is a cartoon showing the likely position of the target site, relative to the histone octamer.

that when used in combination the efficiency of recombination drops to about 60%.

Figure 4.42 shows DNaseI footprinting and bandshift gels for the 360 base pair *tyr*T (43-59,122-133) fragment targeted with PNAs 008, 009, 20 and 21 separately and in combination. When added separately footprints can be seen at site 1 with PNA 20 and 21 and at site 3 with PNA 008 and 009. In combination there are footprint at both sites, PNA 20 and 21 targeting site 1 and PNA 008 and 009 targeting site 3. The distance between sites 1 and 3 on the 360bp fragment could reconstitute one protein octamer and incorporate the PNA complexes at the peripherally regions of the nucleosome. However, when you study the bandshift assays on these samples, which are shown in figure 4.42C there is a decrease in the slowest moving band in the multiple band region, which could indicate that only one protein octamer has bound. The parallel sequence PNA 008 and 21 are reduced to 64% as a function against the control lane and the antiparallel sequence PNA 009 and 20 are reduced to 67%. When targeting individually (figure 4.42B) this band remains contrast, however when compared to the reconstitution of the 360bp fragment which was then targeted with each PNA individually after reconstitution, there are some differences in the multiple bands produced. This is shown in figure 4.43B. These results show that the histone octamer associates with different regions of the 360bp fragment, depending on the location of the PNA/DNA complex. This in turn alters the intensity of the bands representing nucleosome bound DNA.

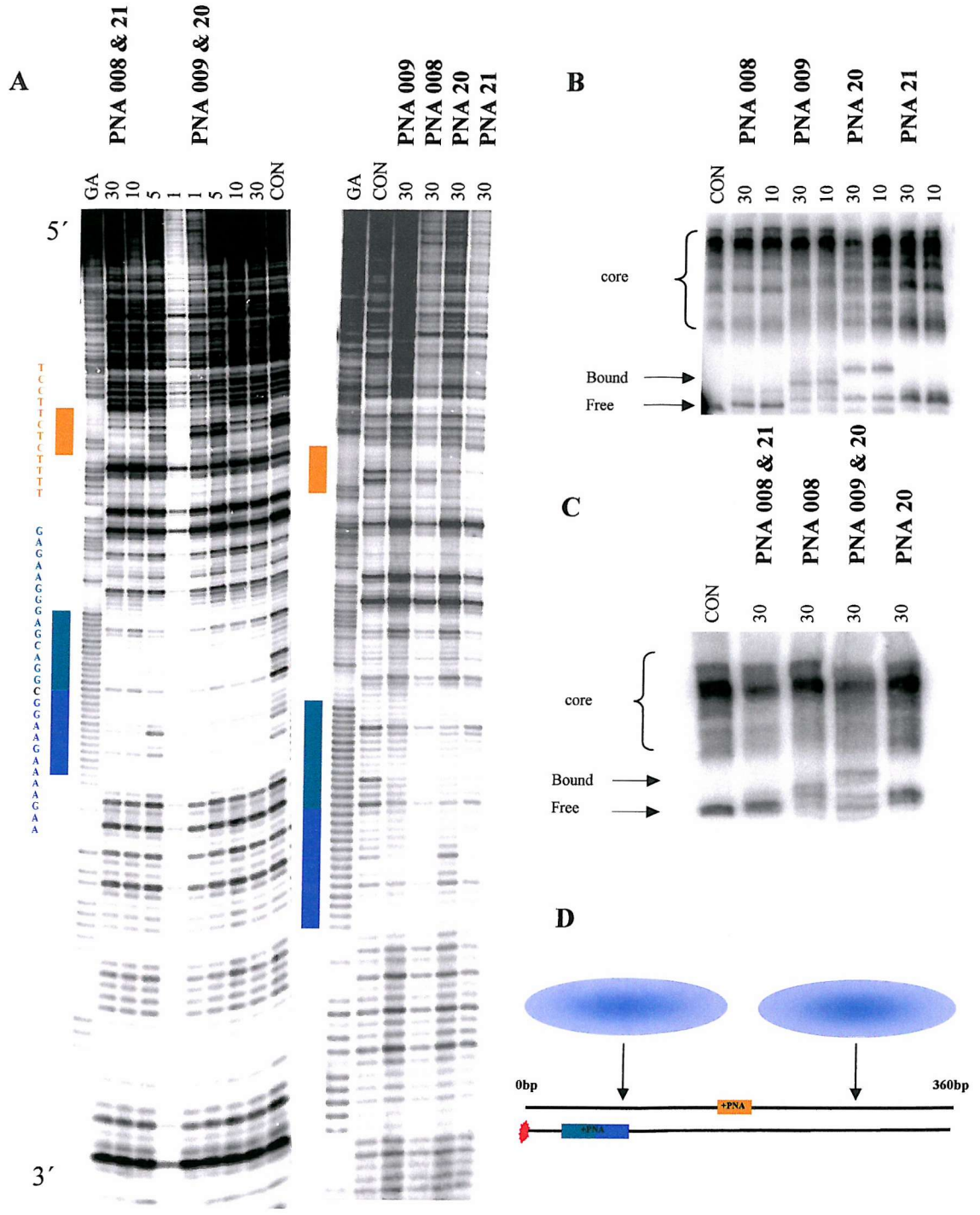

FIGURE 4.42 DNaseI cleavage (A) and bandshift assays on the 360 base pair *tyr*T (43-59,122-133) fragment in the presence or absence of PNA 008, 009, 20 and 21 separately (B) and in combination (C). The PNA-DNA complexes were generated prior to nucleosome reconstitution. The PNA/DNA complexes were prepared before nucleosome reconstitution. The PNA concentration (μM) is indicated at the top of each gel lane. "CON" indicates digestion of the DNA in the absence of PNA and "GA" is a Maxam-Gilbert marker specific for purines. All the complexes were incubated for 24 hours in 50mM sodium acetate pH 5.0 before digestion with DNaseI. The location of site 1 is indicated in orange, while site 3 is shown in blue. D is a cartoon showing the likely position of the target site, relative to the histone octamer.

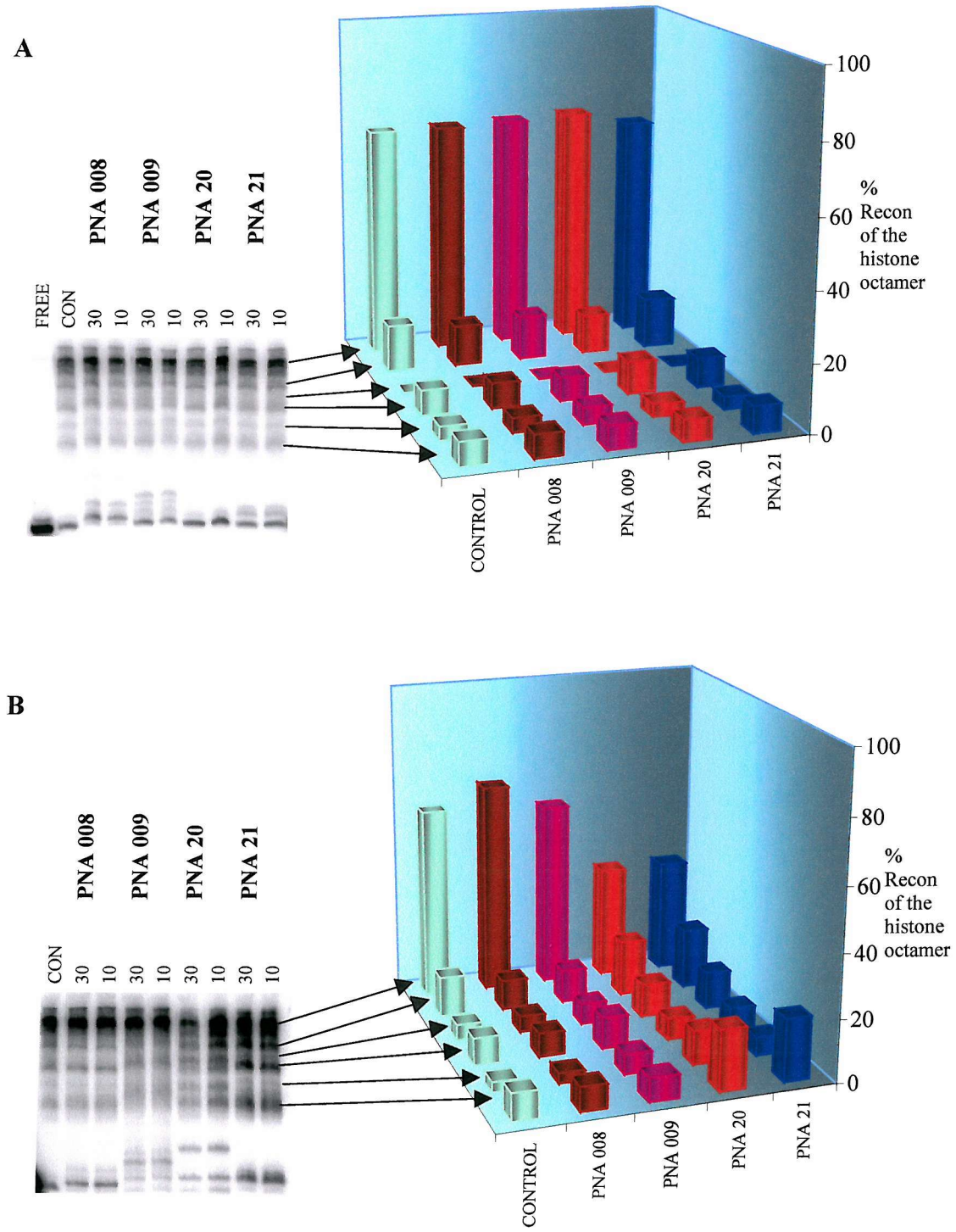

FIGURE 4.43 Graphs representing the percentage reconstitution of the histone octamer onto the 360bp *tyr*T (43-59,122-133) sequence targeted with PNA 008, 009, 20 and 21. (A) post nucleosome reconstitution and (B) prior nucleosome reconstitution. The PNA concentration for each experiment represent on the graph is 30μM.

4.4.3 Discussion

These results have not identified the location of histone binding in relation to site 3, however they have shown whether PNA can interact with these sites and effect nucleosome reconstitution. The 190bp fragment can be targeted at site 1 whereas the bound protein obstructs site 3. This is turn has prevented the interactions at the secondary binding site. Targeting of either site 1 or 3 has indicated that the protein could have translational shifted away from the PNA/DNA complex and in the case of the 360bp, potentially forcing only one protein to bind. DNaseI and bandshift assay show alterations in cleavage and band intensity for the reconstituted DNA indicating a possible translational shift of the protein. Pre-targeting of both sites 1 and 3 has an effect on the nucleosome reconstitution when there is insufficient free DNA present, however this effect is not as severe as seen with the *tyr*T (43-59) and (22-33) fragments. A 70 base pair region is located between sites, 1 and 3, which could be reconstituted into nucleosomes with the two PNA/DNA complexes located at either ends of the nucleosome. Nucleosome reconstitution was reduced under these conditions but not completely abolished. These results do show that both sties are targeted due to normal reconstitution being present when only one site is targeted.

Following on from these studies we attempted to construct the TP48 dimer as explained in chapter 2. This would enable us to examine dinucleosome formation and to selectively target either the linker or the histone-bound DNA. Unfortunately the attempts to produce this fragment were unsuccessful and further experiments are required to complete this work.

Chapter 5

Interaction of PNA with histone octamers lacking the N-terminal tails

5.1 Introduction

All the core histones have a conserved structural domain known as the histone fold, which combine together to form the octamer onto which DNA is associated. The remainder of their structure contains the N-terminal tail regions, which are highly conserved. These are located outside the histone fold and are not required for assembly of the histone octamer. However, these regions have been shown to interact with both DNA and proteins in the nucleus. They modulate nucleosome stability (affecting the DNA binding affinity) and play a key role in gene regulation and in the formation of the chromatin fibre. The structure and molecular contacts of the tail regions within the nucleosome have not been fully defined to date. However, the N-terminal tail domains contain a high level of basic residues that can interact with the DNA backbone, increasing the nucleosome stability by providing additional countercharges to the polyanionic DNA backbone. Proteolytic removal of these tail domains only results in marginal changes to the conformational and hydrodynamic properties of the nucleosome core particle (Widlund *et al* 2000). Remodeling of the chromatin fibre, mediated through processes such as post-translational modifications, alters the strength of the interaction of these tail-domains with DNA (Ausio *et al* 1989).

Core histones have been shown to obstruct the access of the ligands to nucleosomal DNA (Ausio *et al* 1989). Tryptic removal of the N-terminal tail domains of core histones enhances their binding potential and has been shown to enhance the binding of the anticancer antibiotic chromomycin to nucleosomal DNA (Ausio *et al* 1989) relative to intact nucleosomes in which the binding was obstructed. This has

led to the suggestion that the N-terminal tail regions prevent access of external agents, such as anticancer drugs, to the eukaryotic genome.

This short chapter will examine whether tryptic removal of the N-terminal tail regions of the histone octamer affects the interaction with PNA. N-terminal-digested nucleosome core particles were prepared as described in Chapter 2. The illustration in Figure 5.1 shows the regions of the histone octamer that are cleaved by trypsin, leaving the nucleosome fold domain intact. This will affect the interactions with the DNA helix and loosen the contacts between the two. This in turn could affect PNA targeting on the nucleosome core particle and change its ability to be incorporated into a nucleosomal PNA/DNA complex. Figure 5.2 compares the reconstitution of fragment 110 base pair *Tyr*T (43-59) fragment onto intact and tryptic digested nucleosome core particles. This shows an increase in the mobility of the complex formed with the digested protein. Two bands are present in this complex; the higher one corresponds to binding of the DNA to partially cleaved histone octamer while the lower corresponds to the full digested nucleosome fold domain.

5.2 Interaction of PNA with the *tyr*T (43-59) sequence after it has been reconstituted onto digested nucleosomes

This section examines the binding of PNA 20 and 21 to the 110 base pair *tyr*T (43-59) sequence, after it has been reconstituted onto trypsin-digested nucleosomes. Figure 5.3 shows DNase I footprinting and bandshift assays for this interaction. It can be seen that both these PNA interactions with site 1 producing weak footprints. It is difficult to identify the concentrations required because clear footprints are not present. However there is some interaction at site 1 with both PNA

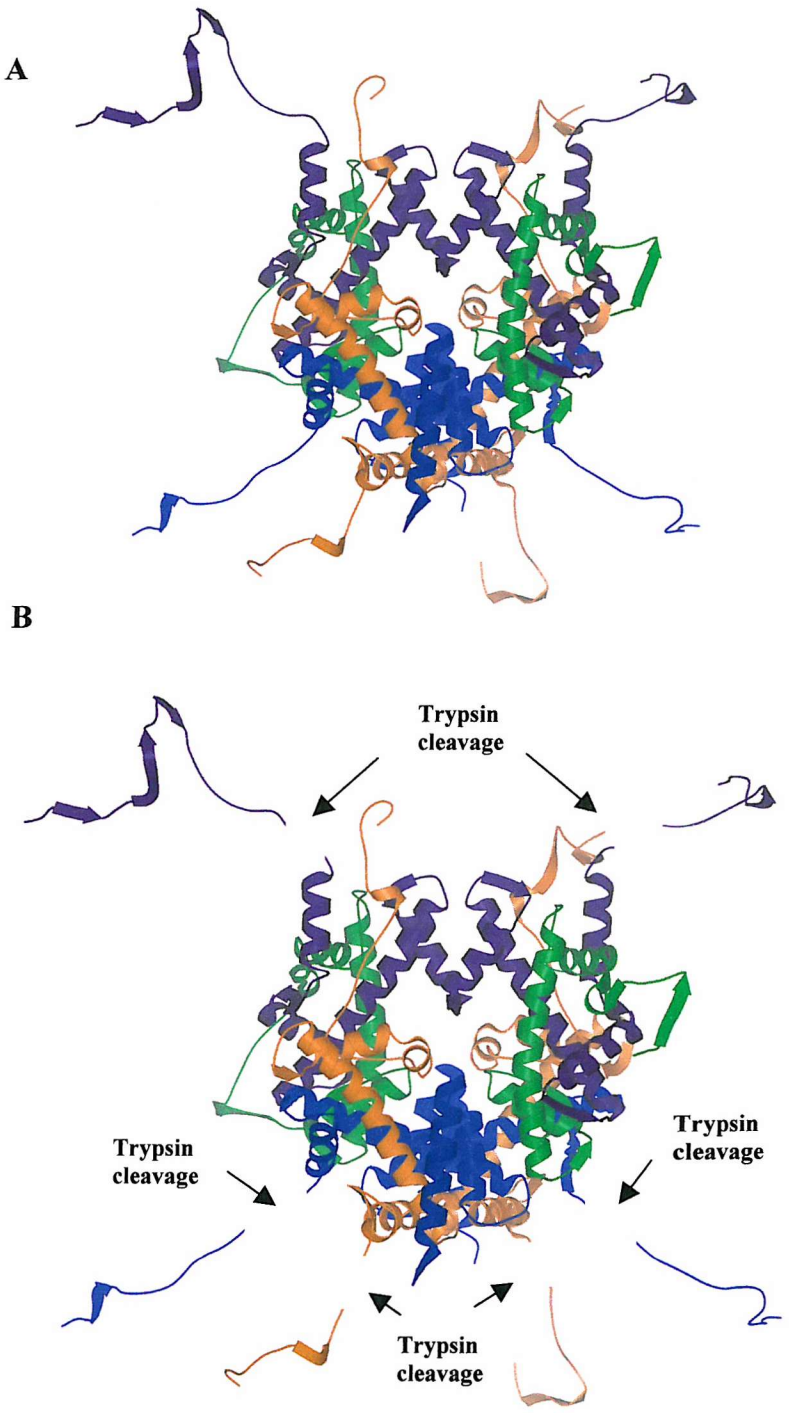

FIGURE 5.1 Three dimensional structure of the histone octamer with the N-terminal tail regions intact (A) and tryptic removal of the N-terminal tail regions (B). Generated from atomic coordinates 1eqz prepared using Molscript, GL render and Raster 3D. The secondary structure and histones are represented as previously described.

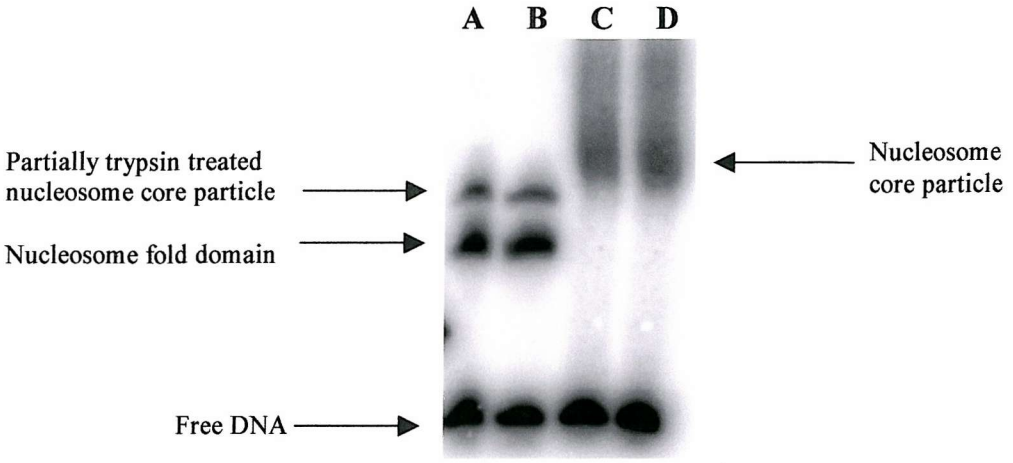

FIGURE 5.2 Native polyacrylamide gel comparing reconstitution of the 110 base pair *Tyr*T (43-59) fragment onto trypsin-digested (A,B) and intact (C,D) nucleosome core particles

20 and 21. These results show that PNA is able to partially interact with site 1 on the 110 base pair fragment, which is situated very close to the dyad axis. Targeting of this region is not expected to produce clear footprints, however weak interactions are present. These results are in contrast to the experiments with intact nucleosomes for which no footprints were observed under similar conditions (see section 4.2.1). A phased DNase I cleavage pattern is evident throughout the sequence, suggesting that the DNA fragment is still associated with the histone proteins and which correlates to the cleavage pattern on the 110 base pair *tyr*T (43-59) sequence. The integrity of the reconstituted nucleosomes is confirmed by the bandshift experiments, shown in figure 5.3B,C, which show that addition of these PNAs has no effect on the amount of DNA in the retarded species. There are two retarded nucleosomal bands present, which correspond to the partly cleaved (top band) and fully cleaved (lower band) nucleosome with trypsin. An additional band is present above the free DNA band, which corresponds to the PNA/DNA complex formed with the contaminating free DNA and has a much lower intensity than when targeting intact nucleosomes

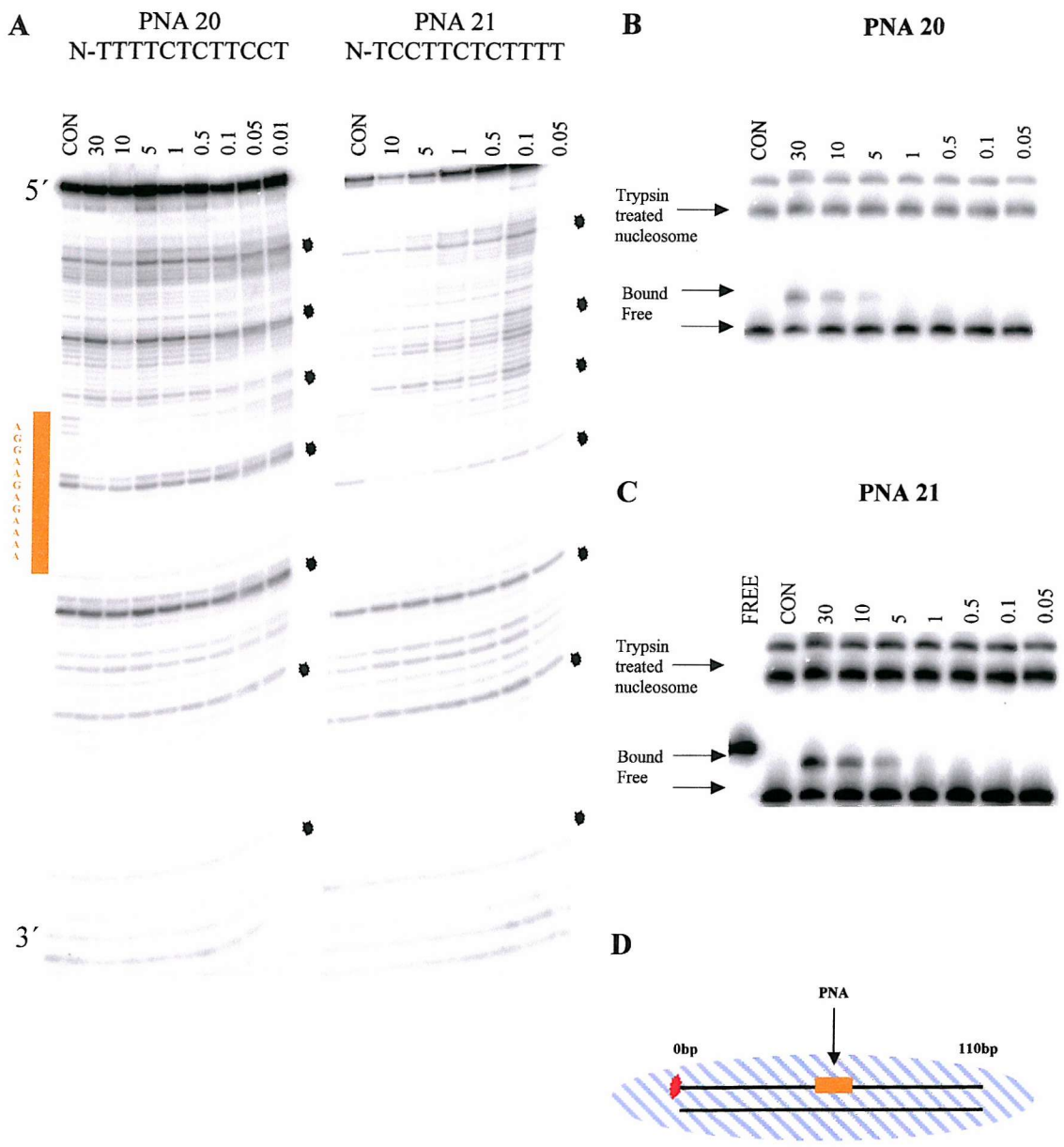

FIGURE 5.3 DNase I cleavage and bandshift assays for the interaction of PNA20 and 21 with the 110 base pair *tyr*T (43-59) DNA fragment which has been reconstituted with trypsin-digested nucleosomes before adding the PNA. The PNA concentration (μM) is indicated at the top of each gel lane. "CON" indicates digestion of the DNA in the absence of PNA and "GA" is a Maxam-Gilbert marker specific for purines. All the complexes were incubated for 24 hours in 50 mM sodium acetate pH 5.0 before digestion with DNase I. The location of site 1 is indicated in orange. The asterisks indicate the sites of maximal cleavage, where the DNA minor groove faces away from the protein core. D is a cartoon showing the likely position of the target site, relative to the histone octamer.

(see section 4.2.1). These bandshifts also show that the percentage reconstitution is also reduced when targeting trypsin-digested nucleosomes. This will be due to the weak association between the DNA and the protein surface created a very loosely associated complex. Figure 5.4 shows footprinting plots, derived from quantitative analysis of bands at site 1 at different PNA concentrations, and the C_{50} values determined from these are presented in table 5.1. As the PNA concentration increases the intensity of bands in site 1 decreases and in a way that is similar to that seen with free DNA (see section 3.2.1) but not at the same rate and higher C_{50} values have been obtained. These results are very different to those obtained with this fragment when bound to intact nucleosomes, which showed no interaction with site 1.

5.3 Reconstitution of PNA/DNA complexes onto trypsin-digestion nucleosomes

The following section examines whether complexes between PNA 20 or 21 and the 110 base pair *tyr*T (43-59) fragment can be reconstituted onto nucleosomes which have had their N-terminal tails removed by trypsin digestion. Figure 5.5 shows the DNase I footprinting experiments and bandshift gels for this interaction. It can be seen that PNA 20 and 21 produce show partial interaction with site 1. With PNA 20 there is a weak reduction in intensity of the bands over site 1 whereas for PNA 21 there is a clearer footprint present at highest concentrations. These results are not as clarified as those shown in chapter 4 (figure 4.9) where the PNA complex formed had remained bound and prevented nucleosome reconstitution. However these results do show that there is an indication that the PNA/DNA complex can be incorporated within the condensed region of near of the dyad axis when the N-terminal tail regions

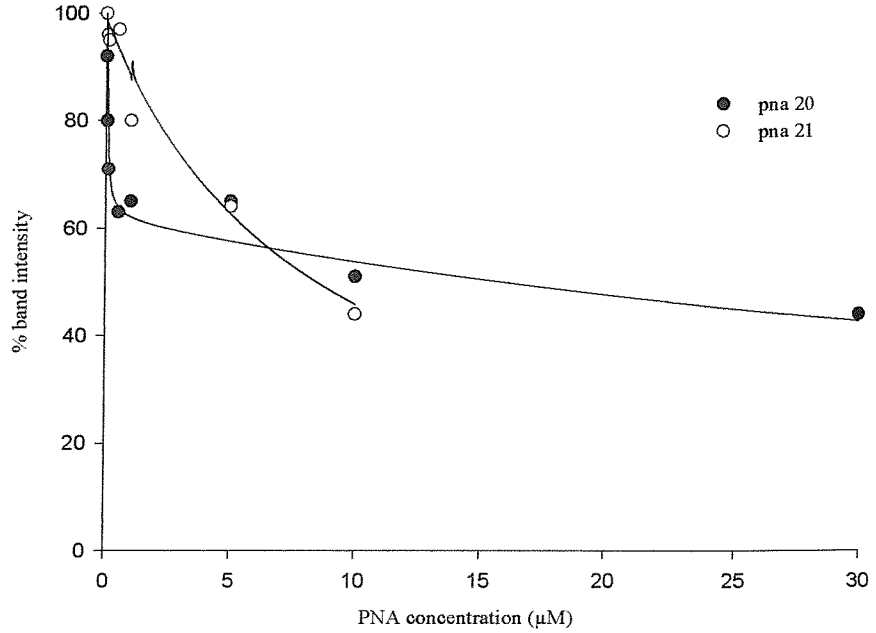

FIGURE 5.4 Footprinting plots showing the interaction of PNA 20 and 21 with site 1 on the 110 base pair *tyr*T (43-59) DNA fragment. The DNA was reconstituted onto trypsin-digested nucleosomes before the addition of PNA.

PNA	C_{50} (μM)	
	Free DNA	Bound to trypsin-digested nucleosomes
20	2.9 ±4	15.8 ±2.4
21	0.2 ±2	8.44 ±3.3

TABLE 5.1 C_{50} values for the interaction of PNA 20 and 21 with the 110 base pair 110 base pair *tyr*T (43-59) fragment, which has been reconstituted with trypsin-digested nucleosome core particles. The values were calculated from the footprinting plots shown in figure 5.4.

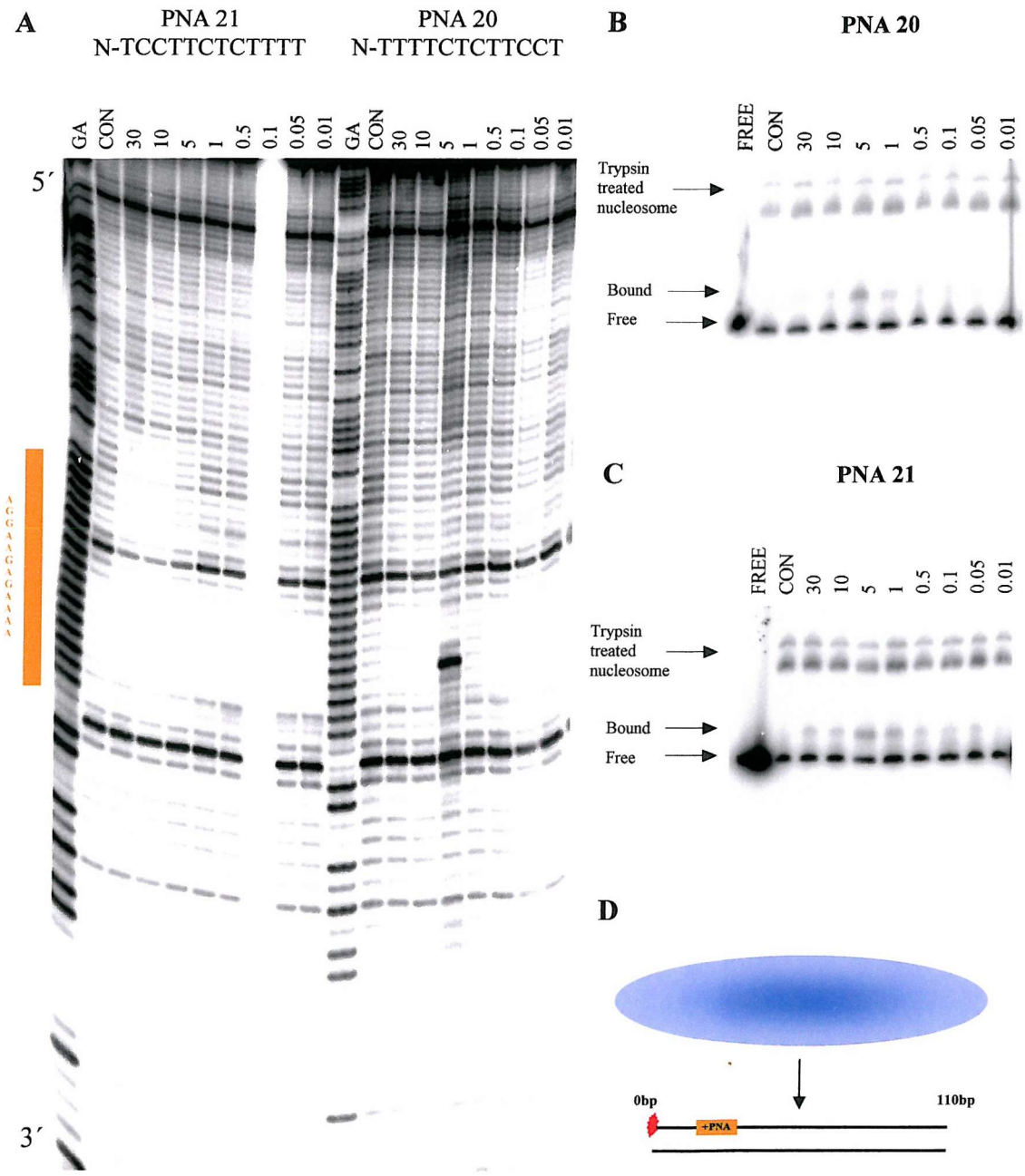

FIGURE 5.5 DNase I cleavage and bandshift assays for the interaction of PNA 20 and 21 with the 110 base pair *tyr*T (43-59) fragment. The PNA-DNA complexes were generated before reconstitution onto trypsin-digested nucleosomes. The PNA concentration (μM) is indicated at the top of each gel lane. "Con" indicates digestion of the DNA in the absence of PNA and "GA" is a Maxam-Gilbert marker specific for purines. All the complexes were incubated for 24 hours in 50 mM sodium acetate pH 5.0 before digestion with DNase I. The location of site 1 is indicated in orange. D is a cartoon showing the likely position of the target site, relative to the histone octamer.

of the protein are not present to effect binding. The corresponding bandshift assays show a clearer picture as to whether the presence of the PNA/DNA complex has effected the reconstitution. Bandshift analysis (Figure 5.5B and C) shows that the PNAs have not affected the formation of nucleosomal DNA, even at high concentrations. Quantitative analysis of this data confirmed that there is no significant decrease in the amount of DNA in the retarded species (not shown). This is in contrast to the results with this fragment on intact nucleosomes for which prior addition of the PNA drastically reduced the efficiency of nucleosome reconstitution (see section 4.2.2).

5.4 Discussion

The result presented in this short chapter show that removal of the N-terminal tails alters the way in which PNA-DNA complexes interact with the histone octamer. The footprinting and bandshift experiments showed PNA-DNA complexes could be generated on trypsin-digested nucleosomes in contrast with the results with intact nucleosomes, which showed an attenuated interaction. This result is surprising since it was obtained with the 110 base pair fragment, for which the entire sequence should be associated with the histone octamer, and the PNA target site is located very close to the dyad axis. However the C_{50} values are higher than those with free DNA, PNA 20 having a C_{50} value of 15.8±2.4 and PNA 21 having a C_{50} value of 8.44±3.3. This suggests that PNA interactions are still effected by the protein however it does show that the N-terminal tails protrude though the DNA helix and somehow influence PNA binding. This could be because the protein-DNA interactions are too strong to allow targeting when it is wrapped around intact histones, or could be because the tails

directly obstruct the target site. It has been well documented that removal of the N-terminal tail regions loosens the histone-DNA interactions (Ausio *et al* 1989), which could increase the capability to bind PNA when these tails are removed. Removal of the N-terminal tail regions has been shown to effect targeting of specific regions within the nucleosome and along the chromatin fibre such as transcription factor binding (Vitolo *et al* 2000). However, removal of the histone tails has been documented to enhance nucleosome sliding (Hamiche *et al* 2001).

The reconstitution of DNA onto trypsin-digested nucleosomes is not as efficient as with intact nucleosomes. Bandshift analysis shows a reconstitution efficiency of around 70%, which is significantly lower than with intact nucleosomes that reconstitute at levels above 95%. This could be due to the loosening effect between the DNA and the histone octamer.

N-terminal tail regions do modulate nucleosome stability (affecting the DNA binding affinity) as well as playing a key role in gene regulation. Due to these regions extending from the protein through the DNA superhelix, modification of the tails by acetyltransferases and deacetylases affect the interactions between the histone proteins and the DNA aswell as a number of metabolic processes. Acetylation of the lysine residues can affect histone assembly and regulate the unfolding and activity of genes, making both RNA polymerase and transcription factors easier to access the promoter region. Tryptic removal of the N-terminal tail domains could be a model for gene regulation and what happens to nucleosomes and the chromatin fibre through acetylation and deacetylation. These results could be used as an experimental model and may give a more accurate idea of how PNA would interact with histone bound DNA with the cell.

Chapter 6

Fluorescence melting studies

6.1 Introduction

As explained in Chapter 1, PNA can interact with double stranded DNA to form several different types of complexes, involving strand invasion and/or triplex formation. The ambiguity in the nature of the complexes that can be formed is evident in the results described in Chapter 3, which seem to involve triplex formation (footprints are only observed at low pH) and strand invasion (the labeled pyrimidine strand is sensitive to cleavage by S1 nuclease). However, for these molecules, strand invasion with triplex formation would require at least one of the PNA strands to bind in a non-canonical orientation (*i.e.* the two pyrimidine strands will be parallel to each other). This chapter investigates the interaction of PNA 20 and 21 with a short DNA duplex by measuring their effects on its melting profile. The experiments used the fluorescence melting technique are described by Darby *et al.* (2002). In this technique, which uses a molecular beacon approach, the complementary DNA strands are labeled with a fluorophore (fluorescein) and a quencher (methyl red), which are positioned so that they are in close proximity in the duplex, thereby quenching the fluorescence. When the duplex melts (on raising the temperature, or as a result of PNA strand invasion) the fluorophore and quencher move part, as they are on different strands, and there is a large increase in the fluorescence signal (see Figure 6.1).

Two complementary 16 base oligonucleotides were synthesized for this work, which are based on site 1 of the *tyr*T (43-59) sequence (see Figure 6.2). The purine-rich strand was labelled with methyl red at the 5'end, while the pyrimidine-containing strand was labelled at the 3' end with flourescein (Figure 6.1). These oligonucleotides were used to study the interaction with PNA 20 and 21 under a range of different conditions. In these studies we reason that simple triplex formation, without strand

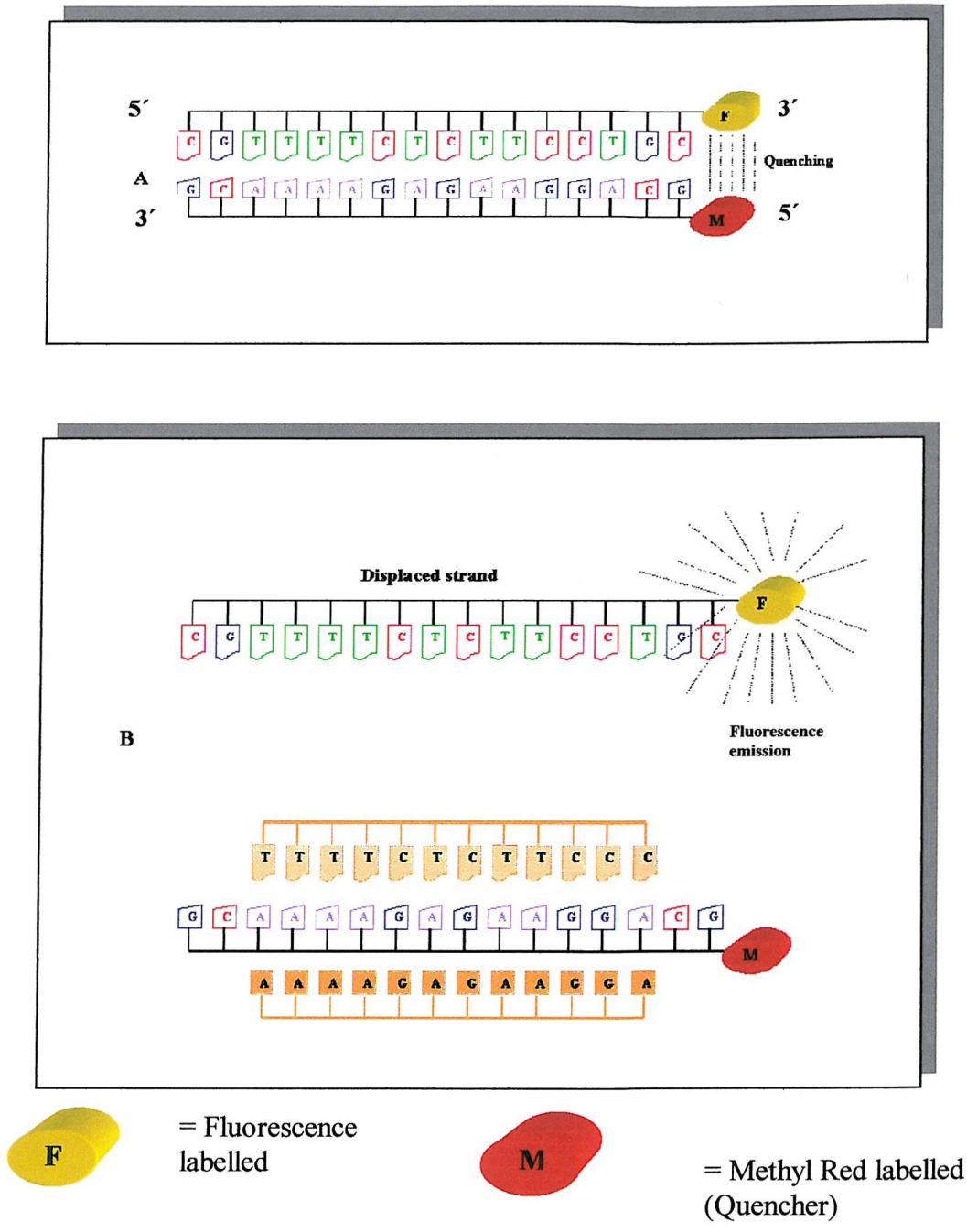

FIGURE 6.1 Illustration of the use of fluorescently labelled oligonucleotides to study the interaction of PNA with the target DNA duplex. (A) Represents the annealed DNA duplex and (B) illustrates the invasion of the DNA duplex with PNA (orange). F indicates the fluorophore (fluorescein) and Q is the quencher (methyl red).

invasion (generating a DNA_2.PNA complex) will either have no effect on the melting profile, or will stabilize the duplex, thereby increasing the T_m. In contrast, any process that involves strand invasion (*i.e.* generating a PNA.DNA duplex or a PNA_2.DNA triplex) will separate the two DNA strands leading to either a large increase in fluorescence, or a reduction in the T_m.

6.1.1 Method

Fluorescence melting curves were determined in a Roche LightCycler, using a total reaction volume of 20 μL. The melting profiles for up to 32 samples could be recorded simultaneously. The LightCycler has one excitation source (488 nm) and three channels for recording fluorescence emission at 520 nm, 640 nm, and 705 nm. For the studies in this work we measured the changes in fluorescence at 520 nm. For each reaction the final oligonucleotide concentration was 0.25 μM, diluted in an appropriate buffer. The samples were first heated to 95°C at 0.1 °C sec^{-1}. These were then annealed by slowly decreasing the temperature from 95 °C to 35 °C at 0.1°C sec^{-1}. In the final step the samples were slowly heated from 35°C to 95°C at 0.1°C sec^{-1}. Recordings were taken during both the melting and annealing cycles. Unless stated otherwise, the results presented refer to the melting profiles. In some instances (described below) there is hysteresis between the annealing and melting profiles, which show different T_m values. This occurs because the reaction is not at thermodynamic equilibrium as the temperature is raised, and is indicative of a slow step in the binding reaction.

6.1.2 PNA and oligonucleotide sequences

The fluorescently labeled DNA oligonucleotides and corresponding PNA sequences are shown in Figure 6.2. DNA oligonucleotides with the same sequence as PNA 20 and 21 were also synthesized (oligo20 and 21) as controls.

5´ CGTTTTCTCTTCCTGC---F 3´	**Pyrimidine strand oligo**
3´GCAAAAGAGAAGGACG---M 5´	**Purine strand oligo**
N-TTTTCTCTTCCT	**PNA 20**
N-TCCTTCTCTTTT	**PNA 21**
5´TTTTCTCTTCCT	**Oligonucleotide 20**
5´TCCTTCTCTTTT	**Oligonucleotide 21**

FIGURE 6.2 Sequences of the PNAs and oligonucleotide used in this chapter. (A) fluorescently labeled oligonucleotides used for generating the DNA duplex. (B) PNA sequences 20 and 21 and (C) Oligos 20 and 21. The flourophore (F) is fluorescein while the quencher (Q) is methyl red.

6.1.3 Reaction conditions

The formation of different types PNA/DNA complexes will be critically dependent on the ionic conditions. In particular, low pHs are usually required for the formation of C^+·GC triplets, and are necessary for triplex formation. In addition, strand invasion is favoured by conditions of low ionic strength and is less likely at high salt concentrations, due to the stronger interaction between the two duplex strands. The experiments described in this chapter therefore used four different

conditions as described below. Conditions 1 and 2 should promote triplex formation as they are at low pH, whereas conditions 1 and 3 should promote strand invasion as they are at low ionic strength.

Condition 1: 5 mM sodium acetate pH 5.0

Condition 2: 50 mM sodium acetate pH 5.0, containing 150 mM NaCl

Condition 3: 5 mM sodium phosphate pH 7.5

Condition 4: 50 mM sodium phosphate pH 7.5, containing 150 mM NaCl

6.2 Duplex melting alone

Figure 6.3 shows melting curves for the fluorescently labelled duplexes alone, under the four conditions outlined above. Each of the duplexes produces a clear sharp transition and the melting temperatures are summarised in Table 6.1. It can be seen that, as expected, the duplex is much less stable in low salt conditions. In addition there is a small dependence on pH, with higher T_ms at pH 7.5 than at 5.0, though this may be partly due to the different buffers used (acetate and phosphate). There is little or no hysteresis between the melting and annealing profiles in the high salt conditions. However, considerable hysteresis was observed in low salt conditions, for both pHs, and the samples did had not completely annealed by the time the LightCyler had returned to 30 °C (not shown).

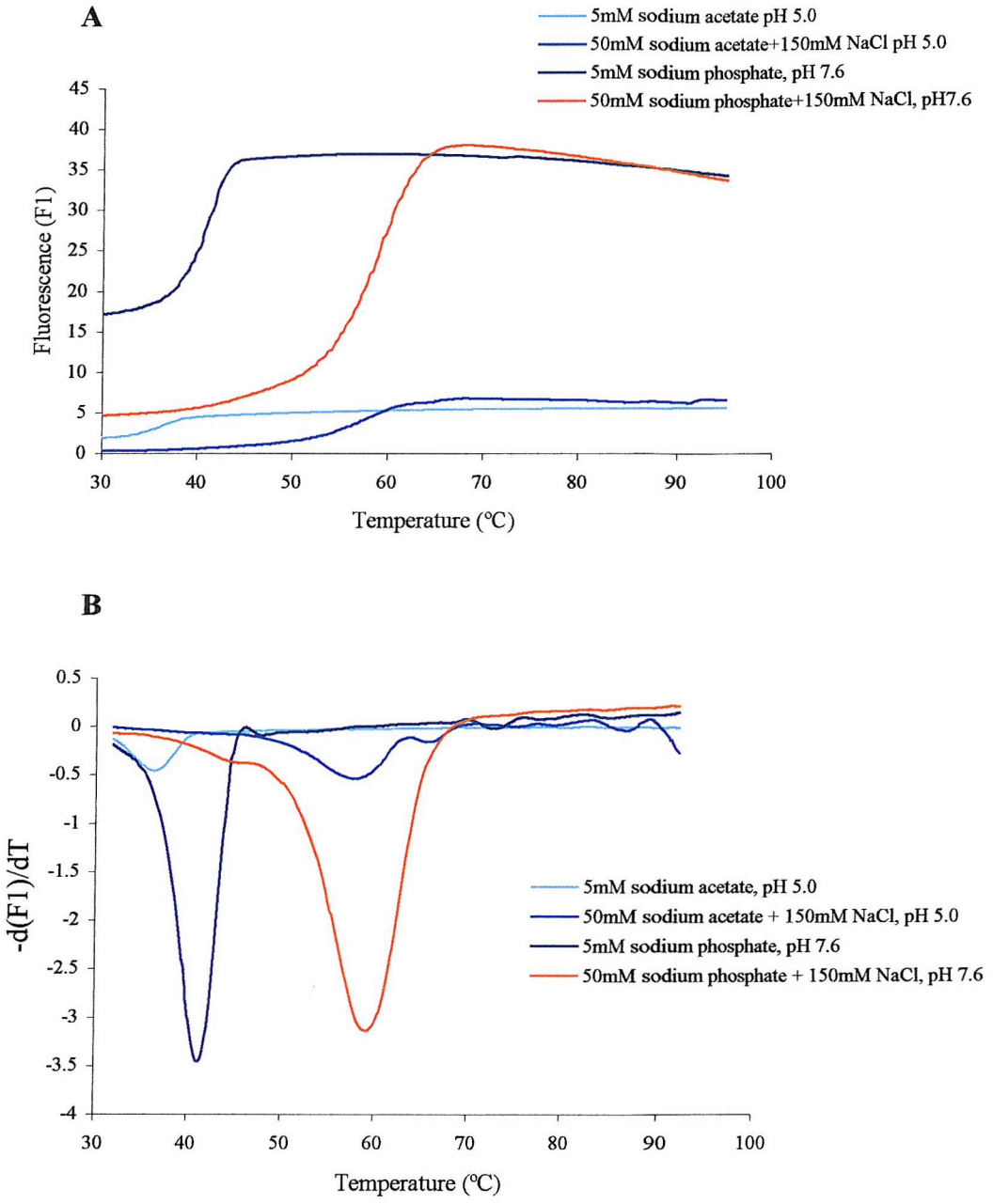

FIGURE 6.3 Fluorescence melting profiles for the DNA duplex alone under different conditions. A) Shows the plots of fluorescence against temperature, while B) shows the first derivative of the melting profile. The fluorescence is expressed in arbitrary units.

Conditions	Melting temperature (°C)
Low salt, low pH	36.9
High salt, low pH	58.4
Low salt, high pH	41.4
High salt, high pH	59.8

TABLE 6.1 Melting temperatures for the DNA duplexes under various conditions.

6.3 Interaction with PNA 21

Initial experiments were performed by mixing PNA 21 with the DNA duplex at concentrations expected to produce 1:1 and 2:1 complexes (*i.e.* by adding 0.25 and 0.5 μM PNA to the solution of 0.25 μM duplex). Surprisingly, these experiments (not shown) did not reveal any significant changes in either the melting or annealing profiles. We therefore examined the effects of higher PNA concentrations, similar to those used in the footprinting and bandshift experiments.

The melting profiles, showing the effects of 10 and 20 μM PNA 21 under condition 1, 3 and 4 (low pH low salt; high pH low salt, and high pH high salt) are shown in Figure 6.4. It can be seen that, in the presence of low salt concentrations, the PNA has caused a large increase in the initial fluorescence signal, which is now as high as that of the denatured species, and does not show a temperature dependent transition. This suggests that the PNA has prevented the two DNA strands from combining together, and is consistent with PNA strand invasion. This effect is seen in the first melt (when the PNA has simply been added to the duplex) suggesting that the PNA has displaced the DNA pyrimidine strand, without requiring prior melting of the

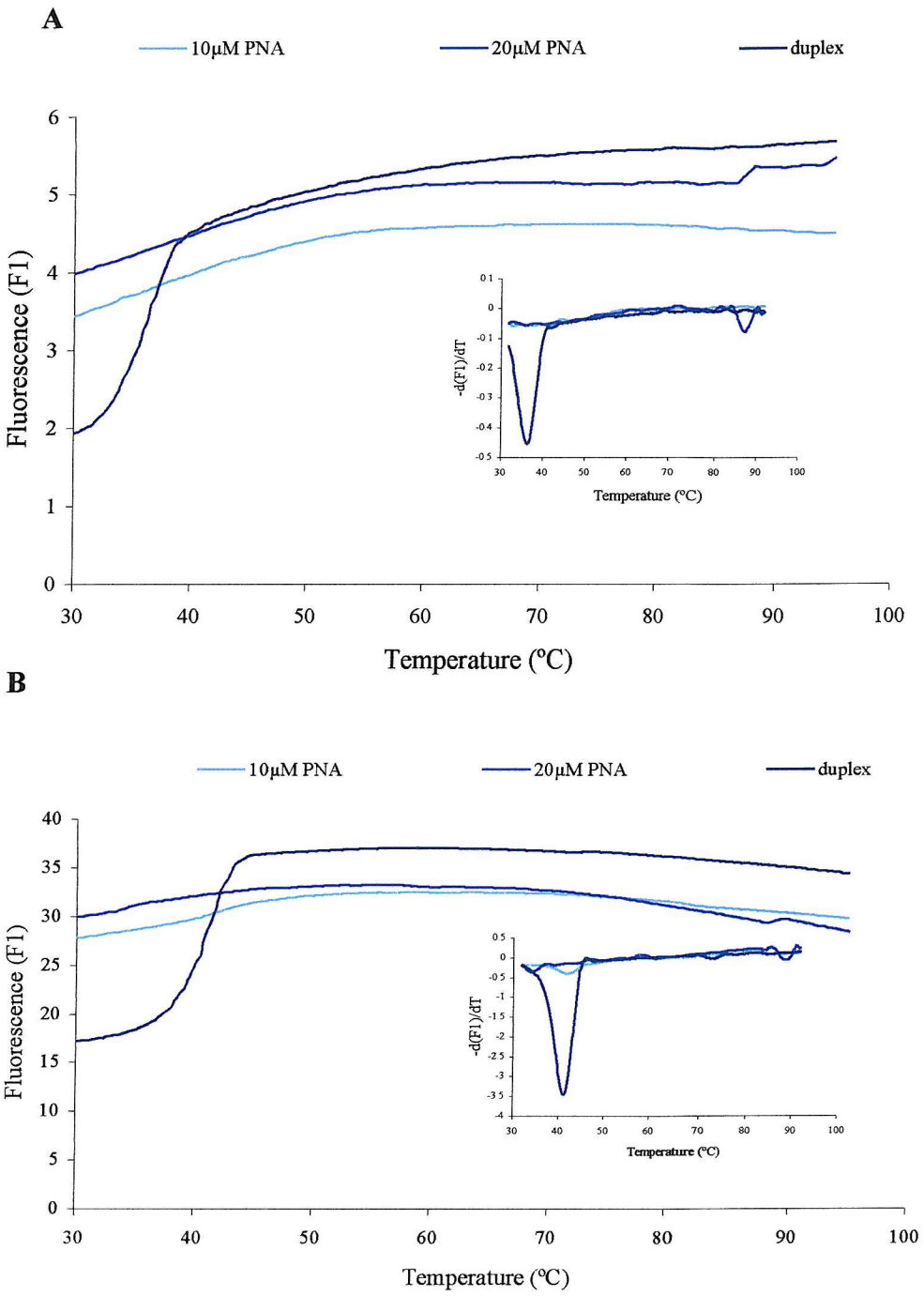

FIGURE 6.4 Fluorescence melting profiles for the DNA duplex in the presence of PNA21 (A) shows the plots of fluorescence against temperature and the inserted panel shows the first derivative of the corresponding melting profile both under conditions of 5mM sodium acetate, pH 5.0. (B) shows the same plots under conditions of 5mM sodium phosphate pH 7.6 and (C) under conditions of 50 mM sodium acetate, pH 7.6. The fluorescence is expressed in arbitrary units.

C

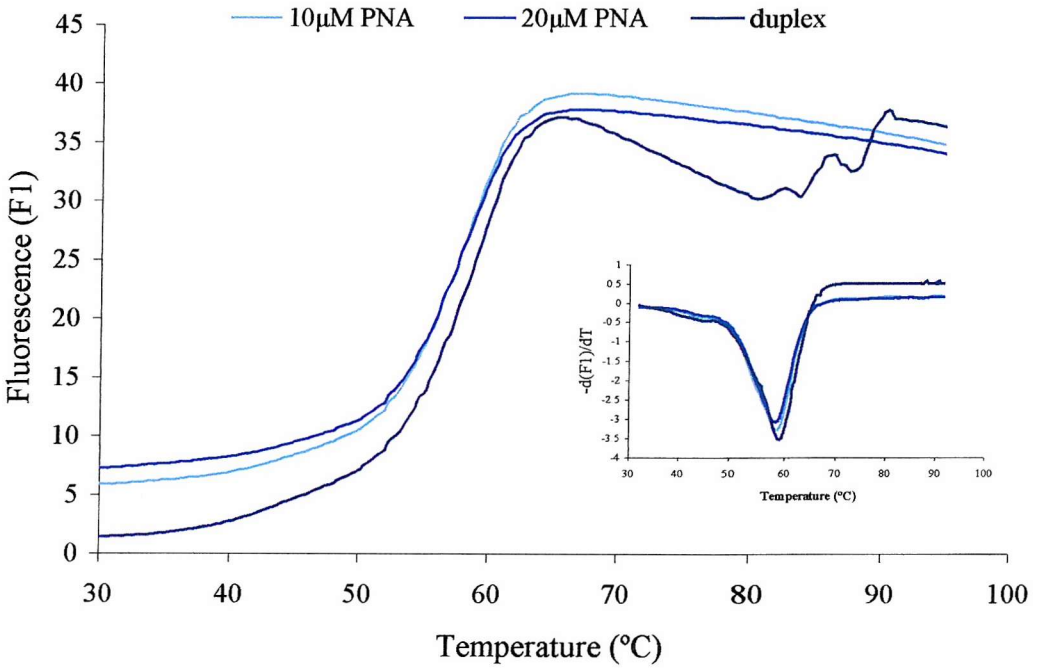
10μM PNA
20μM PNA
duplex
Fluorescence (F1)
Temperature (°C)
-d(F1)/dT
Temperature (°C)

duplex. In contrast, it can be seen that when these experiments are repeated at high pH and high salt (figure 6.4C) addition of PNA does not affect the melting profiles, even at concentrations as high as 20 μM.

Figure 6.5 shows the effects of different concentrations of PNA 21 on the fluorescence melting profiles, measured under condition 2 (low salt, high ionic strength). In these profiles it can be seen that the PNA has a clear effect on the melting transitions. The left hand panels show the first melting curves obtained after mixing the PNA and DNA, and so may not be properly at equilibrium. It can be seen that there is a steady increase in the initial fluorescence signal, consistent with some strand invasion. However the remaining transition moves to higher temperatures, suggesting that the duplex has been stabilized by PNA binding as a third strand. The central panels show the annealing curves for the same samples. In contrast to the melting profiles, these curves all display the same T_m values, though there is again an increase in the fluorescence signal at low temperatures. The difference between the annealing and melting curves suggests that the profiles are not in thermodynamic equilibrium and that there must be at least one slow step in the binding reaction. When these samples are melted for the second time, after 5 minutes equilibration, (right hand panels), the profiles are more similar to those obtained in the first melt. These again show an increase in T_m with increasing PNA concentrations, which would be consistent with the formation of a triplex between duplex DNA and PNA. The T_m values calcuated from these transitions are summarised in Table 6.2. The clear difference between the melting and annealing curves suggests that addition of PNA as a third strand is a slow process, which occurs after annealing of the two DNA strands.

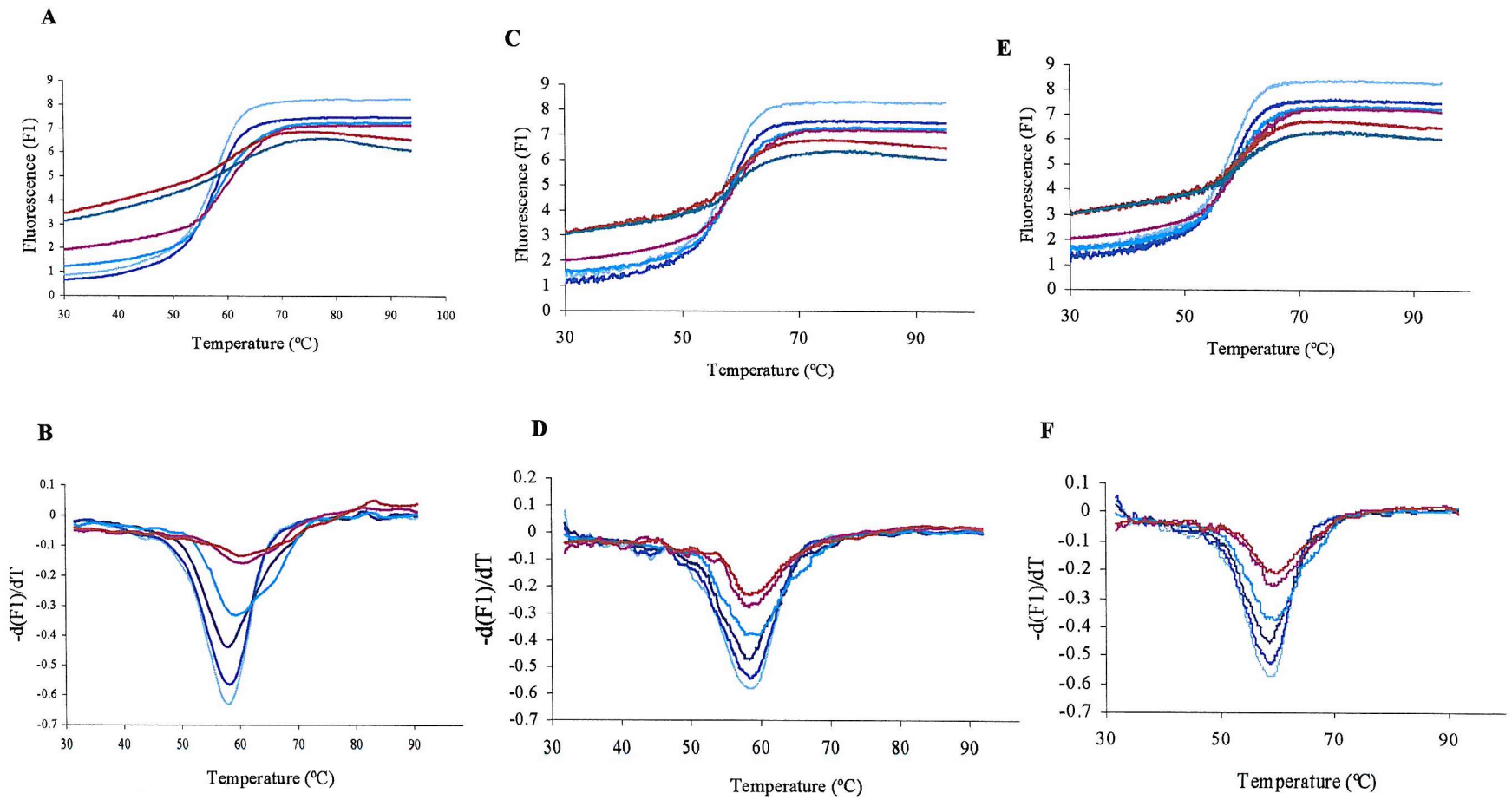

FIGURE 6.5 Fluorescence melting profiles for the DNA duplex in the presence of PNA21 determined in 50mM sodium acetate pH 5.0 containing 150 mM NaCl. (A) the first melting curves of fluorescence against temperature and (B) shows the first derivative of the corresponding melting profile, (C) annealing curves of fluorescence against temperature and (D) shows the first derivative of the corresponding annealing profile, (E) the second melting curves of fluorescence against temperature and (F) shows the derivative of the corresponding melting profile. The fluorescence is expressed in arbitrary units.

PNA (μM)	T_{m1}	T_{m2}	T_{m3}
0	57.9	59.1	59.3
0.25	58.2	59.0	59.3
1	57.9	58.8	59.3
2	59.4	58.9	59.8
5	60.6	58.8	63.2
10	60.6	59.0	62.2

TABLE 6.2 T_m values for the melting of the fluorescently labelled DNA duplex in the presence of different concentrations of PNA 21. T_{m1} corresponds to the first melting curve. T_{m2} corresponds to annealing of these samples, while T_{m3} is the second melting curve.

6.4 Interaction with PNA 20

Figure 6.6 show the melting profiles for the interaction of 10 and 20 μM PNA 20 under conditions 1, 3 and 4 (low pH low salt; high pH low salt, and high pH high salt). These results are very similar to those with PNA 21 (Figure 6.4). It can be seen that the duplex is disrupted at low ionic strength, indicative of strand invasion, and there is no interaction at high pH and high ionic strength.

Figure 6.7 show the results of experiments performed with PNA 20 under consitions of low pH and high salt (condition 2). Again there is a steady increase in the initial fluorescence signal with increasing PNA concentrations, which is consistent with some strand displacement, separating the two labelled DNA strands. However, in contrast to the results with PNA21, there is no increase in the apparent T_m values

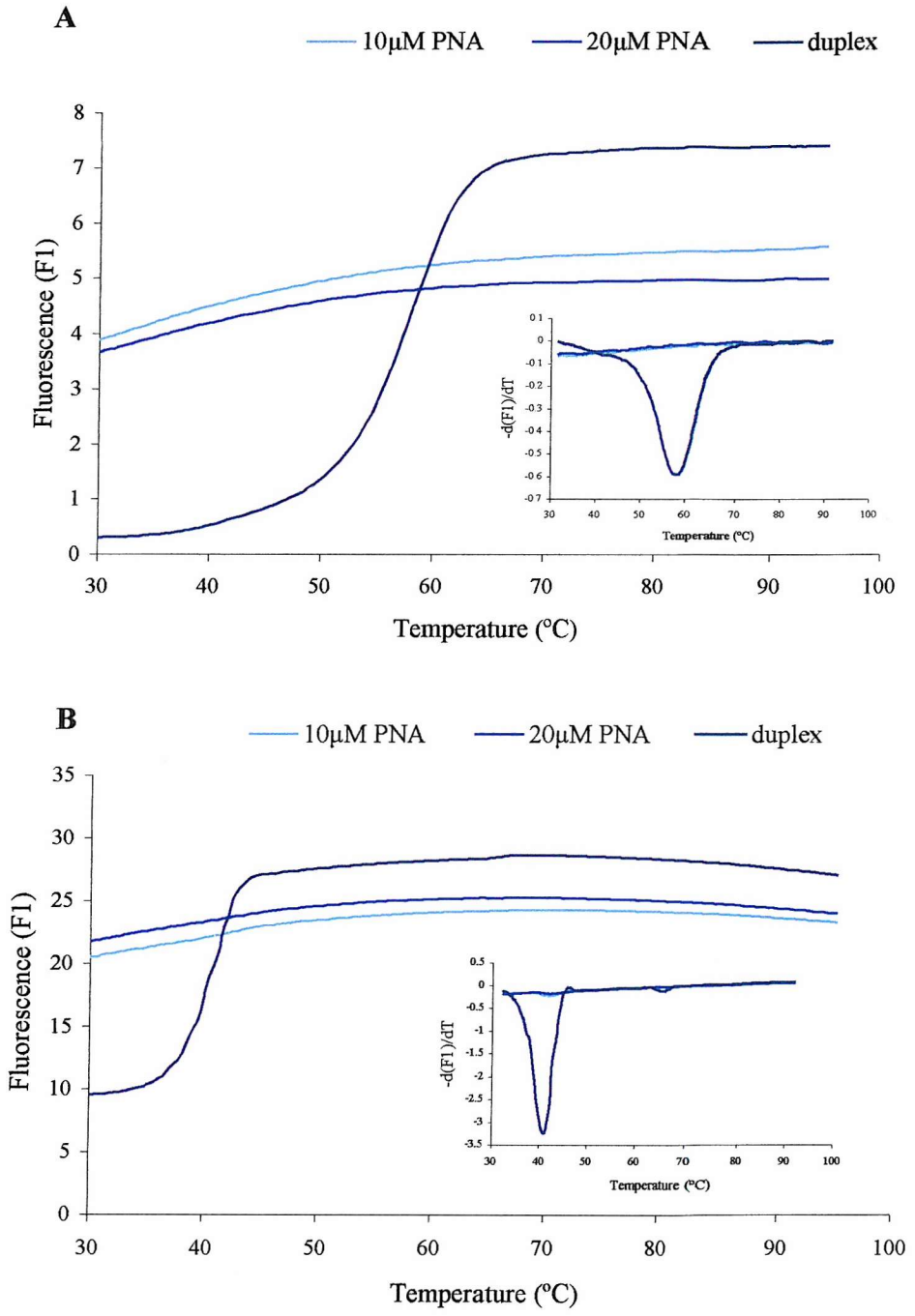

FIGURE 6.6 Fluorescence melting profiles for the DNA duplex in the presence of PNA20 (A) shows the plots of fluorescence against temperature and the inserted panel shows the first derivative of the corresponding melting profile both under conditions of 5mM sodium acetate, pH 5.0. (B) shows the same plots under conditions of 5mM sodium phosphate pH 7.6 and (C) under conditions of 50 mM sodium acetate, pH 7.6. The fluorescence is expressed in arbitrary units.

C

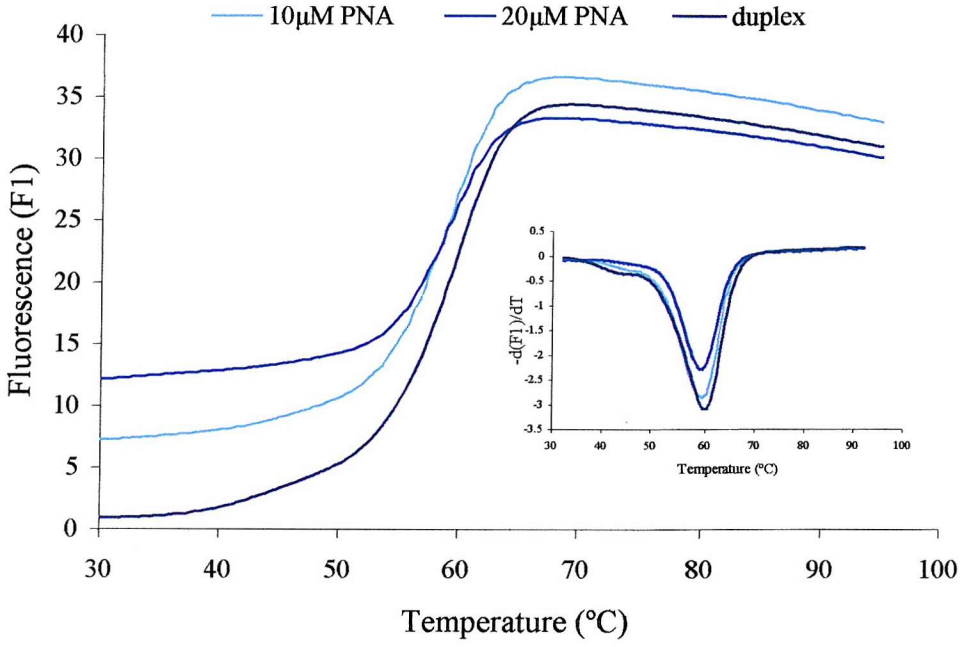
10μM PNA
20μM PNA
duplex
Fluorescence (F1)
Temperature (°C)
-d(F1)/dT
Temperature (°C)

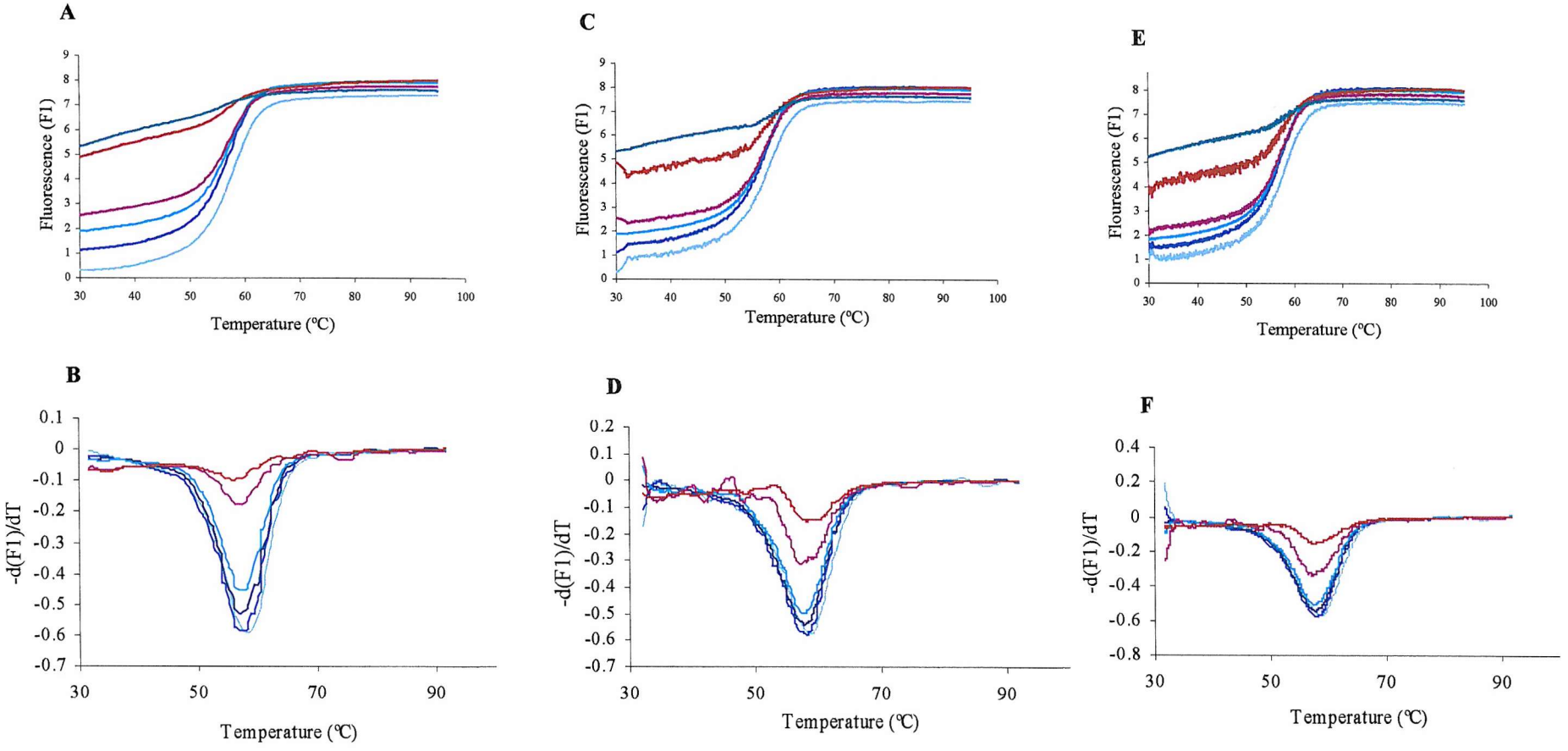

FIGURE 6.7 Fluorescence melting profiles for the DNA duplex in the presence of PNA20 determined in 50mM sodium acetate pH 5.0 containing 150 mM NaCl. (A) the first melting curves of fluorescence against temperature and (B) shows the first derivative of the corresponding melting profile, (C) annealing curves of fluorescence against temperature and (D) shows the first derivative of the corresponding annealing profile, (E) the second melting curves of fluorescence against temperature and (F) shows the derivative of the corresponding melting profile. The fluorescence is expressed in arbitrary units.

for the remaining transition, indeed there appears to be a small decrease in T_m. The melting temperatures for these transitions are summarized in Table 6.3.

6.5 Interaction with PNA 37 and 38

PNA 37 (TTCTCT) is a 6-mer sequence which is can be found within both PNA20 and PNA 21, while PNA 38 is a 7-mer (TCTCTTT) which is contained within PNA21. The effects of these shorter PNAs were examined to test their ability to undergo strand invasion or triplex formation. DNA fluorescence melting profiles with these PNAs are shown in Figure 6.8 and 6.9. It can be seen that at low salt, both these PNAs are able to form strand invasion complexes, as seen from the large increase in fluorescence at low temperatures. Higher concentrations of PNA 37 are required to produce these changes (especially at pH 7.5), as might be expected from its shorter length. In contrast these PNAs do not affect the melting profiles obtained at higher ionic strengths.

PNA (μM)	T_{m1}	T_{m2}	T_{m3}
0	58.2	58.7	58.8
0.25	57.3	58.2	58.3
1	57.4	58.2	58.3
2	57.4	58.0	58.0
5	57.2	58.5	57.8
10	56.5	59.8	56.8

TABLE 6.3 T_m values for the melting of the fluorescently labelled DNA duplex in the presence of different concentrations of PNA 20. T_{m1} corresponds to the first melting curve. T_{m2} corresponds to annealing of these samples, while T_{m3} is the second melting curve.

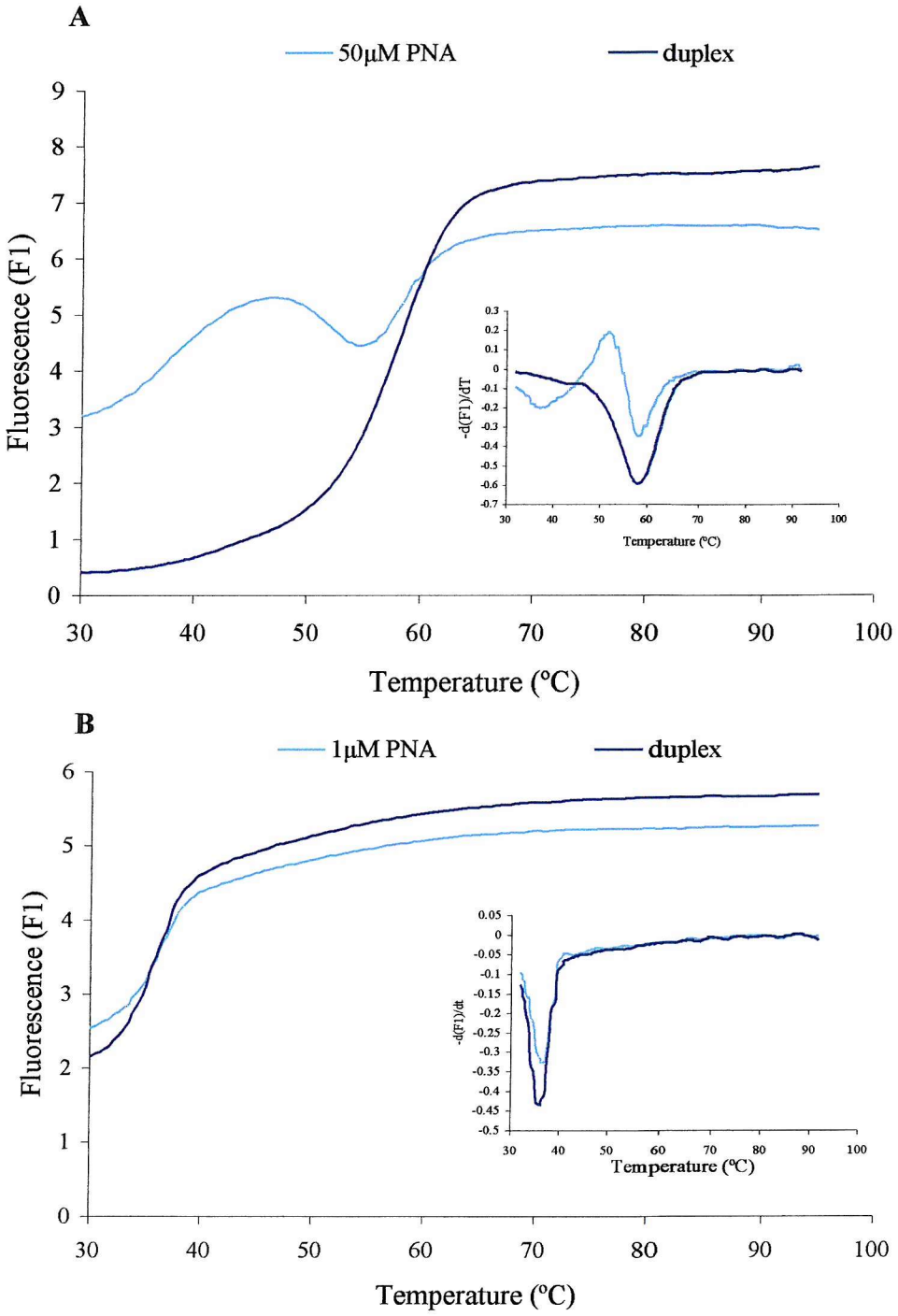

FIGURE 6.8 Fluorescence melting profiles for the DNA duplex in the presence of PNA37 (A) shows the plots of fluorescence against temperature and the inserted panel shows the first derivative of the corresponding melting profile both under conditions of 50mM sodium acetate, pH 5.0. (B) shows the same plots under conditions of 5mM sodium acetate pH 5.0 and (C) under conditions of 50 mM sodium phosphate , pH 7.6 and (D) under conditions of 5mM sodium phosphate , pH 7.6. The fluorescence is expressed in arbitrary units.

C

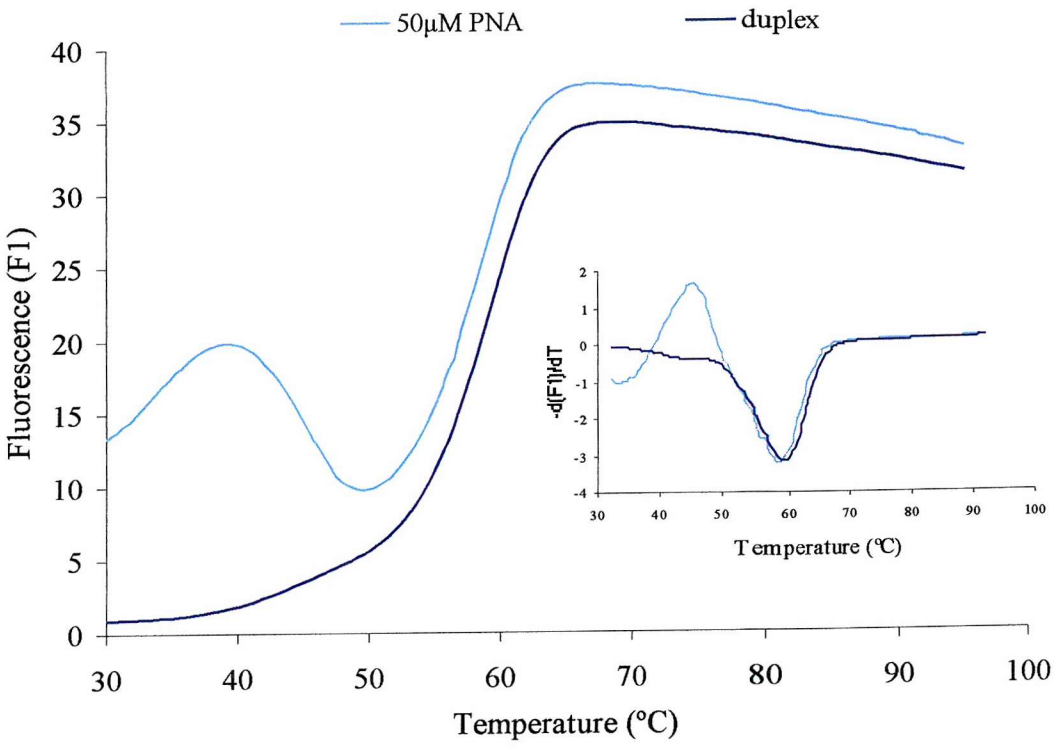
50μM PNA
duplex
Fluorescence (F1)
Temperature (°C)
-d(F1)/dT
Temperature (°C)

D

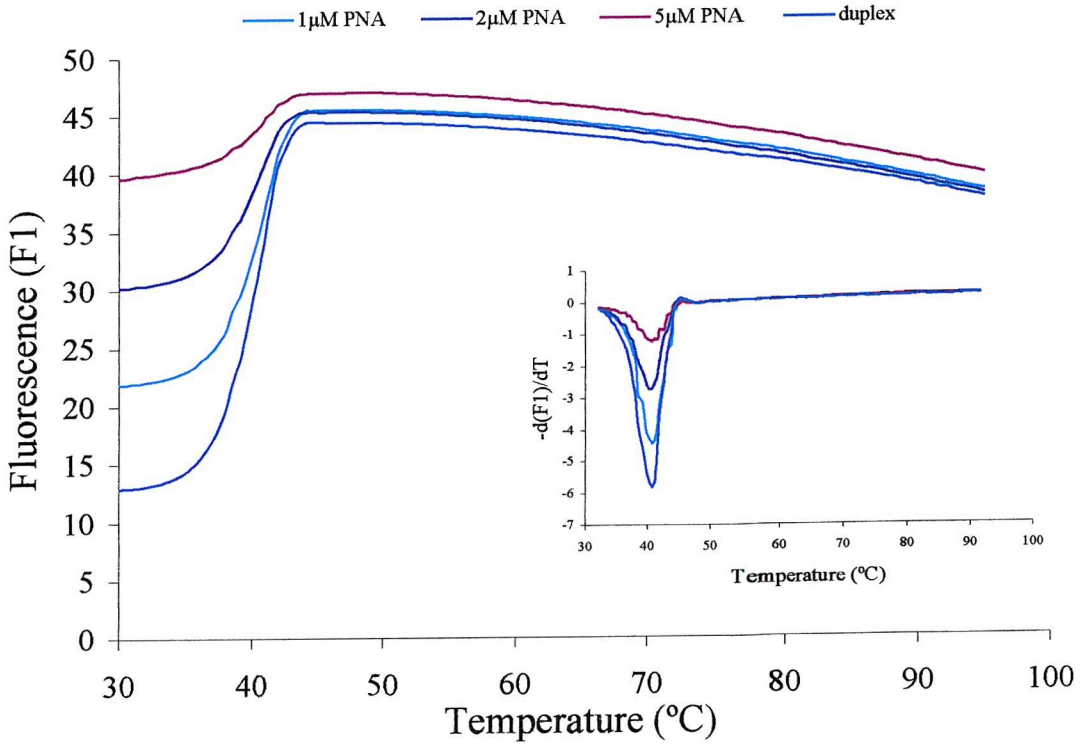
1μM PNA
2μM PNA
5μM PNA
duplex
Fluorescence (F1)
Temperature (°C)
-d(F1)/dT
Temperature (°C)

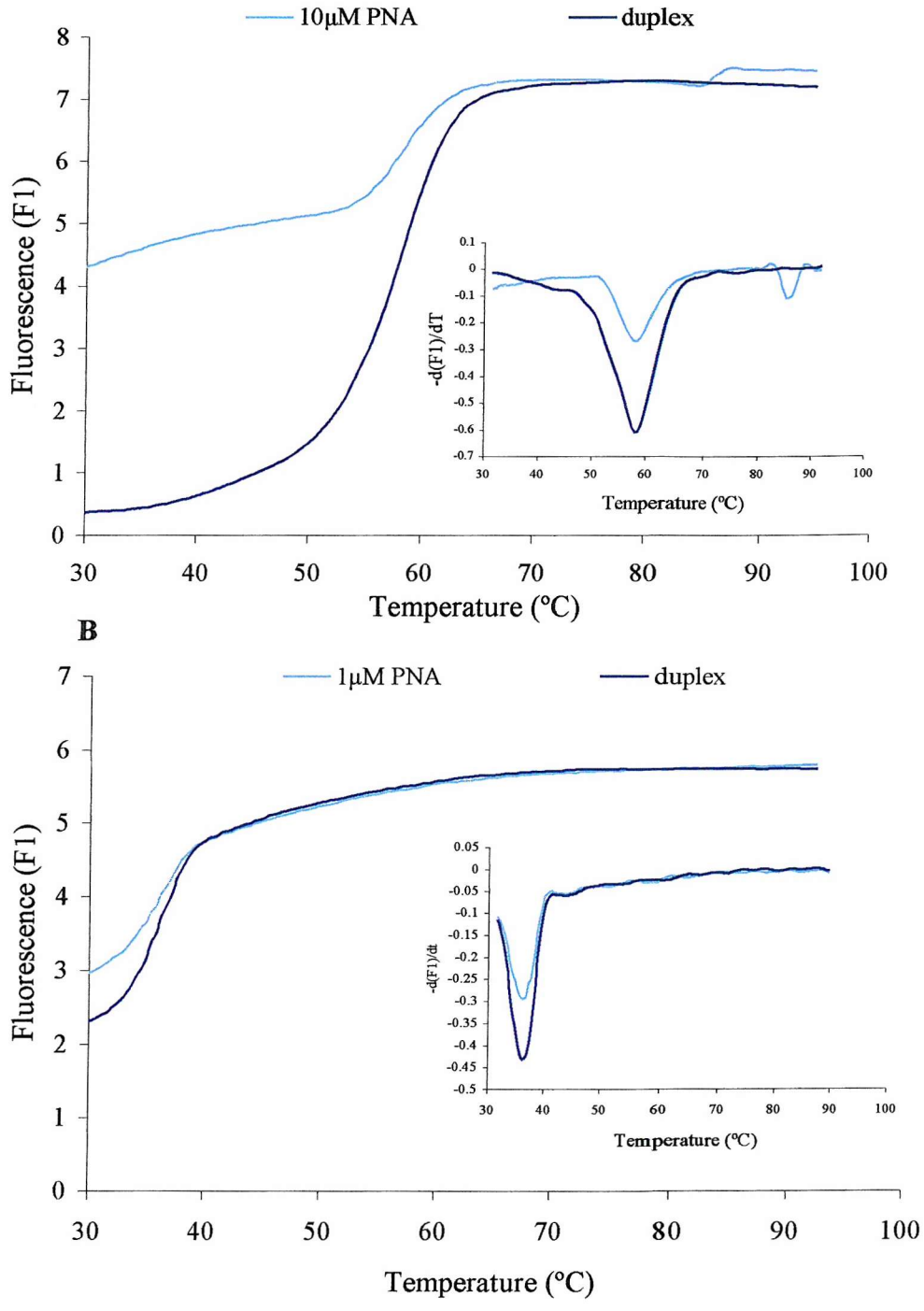

FIGURE 6.9 Fluorescence melting profiles for the DNA duplex in the presence of PNA38 (A) shows the plots of fluorescence against temperature and the inserted panel shows the first derivative of the corresponding melting profile both under conditions of 50mM sodium acetate, pH 5.0. (B) shows the same plots under conditions of 5mM sodium acetate pH 5.0 and (C) under conditions of 50 mM sodium phosphate , pH 7.6 and (D) under conditions of 5mM sodium phosphate , pH 7.6. The fluorescence is expressed in arbitrary units.

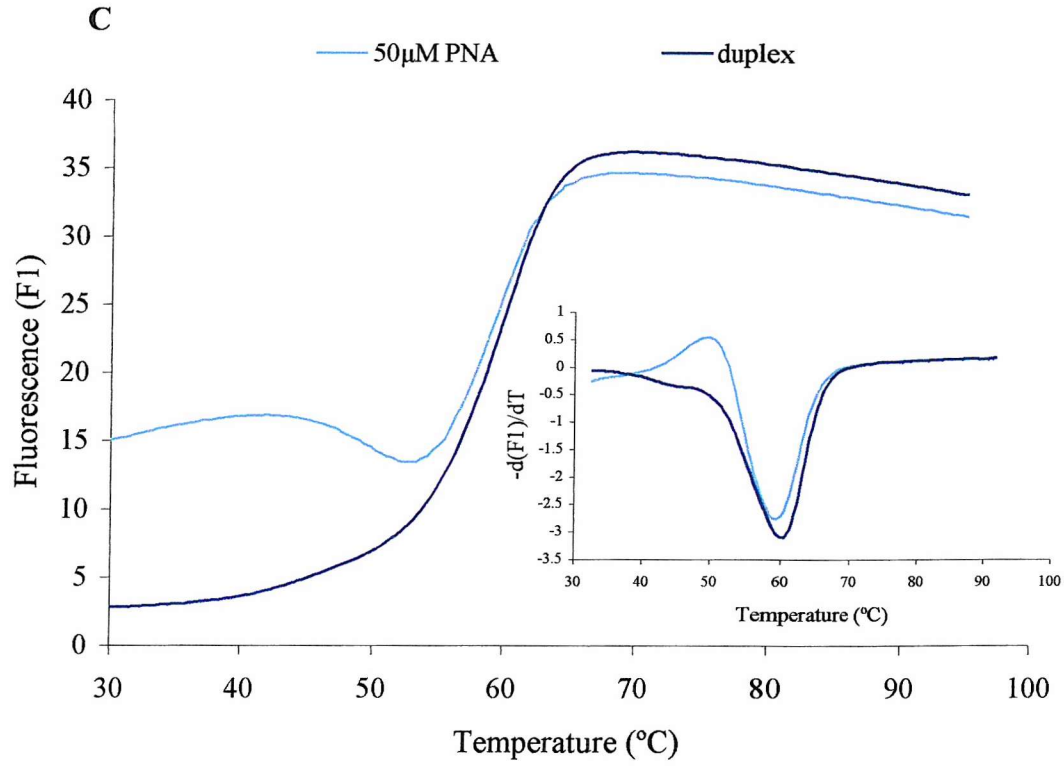
C
50μM PNA
duplex
Fluorescence (F1)
Temperature (°C)
-d(F1)/dT
Temperature (°C)

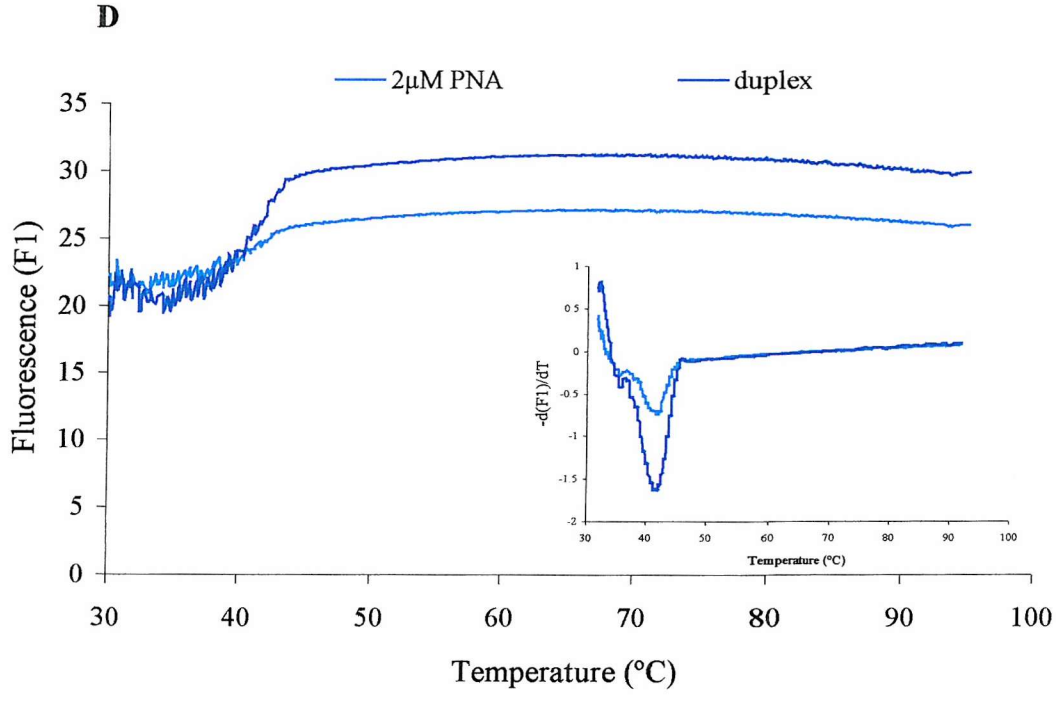
D
2μM PNA
duplex
Fluorescence (F1)
Temperature (°C)
-d(F1)/dT
Temperature (°C)

6.6 Interaction with both PNA 20 and 21 together

PNA 20 and 21 have the same sequences, but with opposite polarities. When used in combination these should therefore be able to form a PNA_2/DNA triplex in which the two pyrimidine-containing PNA strands run in opposite orientations. Figures 6.10 show melting curves when these two PNAs were used in combination under different conditions. It can be seen that, as expected, there is clear evidence for strand displacement in the conditions of low ionic strength. However, in contrast to the results with either PNA alone, this also occurs at high ionic strength, in conditions of both high and low pH. It therefore appears that using these PNAs in combination facilitates the formation of strand invaion complexes, which are formed at much lower concentrations.

6.7 Interaction with oligonucleotides 20 and 21

Oligonucleotides 20 and 21 have the same sequences as PNA 20 and 21 respectively. These DNA oligonucleotides were used as since, unlike PNA, they should not be able to undergo strand invasion. Figures 6.11 and 6.12 show the effects of these two oligonucleotides on the fluorescence melting profiles, in conditions of low pH. The T_m values determined from these profiles are summarised in Table 6.4. It can be seen that, at high ionic strengths, these oligonucleotides have no effect on any of the melting and annealing profiles (not shown) and do not strand invade the duplex. Although oligonucleotide 21 should be able to form a triple helix with this target, we presume that this will have a lower stability than the 16- mer duplex,

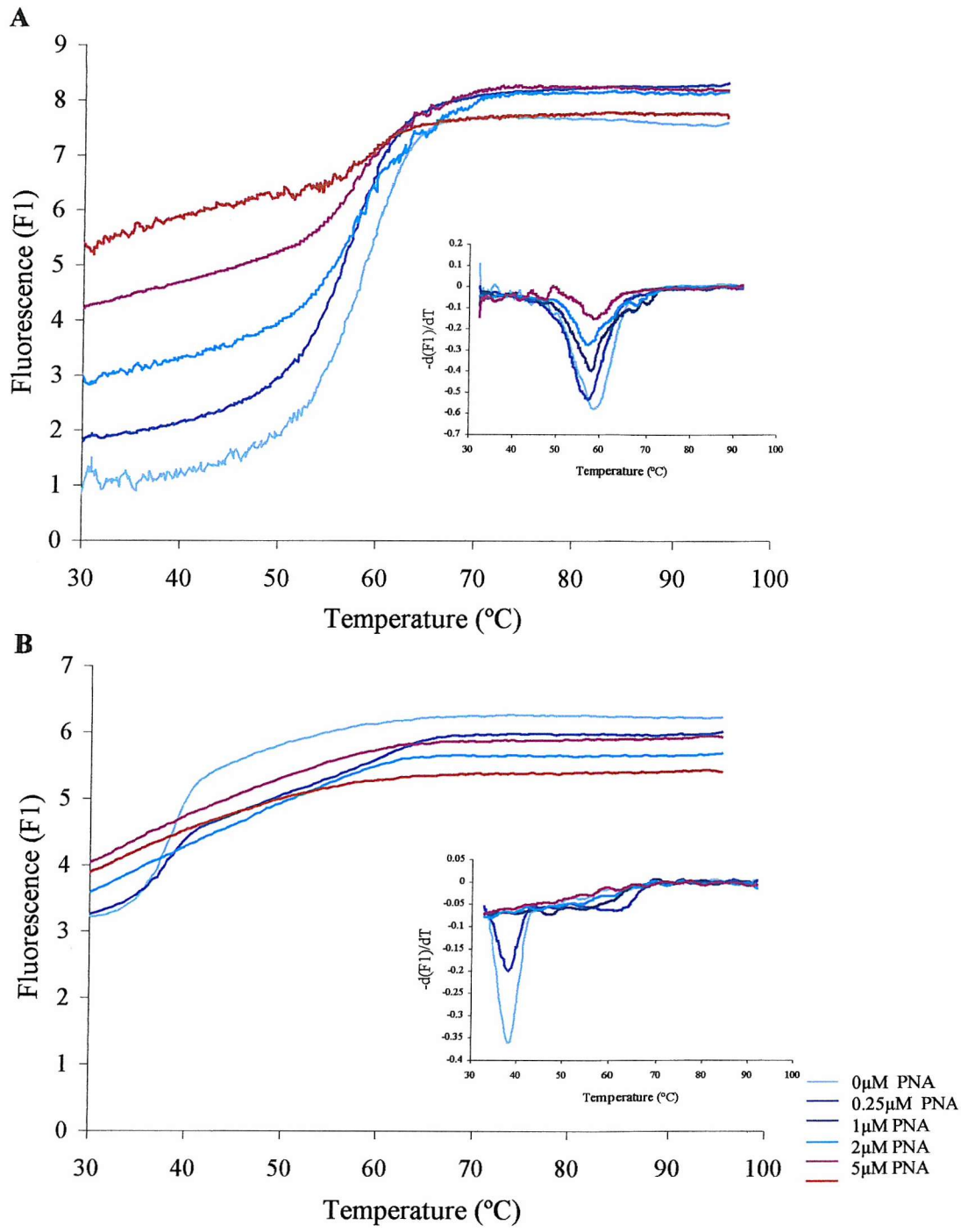

FIGURE 6.10 Fluorescence melting profiles for the DNA duplex in the presence of PNA 20 and 21 added together under different conditions. (A) Melting profile under 50mM sodium acetate, pH 5.0, (B) melting profile under 5mM sodium acetate, pH 5.0, (C) melting profile under 50mM sodium phosphate, pH 7.5 and (D) melting profile under 5mM sodium phosphate, pH 7.5. Inserted panels show the first derivative of the corresponding profile. The fluorescence is expressed in arbitrary units.

C

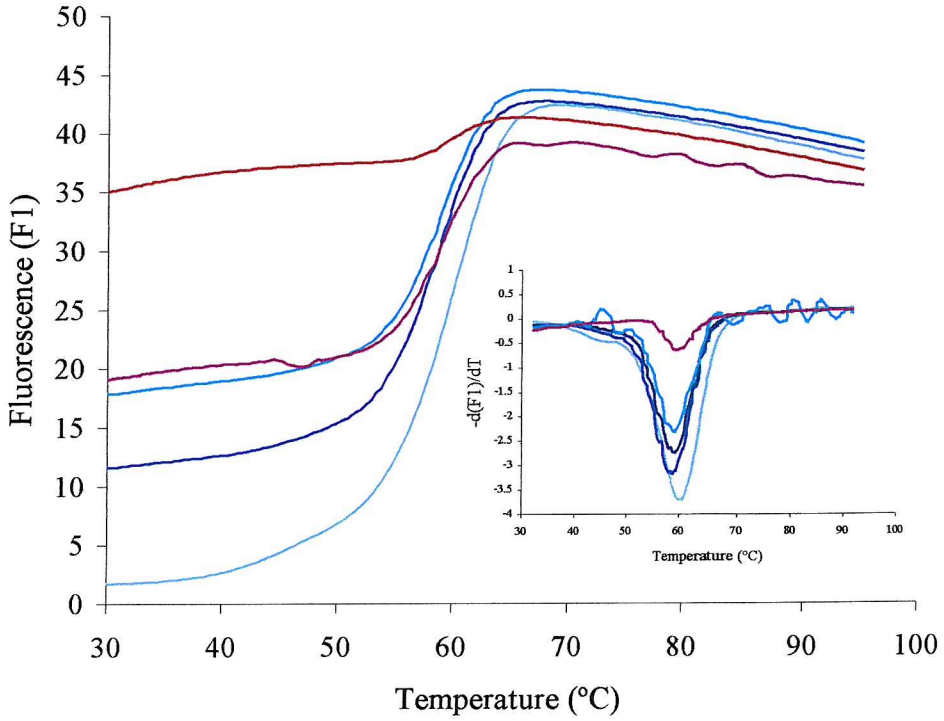
Fluorescence (F1)
Temperature (°C)
-d(F1)/dT
Temperature (°C)

D

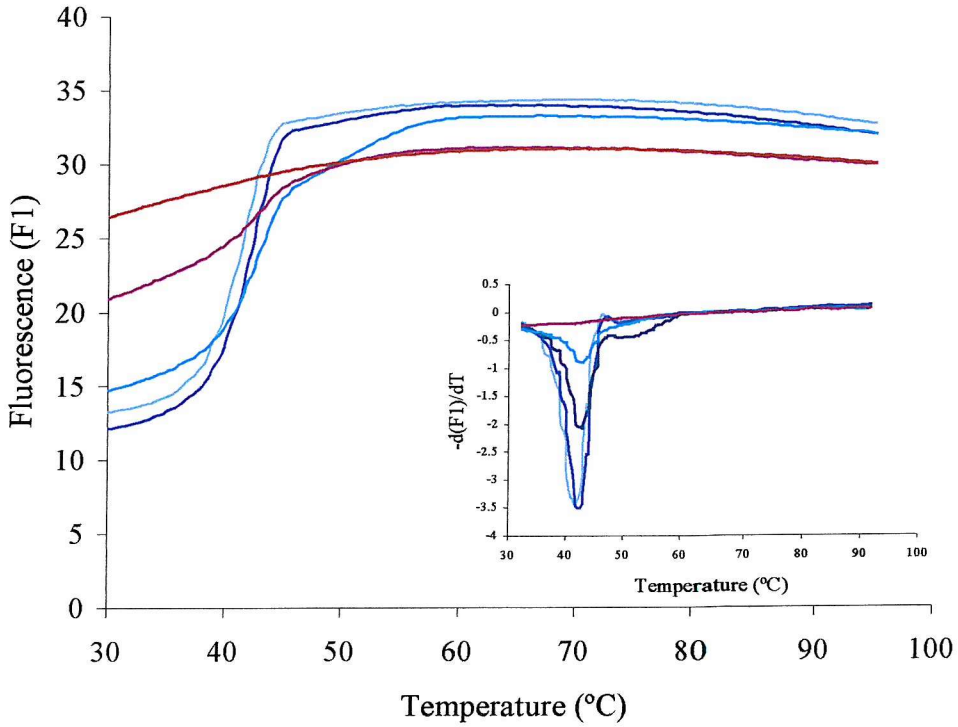
Fluorescence (F1)
Temperature (°C)
-d(F1)/dT
Temperature (°C)

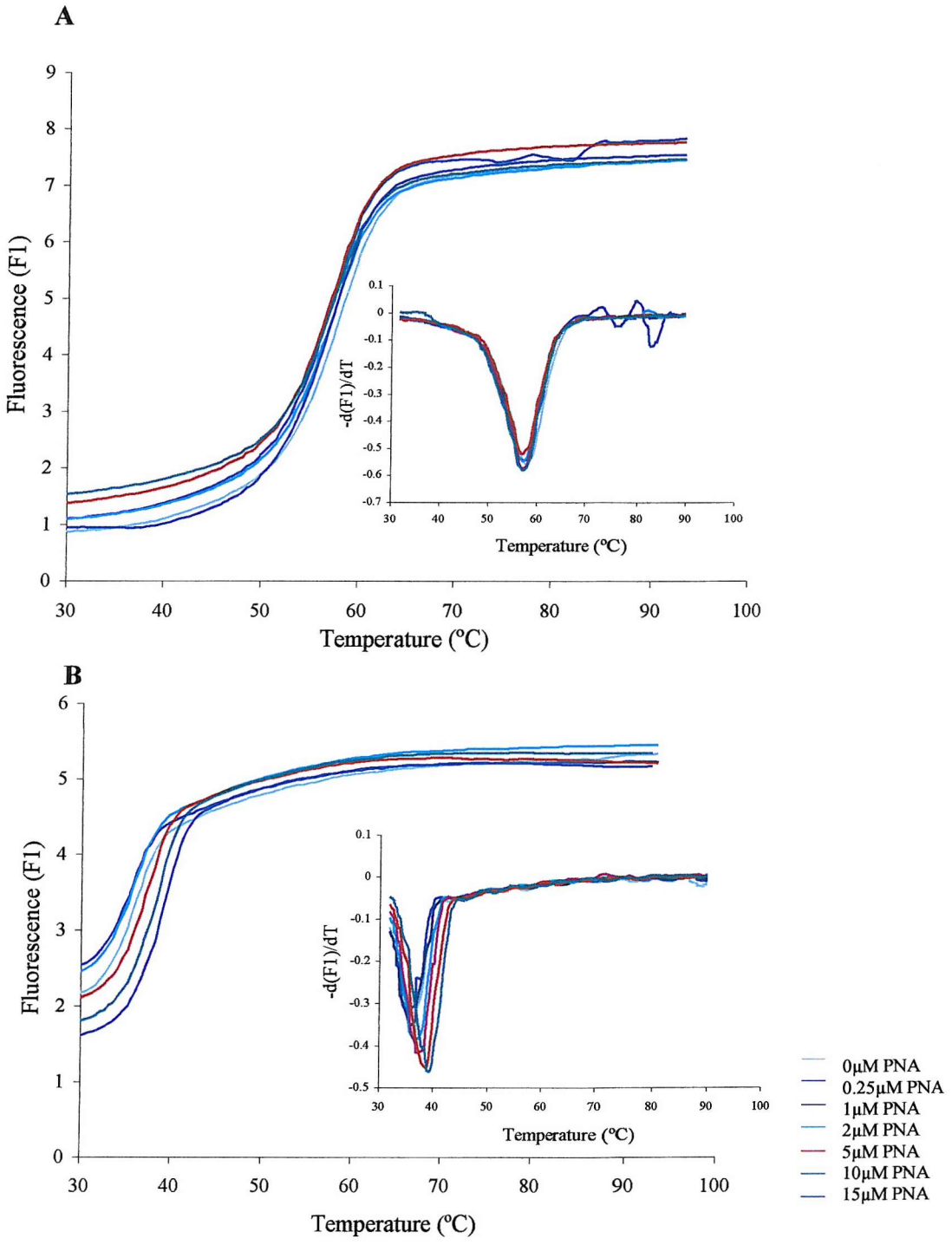

FIGURE 6.11 Fluorescence melting profiles for the DNA duplex in the presence of Oligonucleotide 20 under different conditions. (A) Melting profile under 50mM sodium acetate, pH 5.0, (B) melting profile under 5mM sodium acetate, pH 5.0. Inserted panels show the first derivative of the corresponding melting profile. The fluorescence is expressed in arbitrary units.

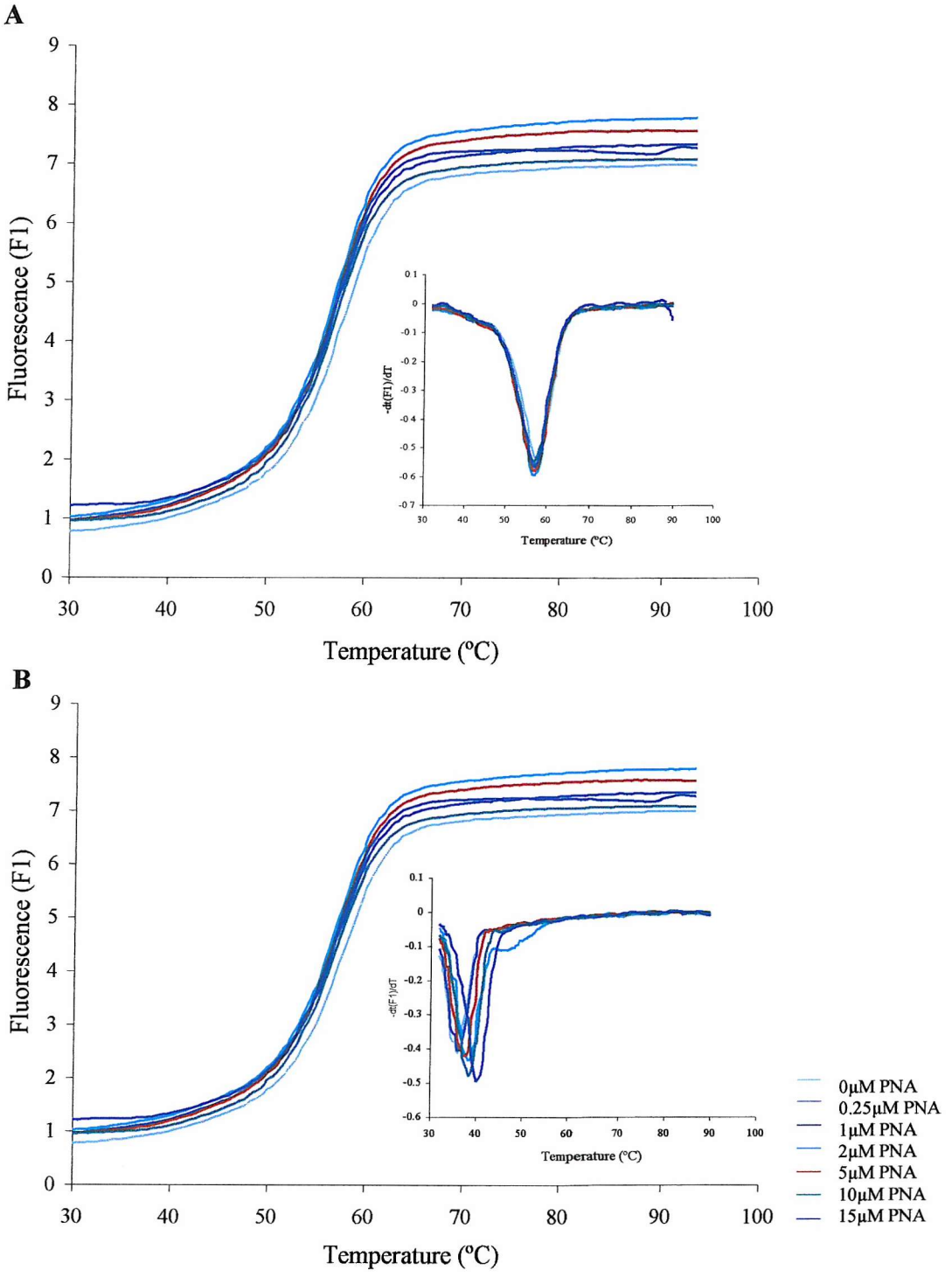

FIGURE 6.12 Fluorescence melting profiles for the DNA duplex in the presence of Oligonucleotide 21 under different conditions. (A) Melting profile under 50mM sodium acetate, pH 5.0, (B) melting profile under 5mM sodium acetate, pH 5.0. Inserted panels show the first derivative of the corresponding melting profile. The fluorescence is expressed in arbitrary units.

A

PNA (μM)	T_{m1}	T_{m2}	T_{m3}
0	57.9	58.3	58.5
0.25	57.2	58.3	58.0
1	57.3	58.0	58.0
2	57.2	57.8	57.7
5	57.2	58.0	58.0
10	57.3	57.9	58.2
15	57.4	57.7	58.0

B

PNA (μM)	T_{m1}	T_{m2}	T_{m3}
0	36.6	36.33	37.6
0.25	35.9	36.73	37.2
1	36.3	38.84	37.6
2	37.1	37.64	38.8
5	37.6	37.64	38.8
10	38.6	38.94	39.9
15	39.5	40.85	40.8

C

PNA (μM)	T_{m1}	T_{m2}	T_{m3}
0	58.0	58.3	58.6
0.25	57.2	58.1	58.2
1	57.3	57.9	58.1
2	57.1	57.7	57.7
5	57.3	57.9	58.1
10	57.2	57.9	58.2
15	57.3	57.7	58.0

D

PNA (μM)	T_{m1}	T_{m2}	T_{m3}
0	36.6	36.73	37.5
0.25	35.9	35.93	37.2
1	36.4	36.43	37.6
2	37.1	37.13	38.7
5	37.6	37.64	38.8
10	38.7	38.74	38.34
15	39.6	39.64	39.14

TABLE 6.4 T_m values for the melting of the fluorescently labelled DNA duplex in the presence of different concentrations of oligo 20 (A and B) and oligo 21(C and D). 50mM sodium acetate, pH 5.0 is the conditions in panels A and C and 5mM sodum acetate, pH 5.0 in panels B and D. T_{m1} corresponds to the first melting curve. T_{m2} corresponds to annealing of these samples, while T_{m3} is the second melting curve.

and so will melt from it at lower temperatures, and so will not affect the duplex-single strand transition. Surprisingly we find that both oligonucleotides increase the melting temperatures at low ionic strengths. This may not be surprising for oligo 21, as it could form a Hoogsteen bonded triplex with this target, though its efects should only be apparent if the triplex is more stable than the duplex under these conditions. The results for oligo 20 at low ionic strength are surprising, since this oligonucleotide has the wrong orientation to form a stable triplex. This effect will considered further in the Discussion below.

6.8 Discussion

These melting studies have identified that the PNAs studied in this thesis generate strand invasion complexes, as expected, at low ionic strengths. PNA 21 appears to form a PNA.DNA_2 triplex, which is consistent with the orientation of the third strand lying parallel. PNA 20 lies antiparallel so consequently does not show that same interaction. In many instances strand invasion does not occur even after melting and annealing the duplex in the presence of an excess of the third strand. At first sight this is surprising, but on reflection this must be because the target is 16 bases long, while the invading PNA is only 12. In theory you can't distinguish between strand invasion and strand invasion plus triplex. However, the previous point suggests that something other than just strand invasion is required to drive the formation of the complex. Triplex formation (without strand invasion) will only lead to an increase in the T_m if the triplex is more stable than the duplex.

Both PNA 20 and 21 in combination shows the formation of a PNA_2/DNA complex with strand displacement in conditions of low and high ionic strength, which

is not seen with each PNA individually and occurs at lower concentrations. The shortest PNA sequences 37 and 38 both form strand invasion complexes however greater concentrations are required the shorter the sequence is. As for oligonucleotides 20 and 21, no displacement of the duplex occured, which showed that strand invasion, is a result of PNA invasion. Triplex formation is present increasing the melting temperature due to forming a more stable complex. Oligonucleotide 20 has the wrong orientation to form a stable triplex however melting profiles shows that the PNA has bound as a third strand, shifting the melting temperature. A clear explanation for this is difficult and it must have bound as an antiparallel strand.

These melting studies have facilitated the DNaseI and bandshift experiments shown in chapter 3 into the more detailed understanding of the complexes and conditions required for PNA to interaction with free DNA.

Chapter 7

Discussion

7.1 Discussion

The results presented in this thesis clearly show that polypyrimidine PNAs interact with homopurine tracts within double strand DNA in a sequence-specific fashion, under specific conditions. In conditions of low pH (5.0), where C^+·GC triplet formation is promoted, PNA appears to strand invade the DNA helix forming a PNA_2/DNA triplex. This is not observed at high pH conditions. Triplex strand invasion complexes have been previously documented as the most stable complexes formed (Wittung *et al* 1996). However, the work presented in this thesis suggests that the formation of this complex is very sequence dependent. At low PNA concentrations a PNA.DNA_2 triplex is formed which only proceeds to form the triplex strand invasion complex at high PNA concentrations.

PNA binding affinity is influenced by a number of factors which include PNA length, base sequence and composition (primarily the cytosine content) and pH and the formation of these complexes requires long incubation times (greater that 24 hours). However, the affinity does not appear to depend on PNA strand polarity and is very similar for related PNAs with opposite orientations. DNase I footprinting studies show changes in the cleavage pattern at much lower concentrations than those required to produce changes in S1 nuclease cleavage or to affect the mobility in bandshift experiments. We know that each PNA forms strand invasion complexes from the increased cleavage by S1 nuclease. However similar PNAs often have very different effects on DNA mobility. In general antiparallel PNAs have a greater effect on the mobility than related parallel PNA sequences. These differences cannot be due to the molecular weight of the complexes, since these are the same (assuming the same stoichiometry), but could be due to local differences in the DNA conformation.

DNA bending or kinking in the PNA complex would reduce the mobility, as too would formation of the P-loop, and we might propose that antiparallel complexes produce a greater distortion than parallel ones. This effect is not thought to reflect the number of PNA molecules bound (1 or 2, in duplex or triplex strand invasion respectively) as both complexes produce DNase I footprints at low concentrations and only induce S1 nuclease cleavage at much higher concentrations. One other explanation might be that, for the parallel complexes, one of the PNA strands is only weakly bound and dissociates in the gel.

The results with free DNA should help understand the interaction with nucleosome-bound DNA more clearly. It is clear that the interaction of PNA with histone-bound DNA is influenced by the location of the PNA target site and the method of preparing the reconstituted DNA. Protein-bound DNA can inhibit the binding of PNA, while prior formation of a PNA-DNA complex can prevent nucleosome assembly.

Although there have been no previous reports on the interaction of PNA with histone-bound DNA, there have been a number of studies on the interaction of sequence specific small molecules with nucleosomal DNA. Echinomycin and distamycin seem to affect the rotational positioning of nucleosomal DNA. From work with the *tyr*T and other natural DNA fragments it was proposed that their interaction with outward facing sites caused the DNA to rotate by 180° on the protein surface. (Low *et al* 1986; Portugal & Waring 1987). However other studies with synthetic DNA fragments containing inward-facing ligand binding sites in well-defined locations also showed that Hoechst 33258 could cause DNA to rotate on the protein surface (Brown & Fox 1996). The rotational position of nucleosomal DNA is less likely to be an important factor for these studies with PNA, as each PNA molecules

will cover more than one turn of the DNA helix, and so interact with both inward and outward facing regions. On the basis of this previous research, we decided to study the interaction of PNA with sites located at different positions along the DNA fragments, in different locations with respect to the nucleosome dyad.

These experiments have shown that PNA can bind to some target sites, but this depends on their translational positioning along the protein. Targeting the regions 10-20 bases away from the dyad was unsuccessful with the two 110 base pair fragments from *tyr*T(43-59) and *tyr*T(22-33). The regions near the nucleosome dyad axis have a helical repeat of 10.7 base pairs, whereas the more peripheral flanking regions have a helical repeat of 10.0 base pairs. These compact DNA regions at the dyad appear to restrict PNA from binding. On increasing the DNA fragment length the target sites can be positioned further away from the nucleosome dyad and we observe the first footprints for the interaction of PNA with histone-bound DNA.

This can be seen by mapping site 1 onto a three-dimensional structure of the nucleosome core particle, as shown in Figure 7.1; a similar structure for site 2 is shown in Figure 7.2. These represent the positions of sites 1 and 2 on the 160 base pair fragment, in which the PNA target sites are located further away from the dyad axis than for the 110 base pair fragments.

The results presented in Chapter 4 show that both these sites can be successfully targeted with PNA, though higher concentrations are required at site 1 compared to site 2, presumably because site 2 is further way from the centre of the nucleosome. Moving these PNA target sites further away from the dyad, towards the peripheral regions of the nucleosome, resulted in PNA targeting at lower concentrations. However, without formal molecular modeling it is difficult to locate

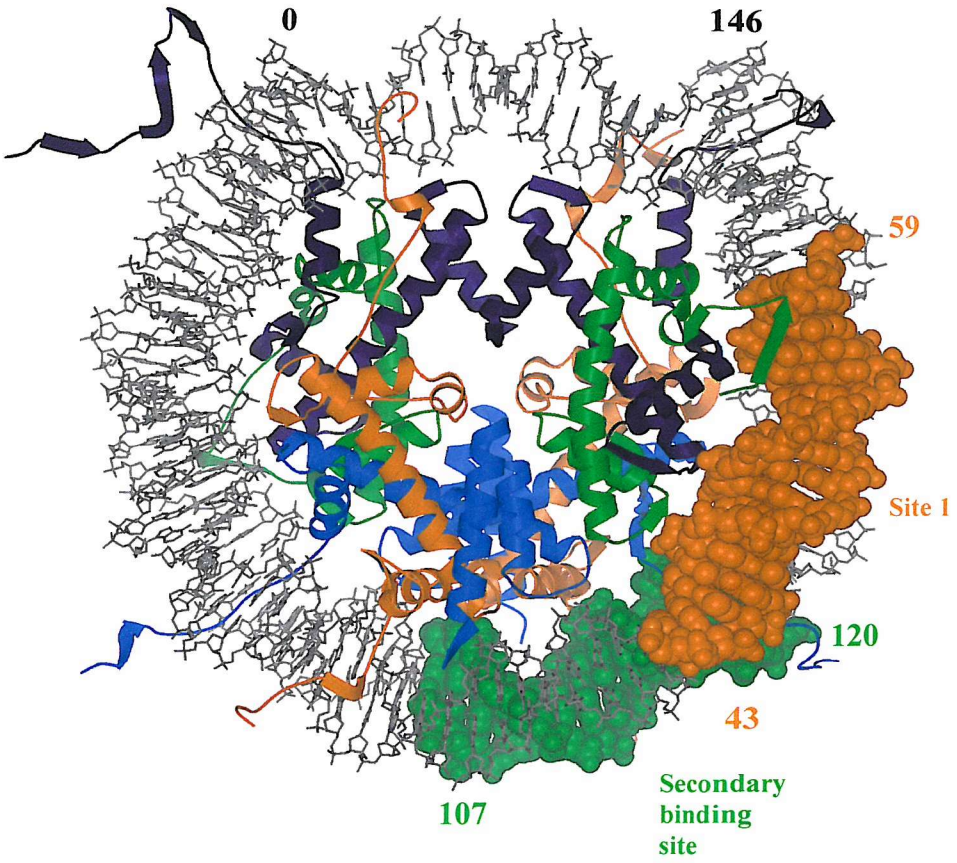

FIGURE 7.1 Three-dimensional structure of the nucleosome core particle. Generated from the atomic coordinates 1eqz (protein data bank) prepared using Molscript, GL Render and Raster3D. A theoretical position for site 1 and the secondary binding site has been incorporated within the DNA sequence. The secondary structure of the core particle is represented as arrows (β-strands), ribbons (α-helices) and cords (loops) and the DNA presented by stick models. H2A is orange, H2B is blue, H3 is purple and H4 is green.

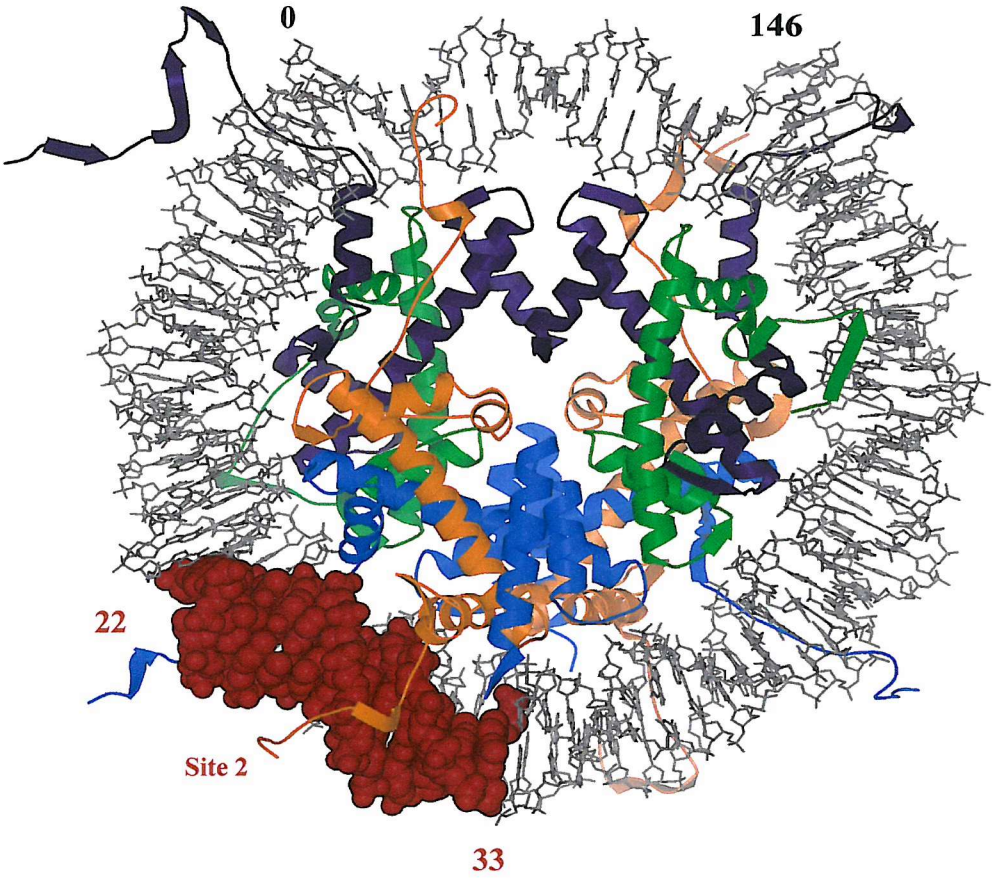

FIGURE 7.2 Three-dimensional structure of the nucleosome core particle. Generated from the atomic coordinates 1eqz (protein data bank) prepared using Molscript, GL Render and Raster3D. A theoretical position for of site 2 has been incorporated within the DNA sequence. The secondary structure of the core particle is represented as arrows (β-strands), ribbons (α-helices) and cords (loops) and the DNA presented by stick models. H2A is orange, H2B is blue, H3 is purple and H4 is green.

the exact positions of sites 1 and 2 in relation to the nucleosome, especially with the shorter (110) and longer (190 and 360) fragments. Experiments with the 360 base pair fragment were performed with the expectation that the PNA target site might be located in the linker region between two nucleosomes within the chromatin fibre. Bandshift experiments with this fragment showed the presence of multiple bands, suggesting that the protein(s) had bound in different locations along the DNA fragment, and that a unique nucleosomal complex had not been formed. Footprints were observed with this reconstituted DNA, however at higher concentrations than expected which must some obstruction by the protein.

A similar pattern was seen for the fragments that contained both sites 1 and 3, again showing that the position of the target site affects the binding of PNA to nucleosomal DNA. A possible structure for the nucleosome containing both sites is shown in Figure 7.3; which is consistent with the observation that site 1 is bound at high PNA concentrations whereas site 3 is obstructed by the protein.

The unexpected secondary binding site, which was observed with free DNA, is not bound when any of these fragments were reconstituted into nucleosome core particles. This raises an important issue regarding the use of PNAs *in vivo,* since it appears that the only interactions will be with those sites which have high binding affinities and which form stable sequence specific complexes. Weakly bound complexes will be excluded from nucleosomal DNA. This increases the likelihood that only the intended sites will be bound by any particular PNA and that secondary binding to related polypurine tracts will be prevented by the chromatin structure.

It seems reasonable to assume that, before it can interact with histone-bound DNA, PNA will have to wait until the DNA (transiently) dissociates from the protein, becoming exposed to targeting. It has previously been shown that the

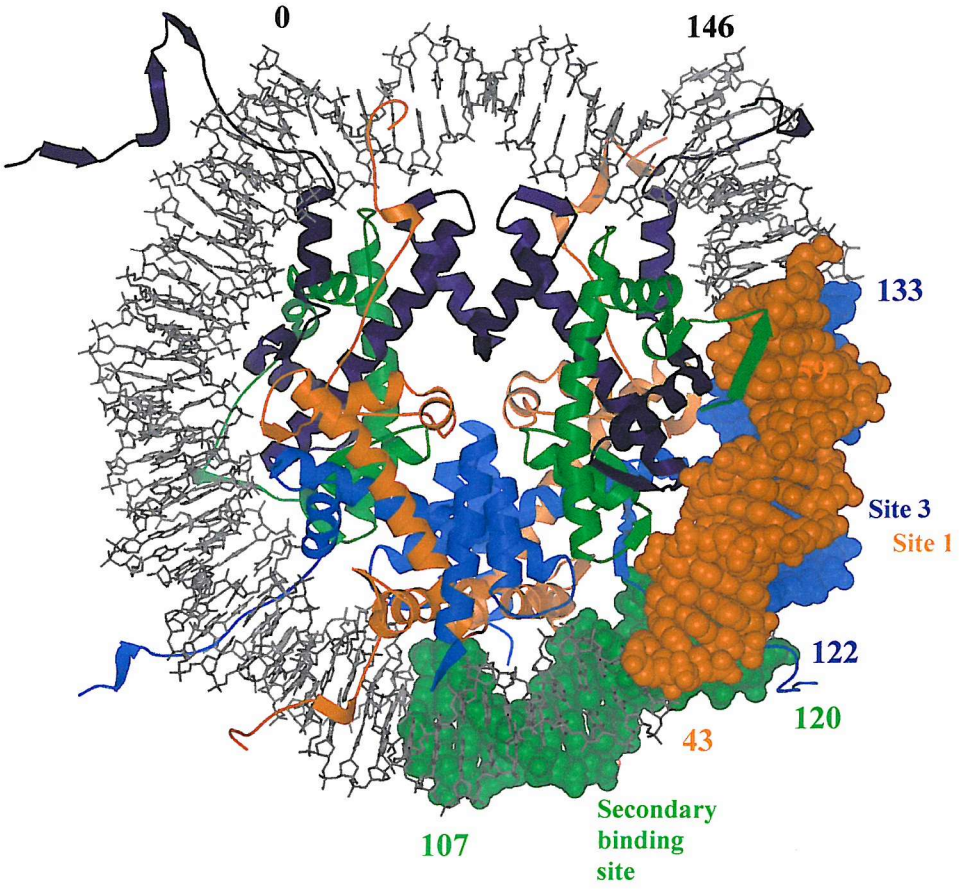

FIGURE 7.3 Three-dimensional structure of the nucleosome core particle. Generated from the atomic coordinates 1eqz (protein data bank) prepared using Molscript, GL Render and Raster3D. A theoretical position for sites 1, 3 and the secondary binding site has been incorporated within the DNA sequence. The secondary structure of the core particle is represented as arrows (β-strands), ribbons (α-helices) and cords (loops) and the DNA presented by stick models. H2A is orange, H2B is blue, H3 is purple and H4 is green.

peripheral regions of the nucleosome core particle are exposed more often than those closer to the dyad axis (Polach & Widom 1995). The PNA will presumably bind when these regions of DNA are exposed, though it is not clear whether this PNA/DNA complex will subsequently refold around the protein core.

As discussed in chapter 4, the inhibition of nucleosome reconstitution is dependent upon the translational position of the PNA target sites. The presence of a PNA/DNA complex close to the dyad axis appears to have a greater effect upon reconstitution than one which is situated closer towards the end of the DNA. For short DNA fragments, when a PNA/DNA complex is located about 10 bases from the dyad nucleosome reconstitution is abolished, as there is insufficient free DNA to bind to the protein surface. When this is moved a further 10 bases away this severely reduces reconstitution, but it is not completely abolished. When situated on the peripheral regions, the PNA/DNA complex is able to associate with the protein core, though it is not clear whether this region is actually incorporated within the nucleosome, or if it is hanging off the end. The histone octamer appears to be located further along the DNA fragment where sufficient PNA-free DNA is present, if not then nucleosome reconstitution is abolished. However, targeting both ends of the fragment prior to nucleosome reconstitution resulted in reduced integrity of the retarded nucleosomes, highlighting the importance for PNA target site positioning.

These interactions with PNA must cause large distortions in the DNA structure, due to the displaced P-loop and the rigid nature of the bulky PNA/DNA complex, which may extend into the surrounding regions. Clearly this complex cannot be easily incorporated within the nucleosome core particle and the protein will have to translationally shift to a more accessible region of the DNA. These results suggest that nucleosome reconstitution is not possible when there are less than 60-80

contiguous PNA-free base pairs, while region of 100 bases and longer are sufficient to obtain high levels of nucleosome reconstitution.

These results suggest that PNA may have a less dramatic effect on the structure of chromatin that is not being actively transcribed. Although the interaction with transcriptionally active chromatin, in which the DNA is more exposed, produces high affinity complexes, this may result in changes in nucleosome reconstitution and its positioning along the DNA. However, it is not clear whether these PNA-induced changes in translational positioning can occur in chromatin *in vivo* with very long DNA fragments, in contrast to the results presented in this thesis which have only concerned the interaction with isolated nucleosome core particles. The experiments with the fragments that have the potential to bind two nucleosomes, suggest that the PNA complexes have affected the reconstitution so that only one nucleosome is bound, but this needs more thorough investigation. The dimeric sequence would have been useful in this regard.

The results presented in chapter 4 highlighted some important issues concerning the interaction of PNA with histone-bound DNA, and showed that the intact protein severely limited the binding. The origin of this obstruction was explored in the experiments in which the N-terminal tails had been removed by trypsin digestion. These regions are known to affect the interaction with DNA (Widlund *et al* 2000). Chromatin structure plays a major role in processes such as transcription, and recent advances have revealed that its structure is highly dynamic and subject to reversible changes in higher-order folding and nucleosome positioning. These structural changes are largely mediated by covalent modification of the N-terminal amino acids in the tails of the core histones. These regions extend from the nucleosomal core through the DNA superhelix and can be modified by

acetyltransferases and deacetylases during the cell cycle. The acetylation patterns may direct histone assembly and regulate the packaging and activity of genes. Acetylation occurs on the lysine residues at the N-terminus of histone proteins, which removes the positive charges, thereby reducing the affinity between histones and DNA. This facilitates the access of transcription factors and RNA polymerase to promoter regions. Therefore, in most cases, histone acetylation enhances transcription, while histone deacetylation represses transcription. This process clearly affects the interaction between the histone octamer and DNA and we therefore removed these N-terminal tail domains by treatment with trypsin, to study their effects on PNA accessibility. The results showed that removal of the N-terminal tails altered the way in which PNA-DNA complexes interact with the histone octamers, and PNA-binding was observed in the regions surrounding the dyad axis, which had previously been inaccessible. It seems reasonable to suppose that N-terminal tail regions affect the tight interactions with the DNA in relation to the histone octamer and that loosening these interactions facilitates the interaction with PNA. The results also showed that the PNA/DNA complex formed near the centre of the short DNA fragment did not reduce reconstitution with these digested nucleosomes.

In summary, this work has shown that some PNA/DNA complexes cannot be incorporated within the nucleosome core particle and that the targeting is dependent on position of the PNA target site. The addition of PNA before nucleosome formation inhibits reconstitution and may change the nucleosome position as it binds to other PNA-free regions.

References

Aldrian-Herrada, G., Desarmenien, M. G., Orcel, H., Boissin-Agasse, L., Mery, J., Brugidou, J., Rabie, A. (1998) *Nucleic Acids Res.* **26**, 4910-4916.

Arents, G., Burlingame, R. W., Wang, B. C., Love, W. E., Moudrianakis, E. N. (1991) *Proc. Natl. Acad. Sci. U. S. A.* **88**, 10148-10152.

Arnott, S., Bond, P. J., Selsing, E., Smith, P. J. (1976) *Nucleic Acids Res.* **3**, 2459-2470.

Ausio, J., Dong, F., van Holde, K. E. (1989) *J. Mol. Biol.* **206**, 451-463.

Bednar, J., Horowitz, R. A., Grigoryev, S. A., Carruthers, L. M., Hansen, J. C., Koster, A. J., Woodcock, C. L. (1998) *Proc. Natl. Acad. Sci. U. S. A.* **95**, 14173-14178.

Bentin, T. & Nielsen, P. E. (1996) *Biochemistry* **35**, 8863-8869.

Berman, H. M., Westbrook, J., Feng, Z., Gilliland, G., Bhat, T. N., Weissig, H., Shindyalov, I. N., Bourne, P. E. (2000) *Nucleic Acids Res.* **28**, 235-242.

Bernardi, G., Ehrlich, S. D., Thiery, J. P. (1973) *Nat. New Biol.* **246**, 36-40.

Betts, L., Josey, J. A., Veal, J. M., Jordan, S. R. (1995) *Science* **270**, 1838-1841.

Blank, T. A. & Becker, P. B. (1996) *J Mol. Biol.* **260**, 1-8.

Bloomfield, V. A., Crothers, D. M., Tinoco, I. (2000) *Nucleic Acids: structures and properties and functions*. University Science Books.

Brown, P. M. & Fox, K. R. (1996) *J. Mol. Biol.* **262**, 671-685.

Brown, P. M., Madden, C. A., Fox, K. R. (1998) *Biochemistry* **37**, 16139-16151.

Brown, S. C., Thomson, S. A., Veal, J. M., Davis, D. G. (1994) *Science* **265**, 777-780.

Buchardt, O., Egholm, M., Berg, R. H., Nielsen, P. E. (1993) *Trends Biotechnol.* **11**, 384-386.

Chann, P. P. & Glazer, P. M. (1997) *J. Mol. Med.* **75**, 267-282.

Collomb, D. (2000) *Nucleic Acids*. Chemis Interactive Molecular Library (http://www.geneticengineering.org/chemis/Chemis-NucleicAcid/DNA.htm).

Costanzo, G. D., Mauro, E., Salino, G., Negri, R. (1990) *J. Mol. Biol.* **216**, 363-374.

Crooke, S. T. (1998) *Antisense Nucleic Acid Drug Dev.* **8**, vii-viii.

Datta, B. & Armitage, B. A. (2001) *J. Am. Chem. Soc.* **123**, 9612-9619.

Demeret, C., Vassetzky, Y., Mechali, M. (2001) *Oncogene* **20**, 3086.

Demidov, V. V., Potaman, V. N., Frank-Kamenetskii, M. D., Egholm, M., Buchard, O., Sonnichsen, S. H., Nielsen, P. E. (1994) *Biochem. Pharmacol.* **48**, 1310-1313.

Demidov, V. V., Yavnilovich, M. V., Belotserkovskii, B. P., Frank-Kamenetskii, M. D., Nielsen, P. E. (1995) *Proc. Natl. Acad. Sci. U. S. A.* **92**, 2637-2641.

Dervan, P. B. & Edelson, B. S. (2003) *Curr. Opin. Struct. Biol.* **13**, 284.

Dickerson, R. E. (1992) *Methods Enzymol.* **211**, 67-111.

Dickerson, R. E. & Ng, H. L. (2001) *Proc. Natl. Acad. Sci. U. S. A.* **98**, 6986-6988.

Doyle, D. F., Braasch, D. A., Simmons, C. G., Janowski, B. A., Corey, D. R. (2001) *Biochemistry* **40**, 53-64.

Drew, H. R. & Travers, A. A. (1985) *J. Mol. Biol.* **186**, 773-790.

Efimov, V. A., Choob, M. V., Buryakova, A. A., Kalinkina, A. L., Chakhmakhcheva, O. G. (1998) *Nucleic Acids Res.* **26**, 566-575.

Eriksson, M. & Nielsen, P. E. (1996) *Nat. Struct. Biol.* **3**, 410-413.

Esser, L. (2001) *Personal communication.*

Faria, M., Wood, C. D., White, M. R., Helene, C., Giovannangeli, C. (2001) *J. Mol. Biol.* **306**, 15-24.

Felsenfeld, G., Davies, D. R., Rich, A. (1957) *J. Am. Chem. Soc.* **79**, 2023-

FitzGerald, D. J. & Anderson, J. N. (1999) *J. Biol. Chem.* **274**, 27128.

Fox, K. R. (2003) *Personal communication.*

Fox, K. R. & Cons, B. M. (1993) *Biochemistry* **32**, 7162.

Fox, K. R. & Waring, M. J. (1987) *Biochim. Biophys. Acta* **909**, 145-155.

Frank-Kamenetskii, M. D. & Mirkin, S. M. (1995) *Annu. Rev. Biochem.* **64**, 65-95.

Galas, D. J. & Schmitz, A. (1978) *Nucleic Acids Res.* **5**, 3157-3170.

Giesen, U., Kleider, W., Berding, C., Geiger, A., Orum, H., Nielsen, P. E. (1998) *Nucleic Acids Res.* **26**, 5004-5006.

Good, L. & Nielsen, P. E. (1998) *Nat. Biotechnol.* **16**, 355-358.

Gottesfeld, J. M, Melander, C., Suto, R. K., Raviol, H., Liger, K., Dervan, P. B. (2001) *J. Mol. Biol.* **309**, 615-629.

Griffin, T. J., Tang, W., Smith, L. M. (1997) *Nat. Biotechnol.* **15**, 1368-1372.

Haaima, G., Lohse, A., Buchardt, O., Nielsen, P. E. (1996) *Angew. Chem. Int. Edit.* **35**, 1939-1942.

Hamiche, A., Kang, J,. Dennis, C., Wu,C. (2001) *Proc. Natl. Acad. Sci. U. S. A.* **98**, 14316-14321.

Hanahan, D. & Weinberg, R. A. (2000) *Cell* **100**, 57-70.

Hansen, G. I., Bentin, T., Larsen, H. J., Nielsen, P. E. (2001) *J. Mol. Biol.* **307**, 67-74.

Hansen, J. C., Tse, C., Wolffe, A. P. (1998) *Biochemistry* **37**, 17637-17641.

Hanvey, J. C., Peffer, N. J., Bisi, J. E., Thomson, S. A., Cadilla, R., Josey, J. A., Ricca, D. J., Hassman, C. F., Bonham, M. A., Au, K. G. (1992) *Science* **258**, 1481-1485.

Harp, J. M., Hanson, B. L., Timm, D. E., Bunick, G. J. (2000) *Acta Crystallogr.* ***D*56**, 1513-1534.

Hayes, J. J., Bashkin, J., Tullius, T. D., Wolffe, A. P. (1991) *Biochemistry* **30**, 8434-8440.

Helene, C. (1998) *Nature* **391**, 436-438.

Hunter, C. A. (1993) *J. Mol. Biol.* **230**, 1025-1054.

Hyrup, B., Egholm, M., Nielsen, P. E., Wittung, P., Buchardt O (1994) *J. Am. Chem. Soc.* **116**, 7964-7970.

Hyrup, B. & Nielsen, P. E. (1996) *Bioorg. Med. Chem.* **4**, 5-23.

Kraulis, P. J. (1991) *J. Appl. Cryst.* **24**, 946-950.

Jordan, S., Schwemler, C., Kosch, W., Kretschmer, A., Stropp, U., Schwenner, E., Mielke, B. (1997) *Bioorg. Med. Chem. Lett.* **7**, 687-690.

Krotz, A. H., Larsen, S., Buchardt, O., Eriksson, M., Nielsen, P. E. (1998) *Bioorg. Med. Chem.* **6**, 1983-1992.

Kushner, D. M. & Silverman, R. H. (2000) *Curr. Oncol. Rep.* **2**, 23-30.

Lagriffoule, P., Buchardt O, Wittung, P., Norden, B., Jensen, K. K., Nielsen, P. E. (1997) *Chem. Eur. J.* **3**, 912-919.

Lansdorp, P. M., Verwoerd, N. P., van de Rijke, F. M., Dragowska, V., Little, M. T., Dirks, R. W., Raap, A. K., Tanke, H. J. (1996) *Hum. Mol. Genet.* **5**, 685-691.

Larsen, H. J. & Nielsen, P. E. (1996) *Nucleic Acids Res.* **24**, 458-463.

Laskowski R A (2001). PDBsum: summaries and analyses of PDB structures. *Nucleic Acids Res.*, **29**, 221-222.

Lee, D. Y., Hayes, J. J., Pruss, D., Wolffe, A. P. (1993) *Cell* **72**, 73-84.

Leijon, M., Graslund, A., Nielsen, P. E., Buchardt, O., Norden, B., Kristensen, S. M., Eriksson, M. (1994) *Biochemistry* **33**, 9820-9825.

Leslie, K. R. & Fox, K. R. (2002) *Biochemistry* **41**, 3484-3497.

Leuba, S. H. & Bustamante, C. (1999) *Methods Mol. Biol.* **119**, 143-160.

Lohse, J., Dahl, O., Nielsen, P. E. (1999) *Proc. Natl. Acad. Sci. U. S. A.* **96**, 11804-11808.

Low, C. M., Drew, H. R., Waring, M. J. (1986) *Nucleic Acids Res.* **14**, 6785.

Luger, K., Mader, A. W., Richmond, R. K., Sargent, D. F., Richmond, T. J. (1997) *Nature* **389**, 251-260.

Lutter, L. C. (1979) *Nucleic Acids Res.* **6**, 41-56.

Merritt, E. A. & Murphy, M. E. P. (1994) *Acta Cryst.* **D50**, 869-873.

Meyer, P. (2001) *Curr. Opin. Plant. Biol.* **4**, 457-462.

Neidle, S. (2002) *Nucleic Acid Structure and recognition.* Oxford University Press.

Nielsen, P. & Haaima, G. (1997) *Chemical Society Reviews.*

Nielsen, P. E. (1999) *Accounts of chemical research* **32**, 624-630.

Nielsen, P. E. & Christensen, L. (1996) *J. Am. Chem. Soc.* **188**, 2287-2288.

Nielsen, P. E. & Egholm, M. (1999) *Peptide Nucleic Acids, Protocols and Applications.* Horizon Scientific Press.

Nielsen, P. E., Egholm, M., Berg, R. H., Buchardt, O. (1991) *Science* **254**, 1497-1500.

Nielsen, P. E., Egholm, M., Buchardt, O. (1994) *Gene* **149**, 139-145.

Orum, H., Nielsen, P. E., Egholm, M., Berg, R. H., Buchardt, O., Stanley, C. (1993) *Nucleic Acids Res.* **21**, 5332-5336.

Polach, K. J. & Widom, J. (1995) *J Mol. Biol.* **254**, 130-149.

Portugal, J. & Waring, M. J. (1986) *Nucleic Acids Res.* **14**, 8735-8754.

Portugal, J. & Waring, M. J. (1987) *Nucleic Acids Res.* **15**, 885-903.

Puschl, A., Sforza, S., Haaima, G., Dahl, O., Nielsen, P. E. (1998) *Terahedron Letters* **39**, 4707-4710.

Rasmussen, H., Kastrup, J. S., Nielsen, J. N., Nielsen, J. M., Nielsen, P. E. (1997) *Nat. Struct. Biol.* **4**, 98-101.

Ratilainen, T., Holmen, A., Tuite, E., Nielsen, P. E., Norden, B. (2000) *Biochemistry* **39**, 7781-7791.

Rhodes, D. (1979) *Nucleic Acids Res.* **6**, 1805-1816.

Rich, A. & Davies, D. R. (1956) *J. Am. Chem. Soc.* **78**, 3548.

Rusckowski, M., Qu, T., Chang, F., Hnatowich, D. J. (1997) *Cancer* **80**, 2699-2705.

Sambrook, J., Fritsch, E. F., Maniatis, T. (1989) *Molecular cloning a laboratory manual.* 2nd edition. Cold Spring Harbor Laboratory Press.

Satchwell, S. C. & Travers, A. A. (1989) *EMBO J.* **8**, 229-238.

Schwarz, F. P., Robinson, S., Butler, J. M. (1999) *Nucleic Acids Res.* **27**, 4792-4800.

Shrader, T. E. & Crothers, D. M. (1989) *Proc. Natl. Acad. Sci. U. S. A.* **86**, 7418-7422.

St John, T., Johnson, J. D., Bonner, J. (1974) *Biochem. Biophys. Res. Commun.* **57**, 240-247.

Suck, D., Lahm, A., Oefner, C. (1988) *Nature* **332**, 464-468.

Sugimoto, N., Satoh, N., Yasuda, K., Nakano, S. (2001) *Biochemistry* **40**, 8444-8451.

Tyler, B. M., McCormick, D. J., Hoshall, C. V., Douglas, C. L., Jansen, K., Lacy, B. W., Cusack, B., Richelson, E. (1998) *FEBS Lett.* **421**, 280-284.

Vitolo, J,M., Thiriet, C., Hayes, J. J., (2000) *Mol. Cell.Biol.* **20**, 2167-2175.

Wang, J., Palecek, E., Nielsen, P. E., Riva, G., Cai, X., Shiraishi, H., Dontha, N., Luo, P., Fairias, M. A. (1996) *J. Am. Chem. Soc.* **118**, 7667-7670.

Watson, J. D. & Crick, F. H. (1953) *Nature* **171**, 737-738.

Weiler, J., Gausepohl, H., Hauser, N., Jensen, O. N., Hoheisel, J. D. (1997) *Nucleic Acids Res.* **25**, 2792-2799.

Westin, L., Blomquist, P., Milligan, J. F., Wrange, O. (1995) *Nucleic Acids Res.* **23**, 2184-2191.

Widlund, H. R., Cao, H., Simonsson, S., Magnusson, E., Simonsson, T., Nielsen, P. E., Kahn, J. D., Crothers, D. M., Kubista, M. (1997) *J. Mol. Biol.* **267**, 807-817.

Widlund, H. R., Vitolo, J. M., Thiriet, C., Hayes, J. J. (2000) *Biochemistry* **39**, 3835-3841.

Wittung, P., Nielsen, P., Norden, B. (1996) *J. Am. Chem. Soc.* **118**, 7049-7054.

Wittung, P., Nielsen, P., Norden, B. (1997) *Biochemistry* **36**, 7973-7979.

Wolffe, A. P. (1995) *Chromatin: Structure and function.* 2nd edition. Academic Press London.

Worcel, A., Han, S., Wong, M. L. (1978) *Cell* **15**, 969-977.

Yanisch-Perron, C, Vieira, J., Messing, J. (1985) *Gene* **33**, 103-119.

Appendix

β-strands

β–strands are extended lengths of polypeptide chains. A number of these strands form β- sheets where they run alongside each other. The β-strands are aligned either in the same (parallel) or opposite (antiparallel) direction, stabilised by hydrogen bonds through the main chain carbonyl and imino groups of adjacent strands.

Helices

Helices are structures where a number of residues rotate and rise in a repeating manor along an axis. The residues are orientated with their carbonyl groups pointing towards the C-terminal and the imino groups towards the N-terminal end. This enables the length of the helix to be stabilised by hydrogen bonding, which in turn creates a dipole moment aligned with the helical axis. Due to the orientation of the main chain atoms, all the C_β carbons are directed towards the N-terminus of the helix. Helices can be either right-handed or left-handed, however left-handed helices only occur in very short sequences. The hydrogen-bonding pattern, number of residues per turn, and the direction of the helices define the helical type. There are two types of right-handed helices, the α-helix and the 3_{10}-helix. Larger helices (over 6-7 residues) are all α-helices. Their consecutive residues have phi and psi angles centred at -60° and -50° respectively, which create a rise of 1.5Å per residue, with 3.6 residues per turn. Hydrogen bonding is formed through the carbonyl of residue *n* with the amide nitrogen of residue *n*+4 creating a hydrogen-bonded ring of 13 atoms.

Histone proteins

H2A

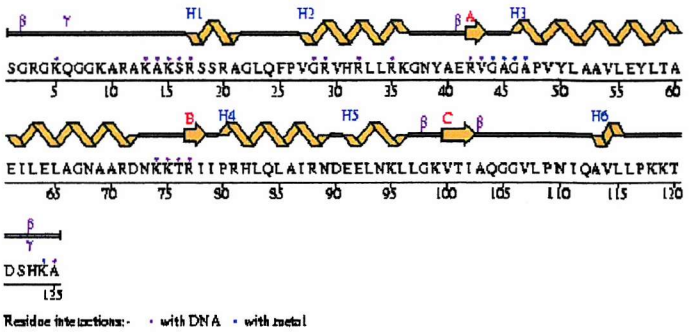

H2B

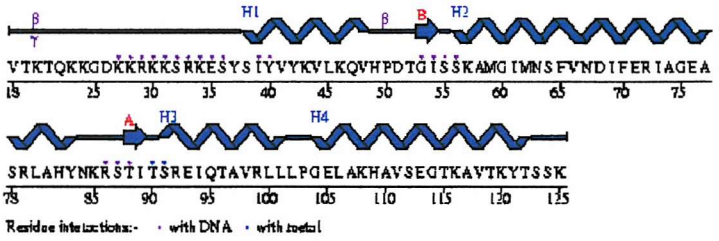

H3

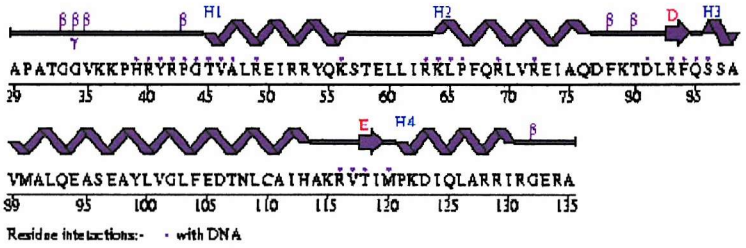

H4